



**HAL**  
open science

# Regeneration by ozonation of catalysts coked during pyrolysis of plastics: process study and comprehension of involved phenomena

Vivien Daligaux

► **To cite this version:**

Vivien Daligaux. Regeneration by ozonation of catalysts coked during pyrolysis of plastics: process study and comprehension of involved phenomena. Chemical and Process Engineering. Institut National Polytechnique de Toulouse - INPT, 2023. English. NNT : 2023INPT0120 . tel-04416857

**HAL Id: tel-04416857**

**<https://theses.hal.science/tel-04416857>**

Submitted on 25 Jan 2024

**HAL** is a multi-disciplinary open access archive for the deposit and dissemination of scientific research documents, whether they are published or not. The documents may come from teaching and research institutions in France or abroad, or from public or private research centers.

L'archive ouverte pluridisciplinaire **HAL**, est destinée au dépôt et à la diffusion de documents scientifiques de niveau recherche, publiés ou non, émanant des établissements d'enseignement et de recherche français ou étrangers, des laboratoires publics ou privés.



Université  
de Toulouse

# THÈSE

En vue de l'obtention du

## DOCTORAT DE L'UNIVERSITÉ DE TOULOUSE

**Délivré par :**

Institut National Polytechnique de Toulouse (Toulouse INP)

**Discipline ou spécialité :**

Génie des Procédés et de l'Environnement

---

**Présentée et soutenue par :**

M. VIVIEN DALIGAUX

le vendredi 8 décembre 2023

**Titre :**

Régénération par ozonation de catalyseurs cokés lors de la pyrolyse de plastiques : étude du procédé et compréhension des phénomènes

---

**École doctorale :**

Mécanique, Énergétique, Génie civil, Procédés (MEGeP)

**Unité de recherche :**

Laboratoire de Génie Chimique (LGC)

**Directeurs de Thèse :**

MME MARIE-HELENE MANERO

M. ROMAIN RICHARD

**Rapporteurs :**

M. ERIC SCHAEER, UNIVERSITE LORRAINE

M. SARY AWAD, IMT ATLANTIQUE NANTES

**Membres du jury :**

MME CARINE JULCOUR, TOULOUSE INP, Présidente

M. LUDOVIC PINARD, ENSICAEN, Membre

MME ISABELLE POLAERT, INSA ROUEN, Membre

MME MARIE-HÉLÈNE MANERO, UNIVERSITE TOULOUSE 3, Membre

MME MYLENE MARIN GALLEGRO, TOULOUSE INP, Invitée

M. ROMAIN RICHARD, UNIVERSITE PAUL SABATIER, Membre

M. STÉPHAN BROSILLON, UNIVERSITE DE MONTPELLIER, Membre



---

# Remerciements

Je tiens dans un premier temps à remercier chaleureusement mes encadrants de thèse, Romain Richard et Marie-Hélène Manero, pour m'avoir permis de vivre ce chapitre de vie de trois années et trois mois, si enrichissant à la fois scientifiquement et humainement. Merci pour la confiance que vous m'avez témoignée en me choisissant pour ce projet de recherche et en me permettant de me l'approprier. La sensation d'aboutissement que j'ai aujourd'hui en écrivant ces lignes montre la qualité de votre accompagnement qui m'a permis de conduire ce projet de recherche. Vous êtes parvenus à me guider dans les périodes de doute, me rediriger quand cela était nécessaire, me rassurer lors de mes remises en question, tout en me laissant libre dans mes choix scientifiques. Merci pour cette expérience tellement riche et formatrice, mais aussi pour les différents moments de partage que nous avons pu avoir, que cela soit au détour d'un congrès à Rome très gastronomique, d'un verre à la Chunga ou d'un simple débat pour déterminer où sont les vraies Pyrénées-Atlantiques. Merci pour tout.

Je souhaite aussi évidemment remercier toutes les personnes avec qui j'ai pu collaborer durant ces trois années, que cela soit au LGC ou d'autres laboratoires. La liste est longue donc il est fort probable que j'oublie du monde mais je vais essayer quand même.

Tout d'abord merci à Thomas Ménager pour son accompagnement technique au cours de ces trois ans, pour la conception et le montage du pilote de pyrolyse durant la première année de thèse, mais aussi pour ses goûts musicaux de qualité. Un grand merci à toi et à toute l'équipe technique du LGC, Quentin, Lahcen, Alek, pour leur aide, leur disponibilité sans lesquelles ces travaux n'auraient pas été aussi aboutis.

Un grand merci à l'équipe du SAP du LGC, Marie-Line de Solan, Gwénaëlle Guittier, Anaïs Vandebossche, Christine Rey-Rouch, pour leur gentillesse et leur réactivité face à mes (nombreuses) demandes d'analyse.

Un grand merci à Sophie Gouy et Philippe de Parseval du Centre de Microcaractérisation Castaing pour leur aide précieuse dans le développement et la réalisation des analyses microsonde pour l'acquisition expérimentale de profils de carbone. Ces résultats représentent une énorme fierté dans mes travaux de thèse et je vous suis donc très reconnaissant.

Je remercie aussi Isabelle Borget et Yannick Coppel du LCC pour la réalisation des analyses élémentaires et RMN venant compléter le volet analytique de la thèse.

Je tiens aussi à remercier Ludovic Pinard et Valérie Ruau du LCS pour la richesse de nos échanges qui a mené à une belle collaboration pour la rédaction d'un article complet et abouti.

Merci beaucoup à Mylène Marin-Gallego avec qui j'ai eu l'opportunité de travailler sur l'axe pyrolyse des travaux grâce à une heureuse coïncidence de demande presque simultanée de pilote. Merci pour ton expertise sur ce sujet ainsi que pour ta gentillesse et ta bienveillance.

Enfin, un grand merci à Jean-Marie Buchot avec qui j'ai eu l'opportunité de travailler sur l'aspect modélisation de la thèse. Même si nous avons commencé à échanger au cours de la dernière année, j'ai vraiment énormément appris grâce à nos réunions et discussions et tu m'as vraiment permis de m'enrichir de ton expérience, de ta pédagogie et de ta vision des méthodes numériques.



---

Merci à tout le personnel du LGC avec qui j'ai pu interagir à maintes reprises pour les démarches administratives ou autres. Je pense notamment à Claudine Lorenzon, Danielle Bouscary ou encore le célèbre Alain Philip. Merci pour votre aide et gentillesse.

La suite de ces remerciements va maintenant se diriger vers tous les collègues doctorants ou autres que j'ai pu côtoyer au laboratoire, certes non impliqués dans la thèse mais sans qui cette traversée aurait été bien moins plaisante. Je vais pas en faire des tonnes parce que j'ai pas envie que les remerciements fassent 10 pages mais bon quand même. Merci à ceux qui m'ont accueilli au labo, Paul, Pierre, Thibaut, Pauline, pour m'avoir si bien intégré et m'avoir mis à l'aise immédiatement par votre soutien constant et par les pauses café vitales pour le bien être psychologique de tout doctorant. Obligé de mentionner la tripléte de rêve, Paul (encore), Thomas et Igor. Que dire. Merci les gars. Merci pour tout. J'espère avoir été un aussi bon pote que vous l'avez été pour moi, votre soutien sans faille et les innombrables bons moments qu'on aura passé ensemble pendant ces trois années resteront à jamais dans mes souvenirs et j'espère de tout coeur qu'on continuera à se voir malgré la vie. Merci aussi à toutes les autres personnes géniales que j'ai eu la chance de rencontrer au labo. Encore une fois je peux pas citer tout le monde donc j'espère que vous vous reconnaîtrez en lisant ces mots. Coeur sur vous.

Pour terminer avec les personnes rencontrées pendant la thèse, il en reste une. Cette personne partage ma vie depuis maintenant presque un an grâce à une sombre histoire de cadenas de vélo, d'anniversaire (merci Thibaut) et de Lion Noir. Merci Kal d'être rentrée dans ma vie, de m'avoir soutenu, aidé, supporté, protégé, d'être toi en fait. J'ai vraiment hâte de démarrer ce nouveau chapitre avec toi et voir ce qu'il nous réservera.

Je tiens aussi à remercier mes amis de plus ou moins tous les moments de ma vie, de la maternelle à l'INSA en passant par le lycée, pour leur soutien plus ou moins à distance dans plus ou moins toute la France. Merci à tous d'être venus à ma soutenance et d'avoir assisté à cette étape de ma vie. Un merci particulier à Yoan et Maxime pour votre soutien pendant la thèse. Le premier pour sa patience à m'écouter déverser ma frustration quand une manip marchait pas au cours de sessions de Rocket thérapeutiques et le deuxième pour nos échanges philosophiques sur l'intérêt d'une thèse et le syndrome de l'imposteur. Enfin, bravo aux nouveaux docteurs, Maxime, Seb et Luca. On l'a fait.

Enfin, je remercie mes parents, ma grand-mère, pour avoir fait de moi la personne que je suis devenue aujourd'hui. Merci d'avoir fait semblant de comprendre quand je vous parlais de mon sujet de thèse, de m'avoir soutenu dans toutes mes décisions, mes choix, mes envies les plus folles comme partir à l'autre bout du monde. Merci pour tout.



---

# Abstract

The work presented in this PhD thesis is embedded in a strategy for the development of innovative processes to answer contemporary challenges, such as the energetic transition of chemical industry. The research project aims to investigate ozonation as an alternative process to classical combustion for the regeneration of coked catalysts. The scope therefore presents a very high industrial relevance as almost 80% of industrial processes involve heterogeneous (or solid) catalysts. The formation of coke over such material leads to an important decrease of catalytic performances during the process. In order to recycle spent catalysts, which are often rare or expensive materials, different regeneration methods were investigated over the years. The most common and industrially implemented process is the combustion of coke with air or oxygen-enriched air at around 500°C, whose main drawbacks are the important energy consumption and the thermal degradation risk for thermo-sensitive catalysts. Due to its high oxidative power, use of ozone for the regeneration of catalysts allows to remove coke in milder conditions at around 100°C. After promising results obtained in the laboratory team, many challenges remain unanswered to acquire a deeper understanding of the ozonation process. This project aims to investigate the different phenomena involved during the oxidation of coke with ozone (competing mechanisms, mass transfer, diffusion, etc.).

The study of ozonation process for the regeneration of coked catalysts was conducted in this work with a combined experimental and numerical approach. Coked catalysts used in this study were industrial HZSM-5 zeolites exposed to pyrolysis of polyethylene at 450°C. This reaction was identified as a promising process for the revalorization of plastics wastes. Comprehensive study of catalysts deactivation by coke formation during pyrolysis and their reuse after regeneration showed the ability of ozonation to restore complete catalytic efficiency and characteristics. The influence of operating conditions on coke removal efficiency was investigated with a lab-scale parametric study in a fixed-bed reactor and by developing robust analytical methodology. The different variable parameters are: time of exposure (between 15 min and 48 h), temperature (50 to 150°C), ozone inlet concentration (10 to 80  $\text{gO}_3/\text{Nm}^3$ ) and volumetric flowrate (50 to 150 L/h). Observations at catalysts pellet and reactor scales using a wide range of characterization methods allowed to provide a better insight of the diffusion-reaction phenomena involved during coke ozonation. Time of exposure and temperature were found to be the most significant parameters as similar behavior to coke combustion was observed: a balance between diffusion and reactivity governs ozonation process. Different regeneration regimes, known in the literature as shrinking-core and homogeneous, are observed depending on the temperature. This equilibrium was illustrated and quantified with the experimental acquisition of carbon profiles over catalyst pellets radius using innovative microprobe application with adequate sample preparation. Exploitation of these results allowed to develop a first modelling approach of the ozonation process at pellet scale. Numerical methods were used for the resolution of partial-differential equations describing the system and for the development of a curve-fitting tool to compare simulated and experimental results. This approach allowed the extraction of key parameters for ozonation that are challenging to obtain experimentally: effective diffusion coefficient of  $\text{O}_3$  in catalysts, global kinetic constants for catalytic degradation of ozone and coke oxidation. Ozonation process appears as a credible alternative to coke combustion to regenerate catalysts at 100°C. Next step would be investigating the energetic viability of the process to consider further industrial development.

---

# Résumé

Le travail présenté dans cette thèse s'inscrit dans une stratégie de développement de procédés innovants visant à répondre aux défis contemporains, notamment la transition énergétique de l'industrie chimique. Le projet de recherche porte sur l'étude d'un procédé d'ozonation comme alternative à la combustion pour la régénération de catalyseurs cokés. De nos jours, près de 80% des procédés de réactions chimiques impliquent des catalyseurs hétérogènes (ou solides), ce qui montre la pertinence industrielle de ce sujet. La formation de coke, qui sont des composés carbonés bloquant la porosité des catalyseurs, entraîne une diminution importante des performances du procédé. Afin de recycler ces catalyseurs usagés, différentes méthodes ont été développées. Le procédé de régénération le plus couramment utilisé est la combustion du coke à l'air à environ 500°C. Bien que ce procédé soit efficace, ses principaux inconvénients sont la consommation énergétique élevée et le risque de dégradation thermique pour certains catalyseurs. Afin de surmonter ces problématiques, différents procédés alternatifs sont étudiés. Parmi eux, l'exposition à l'ozone permet d'éliminer le coke aux alentours de 100°C grâce à son fort pouvoir oxydant. Après avoir obtenu des résultats préliminaires prometteurs, de nombreuses questions demeurent : ce projet vise à étudier les différents phénomènes (mécanismes réactionnels et transfert de matière) mis en jeu lors de l'oxydation du coke par l'ozone.

Le procédé d'ozonation est étudié dans cette thèse à l'aide d'une approche à la fois expérimentale et numérique. Les échantillons cokés utilisés dans cette étude sont issus de la pyrolyse catalytique du polyéthylène avec des catalyseurs zéolithiques HZSM-5. Cette réaction a été identifiée dans la littérature comme un procédé prometteur pour la valorisation des déchets plastiques et s'inscrit donc dans la logique de développement de procédés innovants animant ce projet. Une étude approfondie de la formation de coke lors de cette réaction a permis de décrire la désactivation progressive des catalyseurs au cours de leur utilisation répétée. La réutilisation des catalyseurs régénérés a ensuite permis de démontrer une restauration complète des performances après ozonation. L'influence des conditions opératoires sur l'efficacité du procédé a été examinée à l'aide d'une étude paramétrique et d'une méthodologie analytique robuste. Les différents paramètres variables sont le temps d'exposition (entre 15 min et 48 h), la température (de 50 à 150°C), la concentration d'ozone en entrée (de 10 à 80 gO<sub>3</sub>/Nm<sup>3</sup>) et le débit volumétrique (de 50 à 150 L/h). Des observations à l'échelle du grain et du réacteur ont permis d'obtenir une meilleure compréhension des phénomènes de diffusion-réaction mis en jeu lors de l'ozonation du coke. Différents régimes de régénération, connus dans la littérature sous les noms de cœur rétrécissant et homogène, sont observés. Cet équilibre entre diffusion et réactivité a été illustré et quantifié par l'acquisition expérimentale des profils radiaux de carbone sur les grains de catalyseur à l'aide d'une technique analytique innovante. Ces résultats ont permis de réaliser une première modélisation de l'ozonation à l'échelle du grain. Diverses méthodes numériques ont été utilisées afin de résoudre les équations de transfert de matière décrivant le système afin de comparer les solutions numériques aux résultats expérimentaux. Cette approche a permis de déterminer différents paramètres clés du procédé : le coefficient de diffusion effectif de l'O<sub>3</sub> dans les catalyseurs ainsi que les constantes cinétiques de la dégradation catalytique de l'ozone et de l'oxydation du coke. Au vu des résultats présentés, l'ozonation apparaît comme une alternative crédible à la combustion permettant la régénération des catalyseurs cokés dans des conditions plus douces que la combustion. L'étude de la viabilité énergétique et économique du procédé semble être la prochaine étape pour envisager un développement industriel de cette application de l'ozonation.



# Table of contents

<b>Abstract</b> .....	<b>iii</b>
<b>Résumé</b> .....	<b>vii</b>
<b>Table of contents</b> .....	<b>ix</b>
<b>Introduction générale</b> .....	<b>1</b>
<b>General introduction</b> .....	<b>4</b>
<b>Chapter 1 – Theory and literature review</b> .....	<b>7</b>
1.1. Zeolite materials for heterogeneous catalysis .....	7
1.1.1. General information .....	7
1.1.2. Zeolite reactivity and properties .....	8
1.1.2.1. Acid active sites .....	8
1.1.2.2. Shape selectivity .....	9
1.1.2.3. Influence of shaping .....	9
1.1.3. Focus on ZSM-5 zeolite .....	10
1.2. Catalytic pyrolysis of plastics .....	11
1.2.1. Context: global plastic waste and recycling methods .....	11
1.2.1.1. Plastic production and generated waste .....	11
1.2.1.2. Existing recycling methods .....	12
1.2.2. Catalytic pyrolysis .....	14
1.2.2.1. General information .....	14
1.2.2.2. Reaction mechanisms .....	16
1.2.2.3. Influencing factors .....	16
1.2.3. Focus on pyrolysis of polyethylene using ZSM-5 .....	19
1.3. Catalytic deactivation: mechanisms and key parameters .....	20
1.3.1. Mechanisms of deactivation .....	20
1.3.2. Catalytic deactivation by coking .....	22
1.3.2.1. General information .....	22

1.3.2.2. Coke formation mechanisms.....	23
1.3.2.3. Kinetics of coking and deactivation.....	24
1.3.2.4. Parameters influencing coke formation .....	26
1.3.3. Focus: deactivation of ZSM-5 during PE pyrolysis .....	28
1.4. Regeneration of catalysts deactivated via coking.....	29
1.4.1. Coke combustion with air/oxygen.....	29
1.4.1.1. Oxidation mechanisms.....	29
1.4.1.2. Reaction model: kinetics and mass transfer.....	31
1.4.1.3. Parameters influencing coke oxidation .....	33
1.4.1.4. Limitations of coke combustion .....	35
1.4.2. Ozonation.....	36
1.4.2.1. Ozone molecular properties .....	36
1.4.2.2. Ozone reactivity .....	37
1.4.2.3. Kinetics and mass transfer during ozonation .....	39
1.4.2.4. Ozonation for coke removal: literature review .....	40
1.4.3. Other regenerating methods .....	41
1.4.3.1. Gasification .....	41
1.4.3.2. Hydrogenation.....	41
1.4.3.3. Other Advanced Oxidation Processes.....	42
1.4.4. Focus: regeneration of ZSM-5 coked after PE pyrolysis .....	44
1.5. Conclusion and key takeaways.....	45
<b>Chapter 2 – Analytical review and experimental methods.....</b>	<b>47</b>
2.1. Analytical review .....	47
2.1.1. Catalyst characterization .....	48
2.1.1.1. Structural and physical properties.....	48
2.1.1.2. Chemical properties and reactivity .....	49
2.1.2. Coke analysis .....	50
2.1.2.1. Nature and composition.....	51
2.1.2.2. Reactivity and kinetics .....	53
2.2. Experimental material and methods.....	53
2.2.1. Products and chemicals .....	53
2.2.1.1. Polyethylene.....	53
2.2.1.2. Zeolite catalysts .....	54
2.2.1.3. Chemicals and gases.....	54
2.2.2. Catalytic pyrolysis of polyethylene.....	55
2.2.2.1. Experimental setup.....	55

---

2.2.2.2. Operating procedure .....	57
2.2.2.3. Results exploitation .....	58
2.2.3. Ozonation of coked catalysts .....	59
2.2.3.1. Experimental setup.....	59
2.2.3.2. Operating procedures.....	62
2.2.3.3. Results exploitation .....	63
2.2.4. Analytical techniques .....	64
2.2.4.1. Pyrolysis products .....	65
2.2.4.2. Zeolite characterization .....	65
2.2.4.3. Coke analysis .....	66
2.2.4.4. Pellet cross-section radial carbon profile.....	67
2.3. Conclusion and key takeaways.....	70
<b>Chapter 3 – Deactivation of catalysts by pyrolysis of LDPE .....</b>	<b>71</b>
3.1. Introduction and presentation of work context.....	71
3.2. Results and discussion.....	73
3.2.1. Catalytic deactivation during pyrolysis .....	73
3.2.1.1. Evolution of pyrolysis products selectivity .....	74
3.2.1.2. Influence of coking on catalysts characteristics .....	75
3.2.1.3. Nature and location of coke .....	79
3.2.1.4. Conclusion on catalytic deactivation .....	81
3.2.2. Ozonated catalysts efficiency and properties .....	83
3.2.2.1. Study of regenerated catalysts selectivity .....	83
3.2.2.2. Catalytic properties recovery and evolution.....	84
3.3. Additional considerations .....	87
3.3.1. Repeatability of coking during pyrolysis.....	87
3.3.2. Influence of initial mixing on deactivation .....	88
3.3.2.1. Catalytic selectivity.....	88
3.3.2.2. Catalysts characteristics.....	89
3.3.2.3. Coke nature and location .....	90
3.4. Conclusions and key takeaways .....	92
<b>Chapter 4 – Regeneration of zeolites by ozonation .....</b>	<b>95</b>
4.1. Introduction and context based on previous studies .....	95
4.2. Results and discussion.....	97
4.2.1. Parametric study at pellet scale.....	97
4.2.1.1. Time of exposure .....	97

---



4.2.1.2. Temperature.....	99
4.2.1.3. Inlet O <sub>3</sub> concentration.....	102
4.2.1.4. Volumetric and mass flowrate.....	104
4.2.2. Ozonation study at reactor scale .....	105
4.2.2.1. Thermal and catalytic degradation of ozone .....	105
4.2.2.2. Combined degradation and zeolite deactivation .....	108
4.2.2.3. Coke oxidation in zeolite catalytic bed .....	109
4.3. Comparison tubular/syringe reactor experiments .....	112
4.4. Conclusions and key takeaways .....	114
<b>Chapter 5 – Modelling approach to ozonation reaction .....</b>	<b>117</b>
5.1. Introduction and presentation of work.....	117
5.2. Model of ozonation at pellet scale.....	119
5.2.1. Global approach: diffusion-reaction system .....	119
5.2.2. Effective diffusion in zeolites.....	120
5.2.3. Ozone and coke reactivity.....	121
5.2.4. Simplifications and final PDEs .....	123
5.3. Numerical methods .....	124
5.3.1. PDEs resolution .....	125
5.3.1.1. Crank-Nicolson discretization .....	125
5.3.1.2. Newton method for resolution coupling.....	127
5.3.2. Image processing .....	128
5.3.2.1. Raw image preparation.....	128
5.3.2.2. Profile acquisition .....	128
5.3.2.3. Data normalization .....	130
5.3.3. Profiles fitting optimization.....	130
5.4. Results and discussion .....	131
5.4.1. Influence of key parameters on numerical resolution .....	131
5.4.1.1. Coke oxidation kinetic constant.....	131
5.4.1.2. Effective diffusion coefficient .....	133
5.4.1.3. Catalytic degradation kinetic constant .....	134
5.4.1.4. Initial carbon load.....	135
5.4.2. Parametric identification by profile optimization.....	137
5.4.2.1. Arrhenius correlation for $k_{oxi}$ .....	137
5.4.2.2. Sensibility of effective diffusion coefficient .....	139
5.5. Conclusions and key takeaways .....	141

<b>General conclusion .....</b>	<b>145</b>
<b>Conclusion générale .....</b>	<b>149</b>
<b>References.....</b>	<b>154</b>
<b>List of figures .....</b>	<b>171</b>
<b>List of tables .....</b>	<b>176</b>
<b>Appendices.....</b>	<b>179</b>



# Introduction générale

## (Version française)

La transformation de l'industrie chimique au cours des prochaines années est d'une importance capitale dans le cadre de la transition énergétique. Cette métamorphose est nécessaire afin de surmonter les conséquences environnementales et sociales du changement climatique. En effet, le secteur industriel, couplé à celui de la production d'énergie, est responsable de plus de 60% des émissions mondiales de gaz à effet de serre. Alors que les émissions directes de CO<sub>2</sub> ont atteint 36,8 Gt en 2022, ces secteurs majeurs offrent un potentiel d'amélioration considérable pour réduire ces émissions à l'échelle planétaire [1, 2]. Pour atteindre ces objectifs, il est impératif de mettre en place une stratégie globale de décarbonation et de réduction de consommation énergétique par l'innovation. La recherche scientifique joue un rôle prépondérant afin de permettre et d'encourager cette transition urgente. A cet effet, l'optimisation des procédés existants et le développement de méthodes innovantes sont désormais au cœur des travaux de recherche visant à relever le défi d'une industrie chimique durable.

La catalyse est présente dans la majorité des procédés chimiques. Leur utilisation permet un contrôle accru de la vitesse de réaction et de la sélectivité des produits. De plus, la demande croissante de procédés moins énergivores et générant moins de déchets laisse prévoir une hausse importante des potentielles applications. Les catalyseurs hétérogènes, qui font appel à des matériaux catalytiques solides, sont impliqués dans 80% des processus chimiques (Figure 0.1) en raison de leur facilité de mise en œuvre [3]. Les catalyseurs solides sont donc présents dans de nombreux domaines faisant intervenir une réaction chimique, de la pétrochimie à l'industrie pharmaceutique.

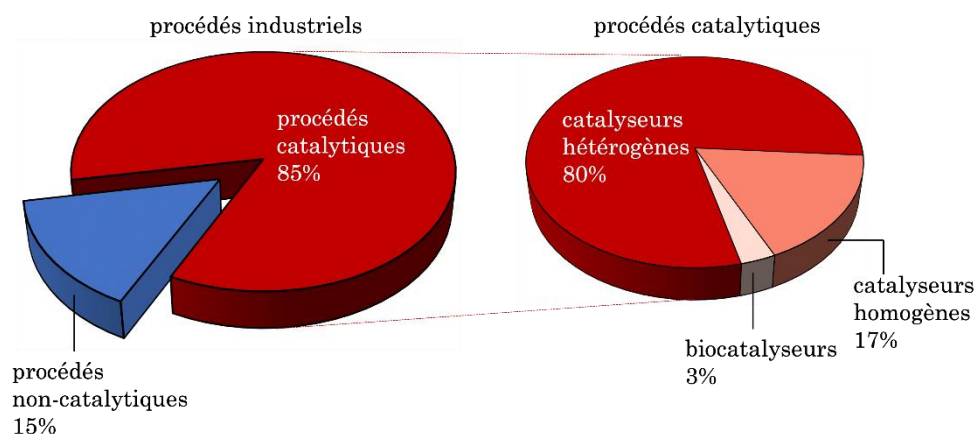


**Figure 0.1.** Importance de la catalyse hétérogène dans les procédés chimiques (Thomas, 2016) [3].

Le principal inconvénient de la catalyse hétérogène est la désactivation des catalyseurs, qui entraîne une perte des performances catalytiques. Se produisant à des degrés différents en fonction du procédé, la désactivation est principalement causée par un encrassement dû à la formation de dépôts de composés carbonés, communément appelés "coke". Celui-ci provoque une importante diminution des propriétés texturales et chimiques des catalyseurs, se traduisant par une baisse de l'activité catalytique [4, 5]. La désactivation par formation de coke est généralement réversible, et les catalyseurs peuvent être recyclés en éliminant le coke. La régénération de ces matériaux est aujourd'hui principalement conduite par oxydation sous air à haute température (400-600°C). Ce procédé requiert une importante consommation d'énergie et ne convient pas aux catalyseurs thermo-sensibles. Le développement d'une alternative pour la régénération des catalyseurs cokés présente donc un intérêt environnemental majeur pour remplacer la combustion du coke par un procédé moins énergivore [6, 7]. Une telle avancée aurait un impact significatif en raison du grand nombre d'applications liées à la désactivation et à la régénération des catalyseurs dans l'industrie chimique. L'objectif de cette thèse est de répondre à ce défi en développant un procédé de régénération opérant dans des conditions plus douces : l'oxydation à l'ozone (ou ozonation). Des études préliminaires prometteuses menées dans le laboratoire ont démontré la capacité de l'ozone à oxyder le coke aux alentours de 100°C grâce à son fort potentiel oxydant [8, 9]. Cependant différents verrous scientifiques et techniques empêchaient d'atteindre une bonne compréhension de ce procédé innovant. Ce projet de recherche vise à surmonter ces défis et à mieux comprendre les phénomènes réactionnels et de transfert ayant lieu durant l'ozonation de catalyseurs cokés. Différentes problématiques sont abordées dans cette étude afin de déterminer : (i) les réactions et mécanismes impliqués dans l'élimination du coke (dégradation thermique et catalytique de l'ozone, oxydation directe et indirecte du coke avec l'ozone moléculaire ou les espèces radicalaires), (ii) l'influence des conditions opératoires sur les limitations de diffusion et l'efficacité du procédé et enfin (iii) l'effet de la nature du coke et le rôle du matériau catalytique. De nombreux aspects de ce travail de recherche, tels que la réactivité des espèces radicalaires ou la diffusion moléculaire dans les milieux microporeux, présentent encore d'importants défis scientifiques à ce jour. Ce projet de recherche constitue donc un défi à la fois académique et industriel pour le développement d'un procédé innovant.

En raison du grand nombre d'applications potentielles, la complexité de cette étude résidait également dans le choix du matériau catalytique et de la réaction désactivante. Cette réaction chimique "modèle" a pour but de conduire à des catalyseurs cokés à régénérer, mais également d'évaluer la restauration des performances catalytiques après ozonation. Il était nécessaire de trouver un équilibre entre la pertinence industrielle actuelle et future pour le choix de ce procédé, offrant ainsi la possibilité d'orienter ce travail de recherche vers des problématiques actuelles. Ayant une importante implantation industrielle depuis de nombreuses années tout en présentant de nombreuses applications émergentes, les zéolithes ont été choisies comme catalyseurs pour cette étude. En effet, leurs propriétés géométriques et acides uniques permettent de réduire la consommation d'énergie et d'augmenter la sélectivité au cours de procédés [10, 11]. La réflexion pour le choix de la réaction désactivante nous a mené vers un procédé présentant d'importantes perspectives à moyen terme, mais dont le développement industriel est retenu à cause de problèmes de désactivation par formation de coke. Ces critères ont été des éléments importants pour le choix final. En effet, même si cette réaction est principalement destinée à obtenir facilement des zéolithes cokées pour l'étude du procédé

d'ozonation, les résultats expérimentaux obtenus peuvent apporter de nouveaux éléments sur ce procédé même s'il ne constitue pas le cœur de la thèse. Répondant à tous ces éléments, la pyrolyse catalytique des déchets plastiques a été choisie en tant que procédé innovant répondant aux défis contemporains, à savoir la pollution plastique [12]. L'utilisation de catalyseurs pendant la pyrolyse permet de revaloriser les déchets plastiques en produits à haute valeur ajoutée, comme du carburant, des monomères ou molécules plateforme [13]. Différents travaux ont étudié ce procédé au cours des dernières années, montrant une importante désactivation par formation de coke, entravant ainsi son développement industriel [14].

L'objet de l'étude présentée dans ce projet de recherche est donc la régénération par ozonation de zéolithes cokées au cours de la pyrolyse catalytique des plastiques, en particulier du polyéthylène. L'étude parallèle conduite sur un procédé de revalorisation des déchets apporte une nouvelle dimension au travail de thèse : il s'inscrit dans une démarche de développement de procédés innovants afin de répondre aux défis environnementaux actuels en promouvant une économie circulaire et une consommation énergétique réduite pour une industrie chimique plus durable. Cette étude cherche ainsi à évaluer la capacité du procédé d'ozonation à régénérer les catalyseurs cokés, à obtenir une compréhension approfondie des phénomènes impliqués, tout en apportant des connaissances supplémentaires sur la désactivation des catalyseurs lors de la pyrolyse des plastiques.

Les principaux aspects de ce travail sont introduits dans le Chapitre 1, avec une revue de l'état de l'art liée à chaque axe du projet de recherche. Après une présentation générale des zéolithes en tant que catalyseurs et de la pyrolyse catalytique des plastiques, un intérêt particulier est porté à la désactivation des catalyseurs par formation de coke ainsi qu'aux différents procédés de régénération. Les connaissances actuelles sur l'ozonation et les phénomènes attendus en faisant le parallèle avec la combustion du coke sont détaillés afin de fournir le contexte et les connaissances nécessaires à une meilleure compréhension des résultats présentés. Dans le chapitre suivant, la méthodologie de ce travail est présentée. A l'aide du contexte fourni par une présentation complète des techniques analytiques utilisées dans le domaine, le matériel, les installations expérimentales, les protocoles et les méthodes de cette étude sont détaillés dans ce Chapitre 2. Les résultats et discussions de cette thèse sont ensuite articulés en trois parties : la désactivation et la réutilisation des catalyseurs ozonés pendant la pyrolyse, l'étude expérimentale de l'oxydation du coke par ozonation et une approche numérique du procédé. Le Chapitre 3 porte sur l'évolution des propriétés des catalyseurs durant la pyrolyse du polyéthylène. Une étude complète de la formation de coke au cours de cette réaction a été menée, examinant l'influence de cette désactivation sur les propriétés et les performances des catalyseurs, avant de réutiliser les zéolithes ozonées en pyrolyse afin d'évaluer la restauration de l'activité catalytique. Dans le Chapitre 4, les aspects expérimentaux du procédé d'ozonation sont présentés : une étude paramétrique est conduite afin de déterminer les conditions optimales pour l'élimination du coke et de mieux comprendre les phénomènes mis en jeu à l'échelle du grain et du réacteur. A l'aide de ces résultats expérimentaux, une approche numérique visant à modéliser ce système de réaction-diffusion complexe est présentée dans le Chapitre 5, afin d'en extraire les paramètres physico-chimiques clés du procédé d'ozonation.

# General introduction

## (English version)

The transformation of chemical industry during the upcoming years represents a key point of the ecological transition required to face environmental and social consequences of climate change. Industrial sector combined with energy production represents more than 60% of global greenhouse gases emissions. While the global direct CO<sub>2</sub> emissions reached 36.8 Gt in 2022, these key sectors present a tremendous potential for the reduction of global emissions [1, 2]. In order to achieve such environmental objectives, a combined strategy of decarbonation and reduction of energy consumption through innovation is required. Scientific research obviously has a crucial role to engage and encourage this urgent transition. The optimization of existing processes or development of innovative methods nowadays animate most of research works to take up the challenge of a sustainable chemical industry.

Catalysts are widely used in industrial processes for chemical reactions as they provide an increase control over reaction rate and product selectivity. Furthermore, due to the increasing need for industrial processes to be less energy intensive and to produce less waste, catalysts demand and applications are expected to grow within the following decades. Heterogeneous catalysts, being the use of solid catalytic material, are involved in 80% of chemical processes (Figure 0.1) due to their ease of implementation [3]. Applications of solid catalysts are therefore found in a wide range of industries when chemical reactions are involved, from petrochemistry to pharmaceutical domains.

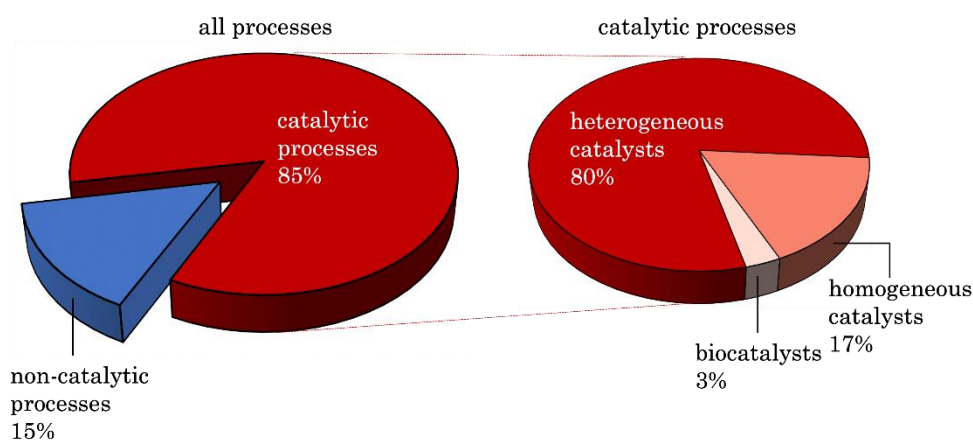


**Figure 0.1.** Industrial relevance of heterogeneous catalysts in chemical processes (Thomas, 2016) [3].

The main drawback of heterogeneous catalysts resides in their deactivation, causing loss of catalytic performances. Occurring at different rates depending on the involved process, deactivation is mainly caused by fouling due to deposition of carbonaceous compounds, referred as “coke”. These molecules cause an important decrease of textural and chemical properties of catalysts leading to lowered efficiency [4, 5]. Deactivation via coking is reversible in most cases and catalysts performances can be recovered by removing coke species. Regeneration of catalytic material is carried out in industry with an oxidation process with air at high temperatures (400-600°C). Such conditions require important energy consumption and are not suitable for thermo-sensitive catalysts. The development of an alternative method for solid catalysts regeneration is therefore of high interest to replace coke combustion by a less energy intensive process [6, 7]. Such advances would have an important effect on chemical industry due to the high industrial relevance and number of applications of catalysts deactivation and regeneration. The aim of this PhD work is to overcome this challenge by investigating a regeneration process operating in milder conditions: oxidation with ozone, also called ozonation. Preliminary studies conducted in the laboratory showed promising results as the high oxidative power of ozone allowed to remove coke over catalysts around 100°C [8, 9]. Different scientific and technical obstacles prevent obtaining a better understanding of this innovative process. This research project aims to overcome these challenges and to gain better insight on the reaction and mass transfer phenomena involved during ozonation of coked catalysts. Different aspects are investigated in this work to determine: (i) the involved reactions and mechanisms leading to coke removal (thermal and catalytic degradation of ozone, direct and indirect coke oxidation with molecular ozone or radical species), (ii) the influence of operating conditions over diffusion limitations and process efficiency and (iii) the effect of deactivating species as well as catalytic material. Many aspects of this research work, such as the reactivity of radical species or diffusion in microporous media, present important scientific challenges even up to date. This research project consequently presents a combined academic and industrial challenge for the development of innovative process.

Due to the wide range of potential applications, the complexity of this study also resides in the choice of a catalytic material and a reaction conducting to the deactivation of catalysts via coking. This “model” chemical reaction is intended to provide coked catalytic material for the regeneration study but also to assess the ability of ozonation to restore catalytic performances. This choice of deactivating process needed to find an appropriate balance between current industrial relevance and future applications, therefore giving the opportunity to direct this work towards contemporary fields of interest. Zeolites were elected as catalytic material for this study, identified in the literature as catalysts with both important industrial implantation for many years and yet presenting many emerging applications. Indeed, their unique acid and shape-selective properties allows minimization of energy consumption and control of appropriate shape and size of products [10, 11]. Moreover, coking is the major deactivation pathway on zeolite-based catalysts and loss of catalytic efficiency is therefore reversible with an appropriate regenerating treatment. The choice for the coking reaction was directed towards a process presenting promising perspectives on a mid-term basis, but whose industrial development is restrained by an important deactivation via coke formation. These criteria were key factors in the final choice as this process is mostly expected to easily provide coked zeolites for ozonation investigations, but even though it is not the core of the PhD work, experimental results can provide new insights on this process. The chosen reaction therefore has to present a recently gained interest, in order to have a sufficient knowledge of the process and yet



being able to bring additional insight. Catalytic pyrolysis of plastics waste was elected as it was identified in the literature as an innovative process answering to contemporary challenges, i.e. plastic pollution, which presents all the aforementioned elements [12]. Use of catalysts during pyrolysis allows the revalorization of plastics waste into high-value products that can be reused as fuel or chemical feedstock [13]. This process was heavily investigated over the past years, showing an important catalytic deactivation via coking that restrains its industrial development [14].

The investigated reaction system in this research project is therefore the regeneration via ozonation of coked zeolites used during catalytic pyrolysis of plastics. The use of this particular deactivating reaction for the study of the ozonation process brings another dimension to the PhD work: it is embedded in a logic of development of innovative processes answering to contemporary challenges for a circular economy and reduction of energy consumption for a sustainable chemical industry. This study intends to evaluate the ability of ozonation to regenerate coked catalysts by providing a deep understanding of involved phenomena, but also to provide additional knowledge on the deactivation occurring during catalytic pyrolysis of plastics.

The main different axes of this work are introduced in Chapter 1 with a literature review related to each relevant aspect of the research project. After a presentation of zeolites material for catalysis and a global overview of catalytic pyrolysis of plastics, a focus on catalysts deactivation via coking and the different existing regenerating processes is conducted. The current knowledge on ozonation and expected phenomena based on comparison with coke combustion are detailed to provide necessary background for the comprehension of further exploitation. In the following chapter, the analytical and technical methodology of this work is presented. Based on the contextual knowledge provided by a complete presentation of the analytical techniques panel used in the domain, the material, experimental setups, protocols and methods of this work are detailed in this Chapter 2. The results and discussions of this PhD work are then articulated in three different axes: the deactivation and reuse of ozonated catalysts during pyrolysis, the experimental study of the ozonation process for coke removal and a modelling approach of coke oxidation with ozone. Chapter 3 focuses on the experimental use of catalysts during pyrolysis of polyethylene. A complete study of coke formation during this process was conducted, investigating the influence of deactivation over catalysts properties and performances, before recycling ozonated catalysts into pyrolysis to assess the ability of the process to restore catalytic activity. In Chapter 4, the experimental aspects regarding ozonation are presented: a parametric study is conducted in order to determine optimal coke removal conditions and to gain better understanding of the phenomena involved during the process both at pellet and reactor scale. Combined with these experimental results, a numerical approach is presented in Chapter 5 intending to model this complex diffusion-reaction system and to extract key physical and chemical parameters of ozonation process.

# Chapter 1

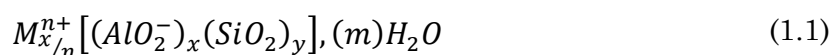
# Theory and literature review

In this chapter, the main axes of this work are introduced with a complete state of art related to each section: zeolite materials, catalytic pyrolysis of plastics, catalysts deactivation mechanisms and regenerating processes. These different aspects are discussed with an important literature review to provide a better understanding of the research context and the project objectives. For every principal aspects, a particular attention is given to the scope of this work in a focus section.

## 1.1. Zeolite materials for heterogeneous catalysis

### 1.1.1. General information

Zeolite catalysts are aluminosilicate sieves with pores and channels forming a three-dimensional microporous framework. While silica-alumina catalysts have an amorphous structure, zeolites have a crystalline structure, composed of primary structural units  $TO_4$  tetrahedron where T is the central atom, typically Si or Al, surrounded by O atoms connecting one unit to the other. The negative charge bore by each tetrahedron with aluminum in the center is compensated by the presence of an exchange cation, usually  $H^+$ ,  $K^+$  or  $Na^+$ . The chemical composition of zeolites is presented by Equation (1.1).



Where M is the exchange cation with its charge n, (x + y) is the total number of primary units and m is the number of adsorbed water molecules. The ratio y/x represents the Si/Al ratio often used to describe zeolite composition. Interconnection between the tetrahedral basic building units (BBU) gives rise to different possibilities of three-dimensional microporous structures with geometries having specific structural properties [10, 15, 16]. As presented in Figure 1.1, each zeolite is defined by its singularities: pore network with related porosity and tortuosity; channels and intersections in one, two or three dimensions; systems of cages connected by windows [16]. Among the most commonly used zeolites, HZSM-5, HUSY, H $\beta$  and HMOR can be cited. Over 200 different zeolite structures, synthetic and natural, have been identified and can be found on the

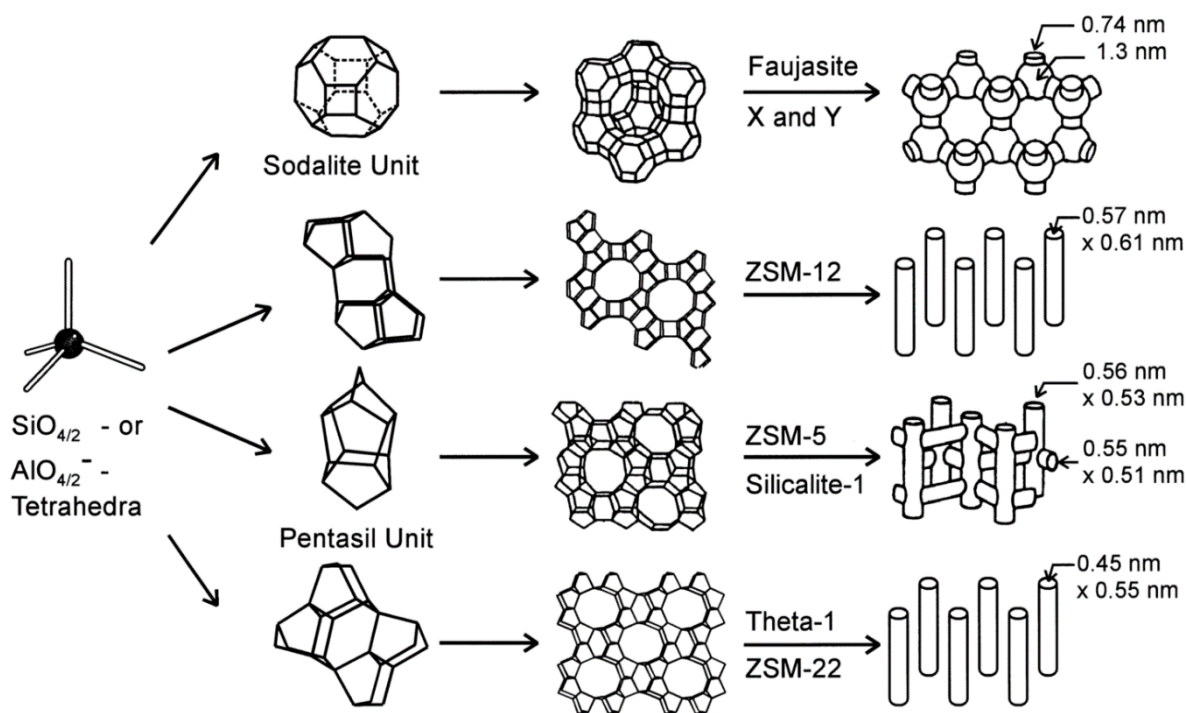


**Figure 1.1.** Structures of four particular zeolites (from top to bottom: faujasite or zeolites X and Y; zeolite ZSM-12; zeolite ZSM-5 or silicalite-1; zeolite Theta-1 or ZSM-22) and their micropore systems and dimensions (Weitkamp *et al.*, 2000) [10].

International Zeolite Association (IZA) website [17]. The possible geometries and composition variations of zeolites offer a wide range of characteristics: Si/Al ratio, specific surface, porosity and nature of compensating cation. Due to their important reactivity and adsorption capacities, zeolites are materials of interest for numerous applications in various domains [18]. Zeolites are nowadays widely used as heterogeneous catalysts in many industrial processes from petrochemistry to water and gas treatment.

## 1.1.2. Zeolite reactivity and properties

### 1.1.2.1. Acid active sites

Zeolite reactivity is due to the presence of surface acid sites which number and strength are determined by its composition. The distribution of aluminum and exchange cation within the structure influences the acidic properties of the zeolite [19]. Two types of acid sites are identified and discussed in the literature: Brønsted (proton donor) and Lewis (electron-pair acceptor) sites [20]. Brønsted acid sites (BAS) appears when trivalent aluminum replaces silicate in the network inducing negative charge compensated by a proton, which leads to the formation of bridging OH groups (Figure 1.2). Lewis acid sites (LAS) are generated either by aluminum electronic default (tri-coordinated) or by interaction with electrons acceptors (Figure 1.2). Extra network aluminum oxides are playing this role on the crystals surface while it occurs in the zeolite bulk due to the compensating cation interaction. However, the latter phenomenon is still debated as the strength of so-formed acid sites is not significant compared to other interactions. Lewis acidity in zeolites is therefore mostly correlated to the interactions with extra framework aluminum species [21]. The following spatial repartition of zeolite active acid sites is accepted: Brønsted sites are mostly embedded in the microporous network while Lewis sites are located on the external surface of the crystals.

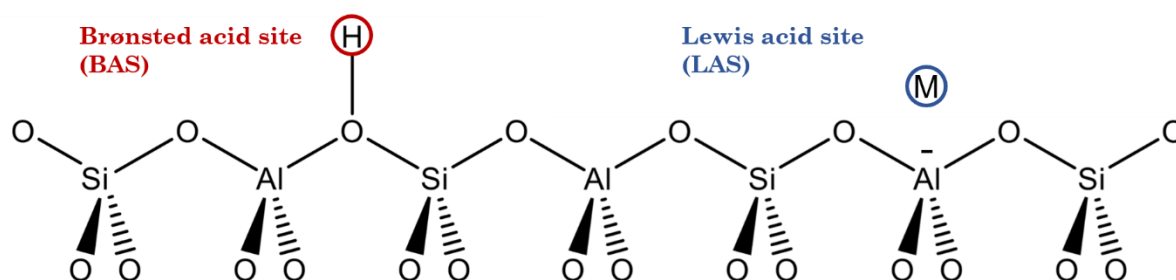


**Figure 1.2.** Formation of acid sites in zeolites. M is an electrons acceptor, can be either a compensating cation or extra framework aluminum oxide ( $\text{Al}_x\text{O}_y^{n+}$ ).

The strength of the different sites differs depending on their type and their direct environment. Most of the catalytic activity of zeolites is attributed to Brønsted acid sites due to their higher reactivity but Lewis sites also affect catalytic activity, either by synergistic effect or by having their own reactivity [21, 22]. The average Si/Al ratio is a key factor of zeolite properties as the strength of Brønsted sites increases with bigger ratio values [23]. However high Si/Al ratio also causes a decrease of total acidity as it means that less tetrahedral aluminum is included in the zeolite network [24].

### 1.1.2.2. Shape selectivity

Due to the wide range of possible geometries and offered shape-selectivity, applications of zeolites are dependent of their structure [25]. The pore size being at the molecular scale, the diffusion of molecules within the zeolite can be limited by steric blocking [26]. The choice of steric limitation can be directed towards selectivity of reactants or products as illustrated in Figure 1.3 (a, b). All catalytic reactions can therefore find an interest in the use of shape-selective materials in order to shift reaction selectivity to products of interest avoiding undesired reactions.

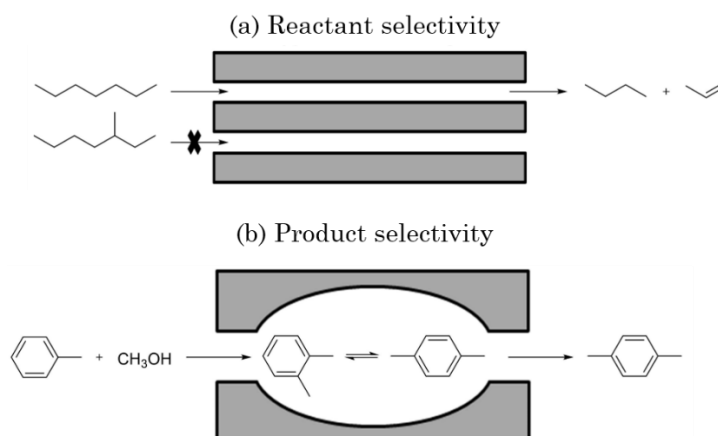


**Figure 1.3.** Illustration of shape-selectivity using zeolites as catalysts in (a) reactant selectivity with the cleavage between linear and branched hydrocarbons and (b) product selectivity during methylation of toluene (Dhakshinamoorthy *et al.*, 2020) [26].

### 1.1.2.3. Influence of shaping

Pure zeolites are usually in the form of a thin white powder and the majority of academic research studies are conducted using powdered zeolites. However, powder is not suitable for fixed beds industrial processes as it causes important charges loss and has a

weak mechanical resistance [27]. Thus, binders are added to the pure zeolites during the shaping step, intending to form catalytic material in pellets form, suitable for scale-up experiments and industrial scale use (Figure 1.4). Classic binders used in industry are alumina, clay, silica or zirconia. The pelletized catalysts are often obtained with an extrusion process followed by a calcination step for activation. Different shapes can be found on the market, from classic spheres and cylinders to more sophisticated geometries developed for hydrodynamics optimization [28].

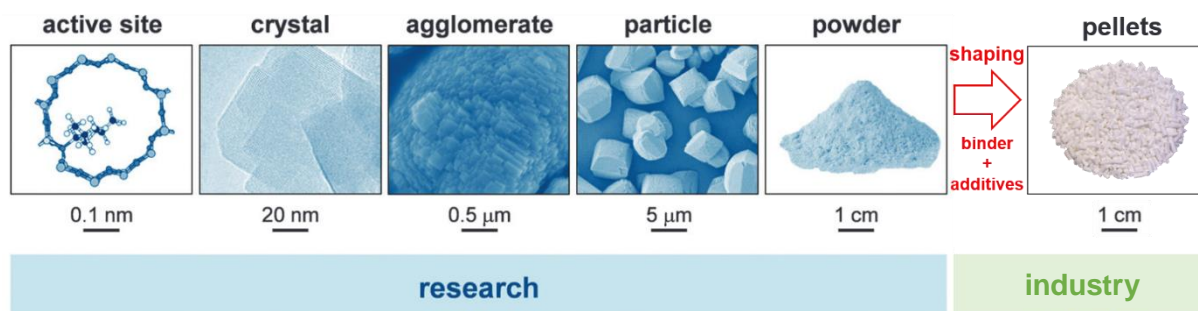


**Figure 1.4.** Representation of zeolite material from atomic scale to its pelletized form for industrial use. Adapted from Mitchell *et al.* (2013) [27].

As other compounds are mixed with pure zeolite during the process, the acidity is diluted in the extrudate. Even though binder may not have a direct catalytic effect, its chemical interactions with zeolite crystals can affect the acidic properties of the material, especially forming Lewis acid sites on the surface as mentioned in Section 1.1.2.1 [29]. The choice of binder is therefore crucial as it has a great influence over the catalyst properties and therefore over the global process [30]. For instance, the use of a binder changes the porosity of the material as it introduces a mesoporous volume in which zeolite crystals (microporous volume) are dispersed. As summary, the reactivity of zeolite pellets is mainly due to the Brønsted acid sites located in microporosity (internal surface), but also to Lewis acid sites located in the mesoporous volume generated by the presence of a binder (external surface). These different levels of porosity greatly affect diffusion and it is therefore necessary to understand mass transfer occurring during the reactions.

### 1.1.3. Focus on ZSM-5 zeolite

ZSM-5 zeolite, standing for Zeolite Socony Mobil-5, has been patented by Mobil Oil Corporation in 1969 [31]. This zeolite presents an MFI type structure and consists in a three-dimensional network with interconnected channels: straight and sinusoidal (Figure 1.5) [32]. A ring of 10 oxygen atoms forms the pore apertures [33]. Despite similar diameters, the circulation path is longer through sinusoidal channels, thus tortuosity is impacted and diffusion is more difficult than through straight channels passage [34]. The intersections form wider voids which diameter is estimated to 9 Å and the Si/Al ratio is between 10 and 1000 [35]. Due to its relatively low aluminum content, ZSM-5 presents good thermal and chemical stability. Its acidic properties combined with its microporosity presents interesting selectivity and is commonly used in a wide number of processes involving hydrocarbon reactions (methanol or olefins conversion to gasoline and diesel, oil refining, xylene isomerization, toluene disproportionation and alkylation, catalytic dewaxing, etc.) [36]. The cracking and reforming capacity of ZSM-5 also lead to recent interest for its use in plastics waste or biomass revalorization processes, which are discussed in the following section [37-39].

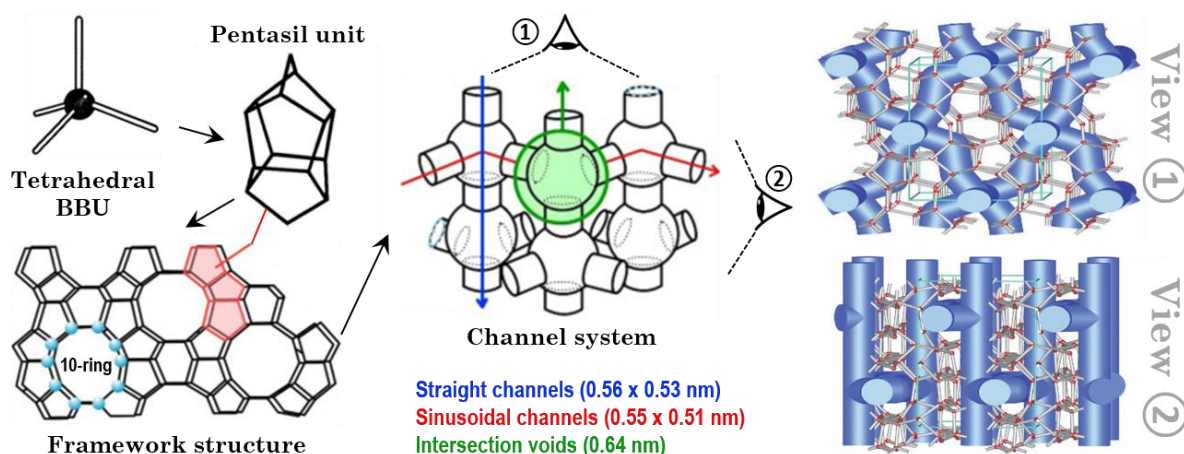


**Figure 1.5.** Spatial representation of ZSM-5 zeolite structure, from tetrahedral primary unit to the framework structure and inherent channel system (blue: straight channels; red: sinusoidal channels; green: intersection voids). Combined scheme adapted from Weitkamp *et al.* (2000) [10], Lounis *et al.* (2018) [32] and Kamaluddin *et al.* (2022) [33].

## 1.2. Catalytic pyrolysis of plastics

### 1.2.1. Context: global plastic waste and recycling methods

#### 1.2.1.1. Plastic production and generated waste

Plastic use has grown extensively during the last decades and is nowadays present in many different sectors, from everyday life to technical applications. As represented in Figure 1.6, combined packaging (household, industrial and commercial) is the main plastic consuming segment and accounts for almost 40% of worldwide consumption [12]. Globally, due to the plastic demand for each segment, the main produced polymers are identified to be polyethylene (PE), with different possible densities, polypropylene (PP), polystyrene (PS), polyethylene terephthalate (PET) and polyvinyl chloride (PVC). Nowadays, plastics are mainly produced from petroleum-based feedstock. To provide an alternative to petroplastics and to face limitation of fossil energy sources, use of biosourced material to produce biobased plastics rises as an interesting and sustainable option because of their biodegradability and renewability [40]. Bioplastics are currently marginal with only about 1% of the annual plastic production, but this market is expected to continuously grow within the next years [41]. Based on their different properties, such as rigidity, ductility, insulation capacity and others, polymers are used for many applications in various domains. For example, polyethylene is very commonly used for packaging purposes. Different densities of PE are possible according to the need: low-density PE (PE-LD) is used for plastic bags and wrapping foils while high-density PE (PE-HD) packaging applications are detergent bottles or oil containers. PP has a lower density than PE-HD and similar to PE-LD but has higher rigidity, making it a rather light and resistant material. This polymer is therefore extensively used in plastic industry for diverse applications such as car bumpers or storage boxes. Cumulative consumption of the five mostly used types of polymers represents almost 75% of the total plastic use, with more than half for PE and PP [42]. Representing the majority of plastics found in landfill, PE and PP are preferentially chosen in recycling R&D investigations.

Even though plastic waste can originate from previous years production, estimation of plastic waste generated per year is usually approximated to the annual production, since



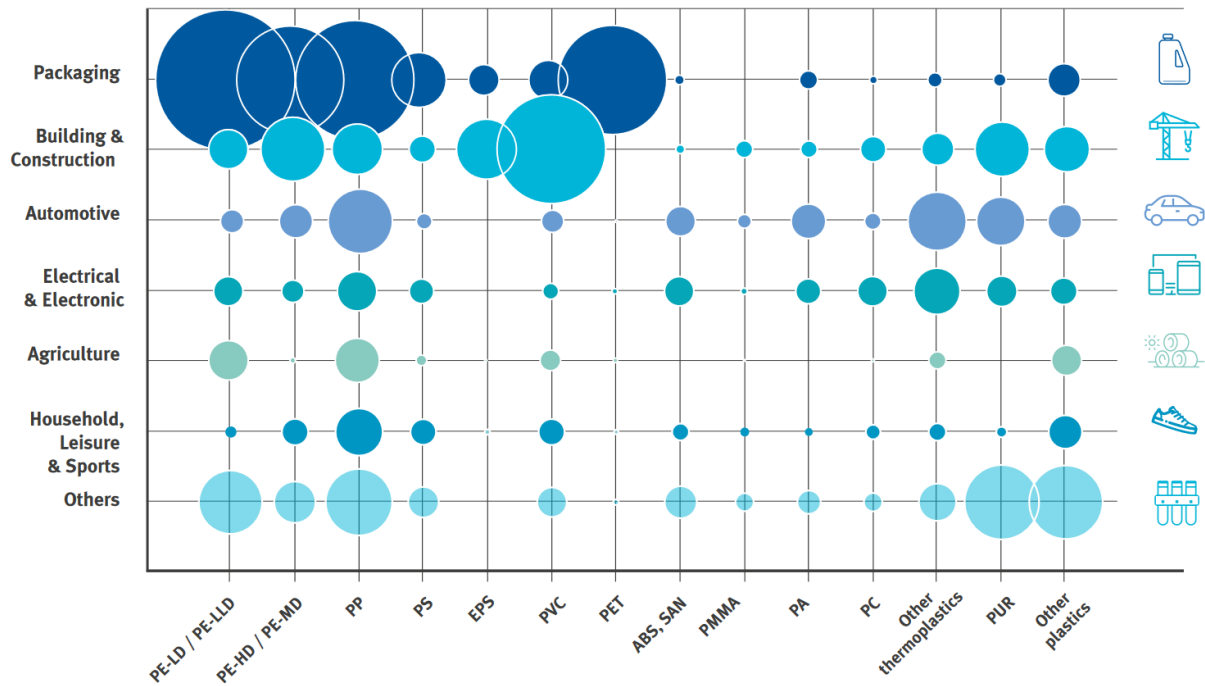


**Figure 1.6.** Plastic demand by domain and type of polymer in 2019. Illustration taken from report “Plastics – the Facts 2020”. Source: PlasticsEurope. Polyethylene PE (LLD: linear low-density; MD: medium-density), polypropylene PP, polystyrene PS, polyvinyl chloride PVC, polyethylene terephthalate PET, acrylonitrile butadiene styrene ABS, styrene acrylonitrile SAN, poly(methyl methacrylate) PMMA, polyamide PA, polycarbonates PC, polyurethane PUR.

almost 50% of the production is aimed for single-use applications and only 9% of the production comes from recycled plastics [43]. Despite recent efforts to limit waste generation and to improve recycling, an important remaining part of plastics is directly disposed to landfill or rejected in the environment causing huge space occupation and dramatic environmental issues. Each year, between 8 and 14 Mt of plastics are dumped into the ocean, mostly deteriorating into tiny pieces also called microplastics, and causing irreversible damages to marine ecosystems and biodiversity [44]. Landfills also have a direct negative environmental impact by poisoning soils, altering land biodiversity, and by emitting greenhouse gases [45]. Because of their stable chemical nature, polymers are very persistent in the environment and may take more than 100 years to undergo natural degradation. Pollution due to plastic waste accumulation and spill in nature is therefore a major environmental issue and the combined reduction of waste and amelioration of recycling have become a worldwide stake. To achieve the model of a circular economy, aiming a complete reuse of plastic waste with the creation of a closed loop between production and waste management, many public and private international actors of research investigate new alternative methods to increase and to improve plastic recycling and revalorization [12, 46].

### 1.2.1.2. Existing recycling methods

The different recycling methods found in the literature can be split into different categories: mechanical, chemical and biological recycling Figure 1.7 represents the different available methods for plastic recycling and their implementation in the aimed circular plastic economy allowing theoretical endless reuse of plastic wastes. The mechanical pathway is already well known and widely applied at industrial scale and is

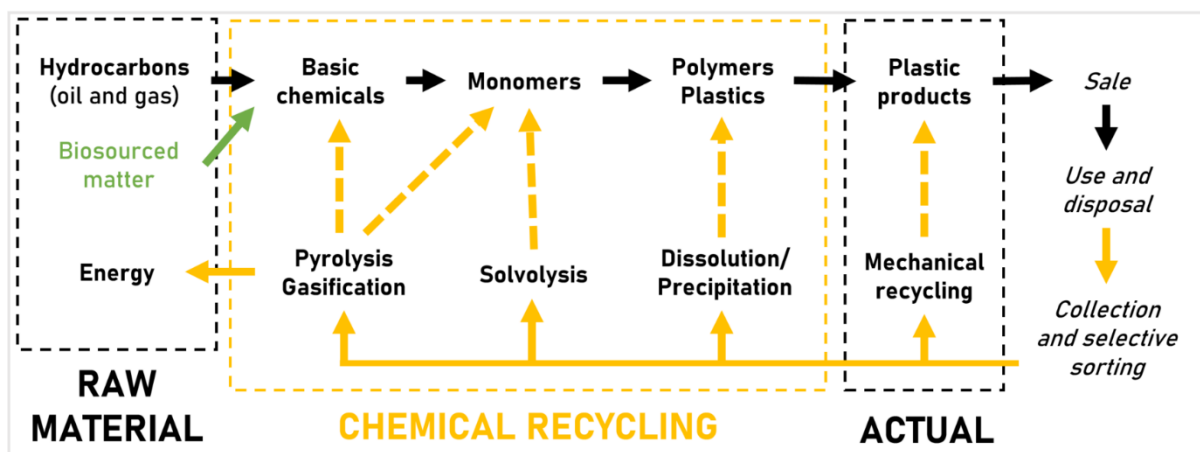


**Figure 1.7.** Schematic representation of the different existing methods for plastic waste recycling and their implementation in the circular economy.

currently the most commonly used method for plastic waste recycling. In fact, the term “recycling” is nowadays mostly associated to mechanical recycling since it represents 99% of recycled quantities in Europe [47]. It consists in reusing and reforming plastic waste without changing its chemical structure to form other consumable products, like clothes made from recycled bottles for example. This pathway involves different steps (collection, sorting, washing and grinding), which may be mixed, repeated several times or not applied according to the composition and origin of treated waste [12]. However, mechanical recycling shows limitations because of the restricted applications of obtained recycled products and to the insufficient capacity facing the enormous quantities of global plastic wastes. Consequently, the need to develop alternative recycling methods appeared and researchers have recently demonstrated a strong interest for chemical and biological pathways. These techniques arised from the recent intensive research for reducing the environmental impact of plastic waste. These alternative recycling processes go further back in the polymer production chain, by modifying the chemical structure of the molecule.

While mechanical processes only use physical methods to sort and separate different types of plastics before grinding and reconditioning them, chemical and biological recycling directly affects the formulation of the plastic or the polymer with treatments modifying its chemical structure in order to obtain reusable raw materials [46]. Even though the term “recycling” is currently associated to the mechanical pathway due to its wide application, these treatments are also referred to as recycling methods since they ensure the recuperation, revalorization and reuse of plastic waste. Chemical processes are based on the effect of solvents or temperature to transform polymer structure in order to obtain different products. Solvent-based methods have two possible outcomes: dissolution/precipitation of the polymer to obtain virgin-grade plastic with all additives removed, or depolymerization by solvolysis to recover monomers, offering greater liberty to produce another grade of polymer with different characteristics from the original one [48]. The first method is based on the solubility of a specific polymer in a particular or a combination of solvents. After a separation step where non-dissolved compounds are removed, an anti-solvent acts as a precipitating agent to recover the polymer in its solid and purified form. The main drawback of this purification is the difficulty to achieve complete removal of residual solvent that may affect polymer properties. In a similar way, solvolysis is based on the use of solvents to achieve removal of additives and to react leading to the monomer, furtherly polymerized again to form “new” plastic products. If



purity is not sufficient for polymer synthesis, these recycled monomers can possibly be purified or mixed with conventionally obtained monomers. Different processes have been investigated for plastic monomer recovery and several processes follow this principle using different solvents: hydrolysis with water [49], alcoholysis using methanol (methanolysis [50]) or ethylene glycol (glycolysis [51]), along with phosphorolysis, ammonolysis and aminolysis [52-54]. Solvents are chosen in function of their affinity for the different polymers and their ability to cleave particular bonds. Indeed, only ester, ether and acid amine bonds can be broken using solvolysis. Its application is consequently limited to polymers containing one of these groups (PET, PUR, PA, PC).

Biological recycling is also characterized by a modification of the chemical structure, occurring via an enzymatic degradation of polymers to form lighter molecules (monomer, dimer, olefins). Gamerith *et al.* investigated and proved the efficiency of enzymatic treatment to recover viable monomers for production of polyesters from polymer blends containing mainly PET and PA [55]. Different companies, such as Carbios, are developing enzymatic recycling to promote plastic and textile circularity. Biodegradation occurs thanks to the action of microorganisms that, after a stage of adherence and colonization of the material, will break polymer chains and eventually form low-molecular weight products as well as byproducts, such as methane, CO<sub>2</sub> or water [56].

In addition to these methods using external reactants, other processes like pyrolysis and gasification rely only on the effect of high-temperature treatments to degrade polymer structure. The main difference between pyrolysis and gasification is the medium where plastics are heated: while pyrolysis is carried out in oxygen-free atmosphere, gasification medium contains limited amount of oxygen. These processes enable the conversion of plastic waste to high-value liquid oils, solid char and high-temperature gases. The yielded products are very similar to raw petroleum feedstock and can be used to be retransformed into polymers, but the obtained oils are generally revalorized as fuel due to their high energetic potential. Pyrolysis is however more embedded in a strategy of energy recovery and revalorization of wastes, transforming plastics into high-added value and reusable products. This promising process can be both thermal or catalytic. Pyrolysis has been heavily investigated during recent years: the mechanisms involved, the influence of operating parameters and reaction system over yielded products have been the subject of numerous articles and reviews [13, 57-59].

## 1.2.2. Catalytic pyrolysis

### 1.2.2.1. General information

Catalytic pyrolysis of plastic waste has recently become a process of interest: its optimization as well as the understanding of its mechanisms and influencing parameters are actual research challenges. While thermal pyrolysis only relies on temperature for polymer cracking, the use of catalyst involves reactivity with an active surface that influences both polymer degradation and reforming reactions. Catalytic pyrolysis, especially with zeolite materials, offers a better selectivity and yields more high-value products than thermal pyrolysis, which contain impurities and residues. Moreover, on top of the improvement of products quality, addition of catalysts in pyrolysis process leads to the reduction of reaction temperature and retention time. It is widely accepted that catalytic acid sites favor cracking reactions. Consequently, catalytic pyrolysis yields lighter products compared to thermal pyrolysis, resulting in an increased gaseous fraction

and reduced liquid fraction [60]. However, this quantity loss of liquid product is compensated by the rise of its quality, containing more molecules of industrial interest, such as light olefins or products having similar properties to automotive fuel such as diesel or gasoline. Figure 1.8 represents the comparative composition of pyrolysis yields for thermal and catalytic process of HDPE showing the difference in phase repartition and liquid composition [58]. This observation is explained by the enhanced conversion of heavy and long chain olefins to lighter compounds thanks to the reactivity of acid sites on the catalytic surface. Catalysis for pyrolysis of plastics can be homogeneous or heterogeneous. The latter is preferred due to the convenience for separation of catalyst from fluid product or remaining solidified molten polymer, while further separation process steps are required for homogeneous catalyst recovery after reaction. Either the solid catalyst can be directly mixed with the feedstock in the reactor or it can be placed in a separate column where only the organic pyrolysis vapors pass through. Direct contact improves strongly the cracking process while, in a two-stage reactor, catalyst only takes part to the following reforming reactions. Therefore, catalytic pyrolysis with direct contact yields better quality of liquid oils but is also more exposed to deactivation by coke formation or poisoning due to the deposition of other impurities, such as chlorine during PVC pyrolysis.

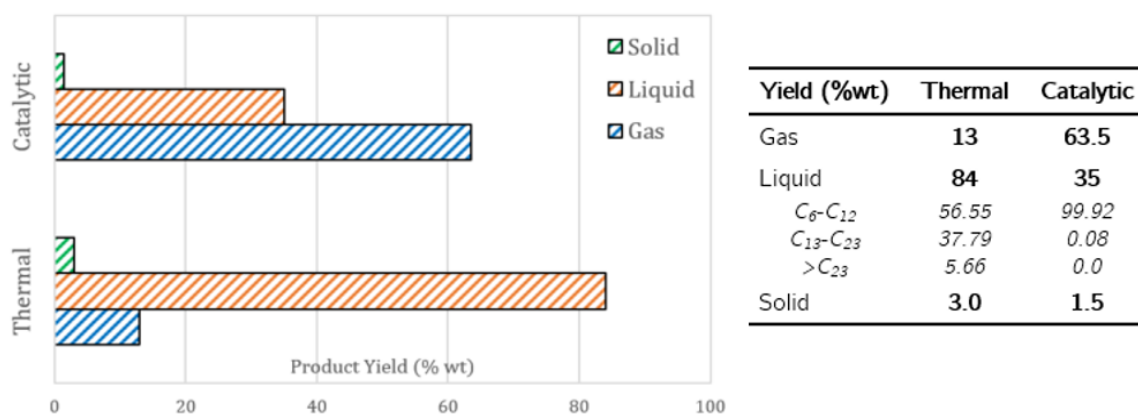


**Figure 1.8.** Product yield comparison between thermal and catalytic pyrolysis of HDPE. Graph adapted from Seo *et al.* (2003) [74].

Catalysts used for pyrolysis are part of three main categories: FCC (Fluid Catalytic Cracking) catalysts, zeolites and silica-alumina catalysts. Their reactivity is due to metallic or acid sites contained over the surface area. FCC catalysts, heavily used in petrochemical industry, mainly yield liquid oil as investigated by Lee *et al.* who reported between 80 and 90% of liquid oil production during pyrolysis of different polymer feedstock [61]. Silica-alumina and zeolite catalysts show different results with a more important gaseous fraction. This behavior is attributed to their improved acidic properties, depending on the Si/Al molar ratio. The increased cracking reaction rate due to acidity is responsible for the formation of lighter molecules, favoring gas formation. Sakata *et al.* compared liquid yield with catalysts of varying acidity and confirmed this statement: while a low acidity catalyst produced 74.3 wt.% of liquid oil, high acidity ZSM-5 yielded only 49.8 wt.% [62]. Among catalyst characteristics, structure and pore distribution have an influence due to the shape-selectivity of the reaction with different size distributions of products and intermediates. Many studies focused on the determination of catalytic pyrolysis yield with various feedstock, catalysts and operating conditions. In the literature, most commonly used catalysts for catalytic pyrolysis are zeolites.

### 1.2.2.2. Reaction mechanisms

During catalytic degradation of plastics, as temperature rises, the polymer firstly melts and is dispersed over catalyst surface where it is broken due to its reactivity with acid sites. Different mechanisms involving ionic and free radicals have been proposed by many researchers and have been summarized in comprehensive reviews [63]. Mechanisms of catalytic pyrolysis usually involve chain scission, isomerization, oligomerization, H-transfer and aromatization. The initial step of polymer cracking is agreed to be the adsorption of the reactant molecule on the acid site where it is protonated to obtain carbonium ions. This intermediate is known to promote the cracking of molecules. Reaction rate is therefore mainly influenced by acid site strength, density and distribution. Indeed, acid active sites of the catalyst support the cracking of olefinic compounds and favor hydrogen transfer reactions [64]. Catalytic cracking can proceed by end-chain scission when catalyst acidity is strong, forming olefins, or by random scission in weak acidic medium leading to the formation of waxes. Those primary formed products undergo further reactions to eventually produce low molecular weight compounds, as represented on Figure 1.9 [65]. It has been suggested that initiating decomposition reactions can only occur over external catalyst surface due to the important size of polymeric molecules. Further transformations take place at the internal surface as initial cracking products have lower molecular size and consequently can diffuse through the molten polymer and enter catalyst pores to undergo the aforementioned secondary reactions. The equilibrium reached with these reactions, sometimes competing with one another, yields light hydrocarbon molecules in different phases forming char, liquid and gases, which repartition and nature depend on operating parameters.

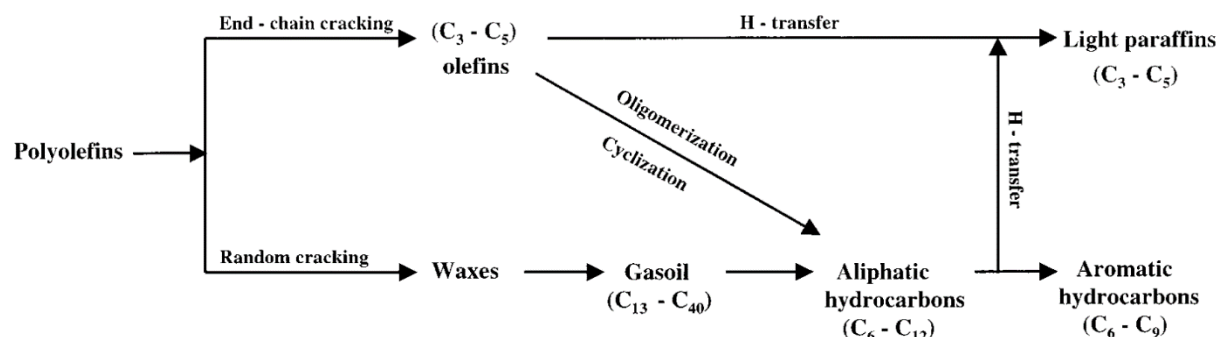


**Figure 1.9.** Reaction pathways for catalytic pyrolysis of polyolefins (Aguado *et al.*, 2001) [65].

### 1.2.2.3. Influencing factors

#### a. Operating parameters

Among the different operating parameters, temperature is considered as the most important factor by influencing both repartition and nature of yield [66, 67]. High temperature pyrolysis enhances cracking reactions, consequently favoring the formation of small molecules, whereas long chain hydrocarbons are produced at lower temperatures. During pyrolysis of plastic wastes in a semi-batch reactor, Lopez *et al.* found a variation of yield repartition between liquid and gaseous phase due to temperature [67]. From the comparison between yield at 500 and 600°C, decrease of liquid phase quantity from 65.2 to 42.9 wt.% is correlated with an increase of light gaseous phase from 34.0 to 56.2 wt.%. Temperature rise also enables the activation of secondary reactions leading to the

formation of aromatics [68]. Consequently, a high gaseous product fraction is obtained at 600°C while the liquid fraction is more important for lower temperatures between 300°C and 500°C, and the liquid fraction contains more aromatic products at 500°C. The composition of each of these fractions is highly influenced by pyrolysis temperature. However, different heating ramps to reach the targeted temperature were tested during pyrolysis experimentations and did not appear as a major impacting factor [13]. Reaction temperature has to be set in function of feedstock, as degradation temperature is different according to the polymer, as shown in Figure 1.10, which represents ThermoGravimetric Analysis (TGA) for different polymers. PVC is partially degraded at 300°C and PS is completely decomposed at around 410°C, while PET, PP and PE degradation occur between 450 and 500°C. As reactivity of plastics increase with temperature, the sole limitation is set by the maximum temperature before thermal damages of the catalyst. Products yield phase repartition varies slightly with nature of feedstock, as investigated in some studies carrying out pyrolysis experiments with different polymers or with mixed plastics [69].

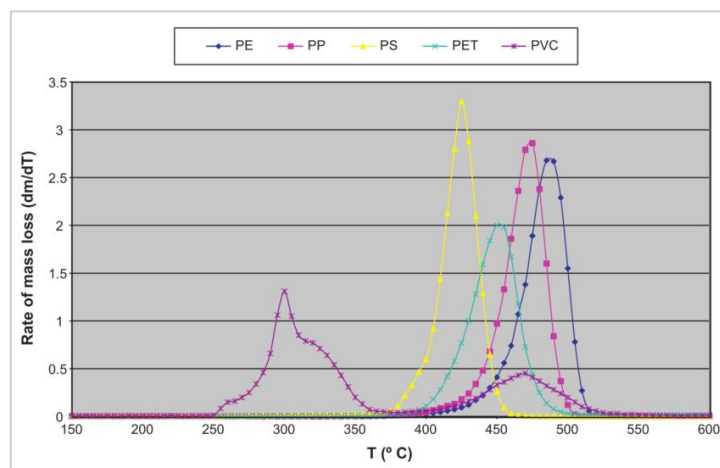


**Figure 1.10.** Thermogravimetric analysis (TGA) for determination of degradation temperature for different polymers (Lopez *et al.*, 2011) [67].

Other operating parameters, such as pressure and retention time, were studied to determine their influence over pyrolysis yield. Murata *et al.* carried out thermal pyrolysis of HDPE at different pressures within 1-8 bars range in a continuous stirred tank reactor and observed an increase of gaseous products fraction from 6 to 13 wt.% at 410°C [70]. This effect tends to decrease as temperature rises. Moreover, pressure has been shown to affect nature of products by shifting the average molecular weight to lighter compounds due to its direct impact over scission of C-C links. Pressure is consequently considered as an influencing parameter for pyrolysis and could be used to control distribution of pyrolysis products, especially at low temperatures. However, the influence of pressure during catalytic pyrolysis still has to be investigated. Residence time, defined as the average time of retention of species in the reactor, may also influence product distribution since it directly affects conversion of reactants and secondary products to light hydrocarbons and non-condensable gases. However, Lopez *et al.* observed that product distribution did not change much between 30 min and 120 min pyrolysis experiments and determined that residence time is a highly influential parameter only up to 15min of reaction, which is not sufficient for total reactant conversion [67]. Lee and Shen focused on the composition of pyrolysis oil for different lapse time of reaction, between 0 and 400 min, and observed a varying repartition of known paraffin, olefin, naphthene and

aromatic products between 350°C and 400°C [71]. Pressure and residence time can therefore be considered as influencing parameters for pyrolysis reactions, but remain temperature-dependent, their effect being less apparent at higher temperatures due to the temperature limitation in the process [72]. Based on the different studies available in literature, pyrolysis experiments are usually carried out at atmospheric pressure with a temperature around 500°C during 30 min. The operating conditions will also vary depending on the nature of feedstock and the type of reactor used during the experiment.

### *b. Reactor type*

The type of reactor has an important impact during catalytic pyrolysis as it influences mixing of reactants and catalysts. Polymers are often used as provided in solid pellets of about 3 mm diameter, but can also undergo a grinding step to form solid powder (<1 mm). Ratio between catalyst and polymer commonly vary from 5 to 20 wt% of catalyst [73]. The type of reactor also affects residence time and heat transfer.

Use of batch or semi-batch reactors is very common in lab-scale experiments due to their ability to control operating parameters. In batch reactors, reactants are left during all reaction time, while a product extraction is performed with semi-batch reactors. They are particularly suitable for thermal pyrolysis. The main drawback is the variability of results due to the non-homogeneity of reaction medium. Seo *et al.* therefore embedded a stirrer in the experimental reactor for HDPE pyrolysis at 450°C [74]. The provided agitation led to an increase of liquid fraction for both thermal and catalytic pyrolysis compared to experiments carried out in similar conditions by Sakata *et al.* without agitation [75]. Indeed, stirring provides appropriate heat transfer leading to better efficiency and viability of the process [76]. The addition of catalysts in this type of reactor has proved to influence the phase repartition of products as expected from previous observations [75, 76]. Direct contact between plastic and catalyst is preferable for enhanced reactivity and improved liquid yield, but it also favors coke formation over the catalytic surface leading to deactivation. Combined with the high operating cost, the tendency to fast deactivation is the reason why this type of reactor is not recommended for catalytic pyrolysis for large scale production and remains mostly used for lab-scale experiments.

Continuous flow reactors, especially fluidized bed reactors, are suggested to be the most efficient reactor shape for industrial application of catalytic pyrolysis because of improved heat and mass transfer as well as reduced deactivation providing to the catalyst an improved lifetime. The different types of continuous flow reactors are represented Figure 1.11. Fixed-bed reactor is the easiest geometry to design but the packed catalyst bed causes issues related to mass transfer in the reactor, which could lead to reactor plugging due to the heavy and sticky nature of molten plastics. Moreover, the available catalytic surface area in a fixed bed is limited and catalyst efficiency is reduced. In studies carried out with fixed bed reactors, catalysts and plastic feedstock are not directly mixed: polymer is placed over the catalyst or even in a separate porous recipient [77-79]. To avoid direct catalyst exposure to molten polymer, some studies preferred to separate the pyrolysis reactor in two stages, one for pyrolysis followed by a fixed-bed column for reforming reactions with only pyrolysis gases passing through [80, 81]. Use of a fluidized bed reactor solves some of the issues of fixed-bed as it provides a good mixing, leading to a higher accessible surface area and an improved mass and heat transfer. Consequently, catalytic pyrolysis needs shorter residence time and yields less variable products. Due to

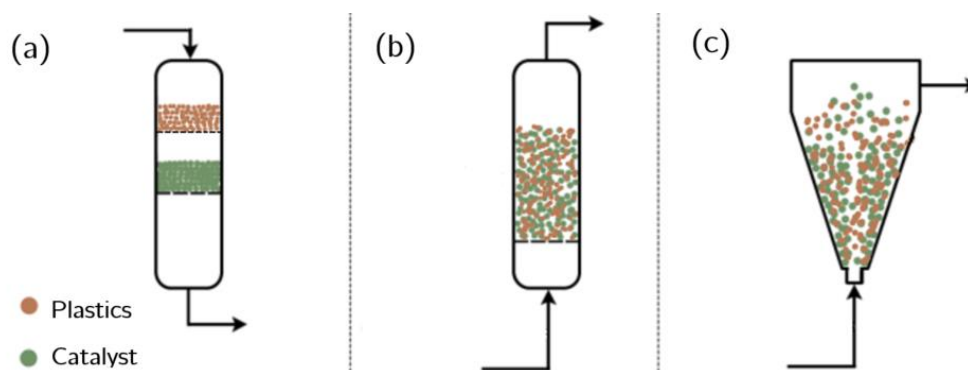


**Figure 1.11.** Different possible continuous reactor configurations for catalytic pyrolysis of plastics: (a) fixed bed reactor, (b) fluidized bed reactor, (c) conical spouted bed reactor. Adapted scheme from Ochoa *et al.* (2020) [14].

the industrial interest for this type of reactor because of low operating costs, pyrolysis in fluidized-bed reactor has been heavily investigated over the last decade [82-84]. In addition to these “classic” reactors commonly used for other processes, a new reactor geometry for catalytic pyrolysis has been investigated. Elordi *et al.* carried out pyrolysis experiments in a conical spouted bed reactor (CSBR) that, similarly to fluidized-bed reactors, insures a good mixing of catalyst with reactants yielding high quality products [85]. With this reactor, a wider range of solid particle size and density can be handled and, according to Olazar *et al.*, it helps reducing the attrition and low bed segregation compared to fluidized bed [86]. Even though pyrolysis reactors and processes are often designed to postpone catalyst deactivation as much as possible, loss of catalytic activity via different mechanisms of deactivation remains an important challenge for wider use of catalytic pyrolysis.

### 1.2.3. Focus on pyrolysis of polyethylene using ZSM-5

Due to its important part in generated plastics waste each year and its simple molecular structure, polyethylene has been extensively used as a “model” feedstock material for the development of new and innovative recycling processes. Nowadays, even though pyrolysis is more and more carried out with real landfill waste, polymers mix or biomass, the use of polyethylene in thermal and catalytic pyrolysis presents a substantial database of research articles. As mentioned in Section 1.2.2.1, integration of catalysts in pyrolysis, especially zeolites, has been reported to have a positive effect on the quality of obtained products. Among them, ZSM-5 is of high interest at it yields higher proportions of gases and aromatics, including high-added value products such as toluene or xylenes.

Similarly to pyrolysis with other catalytic material, the use of ZSM-5 produces three different fractions: gas (light fraction), liquid (oil) and solid (char). According to the literature, the microporosity of ZSM-5 leads to the formation of a more important gas fraction and limits the amount of char [13]. Due to the steric limitation, the molecules entering the zeolite crystals have already been cracked and undergo further cracking on the internal active sites, forming light molecules. The important reactivity of internal acid sites also favors the formation of aromatic products during steps referred as reforming or rearrangement reactions. Lopez *et al.* reported the formation of over 95% of aromatic products in the oil fraction during pyrolysis of plastics with ZSM-5, while only around 70% was produced with thermal pyrolysis in similar conditions [67]. The pyrolysis oils are usually split into different fractions according to the carbon number repartition and their



potential applications as shown in Figure 1.12: gasoline (C6-C9), kerosene (C10-C14) and waxes (C15+). High quality oils present low waxes and high aromatics proportions. Even though deactivation is reported to be less important for ZSM-5, important carbon deposition occurs causing catalytic activity loss [57]. This deactivation mechanism, known as “coking”, is introduced and discussed in the following section.

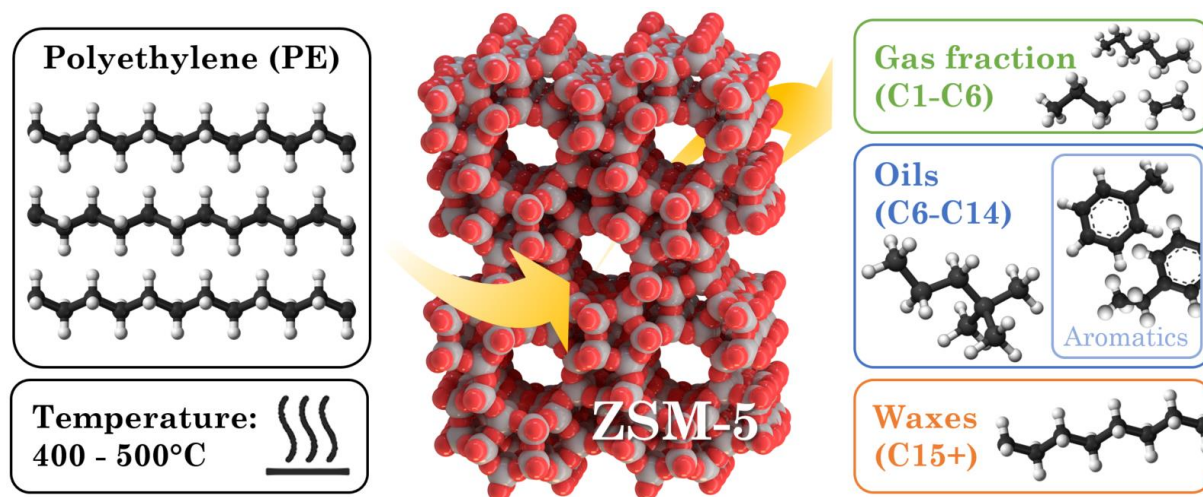


**Figure 1.12.** Schematic representation of catalytic pyrolysis of polyethylene over ZSM-5 with repartition of obtained products. Source molecules 3D models: Wikipedia.

### 1.3. Catalytic deactivation: mechanisms and key parameters

Catalyst deactivation is a well-known issue that has been heavily investigated over the past decades. While catalyst deactivation is inevitable for most cases, some of its immediate and/or drastic consequences can be avoided, postponed or even reversed. Therefore, deactivation phenomenon greatly influences research, development, design and operation of commercial processes leading to a considerable motivation to understand and treat catalyst decay.

#### 1.3.1. Mechanisms of deactivation

Industrial processes involving organic compounds in the presence of solid catalysts are widely carried out in industries, such as petrochemical industry, and catalyst deactivation is often observed. There are different paths for heterogeneous catalyst decay leading to catalyst deactivation and loss of catalytic activity (Figure 1.13). Generally, five main ways leading to catalyst deactivation are reported in literature: poisoning (1), gas/vapor-solid and solid-state reactions (2), mechanical failure of catalyst (3), thermal degradation and sintering (4) and fouling, coking and carbon deposition (5). Poisoning is a very common deactivating mechanism and is known as a strong chemisorption of species which are not taking part to the reaction and therefore “blocking” the active catalyst sites. This phenomenon happens when the chemisorption of these poisoning species is stronger than the affinity of reactants with active sites. Deactivation can also be due to unwanted reactivity of catalyst with species present in the reaction. Different types of reactions leading to deactivation can take place: gas-vapor solid reactions between the catalyst and gas phase turning active catalytic surface into inert phases or into volatile compounds leaving the reactor as by-products, or solid-state reaction with catalyst phase

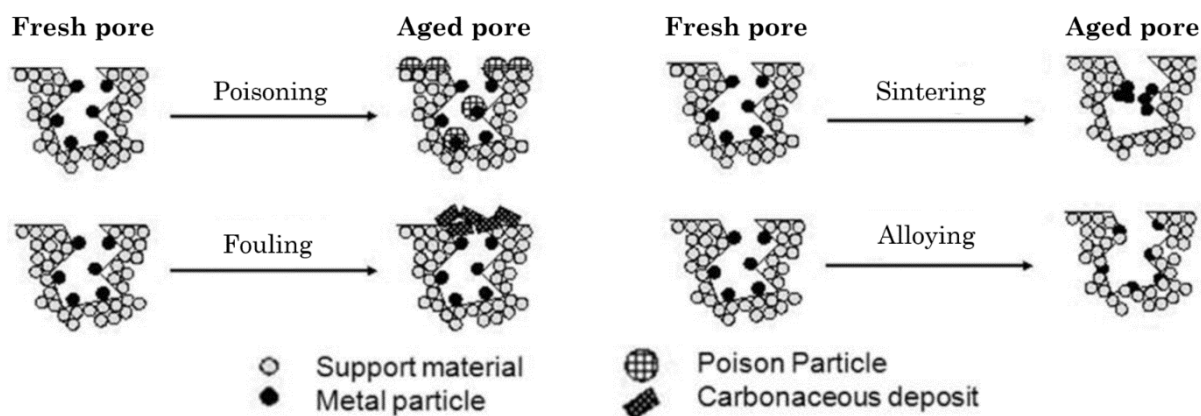


**Figure 1.13.** Illustration of main catalytic deactivation pathways (Bartholomew *et al.*, 2003) [4].

transformation during process. Moreover, mechanical failure of catalyst can occur in some cases and manifests in different ways: crushing, attrition and/or erosion of catalyst pellets, all leading to a generally irreversible structural damage of the catalyst [6]. In this review, a particular attention is given to thermal degradation and fouling/coking as they represent the main deactivation risks for catalysts used for pyrolysis of plastics.

Thermal degradation of catalyst is the loss of catalytic surface area resulting from the crystallite growth of catalytic phase or the loss of support/catalytic surface area due to support/pore collapse. These two phenomena are usually referred to as “sintering” in the literature. These processes generally take place during high-temperature reactions and are accelerated by the presence of water vapor. The principal sintering mechanisms, represented on Figure 1.14, are based on adatoms migration from small particles to larger ones (a), and direct migration of small particles to agglomerate with larger particles (b). This process results in crystallite size growth, therefore reducing the active surface area and decreasing the catalytic activity. However, sintering is reversible and redispersion of metal particles is achievable to recover catalytic activity [87]. Nevertheless, structural degradation represents irreversible damages for catalyst crystallinity, leading to permanent loss of catalytic activity. As plastic pyrolysis is carried out at high temperatures, a particular attention has to be paid to the maximal temperature accepted by the catalyst to avoid deactivation by thermal degradation. Consequently, processes are designed to avoid this type of deactivation and thermal damages are usually not observed in normal operating conditions. Fouling and coking deactivation pathway is much more difficult to avoid as it usually occurs within operating conditions. The latter are defined by the deposition of chemical species, especially carbonaceous compounds referred as coke,

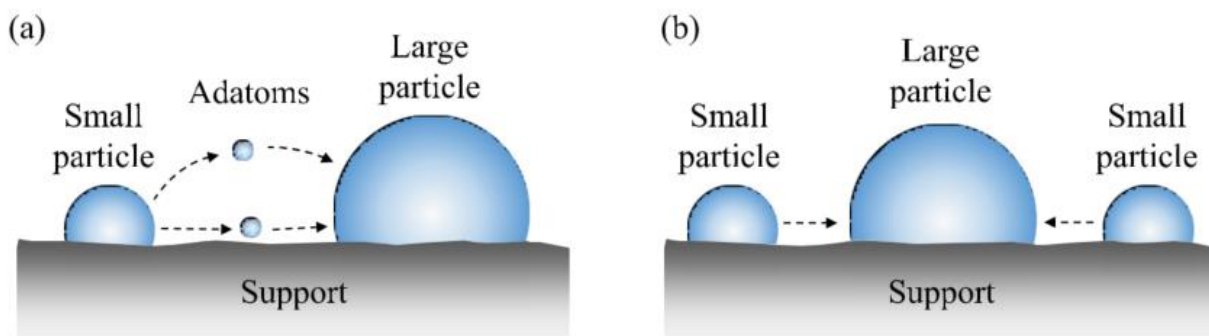


**Figure 1.14.** Conceptual models representing main mechanisms of metal particles sintering due to thermal degradation (Ochoa *et al.*, 2020) [14].



onto the catalyst internal and external surface, resulting in catalytic activity loss due to lowered access to active sites [88]. Being the main cause of catalytic deactivation in many processes, this type of deactivation has been heavily studied under the name of “coking”.

### 1.3.2. Catalytic deactivation by coking

#### 1.3.2.1. General information

According to numerous works that studied coke formation and nature with several types of catalysts, coke is defined as a solid carbonaceous compound with no heteroatoms [4-6, 89]. Coke nature can therefore vary from alkanes or alkenes to cyclic and aromatic molecules depending on coke formation advancement [89, 90]. An average coke molecule consists in polycyclic aromatic hydrocarbons interconnected by aliphatic bridges. Its composition may be represented as  $C_nH_m$ , with  $m/n$ , or H/C ratio, usually being between 0.2 and 1.5. As an example, H/C ratio value is 1 for benzene and 0.8 for naphthalene. Coke is usually described with this H/C ratio, defining the nature of its average component. High H/C ratio is mainly aliphatic hydrocarbons, such as co-oligomers and polymers, while more condensed molecules such as polyaromatics have lower H/C value. These two “classes” of coke are respectively designated as “light” or “soft” coke and “heavy” or “hard” coke. This notion has been introduced to describe the different behavior of coke according to its nature. The chemical structure of coke formed in catalytic processes varies with the type of reaction, catalyst and reaction conditions. This type of deactivation is the most difficult to investigate because coke matter is constituted of multiple products from secondary reactions that contain variable amounts of carbon and hydrogen. The deactivation effect of coke is not the same according to its content, its location on the catalyst surface, its morphology and its chemical nature, which are the four main features used in literature to describe coke properties and its effect on catalytic activity. It is consequently important to understand the composition of the carbonaceous compounds in

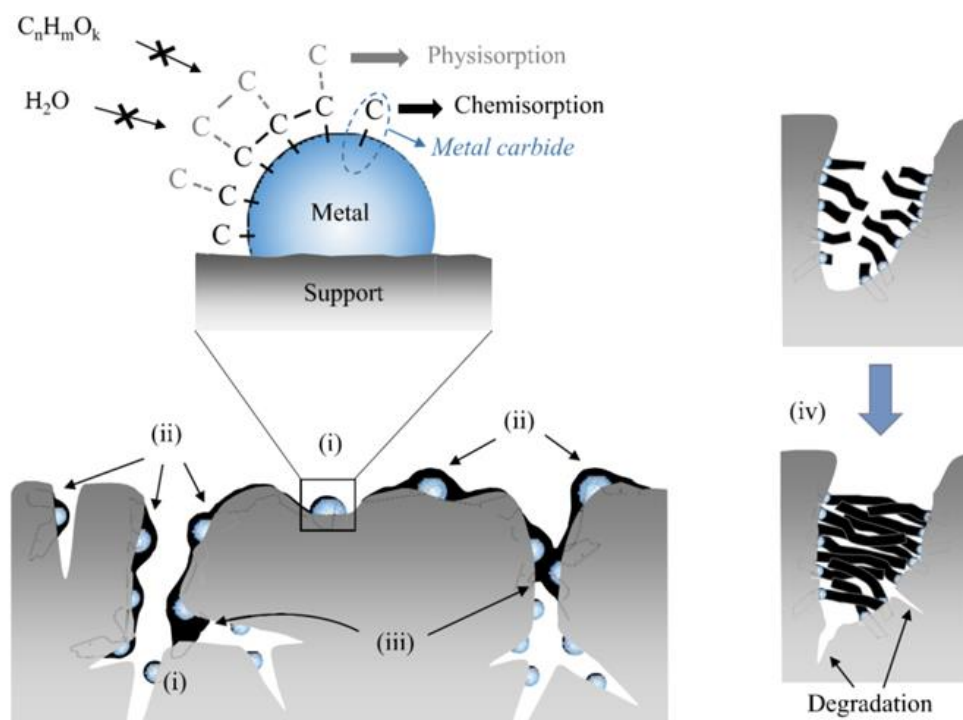


**Figure 1.15.** Deactivation pathways by coke formation from precursors adsorption to structural damages at advanced coke growth stages (Ochoa *et al.*, 2020) [14].

order to deduce the implied deactivation effects of the various coke molecules, but also to study the involved formation rates, mechanisms and affecting parameters. Different studies investigated coke formation in catalytic pyrolysis of plastics determining the effect of operating parameters [85, 91-93].

Deactivation via coke formation is a complex phenomenon combining successive physical and chemical interactions. In catalytic processes involving hydrocarbon feedstock, coke formation usually starts with strong chemisorption as a monolayer of coke precursor or physisorption in multilayers over active sites. As illustrated in Figure 1.15, this results in a partial hindering of active sites (i). As carbonaceous compounds accumulate, other deactivating phenomena can occur: total encapsulation of the active site, making it inaccessible to the reactants (ii), and plugging of pores of the catalyst, blocking the access to free active sites in inner pores (iii). In advanced coke growth stages, the apparition of filamentous coke can cause changes or even disintegration of catalyst structure (iv). In addition to these chemical steps, formation of coke molecules also requires retention within the pores or on the outer surface of the catalyst. This retention may be due to trapping (steric blockage), strong chemisorption on active sites and confinement in the pores but also low volatility or solubility. The following sections provide more details about molecular mechanisms and kinetics involved in coke formation.

### 1.3.2.2. Coke formation mechanisms

Over the years, intensive researches have been carried out to understand the mechanisms leading to the formation of complex coke molecules [89, 90]. In reactions involving hydrocarbons, coke may be formed on both active sites and noncatalytic supports. Due to its important stability, coke formation is catalyzed by acid sites. As mentioned in the previous section, coke formation starts with the adsorption of coke precursors, typically olefins or light aromatics depending on the nature of the reactants. As reaction proceeds, these precursors will further react with other molecules. Coke formation involves many steps with intermolecular and intramolecular reactions. Distinction is made between low and high temperature coke. At low reaction temperatures (under 200°C), mostly condensation and rearrangement reactions occur with the oligomerization of coke precursors. Resulting coke is mainly co-oligomers and polymers with high H/C ratios. This “light” coke formation is often reversible under specific operating conditions, making the concentration of condensation products limited by

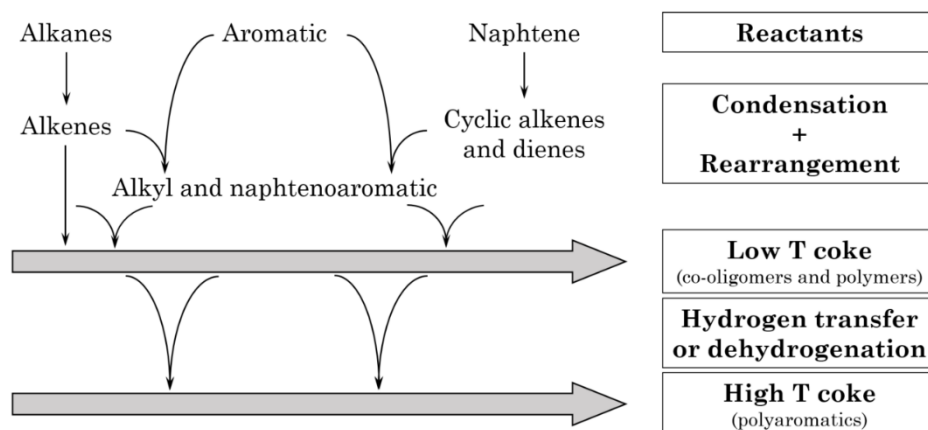


**Figure 1.16.** Simplified scheme of coke formation from hydrocarbons and molecular coke over acid zeolite catalysts (Guisnet *et al.*, 2001) [89].

thermodynamic equilibrium. Therefore, in absence of reactant mixture, light coke molecules are retransformed to their initial compounds, referred to as “reversible coke”. At high temperatures (over 350°C), carbonaceous molecules undergo additional reactions such as hydrogen transfer and dehydrogenation, leading to the formation of polyaromatic components. This “heavy” coke is much more difficult to remove because of its high stability and its imposing size causing steric blockage. At intermediate temperatures, a mix of these different mechanisms is observed, as represented in Figure 1.16 [89]. Indeed, as coking proceeds, primarily formed light coke can undergo intramolecular condensation reactions. Carbocation intermediates that can be produced on catalyst acid sites can consequently form aromatics via dehydrogenation and cyclization reactions. These aromatics can then further react to polynuclear aromatics, which ultimately condense as coke molecules. The formation of polynuclear carbocations not only lead to the production of coke molecules but also are relatively stable, meaning they can sustain growth of molecules for quite long periods until a termination reaction occurs. At advanced coking stages, heavy polyaromatic structures are observed and can lead to both encapsulation and filamentous coke mechanisms as aforementioned. The main conditions and parameters for coke formation are summarized in Figure 1.17. The features of the reaction, the operating conditions and the studied catalyst are the main parameters determining the composition, location and rate of coke formation and therefore the involved mechanisms.

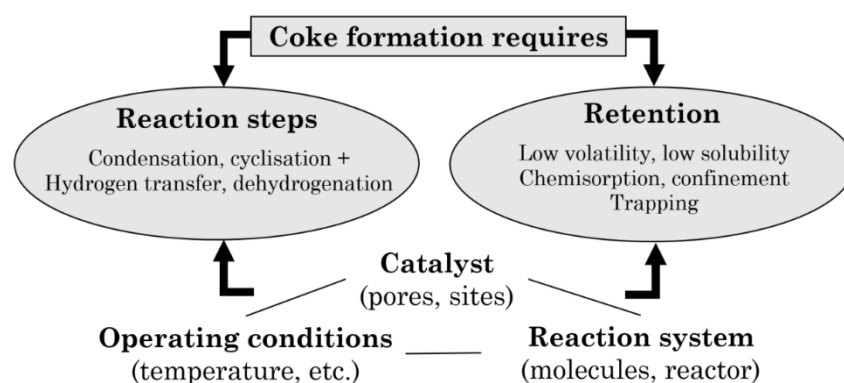


**Figure 1.17.** Necessary conditions for coke formation over catalysts and major influencing parameters (Guisnet *et al.*, 2001) [89].

### 1.3.2.3. Kinetics of coking and deactivation

Kinetic studies of coke formation are carried out using thermogravimetric analysis which provides mass evolution monitoring of the catalyst sample during the reaction. The increase of coking rate with coke content during early stages of the reaction suggests that coke formation is an autocatalytic reaction, which is coherent with the described mechanisms consisting in initial adsorption of coke precursors leading to further reactions to form coke molecules via rapid steps [94]. This type of analysis leads to the determination of coking rates thanks to the relation between coke content in catalyst and process time. The typical profile for coke formation reaction rate is represented Figure 1.18: the high initial coke formation rate is due to the occurrence of both catalytic and radical mechanisms, then when all active sites are blocked, the coking rate becomes approximately constant as only radical coke is formed [95]. Coke content and catalytic activity are generally compared to better understand the effect of coke over catalyst [96]. It is important to notice that kinetics of deactivation is not necessarily proportional to coke

content on the catalyst. Indeed, this depends on the selectivity of the coke formation and on the deactivation pathway. This observation is due to the variability of coke toxicity ( $T_{ox}$ ), which could be defined as the number of active sites being inactive due to the action of one coke molecule. When a coke molecule is chemisorbed and blocks a single active site, the value of  $T_{ox}=1$ .

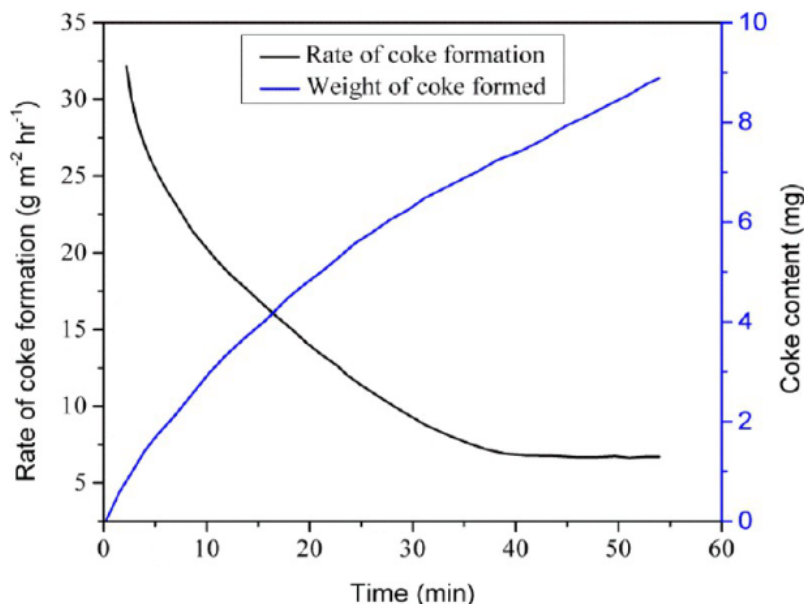


**Figure 1.18.** Rate of coke formation and weight content over steel cylinder during thermal cracking of ethane between 750 and 850°C (Mahamulkar *et al.*, 2016) [95].

Deactivation can be limited if reactant interaction with an active site leads to coke molecule desorption ( $T_{ox}<1$ ) or more important if the molecule is big enough to interact with several active sites ( $T_{ox}>1$ ). In this case, deactivation is similar to a poisoning mechanism. However, coke can also lead to fouling or blockage in which case a single coke molecule can block access to all active sites present in a pore or in a channel ( $T_{ox}\gg>1$ ). Therefore, residual activity during coke deactivation cannot be directly determined from coke content. Coke formation is highly dependent of the reactants, used catalyst and operating parameters as developed in the following section. Many studies aimed to develop kinetic models of coke formation for particular applications. The usual approach consists in splitting global coke formation phenomenon into successive elementary steps based on different hypothesized mechanisms dependent of the studied reaction [97-99]. The difficulty of developing such a model is the very large number of possible reactions having their own kinetic constant. A reaction scheme can be used to represent schematically all the possible reactions leading to the formation of coke. The reaction scheme developed by Moustafa *et al.* to represent coke formation during catalytic cracking of Vacuum Gas Oil is presented in Figure 1.19 [98]. In order to simplify the models, the number of needed kinetic parameters is substantially reduced by predicting the most important pathways of reaction and by analyzing the favorable conditions for coke formation. For instance, the kinetic model for coke formation during ethane cracking developed by Wauters *et al.* uses ethane, ethyne, propene and propyne as coke precursors, reacting with gas-phase radicals H, CH<sub>3</sub>, C<sub>2</sub>H<sub>5</sub> and C<sub>3</sub>H<sub>5</sub> [97]. Combination of this type of coke formation model with existing models for the studied reaction provides a prediction with high precision of the reaction rate, the catalyst deactivation but also the effect of operating parameters which are discussed below [98, 99].

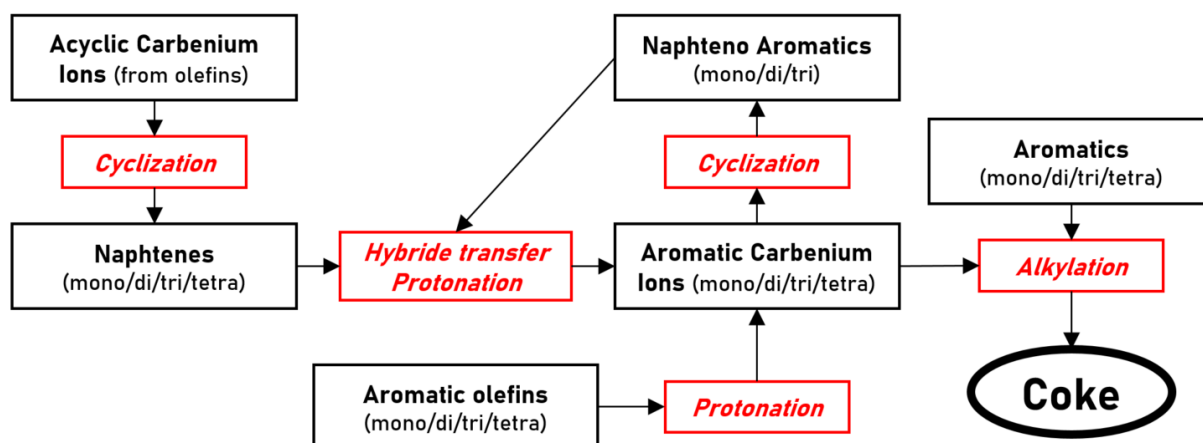


**Figure 1.19.** Reaction scheme for coke formation during catalytic cracking of VGO. Adapted from Moustafa *et al.* (2003) [98]. Black: chemical compounds. Red: reaction mechanisms.

### 1.3.2.4. Parameters influencing coke formation

#### a. Reaction system

As detailed in the previous section, formation of coke is the result of rearrangement and condensation reactions. Some particular molecules commonly referred to as coke precursors initiate coke formation by undergoing further reactions [100-102]. The nature of coke precursors differs according to the studied reaction and is dependent of reacting phase. Coke maker molecules can be the reactant itself, intermediates or desired products [102]. Coke precursors can be formed from light unsaturated species, such as alkenes, but also from heavier compounds like olefins, benzene and benzene derivatives or even polyaromatics. The formation of coke makers from these molecules is very slow due to their low reactivity and is therefore the rate-determining step of coke formation. Both retention within catalyst pores and reactivity with catalytic surface have to be satisfied and sufficient to allow initiation of coke precursors [90]. Nature of reactants and catalyst used in the process being known, the coking behavior of a reaction system is predictable [103]. Generally, precursors from short chain alkenes and dienes undergo very fast condensation reactions leading to polar products that are easily retained on the active sites of the zeolite. On the other hand, polyaromatic precursors reactivity is not very high, but these compounds are polar enough to be retained over acid zeolites. The affinity of coke precursors with catalytic surface has a great impact on the coking behavior of a particular reaction system. Investigating the deactivation of HZSM-5 zeolite during bio-oil cracking, Guo *et al.* observed that coke precursor nature is different between external and internal surface, suggesting that catalyst structure impacts coke formation mechanisms [101]. The influence of catalyst structure and composition is discussed in next paragraph.

As coke precursors are often intermediates or desired products, coking appears as an inevitable phenomenon. All the different features of the reaction system have an impact by influencing rate of the different possible reactions that reactants, intermediates and by-products may undergo leading to coke formation. Deactivation studies for specific processes are usually carried out to study coke formation effects over catalytic activity loss, involved mechanisms and influence of operating conditions in order to provide solutions to limit catalyst deactivation by coke deposition [89].

#### *b. Operating conditions*

As for every process involving chemical reactions, temperature influences equilibrium and kinetics of reaction rates but also thermodynamic and diffusion phenomena. Temperature therefore affects both the reactivity and retention necessary for coke formation. Considering a system where feedstock contains poorly reactive coke precursors, coke formation increases with temperature as it favors formation of intermediate coke makers. It is commonly accepted that higher temperatures enhances coke formation [104]. Analyzing coke characteristics leads to determining whether coke retention is due to low volatility, comparing normal boiling point with reaction temperature, or to steric blockage, comparing molecular coke size with pore aperture. It has been proved that, at low temperatures, retention is due to low volatility of coke compounds, whereas at high temperatures, its results from their trapping within micropores [105]. As temperature has a significant effect on coke nature, it is usual to classify coke into low temperature and high temperature cokes: whatever the nature of reactants, polyaromatic coke cannot be formed at low temperatures as only condensation and rearrangement reactions are possible. On the other hand, at high temperatures, the occurrence of hydrogen transfer and dehydrogenation reactions leads to the formation of large amount of polyaromatic molecules (low H/C ratio), which composition is practically independent of the reactant and is mainly determined by the catalyst structure [90].

Reaction time is also influencing coke formation since long contact time with deactivating species will ensure extensive growth of coke structures, forming long olefin chains or increasing aromatic core number in polyaromatics. At intermediate temperatures, sufficient time of exposure leads to cyclization reactions and initiation of polyaromatic coke formation normally occurring at high temperatures. As coking proceeds, there is an accumulation of carbonaceous content over catalyst surface, being measured by its coke content (expressed in %C). Average coke nature gradually shifts from light to heavy compounds [106].

#### *c. Catalyst structure and surface*

In terms of coke formation on zeolite catalysts, there has been extensive research carried out on the topic, including some significant findings [107-109]. The process of zeolite deactivation via coking is predominantly influenced by the pore structure of the catalyst responsible of heavy aromatic clusters. Indeed, catalyst geometry affects coke location and size since the aperture of the pores and width of channels will affect the diffusion and accessibility of coke precursors within the catalyst framework [104, 110, 111]. In most cases, initial molecules are relatively small and can diffuse within the catalyst where they are chemically retained and react to form coke molecules. The growth of coke molecules is limited by pore dimension, varying according to the type of catalyst (micro and macropores). The formed heavy polyaromatic coke is too imposing and is retained in the pore due to steric blockage, causing pore plugging. In industrial processes, pore size and structure have been determined to be more influential than the acidic properties of the catalysts [6]. Hence, coke formation is qualified as a shape-selective process. Coking is controlled by diffusion limitations depending on how film mass transfer and pore diffusional resistance affect the reaction of interest, but also the secondary deactivating reactions [107]. Consequently, coke yield varies within the catalyst pores and along the catalyst bed depending on the reactor dimensions and shape. However, nature and reactivity of catalyst surface also affect coking rate. Catalyst acidity, indicated by



Si/Al ratio, influences the various successive chemical steps implied during coke formation [109]. The concentration, strength and proximity of the acid sites impact coke precursor reactivity, mostly during early stages of coke formation. The quantification of the influence of these parameters is a challenge because of the difficulty to obtain zeolites with acidities and pore structures varying separately. Nevertheless, it is expected that a stronger acidic state implies faster chemical steps and stronger retention of coke molecules and precursors. Besides, higher density of acid sites leads reactant molecules to undergo more successive chemical steps along the diffusion path within zeolite crystallites promoting condensation reactions. Strength, density and number of acid sites consequently enhance coking rate [89]. Catalyst deactivation by coke is in most cases a reversible phenomenon and deposited carbonaceous compounds can be removed. Regenerating processes have been investigated over the years and the different existing methods are presented in Section 1.4.

### 1.3.3. Focus: deactivation of ZSM-5 during PE pyrolysis

As ZSM-5 is one of the most used zeolite in pyrolysis, its deactivation has been extensively investigated using different feedstock, from virgin plastics to real waste combined with biomass [85, 91, 93, 112, 113]. These different studies show the impact of coke deposition over the textural and chemical properties of the zeolite. Surface hindering and porosity blockage causes an important decrease of acid sites available for reaction. Due to the small size of ZSM-5 channels, it is suggested that part of the porous volume is lost because of porosity blockage [4]. As schematic representation of coke deposition over catalyst pellets is presented in Figure 1.20. The important temperature operated during pyrolysis leads to the formation of heavy coke composed of aromatic coke molecules [79]. However, mechanisms of coke growth are limited by steric blockage in micropores [112]. In pelletized catalysts, it is therefore necessary to distinguish internal coke located in zeolite crystals and external coke formed in the mesoporous volume generated by the binder. The decrease of acid sites generated by coke deposition causes a catalytic activity loss. During pyrolysis of PE, this phenomenon is traduced by a diminution of cracking and reforming performances of the zeolite. An evolution of obtained products is therefore observed: the composition globally shifts towards molecules with higher carbon number accompanied by a diminution of aromatics proportion [93].

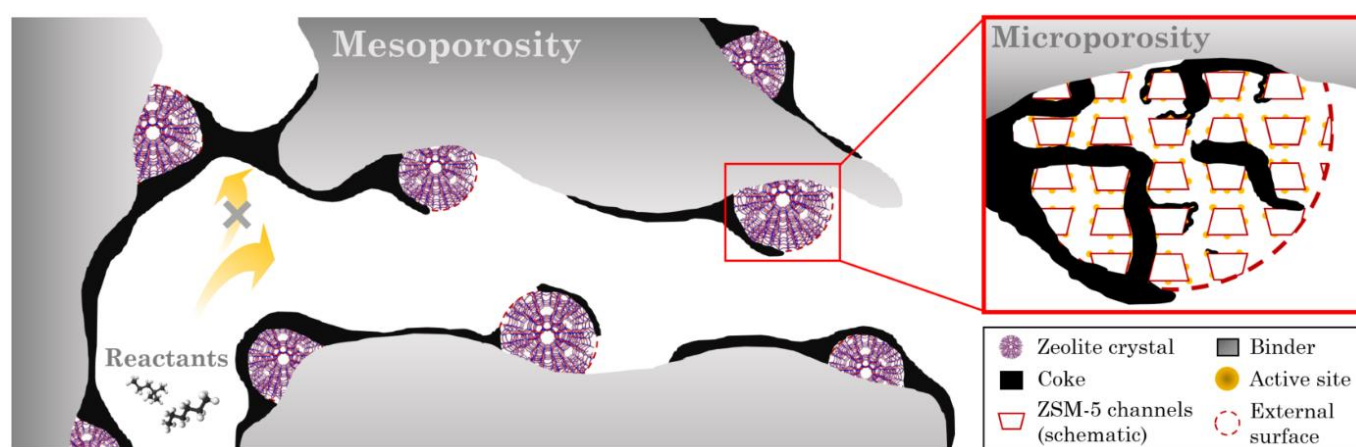


**Figure 1.20.** Scheme of coke formation over pelletized ZSM-5 zeolite, representing coke deposition and pore blocking both at mesopore and micropore level.

### 1.4. Regeneration of catalysts deactivated via coking

For combined economic and environmental concerns, processes for catalyst regeneration have been investigated over the years. Coke removal is achieved via three methods as summarized in Figure 1.21: oxidation, including classic or advanced processes, gasification or hydrogenation. Each process has its advantages and drawbacks according to the catalyst type to be regenerated and to the nature and structure of coke. Particular attention is given to the regeneration of zeolite materials commonly used during catalytic pyrolysis of plastic wastes.

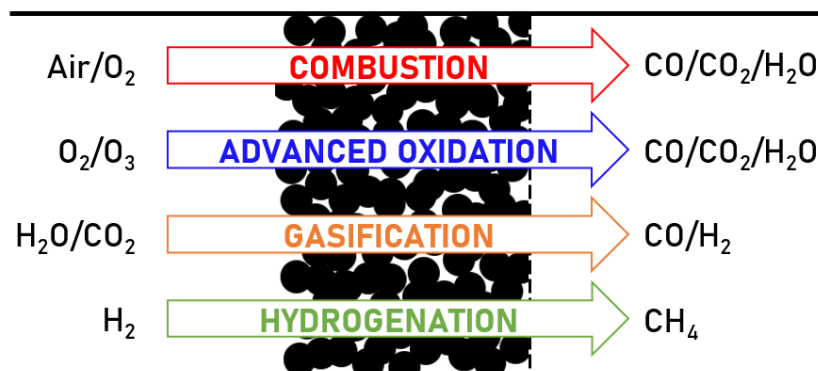


**Figure 1.21.** Schematic representation of the main coked zeolites regeneration methods with the principal generated products. Operating conditions are discussed in respective section.

#### 1.4.1. Coke combustion with air/oxygen

The most frequently used method to regenerate coked catalysts in the industry is coke combustion using air or oxygen. Spent catalysts are usually placed in a fixed-bed reactor and are treated with oxygen-containing gas at a high temperature. While nitrogen is mostly used as a diluent in laboratory-scale tests, steam is used in full-scale plant operations [4]. Coke removal reaction with air or oxygen is a rapid process occurring at moderate-high temperatures (usually around 400-500°C). Coke combustion with oxygen is used for catalyst regeneration of common industrial processes such as cracking or catalytic reforming [4-6].

##### 1.4.1.1. Oxidation mechanisms

Coke oxidation with oxygen is an exothermic reaction that is usually described by the following set of equations (Equations (1.2) to (1.5)) representing total oxidation of solid unspecified carbonaceous compounds, where H(s) represents hydrogen atoms attached to solid coke compounds [7]:



From the determined reaction enthalpies, it can be shown that the exothermicity of the process is mostly due to oxidation of carbon, even though energy emission of hydrogen



oxidation is not negligible. From Temperature-Programed Oxidation (TPO) experiments, it has been shown that light coke is primarily oxidized, as hydrogen oxidation is easier, leading to light coke dehydrogenation forming heavier coke. High carbon content coke is burnt off afterwards at higher temperatures [114, 115]. This is why water is the first molecule observed on a classical TPO spectrum, followed by CO and CO<sub>2</sub> production that corresponds to competing mechanisms of carbon oxidation [114, 116, 117]. Intrinsic mechanisms of coke have not been formally determined yet since coke nature has a great influence over the oxygenated intermediates formed during oxidation, which are considered as precursors for carbon oxide formation [118]. The following equations presented in Table 1.1 are commonly used to describe more precisely the steps of coke combustion, from light coke dehydrogenation to heavy coke oxidation via the formation of oxygenated intermediates [116, 117]:

**Table 1.1.** Overall mechanism for light and heavy coke oxidation with oxygen.

<b>Light coke combustion</b> <i>Hydrogen oxidation</i>	$-C_nH_{2n} + \frac{n}{2}O_2 \rightarrow -C_n + nH_2O$	(1.6)
	$-C_f + O_2 \rightarrow -C(O_2)$	(1.7)
	$-C(O_2) + -C_f \rightarrow -C(O) + CO$	(1.8)
<b>Heavy coke combustion</b> <i>Carbon oxidation</i>	$-C(O) \rightarrow CO$	(1.9)
	$-C_f + O_2 \xrightarrow{-C(O)} CO_2$	(1.10)
	$-C(O_2) \rightarrow CO_2$	(1.11)

In these equations,  $-C_nH_{2n}$  and  $C_n$  represent respectively light coke and hard coke, while  $-C_f$  is used to describe a free carbon site available for dioxygen chemisorption. The latter ensures the formation of dissociated ( $-C(O)$ ) and undissociated ( $-C(O_2)$ ) surface oxides turning into the corresponding molecular gases once atom binding is completed. The competition between rearrangement (1.8) and desorption (1.10) of the formed complexes is responsible for the complexity of the coke oxidation process. The latter is usually qualified as completely achieved when CO<sub>2</sub> is formed while partial oxidation leads to CO formation. As for every reaction, coke oxidation is influenced by different parameters as developed in Section 1.4.1.3 [117, 119].

The evolution of reactivity is studied following the composition of oxidation products, especially the CO/CO<sub>2</sub> ratio, to monitor which reaction is favored. Overall, coke oxidation mechanisms are governed by combustion temperature and coke nature: the more coke is condensed and “heavy”, the more temperature needs to be high for the oxygen to oxidize solid carbon compounds [119]. Coke location and therefore catalyst geometry are also determining parameters as they govern the diffusion of oxygen within catalyst pores and the accessibility of coke. Process of coke oxidation is consequently often qualified as a shape-selective process [107]. However, this problematic is more related to mass transfer and diffusion limits than to reaction mechanisms and will be further developed in a following paragraph (Section 1.4.1.2.b).

### 1.4.1.2. Reaction model: kinetics and mass transfer

#### a. Kinetics

Determining reaction rates is important for process design and optimization to avoid the apparition of hot spots leading to catalyst attrition. Consequently, over the last decades, many studies worked on the determination of kinetic parameters for coke combustion applied to various catalysts and deactivating reactions. Two approaches are possible for kinetic study completion: coke oxidation can be considered in its overall form, thus considering a global reaction rate for the direct combustion of coke to carbon oxides. Otherwise, intrinsic coke burning reactions may also be considered to approach hypothesized intermediate mechanisms occurring at the reaction site within the catalyst [120]. Results from both approaches being similar, the determination of a global reaction rate for the overall coke combustion is usually used for process design needs as it provides a sufficient approximation to study oxidation kinetics. Models considering intrinsic reactions are based on various assumptions aiming to describe reality as close as possible. Complexity of coke compounds leads to a limitation for coke oxidation modelling as reaction rate is correlated with numerous varying parameters such as coke and catalyst nature and structure among others [107, 119, 121, 122]. While kinetic studies only focused on carbon oxidation rate, some works noticed that hydrogen oxidation effect in oxidation exothermicity was not negligible in the early stages of combustion and pointed out the importance of integrating the hydrogen reaction rate in kinetic studies especially to evaluate the risk of sintering related to the apparition of hot spots [114]. The multiple-reaction model detailed in Table 1.2 is based on the overall oxidation reaction and offers a relatively simple description of the coke burning process [123, 124].

**Table 1.2.** Stoichiometry and overall reaction rates for solid carbon and hydrogen oxidation.

Stoichiometry and kinetics		Reaction rates
$2\text{H}(\text{s}) + \frac{1}{2}\text{O}_2(\text{g}) \rightarrow \text{H}_2\text{O}(\text{g})$	$r_1 = k_{\text{H}_s} C'_{\text{H}_0} p_{\text{A}}$ (1.12)	[Hydrogen] $r_{\text{H}_c} = k_{\text{H}_s} C'_{\text{H}_0} p_{\text{A}}$
$\text{C}(\text{s}) + \text{O}_2(\text{g}) \rightarrow \text{CO}_2(\text{g})$	$r_2 = k_2 C'_c p_{\text{A}}$ (1.13)	[Carbon]
$\text{C}(\text{s}) + \frac{1}{2}\text{O}_2(\text{g}) \rightarrow \text{CO}(\text{g})$	$r_3 = k_3 C'_c p_{\text{A}}$ (1.14)	$r_{\text{C}_c} = (k_2 + k_3) C'_c p_{\text{A}} = k_{\text{C}} C'_c p_{\text{A}}$

$k_{\text{H}_s}$  and  $k_{\text{C}}$  are respectively rate constants for hydrogen and global carbon oxidation, while  $k_2$  and  $k_3$  are separate rate constants for carbon oxidation to  $\text{CO}_2$  and  $\text{CO}$ .  $C'_c$  and  $C'_{\text{H}_0}$  represent the carbon content and the initial hydrogen content in coke respectively, while  $p_{\text{A}}$  is the oxygen partial pressure. This simplified model gives a reliable representation of coke burning process where equations are expressed as first order with respect to the oxygen partial pressure and reactants concentration. Determination of kinetic parameters confirmed that hydrogen is oxidized faster than carbon, thus “soft” coke is firstly oxidized and turned into “hard” coke, which is more difficult to oxidize. Both hydrogen and carbon reaction rates were correlated with the Arrhenius equation determining temperature effect over kinetic constants and activation energies for specific applications. Indeed, as coke nature and catalyst structure vary from a process to another, it has been proved that mass transfer within the catalyst mostly limits coke oxidation. Therefore, kinetic parameters vary for each application, requiring a different study for

each process. The importance of diffusion and mass transfer for coke oxidation will be discussed in the next section.

*b. Diffusion and mass transfer*

Being a fast equilibrium reaction, coke oxidation of both carbon and hydrogen in coke is mainly controlled by oxygen diffusion within the pores of the inert catalyst pellet towards coke reactive surface. Consequently, coke is firstly removed from the edge of the pellet and oxidation progresses to the center core of the pellet as oxygen diffuses farther into the solid catalyst matrix. This model of diffusion, known as shrinking-core model (SCM), is used to describe heterogeneous reactions where a gas-phase reactant reacts with species contained in a porous solid material. The shrinking-core model provides a mathematical representation of gas-phase diffusion, here oxygen, throughout the catalyst and its reactivity with coke [125]. Using diffusivity and molar balance equations finally offers an ideal prediction of oxygen concentrations across the catalyst pellet at various times. This model implies catalyst particle to be divided into two distinct regions, a non-reacted carbon-rich core at the center of the pellet surrounded by a carbon-free outer shell where coke removal is achieved. The delimitation of these zones is the reaction interface where oxidation exclusively occurs, which is not representative of the real phenomenon. As coke oxidation advances, this boundary moves towards the center of the grain as illustrated on Figure 1.22.a.

Even though SCM provides a good estimation of coke oxidation progression within a single catalyst grain, some assumptions lead to a lack of accuracy representing reality. For instance, in this model, reaction rates are ignored and coke oxidation is considered immediate at the unreacted coke external surface. During the real oxidation process, all oxygen does not stop instantaneously to react at the unreacted core surface and pursue its way within coked pores, generating the apparition of a “partially” oxidized zone where carbon content decreases from  $C_0$  (unreacted core carbon content) down to carbon-free region as represented on Figure 1.22.b [126]. Kern *et al.* completed the existing shrinking-core model (SCM) including the influence of pore diffusion as well as the intrinsic kinetics to model more precisely the effective rate of coke oxidation [127]. Some studies adapted this work on a single catalyst grain to a fixed-bed regenerating reactor, modelling carbon concentration profiles alongside the deactivated bed. As expected, by transposition from

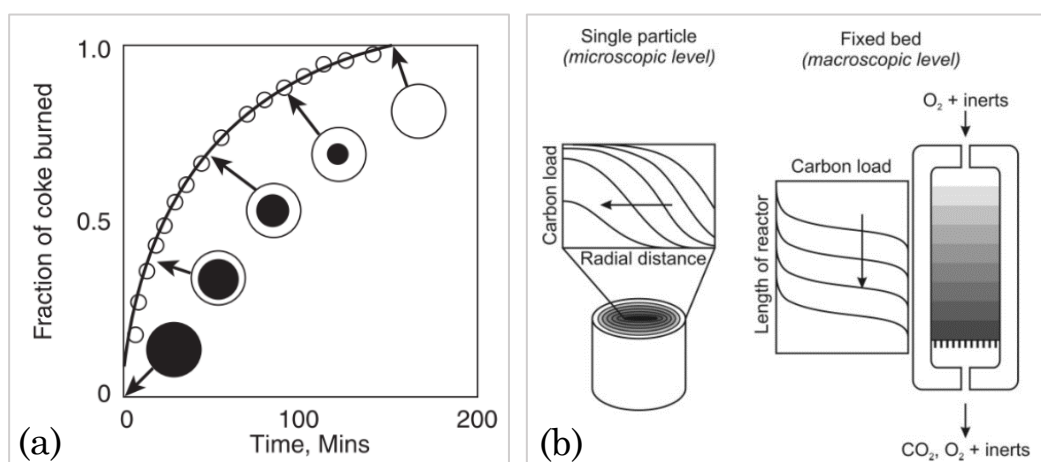


**Figure 1.22.** (a) Shell progressive regeneration of fouled pellet following shrinking-core mode (Fogler *et al.*, 2011) [125]; (b) Coke removal during combustion of catalyst pellets in a fixed bed reactor (Müller *et al.*, 2010) [126].

the grain scale to the bed scale, when oxygen is fed by the top of the reactor, it was proved that a greater coke removal is achieved in the upper fraction of the fixed bed as it is more exposed to oxygen flow, while on the other hand, carbon-rich coke remained in the bottom fraction. Therefore, coke oxidation is controlled by oxygen diffusion within both a single catalyst particle (microscopic) and a fixed-bed reactor (macroscopic) [124, 126-128].

#### **1.4.1.3. Parameters influencing coke oxidation**

##### *a. Catalyst structure and composition*

Coke oxidation being a shape-selective process where reaction rate is limited by oxidant diffusion, catalyst structure appears as an important parameter since geometry of internal pores will influence mass transfer within the catalyst. Several works demonstrated the correlation between catalyst structure and coke removal rate, mainly related to the variable coke accessibility to oxygen due to the difference of pore structures according to the catalyst geometry [92, 105, 107, 129]. Indeed, following the size and aperture of pores, coke location will change and will deposit preferentially on the outer or internal surface, being more or less accessible to oxygen. Therefore, while coke on the outer surface will be easily removed, oxidation of inner compounds will be more difficult and dependent of oxygen diffusion within the pores. As an illustration, easier coke removal is observed on a HFAU-type catalyst at 550°C while a temperature of 600°C is necessary for coke removal from HEMT zeolite, regardless of framework composition and coke content. [105]. This has been attributed to the preferential deposition of coke on the outer surface because of the small pore apertures of HFAU structure, making coke more accessible for oxidation. Similar results were observed by Magnoux *et al.* comparing oxidation of coke formed on HY, H-mordenite and HZSM-5 zeolites during n-heptane cracking. In addition to the faster oxidation of coke deposited on the outer surface, the influence of internal channels and pore size for oxygen diffusion has been proved: macropores, supercages and interconnected channels offer a better circulation of oxygen, subsequently affecting contact between oxygen and coke deposits located over the inner surface [107, 129].

Zeolite framework as well as the number and strength of active sites are also implied in catalyst regeneration and coke removal efficiency. Influence of catalyst composition over coke oxidation is observed on both metal and zeolite catalysts since both the metallic and acidic acid sites participate in the coke removal process. Interactions between oxygen and catalyst may vary according to the composition of the active sites or even its support. Moljord *et al.* observed that a high density of framework aluminum atoms facilitates coke oxidation over HY zeolites with Si/Al ratios from 4 to 100 [130]. Another study proved that, over a Pt-Sn/Al<sub>2</sub>O<sub>3</sub> catalyst, oxygen is activated by platinum particles rather than alumina support, therefore coke located over metallic Pt sites is preferentially oxidized [131]. Consequently, knowledge of catalyst composition is also important to understand coke oxidation mechanisms since nature of deactivated surface has also a role in coke removal rate as it determines intrinsic mechanisms of oxidation. Even though diffusion is the limiting step of the reaction, nature of deactivated surface has also a role in coke removal rate as it determines intrinsic mechanisms of oxidation. Due to the variety of catalysts, different activation step mechanisms for the reaction of an aromatic core in coke are proposed. A mechanism suggested by Dong *et al.* suggests that the initiation step for coke oxidation involves the formation of radical carbocations from any accessible aromatic cores of coke molecules. This mechanism, represented Figure 1.23, is commonly accepted as the main reaction for coke oxidation [132]. The relative acidity of the coke-

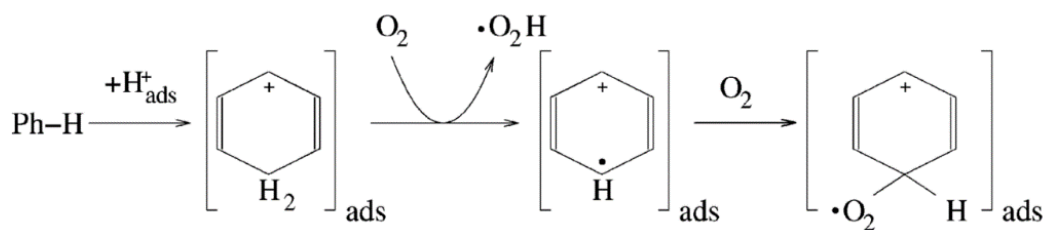


**Figure 1.23.** Carbocation mechanism for the reaction of oxygen with an adsorbed coke molecule Presented by Dong *et al.* (1991) [132] and adapted by Keskitalo *et al.* (2006) [118].

carrier surface accounts for the existence of preferential coke removal sites, as the formation of carbocation intermediates from deposited coke is more or less favored. Therefore, oxygen reactivity is not only determined by the nature of coke itself but also by the composition of the deactivated surface.

### *b. Operating parameters*

For process optimization purposes, the influence of operating parameters on coke oxidation efficiency has been heavily studied. The main four parameters that can be easily modulated at an industrial scale are temperature, time on stream, oxygen concentration and flowrate. While oxygen is diluted in N<sub>2</sub> in laboratory experiments, industrial processes often use a steam and air mixture. In classical conditions, coke oxidation is operated in a temperature range of 400-600°C and an oxygen concentration in gas from 0.05 to 10 vol.%, with a time of exposure varying according to the degree of coke removal to be achieved [133]. For example, during the regeneration of HZSM-5 catalyst coked during ethylbenzene conversion, Jong *et al.* observed that 67% of coke was removed after 0.5 h and 93% after 2 h, while 6 h are needed to achieve complete coke removal [134]. As the oxidation reaction rate is correlated with Arrhenius equation, higher temperatures could accelerate the reaction to achieve better coke removal. However, temperature is limited by the catalyst material which could be altered in case of excessive temperature exposition. Operating temperature can therefore vary according to the deactivated catalyst and is set at the maximum value allowed by the catalyst to increase coke removal efficiency but also to insure catalyst structure is not damaged. Marcilla *et al.* observed a structural change in HZSM-5 zeolite after a 900°C treatment leading to further catalytic activity loss, while a HUSY-type zeolite exposed to the same treatment recovered all its activity without any structural alteration [92]. To avoid the apparition of hot spots and catalyst sintering, the oxygen concentration in incident gas also has to be controlled. Indeed, as coke oxidation is exothermic, a too important concentration of reactant could lead to local temperature rises,

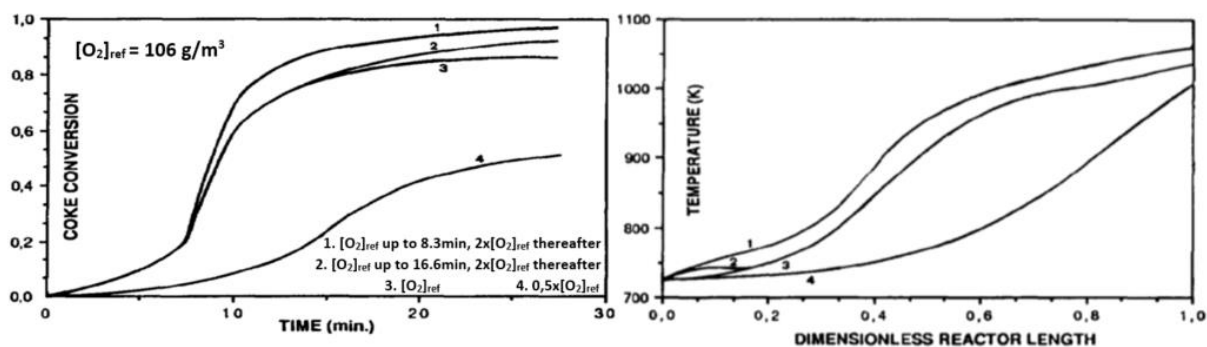


**Figure 1.24.** Average coke conversion and temperature profiles in the reactor for different oxygen-inlet concentration strategies. Adapted from Santamaria *et al.* (1991) [115].

which could further deactivate the catalyst. Santamaria *et al.* investigated the temperature behavior within a reactor during coke oxidation with different oxygen inlet strategies as illustrated Figure 1.24 [115]. Even though this experiment shows that temperature is reduced in the reactor with lower oxygen concentrations, coke removal efficiency is also greatly impacted. Therefore, a balance has to be found between thermal risk and oxidation efficiency. As the risk is mainly present at high coke contents, the combustion process is typically controlled by initially feeding low concentrations of air before increasing oxygen concentration gradually as carbon content decreases [135]. Coke oxidation being limited by mass transfer and following shrinking-core model, coke removal increases with time and complete regeneration is theoretically achieved at infinite time. Time of exposure is a parameter determined to comply with industrial needs in term of coke removal and catalytic activity recovery. For economic reasons, optimization studies of oxidation processes tend to maximize catalytic activity recovery, which is correlated to coke removal, and to minimize time on stream by variation of all the aforementioned parameters [136].

#### 1.4.1.4. Limitations of coke combustion

The main drawback to coke oxidation with air or oxygen is the temperature limitation to avoid irreversible damage to catalyst and a loss of catalytic activity after regeneration. Among the principal possible structural changes due to thermal degradation, dealumination has been studied in zeolite materials for its capacity to promote formation of mesoporous systems, giving an interest to determine reaction rate and influencing parameters [137, 138]. In some particular cases, dealumination turns out to be a way to improve catalytic activity due to the modification of acidic properties in the structure [139]. However, structural changes during a regeneration process are not desired as it often causes a decrease of active sites by sintering or damages on the crystallinity of the catalyst framework, leading to an irreversible loss of catalytic activity [92, 140].

Intensive work was carried out to achieve coke oxidation reducing temperature of the regeneration process, therefore avoiding thermal damage. A well-known technique is catalyst improvement with metal impregnation, offering both inhibition of heavy polyaromatic coke and temperature reduction during regeneration [141]. Moreover, it was shown that coke removal close to the metal is easier, with lower temperatures and shorter

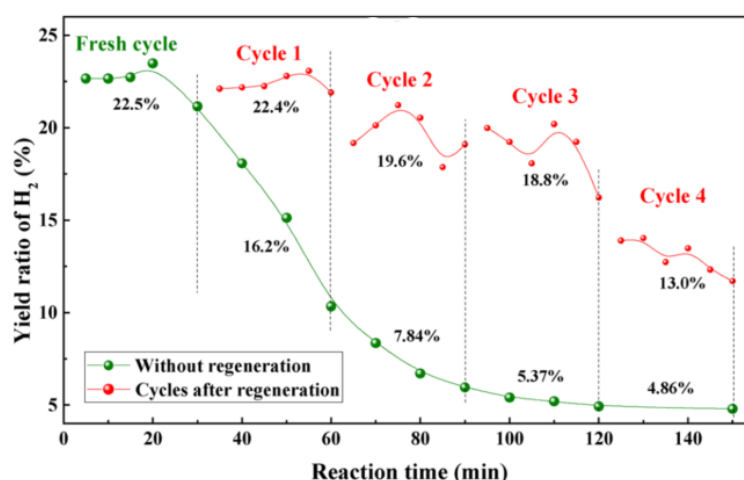


**Figure 1.25.** H<sub>2</sub> yield of a metal-impregnated cracking Ni/γ-Al<sub>2</sub>O<sub>3</sub> catalyst after different cycles of regeneration with oxygen for 3h (Lu *et al.*, 2017) [144].



exposition times, suggesting that coke oxidation is promoted by the presence of metal particles [142]. However, metal-impregnation also has the disadvantage to not guarantee catalyst stability after several regenerations. Different studies have shown a significant catalytic activity loss compared to the fresh catalyst after repetition of deactivation/regeneration cycles suggesting that metal-impregnation may not be suitable for long-time reuse of catalysts [143]. Lu *et al.* observed this loss of catalytic activity during catalytic cracking of toluene over Ni/ $\gamma$ -Al<sub>2</sub>O<sub>3</sub> after successive regeneration cycles as illustrated Figure 1.25 [144]. They attributed the loss of surface area to sintering of metal particles and to remaining coke. In order to avoid the issues related to coke combustion, the use of an oxidant other than oxygen has also been investigated to achieve improved catalyst regeneration in milder conditions. These alternative methods for oxidative processes are discussed in following sections.

### 1.4.2. Ozonation

The regeneration of coked catalysts using ozone is a process that has been gaining increasing amounts of interest recently [8, 9, 145]. The strong oxidizing power of this molecule allows a high reactivity with coke but also the production of highly reactive radical species, making ozonation a favorable alternative process to regenerate coked catalysts. In fact, the high reactive nature of ozone enables regeneration to take place at much lower temperatures, thus mitigating the issue of catalyst thermal deactivation but also lowering energy consumptions. This type of regeneration is therefore promising both from environmental and economical point of view.

#### 1.4.2.1. Ozone molecular properties

Ozone molecule is a very unstable molecule comprising three oxygen atoms, thus including two O-O bindings 1.276 Å long with an angle of 116.8° as illustrated in Figure 1.26. Even though gas-kinetic diameter of ozone diverges in literature, the value of 5.8 Å is commonly used [146]. Ozone is an allotropic molecule as the electronic density moves from one oxygen to another, leading to different resonance structures represented in Figure 1.26. Ozone is described as a hybrid between all these configurations, conferring various characteristics like electrophilic properties or oxidizing power [147].

Its strong oxidizing power turns ozone into a very interesting molecule used for industrial purposes (chemical, pharmaceutical, etc.) and for environmental applications (water, soils and air treatment). Ozone applications are detailed in Rakovsky *et al.* review article [148]. The oxidizing ability of ozone is related to its high redox potential comparatively to oxygen, as shown in Table 1.3. Due to its instability, ozone decomposes naturally to oxygen but can also form oxygenated radicals which oxidizing power is even stronger. Some processes, mentioned in literature as Advanced Oxidation Processes (AOPs), decompose ozone intentionally into radicals to achieve further oxidation. These specific processes and applications are discussed in a dedicated section of this review.

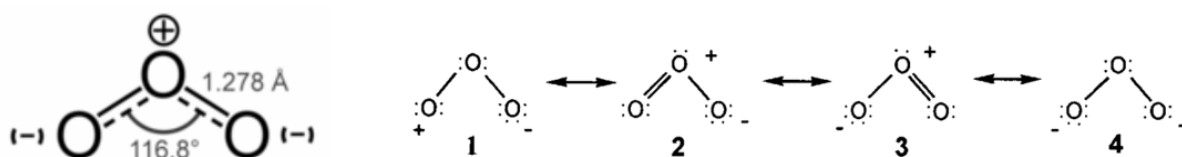


**Figure 1.26.** Ozone molecule dimensions and resonance structures. Adapted from Chao *et al.* (2007) [146] and Oyama *et al.* (2000) [147].

**Table 1.3.** Standard potential of oxygen, ozone and principal oxygenated radicals under normal conditions (25°C and 1 atm).

Oxydant	Redox couple	Redox potential (V)
Oxygen molecule	O <sub>2</sub> /H <sub>2</sub> O	1.23
Ozone	O <sub>3</sub> /O <sub>2</sub>	2.07
Atomic oxygen	O•/H <sub>2</sub> O	2.42
Hydroxyl radical	OH•/H <sub>2</sub> O	2.80

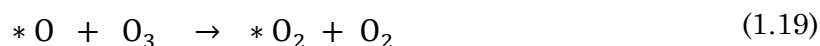
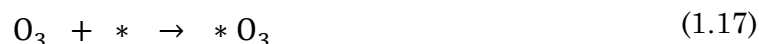
### 1.4.2.2. Ozone reactivity

#### a. Thermal and catalytic degradation

Ozone is artificially generated with different methods such as electrical discharge (ED), electrolysis or irradiation. The most common technique is electrical discharge, treating oxygen-containing gases with extremely high voltages. Although useful as a strong oxidant, ozone has a very short life of only tens of minutes at ambient temperature and significantly lower at higher temperatures [149]. The thermal gas-phase decomposition of ozone is described by the following mechanism [150]:



Where M is a third molecule being O<sub>2</sub>, O<sub>3</sub>, CO<sub>2</sub>, N<sub>2</sub>, He or other gaseous body. The kinetic constant of each reaction is dependent of this last reactant and varies accordingly. Different researchers worked on the determination of these parameters to study the kinetics of ozone thermal degradation [147, 150]. At low temperatures, the “natural” thermal degradation of ozone represented by this mechanism occurs relatively slowly if not exposed to UV radiations or catalysts. In fact, many solids used in the industry as catalysts or absorbents have been proved to interact with ozone and to enhance its decomposition. This “catalytic” thermal degradation has been heavily studied over metal oxides but also over zeolite materials. Both of them have active surface presenting different possible interactions with gaseous ozone: simple physisorption or molecular adsorption over silanol functions and Lewis acid sites, which can further lead to ozone decomposition if the acidity of the adsorption site is strong enough [151]. The following set of equations describes ozone decomposition over metal oxides and zeolites. In this mechanism proposed by Li *et al.* and adopted in many studies afterwards, \* represents surface active sites [152].





This mechanism illustrates the decomposition of ozone to oxygen but also emphasizes the formation of adsorbed oxygenated species such as atomic oxygen (Equations (1.18) and (1.19)). Hydroxyl radicals are also susceptible to form in case of proximity with hydrogen, due to humidity or to the presence of other species (Equation (1.22)) [153]. Different studies focused on the location of the active sites leading to ozone decomposition on zeolites and showed that Lewis acid sites are mainly responsible of this phenomenon. Studies over faujasite and natural zeolites show that acidity strength has an influence: ozone is adsorbed over weak acid sites while it is decomposed over strong ones [146, 154]. Alejandro *et al.* added that molecular ozone has no affinity with Brønsted acid sites [155]. The decomposition of ozone thus produces a diversity of adsorbed oxygenated species: molecular and atomic oxygen, peroxide ions and hydroxyl radicals. Operating conditions such as oxygen concentration, humidity of ozonized air and temperature have a great influence over the kinetics of decomposition and consequently strongly affect the repartition of reactive species. When temperature is high enough, these are desorbed from active sites and are susceptible to take part to other reactions with reactants in the gaseous or solid phase. Over inert raw material, the intermediate oxygenated species react to form oxygen but, in the presence of other molecules, they can also participate to further oxidation reactions as they readily react with most organic compounds in an unselective manner with aggressive attacks due to their strong reactivity.

#### *b. Coke oxidation mechanisms*

Ozonation is based on two different pathways for coke oxidation: direct and indirect. The direct mechanism utilizes ozone as the dominant oxidizing agent via a direct electrophilic attack of molecular ozone on organic species, whereas indirect mechanism relies on the participation of aforementioned oxygenated intermediates formed from ozone decomposition [156]. These highly reactive compounds attack organic species aggressively by either extracting hydrogen from water, as is the case with alkanes and alcohols, or attaching itself to the organic molecule, as is the case with olefins and aromatics. The combination of these mechanisms are forming a simple overall oxidation (Equation (1.23)) where a, b, c and d depend on the feed ratio and X and Y are related to coke nature.



From previous studies, it was found that molecular ozone can attack directly organic coke in different ways according to the nature of the carbonaceous compounds present [157]. Due to its strong electronegativity, ozone favors electrophilic attacks and therefore reacts with electron-donating groups such as alcohols, aromatics, ethers, aldehydes and amines. As there is a wide range of possible constituents, it is difficult to specify a unique pathway through which ozone attacks coke. However, one largely accepted mechanism for the oxidation of alkenes, and more generally double bounds including in aromatic compounds, was suggested by Criegee [158]. The initial attack of ozone is thought to proceed in three distinct steps as illustrated on Figure 1.27: ozone first attacks the double bound to form a primary ozonide (1), which decomposes into stable carbonyl compounds (aldehyde or ketone) (2) forming a more stable secondary ozonide (3). The resulting products are compounds that will more readily undergo further oxidation reactions to decompose completely to carbon dioxide and water.

The indirect pathway for coke oxidation implies the radical oxygenated species directly or indirectly formed from ozone decomposition. Similarly to the direct mechanism, radicals

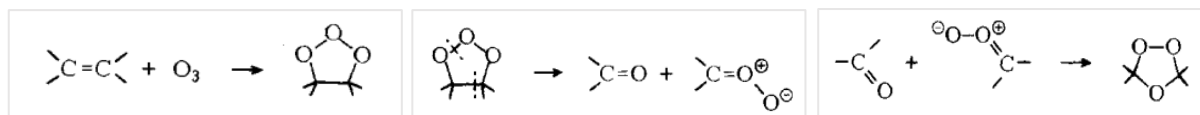


**Figure 1.27.** Criegee mechanism for initial attack of  $O_3$  on alkenes (Criegee *et al.*, 1975) [158].

react with organic compounds to form oxygenated coke which will further react until total oxidation. Due to the poor hydrogen content in coke, it is theorized that radical is attaching itself to carbon atom by breaking the double bond. The behavior and formation of these radicals, such as ozonide and peroxide ions or hydroxyl radicals, have been heavily investigated in the liquid phase with the growing interest in AOPs over the last decade [156, 159]. Due to the more recent interest of ozone use in the gas-phase, mechanisms are less detailed even though some similarities of ozone decomposition have been observed in the two different phases.

### 1.4.2.3. Kinetics and mass transfer during ozonation

Due to the recent interest for ozone use for oxidation processes in gas-phase, very few studies focused on ozonation kinetics rather than materials and operating conditions influence over coke removal and regeneration efficiency [8, 9, 131, 146]. However, from the observations made in these studies, similarities with oxygen oxidation are expected. Khangkham *et al.* observed that after ozonation of ZSM-5 zeolite used for PMMA cracking in a fixed-bed reactor, the H/C ratio of remaining coke in the catalyst pellet decreased compared to deactivated catalysts [160]. This observation suggests that ozone oxidation, similarly to oxygen, starts with hydrogen contained in coke. Direct oxidation with molecular ozone is a very selective reaction. Kinetic constants for ozone reactivity with principal families of hydrocarbons are listed in Table 1.4 [161]. More recent studies have been carried out determining rate coefficients of ozone reactivity with unsaturated molecules [162]. These results show the complexity of coke oxidation kinetics as coke molecules are complex structures with a mix of functional groups organized in an infinite number of combinations. Organic compounds reactivity with ozone is globally weak at ambient conditions but is enhanced at higher temperatures. However, as temperature increases, thermal degradation of ozone is also favored rather than catalytic decomposition, lowering radical formation leading to a decreased coke oxidation yield. A kinetic study for the indirect oxidation mechanism has not been carried out yet and would be relevant to better understand the repartition between direct and indirect pathways during ozonation as well as mechanisms involved in oxidation with radical species.

**Table 1.4.** Kinetic constants for hydrocarbons reactivity towards molecular ozone at ambient temperature (Treacy *et al.*, 1992) [161].

Pollutant	$k$ ( $\text{cm}^3 \cdot \text{molecule}^{-1} \cdot \text{s}^{-1}$ )
Alkanes	$10^{-23}$ - $10^{-24}$
Alkenes	$10^{-16}$ - $10^{-18}$
Aromatics	$10^{-20}$ - $10^{-22}$
Oxygenated compounds $C_1$ - $C_3$	$10^{-19}$ - $10^{-21}$
Oxygenated compounds $C_{4+}$	$10^{-17}$ - $10^{-18}$

Because of ozone short lifetime, diffusion and mass transfer is, similarly to oxygen, a limiting parameter for coke oxidation with ozone. Microscopic and macroscopic coke profiles within catalyst pellet and alongside fixed-bed respectively were found to be similar showing that ozone reacts primarily with external coke and progresses towards the center of the pellet starting by the top of the catalyst bed [160, 163]. However, diffusion limitations seem to be even more important as coke located in the center of pellets may remain unreacted when rate of ozone decomposition is faster than its diffusion rate. Thus, regeneration of coked catalysts via ozonation is a complex process involving both complex chemical reactions (direct and indirect pathways) and transport processes (pore diffusion to the internal coke surface).

#### 1.4.2.4. Ozonation for coke removal: literature review

The investigated ozonation conditions found in literature for coke oxidation using ozone are summarized in Table 1.5. Various solid catalysts, from bi-functional to zeolite materials, as well as different coking reactions are investigated.

**Table 1.5.** Experiments of coke removal from catalysts using ozone found in literature.

Ozonation conditions	Deactivated catalyst	Deactivating reaction	Ref.
O <sub>2</sub> + O <sub>3</sub> flow 120 cm <sup>3</sup> .min <sup>-1</sup> (ratio not given), 137°C.	HY and HYS zeolite	Exposition to cyclohexene at 347°C.	[164]
O <sub>3</sub> /O <sub>2</sub> mole ratio 0.05-0.06, 150°C, 90 min.	HZSM-5 zeolites (Si/Al: 35 and 70)	Methanol conversion to hydrocarbons and o-xylene isomerization.	[163]
O <sub>3</sub> /O <sub>2</sub> mole ratio 0.05, 200°C, 4h (bed agitation).	HY zeolite	Exposition to various alkanes and alkenes at 500°C.	[165]
O <sub>3</sub> conc. from 16 to 50 g/m <sup>3</sup> , 20-150°C, 0.5-4h.	HZSM-5 zeolite	PMMA cracking at 250-300°C.	[8]
O <sub>3</sub> conc. from 4 to 25 g/m <sup>3</sup> , 50-200°C, 2-8.5h.	Undefined zeolite	Not given.	[9]
O <sub>3</sub> /O <sub>2</sub> mole ratio 0.01, 125°C, 4h + H <sub>2</sub> regeneration	Y-zeolite (UOP, Y-54)	Isobutane alkylation (liquid, 25-80°C).	[166]

### 1.4.3. Other regenerating methods

#### 1.4.3.1. Gasification

Although oxidative treatments are very commonly used for coked catalysts regeneration, the main drawback of these techniques is the formation and emission of carbon dioxide. While reduction of greenhouse gases emission is an actual industrial challenge, coke combustion for spent catalysts regeneration produces almost half of the emitted CO<sub>2</sub> in a FCC unit [167]. Gasification provides an alternative method to mitigate CO<sub>2</sub> emission during catalyst regeneration, using H<sub>2</sub>O or even CO<sub>2</sub> as feedstock to remove coke at around 700-900°C (see corresponding reactions Table 1.6). The latter uses CO<sub>2</sub> as an oxidizing agent (redox potential 1.33 V) reacting with coke to form carbon monoxide (Equation (1.24)). The equilibrium of this highly endothermic reaction favors CO production at temperatures above 700°C [168]. Due to low CO<sub>2</sub> reactivity and the high temperatures needed, the scope of application is limited to catalysts with high resistance to heat. Otherwise, in such conditions, catalysts may suffer structural damages or sintering. Use of H<sub>2</sub>O as reactant for gasification ensures the direct formation of syngas (H<sub>2</sub> and CO) in a temperature range between 700 and 900°C. Steam gasification, represented by Equation (1.25), also present risks of catalyst structure damage because of high temperature and possible attack Al-O bonds causing catalyst support collapse [169]. Therefore, regeneration via gasification is not suitable for coke removal from zeolite material and no studies dealing with gasification over zeolites have been found in literature. Studies carried out in this field are mostly focused on spent FCC catalysts used in refineries and are consequently out of the scope of the research project [170-173].

**Table 1.6.** Coke gasification reactions using H<sub>2</sub>O or CO<sub>2</sub>.

<b>CO<sub>2</sub> gasification</b>	$C(s) + CO_2(g) \rightarrow 2CO(g)$	+172 kJ/mol	(1.24)
<b>Steam gasification</b>	$C(s) + H_2O(g) \rightarrow CO(g) + H_2(g)$	+131 kJ/mol	(1.25)

#### 1.4.3.2. Hydrogenation

Another method used in literature for coke removal over catalytic material is based on the reactivity of coke with hydrogen or light carbonaceous gases such as alkanes [174]. In particular conditions, hydrocracking reactions are observed and coke is decomposed in lighter volatile gases. When hydrogen is used as a reactant, Marecot *et al.* observed that methane is the only product formed from coke decomposition over Pt/Al<sub>2</sub>O<sub>3</sub> catalyst [175]. Therefore, the accepted hydrogenation of coke is represented by the equation:



Nevertheless, Walker *et al.* demonstrated the low efficiency of this process by comparison with the previously mentioned methods at 800°C (O<sub>2</sub>, H<sub>2</sub>O and CO<sub>2</sub>), finding the lowest coke removal performance for H<sub>2</sub> treatment [176]. Indeed, to achieve coke removal via hydrogenation, severe temperature or pressure conditions are needed to thwart hydrogen low reactivity. To limit temperature rise due to reaction exothermicity during catalyst regeneration, several works observed that elevated pressure, between 1 and 10 atm, can be applied to achieve coke elimination [177, 178]. Moreover, based on the observations of different studies, coke nature and location seem to influence greatly

hydrogenation of coke. In most cases, coke is only partially removed, with an increase of H/C ratio of remaining coke, suggesting that heavy coke partially reacted to form lighter compounds [179]. According to Gnep *et al.*, reactivity of hydrogen with coke compounds over mordenite zeolite is limited to soft coke (high H/C ratio) while heavy polyaromatic molecules remain unreacted [180]. Other studies determined that coke is preferentially removed near Brønsted acid sites on the internal surface of the catalyst while external coke remained unreacted [134, 181]. Consequently, complete coke removal via hydrogenation alone is usually not possible unless with severe operating conditions, which could cause catalyst degradation.

### 1.4.3.3. Other Advanced Oxidation Processes

Advanced Oxidation Processes (AOPs) or microwave-assisted processes can be used for the regeneration of adsorbents used for wastewater and gas treatments [182-187]. Their application to coke removal from heterogeneous catalysts gained recent interest in order to develop new alternative methods for coke oxidation processes. Additionally to the aforementioned ozone-based process, other AOPs methods can be found in the literature.

#### a. Non-thermal plasma (NTP)

Among the alternative techniques to regenerate coked catalysts, use of non-thermal plasma (NTP) has been proved to be an efficient technique for coke removal from zeolite materials at ambient temperature [188]. This method is based on the formation of reactive oxygenated species (ROS), such as radicals, excited atoms, ions and molecules, thanks to the generation of highly energetic electrons in plasma discharge. Generated species from dioxygen exposition to plasma are mostly positive and negative ions ( $O^{2+}$ ,  $O^-$ ,  $O_2^-$ ) but also atoms and molecules such as O-atoms or ozone, which are able to form radicals or other reactive species. This type of regeneration is carried out in a dielectric barrier discharge (DBD) reactor where spent catalysts are placed between two electrodes. The oxidative species are generated thanks to the plasma discharge from oxygen contained in the gas

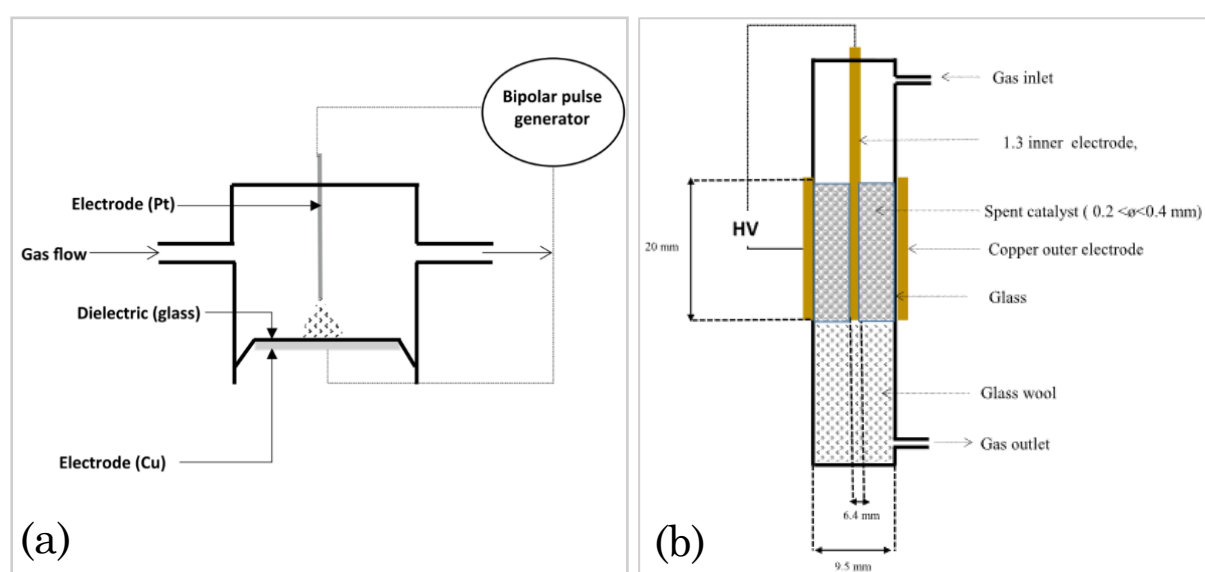
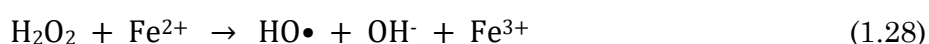
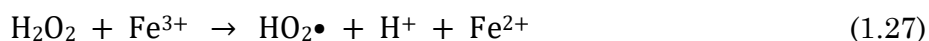


**Figure 1.28.** Schematic representation of (a) point-to-plate reactor (Pinard *et al.*, 2019) [129] and (b) fixed-bed dielectric barrier discharge (DBD) reactor for coked catalyst regeneration via NTP (Astafan *et al.*, 2019) [190].

passing through the reactor. This type of reactor, which generates plasma at atmospheric pressure, is experimented by Hafezkhiani *et al.* to perform Pt-Sn/Al<sub>2</sub>O<sub>3</sub> decoking [189]. Two different geometries of DBD reactors are found in literature: point to plate (Figure 1.28.a) and fixed-bed reactor (Figure 1.28.b). The latter was used by Astafan *et al.* who studied the NTP regeneration of faujasite zeolite coked from propene transformation at 623 K and achieved complete regeneration of the catalyst at ambient temperature with a deposited power of 12 W [190]. Consequently, coke removal can be achieved thanks to the generation of these oxidizing species that are diffusing within catalyst structure and oxidize coke organic compounds. Similarly to coke combustion and ozonation, this process is highly dependent of catalyst structure due to the diffusion limitations, as demonstrated by Pinard *et al.* who studied NTP catalyst regeneration over MFI, MOR and FAU zeolites [129]. Different parameters, such as input power, gap between electrodes, gas flowrate and nature of diluent (N<sub>2</sub>, He, Ar), as well as catalyst mass and compactness, have been investigated to provide deeper understanding of this process, which remains a relatively new and unknown method despite its promising aspects [191].

#### *b. Hydrogen peroxide and OH-derived Fenton radicals*

Oxidation processes based of Fenton reaction have applications in various domains such as soil or wastewater treatments. However, its application for deactivated catalytic materials is relatively recent and, consequently, there is currently no studies mentioning application of Fenton chemistry over coked catalysts and only very few papers dealing with fouled zeolite [192-194]. These papers are not properly dealing with coke removal as defined earlier but with deactivating species referred as humins, having similar behavior with coke (adsorption, steric blockage). Application of Fenton reaction could therefore be relevant for coke removal. These processes, occurring in liquid acidic medium, are based on the generation of OH radicals from hydrogen peroxide in the presence of Fe salt, which acts as a catalyst taking part in Fe<sup>3+</sup>/Fe<sup>2+</sup> redox cycle. The so-called Fenton reaction is described by the following mechanism:



Where reactions described by Equations (1.27) and (1.28) are desired because they lead to the formation of radicals OH, other reactions are undesired pathways (Equations (1.29) and (1.30)). Highly reactive hydroxyl radicals are consequently produced at low temperature. Using this method, Morales *et al.* reported total coke removal and catalytic activity recovery below 100°C for ZSM-5 zeolite fouled during glucose dehydration [194]. According to them, similar diffusion limitation issues are observed due to the rapid recombination of highly oxidative radicals and the selection of appropriate reaction conditions is a key factor to achieve coke removal. Oxidation mechanism can be, similarly to ozonation, direct from hydrogen peroxide or indirect with formed OH radicals. However, further research is needed to verify the efficiency of this method over “real” coke, and especially the potential Fe impurities generated by this method. Fenton-reaction-based processes may be a new alternative method for catalysts regeneration via oxidation under mild conditions.



#### 1.4.4. Focus: regeneration of ZSM-5 coked after PE pyrolysis

The regeneration of zeolite catalysts coked during pyrolysis is the object of limited research in the literature. Most of them are carried out using classic combustion process for coke removal. Lopez *et al.* studied the regeneration of ZSM-5 used in pyrolysis of polymer mix and showed almost complete recovery of textural properties with 99% of recovered BET surface area and 83% of microporous area between spent and regenerated catalysts [93]. Similar pyrolysis products to fresh catalysts use was obtained by reusing regenerated ZSM-5 samples with around 97% of aromatics and 78% of C5-C9 fraction in pyrolysis oils, showing that catalytic initial activity is restored. Complete regeneration is also achieved in a different study over ZSM-5 coked during the oligomerization of 1-butene despite the heavy nature of coke formed [195]. Marcilla *et al.* investigated the importance of treatment conditions (temperature and time) on the capacity of coke combustion to achieve complete coke removal and recovery of initial catalytic performances [92]. In this study, ZSM-5 showed a very sensitive behavior during coke combustion as its catalytic activity during pyrolysis of LDPE is not fully recovered at regeneration temperatures over 600°C. Ma *et al.* made similar observations with a different zeolite geometry during the regeneration of H-USY zeolites used in fast catalytic pyrolysis of lignin [196]. The incomplete catalytic activity recovery observed in these studies is attributed to structural changes and dealumination in the catalyst during the coke combustion process. However, as mentioned previously, regeneration via combustion can fully restore catalytic activity using adequate operating conditions to avoid thermal damages (around 500°C for ZSM-5). While catalysts performances are retrieved after one cycle, some studies demonstrated the gradual loss of catalytic performances after multiple cycles of reaction/regeneration as a complete regeneration is harder to achieve due to the accumulation of residual coke over the catalysts after each reuse [197].

Consequently, there is a need to develop alternative methods for regeneration in milder conditions to achieve complete coke removal while avoiding possible thermal damages. Using NTP at ambient temperature, the work of Jia *et al.* showed partial coke removal from ZSM-5 deactivated during pyrolysis of oak [188]. Promising primary results were also obtained using the ozonation process, being the core of the research project of this thesis, which allowed to achieve partial coke removal and catalytic activity recovery in PMMA cracking with pelletized ZSM-5 [8].

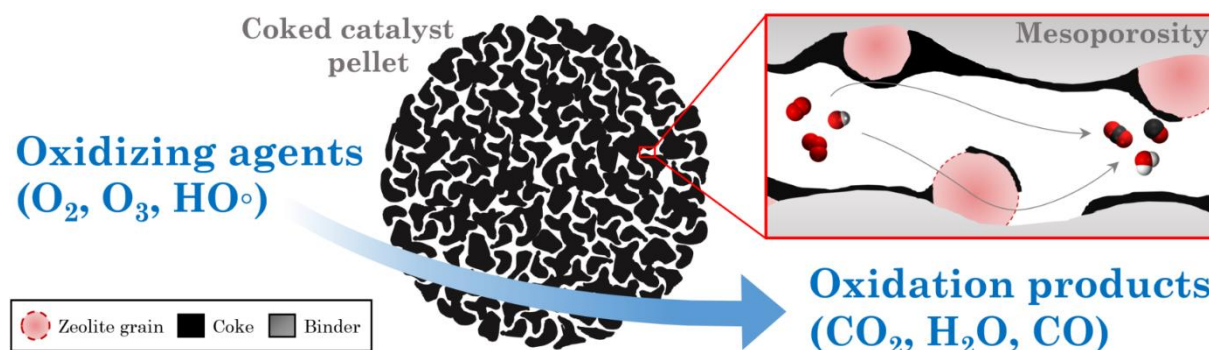
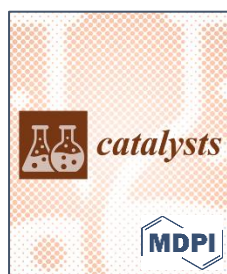


**Figure 1.29.** Schematic representation of oxidation processes for coke removal from catalysts at pellet and mesoporous scale.

## 1.5. Conclusion and key takeaways

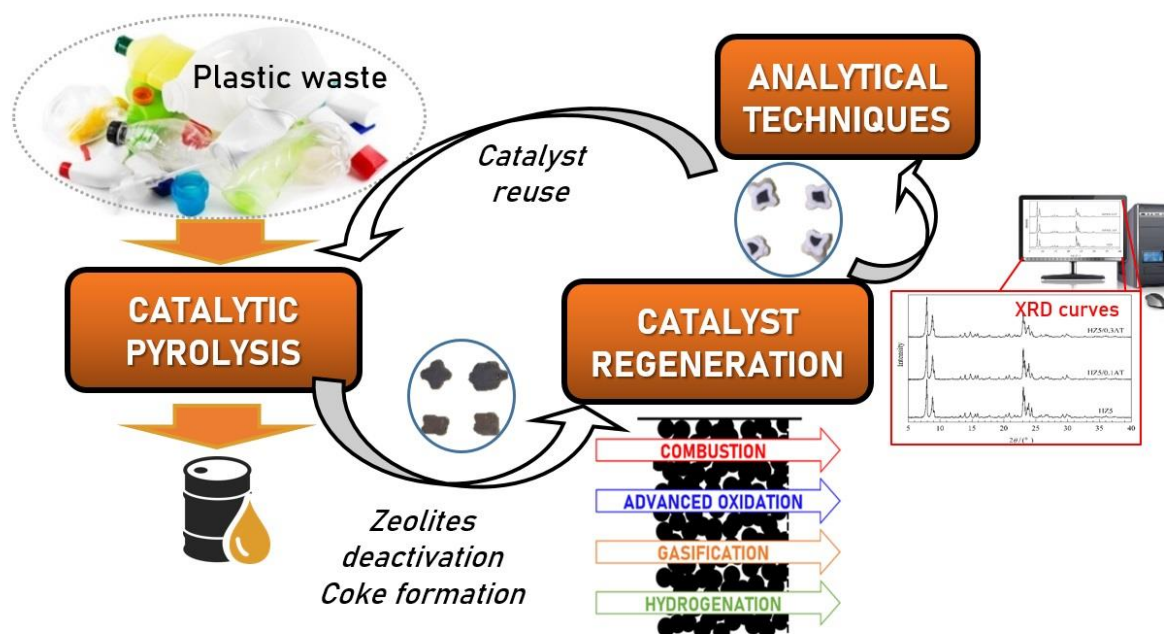
This chapter presented the theoretical background necessary to approach the research project developed in this PhD thesis: ozonation regeneration of ZSM-5 deactivated by coke formation during catalytic pyrolysis of polyethylene. As this combined scope is really precise and has not been treated so far in the literature, its main different aspects were presented in separate sections: zeolites properties and applications, catalytic pyrolysis of plastics, deactivation via coke formation of catalysts and regeneration of so-deactivated materials. The key takeaways of this chapter are summarized in Figure 1.30.



A review article based on this chapter was published in *Catalysts* (MDPI) in June 2021 (Volume 11, Issue 7, 770).

“Deactivation and Regeneration of Zeolite Catalysts Used in Pyrolysis of Plastic Wastes – A Process and Analytical Review” – V. Daligaux, R. Richard, M.-H. Manero

Access: <https://doi.org/10.3390/catal11070770>





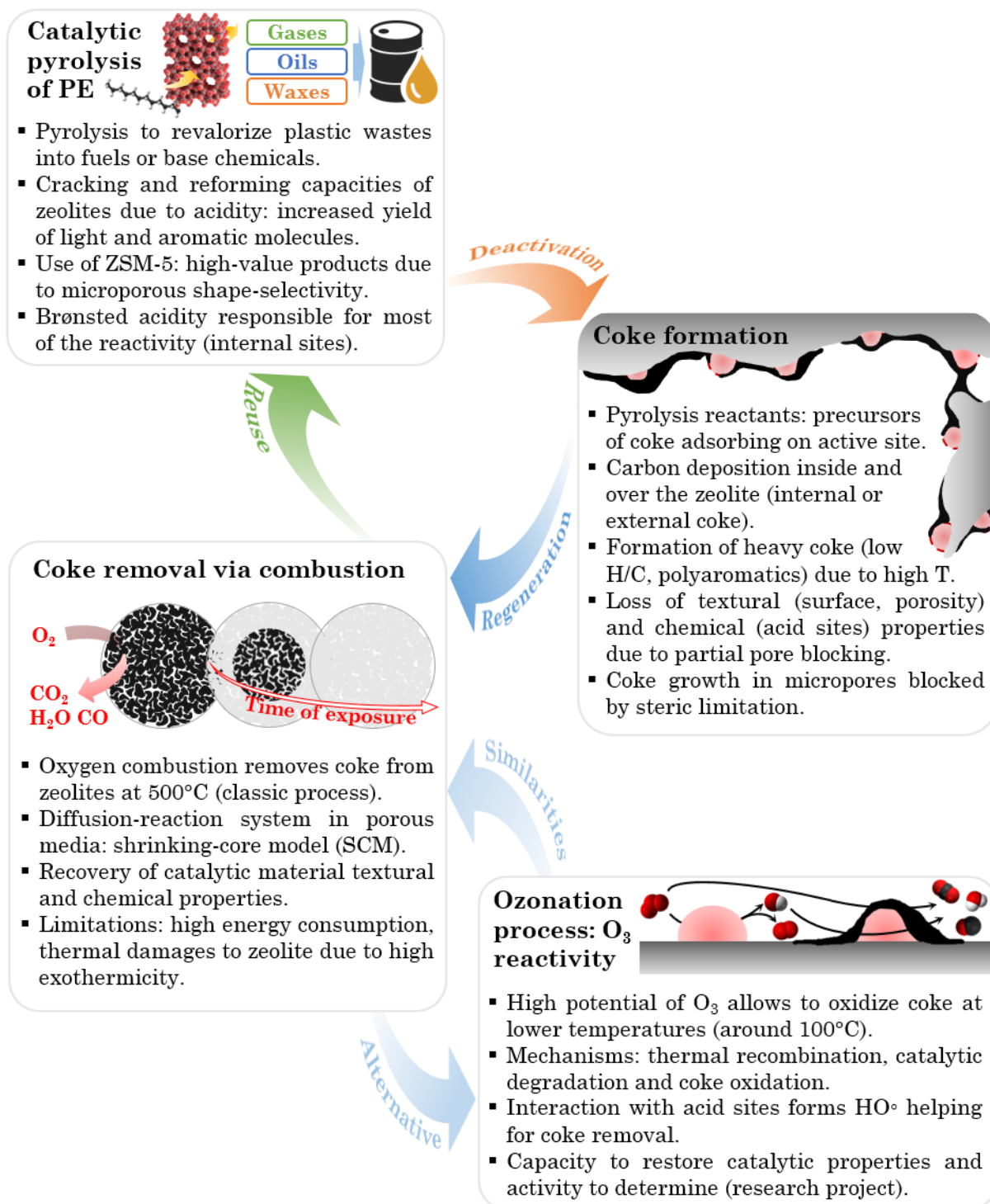


Figure 1.30. Key takeaways of “Chapter 1 - Theory and literature review”.

# Chapter 2

## Analytical review and experimental methods

In this chapter, an overview of analytical techniques used in the literature for the characterization of zeolites and coke compounds is presented in Section 2.1. Methods presented in this analytical review are not all used in the PhD work but it provides better insight of what is usually done and where the research project stands in the domain. Based on this contextual knowledge, the methodology of the two main experimental parts investigated in this work are detailed in Section 2.2: catalytic pyrolysis of polyethylene using zeolites and regeneration by ozonation of so-used catalysts. The experimental setups and procedures, as well as implemented analytical techniques are described for each process in Section 2.2.2 and 2.2.3 respectively.

### 2.1. Analytical review

The following section presents the main relevant analytical techniques used in the field of catalyst deactivation and regeneration, from fresh, spent and regenerated catalysts to the analysis of deactivating species, allowing the characterization of both crystalline zeolites and coke molecules structure. The different possible analytical techniques found in the literature are categorized by type of information provided.

**Table 2.1.** Principal analytical techniques found in the literature used for the characterization of fresh and deactivated catalysts.

Desired information	Analytical technique
Crystalline structure: zeolite type, PSD.	X-Ray Diffraction (XRD) + SAXS
Surface aspect image, particle size.	Electron microscopy (SEM, TEM)
Elemental analysis: Si/Al ratio for zeolites.	X-Ray Fluorescence spectrometry (XRF)
Porosimetry analysis: surface area, pore volume	Physisorption of N <sub>2</sub> (or other inert mol.)
Surface acidity: concentration, strength, type.	Chemisorption of NH <sub>3</sub> (or other probe mol.)

### 2.1.1.1. Catalyst characterization

Table 2.1 gathers the main different analytical techniques that are used for the study and characterization of fresh, spent and regenerated catalysts. A combination of several of these analyses provides complete description of catalyst characteristics in order to follow the evolution of new virgin catalyst, deactivated catalyst after process use and recycled catalyst after regeneration.

#### 2.1.1.1.1. Structural and physical properties

The most commonly used technique for the study of catalyst structure is X-Ray Diffraction (XRD), which determines the bulk structure and composition of heterogeneous catalysts with crystalline structures, but also the average crystallite grain size and the particle size distribution (PSD). The characteristic patterns of common zeolite structure are used to identify catalyst. XRD analysis can be used as a comparative tool between fresh and deactivated catalysts, before and after reaction, to check any possible structural changes or damages. Alvarez *et al.* observed a structural change of ZSM-5 zeolite from orthorhombic to tetragonal structure using XRD method [181]. This modification was attributed to zeolite channel occupation by coke molecules formed during the conversion of methanol to hydrocarbon. However, XRD analysis technique is limited to crystalline phases and is not suitable to analyze amorphous or highly dispersed phases. Use of electron microscopy (EM) is also very common as it provides a visual representation of the catalyst surface. Comparison of surface images of the catalyst are often compared to visually illustrate formation of coke. Thanks to the SEM photographs represented Figure 2.1, Lopez *et al.* observed a difference between fresh (a) and spent (c) surface of ZSM-5 zeolite used for catalytic pyrolysis of plastic wastes [93]. While crystal size of fresh zeolite is in the range of 100-300 nm, deposition of coke leads to the agglomeration of particles and to crystal size growth in the range of 300-900 nm. Two modes of electron microscopy are possible: by scanning (SEM), used for imaging at a micrometer scale, or by transmitting (TEM), providing images down to the nanometer scale and therefore mostly used for nanosized catalysts such as metal oxide particles, supported metals and catalysts with nanopores [198, 199]. Electron microscopy is often coupled with energy-dispersive analysis of X-Rays (EDX) to add elemental data. Catalyst composition provides important data on zeolites such as silica to alumina ratio giving an indication on catalyst acidity [184]. This characteristic is commonly determined with X-Ray fluorescence (XRF) spectrometry, which is particularly well suited to investigate the bulk chemical analysis of major elements. XRF is very commonly used as a primary analysis for catalyst characterization. For example, Ajibola *et al.* used XRF analysis to compare Si/Al ratio of natural and synthesized Y-zeolite Nigerian kaolin zeolite, with respectively 3.22 and 1.45 ratios, furtherly used for catalytic cracking of polyethylene [200]. Many other optical and surface-sensitive techniques are relevant for fresh or deactivated catalyst characterization, which are classified following their capacity to emit or absorb photons (i.e. NMR, IRFT, DRX, UV, etc.), electrons (i.e. XRF, TEM, ESR, etc.) or neutrons and ions (i.e. SIMS, LEIS, etc.) [201, 202]. These techniques are used for elemental analysis but can also provide relevant data on the adsorbed species. As an example, Chen *et al.* used a combination of <sup>13</sup>C NMR, FTIR and UV-Vis to characterize coke formed over a Y-zeolite during catalytic pyrolysis of PE [79]. Deconvolution of NMR spectra provided them with a very precise description of coke nature (aliphatic, aromatic), amount and repartition.

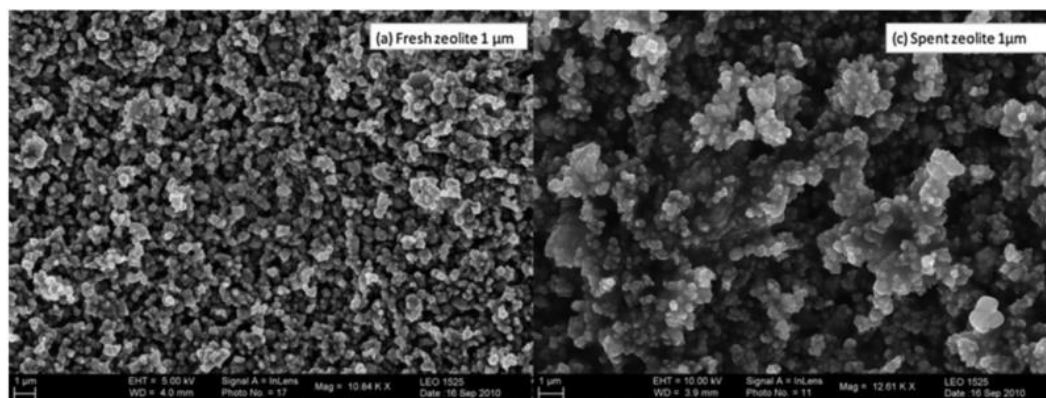


**Figure 2.1.** SEM images of fresh and aged ZSM-5 zeolite used for catalytic pyrolysis of plastic wastes (López *et al.*, 2011) [93].

In spite of the overall structure and composition of the catalyst, the determination of the surface area and volume of pores is very important for the characterization of solid catalysts since these parameters have been proved to be correlated with catalytic activity [77, 79]. The most common technique used for this measure is the N<sub>2</sub> adsorption and desorption experiment. Comparison of results for a fresh and deactivated catalyst emphasizes the direct impact of carbon deposition on catalyst surface area and pore characteristics [149]. During the catalytic pyrolysis of PE in a conical-spouted bed reactor carried out by Elordi *et al.* with different zeolites, coke deposition led to the reduction of BET surface area, 19% and 39% for HZSM-5 and HY zeolites respectively, as well as micropore area [71]. By comparing results between fresh and spent catalyst, relative accessibility to catalytic active sites can be determined and coke location can be hypothesized from pore volume repartition and variation. Other inert molecules can be used to get as close as possible to the real reaction conditions: use of an inert probe molecule having a similar size to the reactant leads to the determination of the surface area effectively accessible during the reaction. For zeolites used for n-heptane cracking, Magnoux *et al.* used inert n-hexane as a probe having similar dimensions with the reactant and, for some of the investigated zeolites, observed a variation of accessible surface area compared to N<sub>2</sub> measurement due to their shape-selectivity [93]. As re-reported in the following paragraph, adsorption experiments are also useful for the de-termination of chemical properties of catalysts by analyzing interactions between the probe molecule and catalytic surface.

### **2.1.1.2. Chemical properties and reactivity**

As mentioned previously, using specific probe molecules interacting with active sites in adsorption-desorption experiments ensure the extraction of additional chemical information. This technique, referred to as Temperature-Programmed Desorption (TPD), is commonly used to study the reactivity and acidity of catalytic active sites. Temperature at which desorption occurs indicates the strength of the acid sites while probe molecule quantity consumed or released is related to their concentration over the external and internal accessible surface of the catalyst. Formation of coke leads to an inevitable decrease of catalytic acid site concentration due to the loss of active surface. The most common molecules used as probes are NH<sub>3</sub> and CO<sub>2</sub> for acidic and basic site identification respectively. Experiments with some other molecules, such as H<sub>2</sub>O or pyridine, were also carried out in literature to get more specific information [202]. For instance, using pyridine

as probe molecule ensures the differentiation between Brønsted and Lewis acid sites, which is not possible with  $\text{NH}_3$ . Engtrakul *et al.* used combined  $\text{NH}_3$ -TPD, to quantify the total number of acid sites, and pyridine DRIFTS (diffuse-reflectance FTIR spectroscopy) to probe their nature and repartition (Lewis or Brønsted sites) over a ZSM-5 zeolite used for pine pyrolysis vapor reforming [203]. Moreover, combined reactor and analysis (FTIR, UV-Vis, etc.) over aged catalysts can be used to study the effect of coke over active sites, especially if used operando, offering observation of catalyst acidity evolution and coke nature as deactivation progresses. Goetze *et al.* used operando UV-Vis spectroscopy to monitor the formation of hydrocarbon pool species leading to the accumulation of coke during the methanol-to-olefins process over HZSM-5 zeolite [204]. Pyridine being a relatively large molecule, its use is limited to catalysts with particular geometry, especially pore apertures, allowing its diffusion within its pores, and is not applicable to zeolite material with small pores and channels, such as HFER [205]. Consequently,  $\text{NH}_3$ -TPD experiment remains the most commonly used method for catalyst acidity measurement due to its wide application range and to its weak basicity, avoiding coke molecule “replacement” when analyzing aged catalysts. Comparison of fresh and spent catalyst  $\text{NH}_3$ -TPD spectra provide information about the remaining acid sites and therefore catalytic activity. Figure 2.2 represents comparative TPD experiments for a USHY zeolite deactivated by 1-pentene with and without  $\text{NH}_3$  probe adsorption. The difference between desorption behavior in the presence or absence of  $\text{NH}_3$  ensures the determination of free acidity since desorption without a probe molecule is only due to coke [206]. From raw TPD experiment curves, deconvolution calculations are necessary to determine the total amount and the strength of catalytic acid sites, as carried out by Khangkham *et al.* for the characterization of zeolites furtherly coked during PMMA cracking [160].

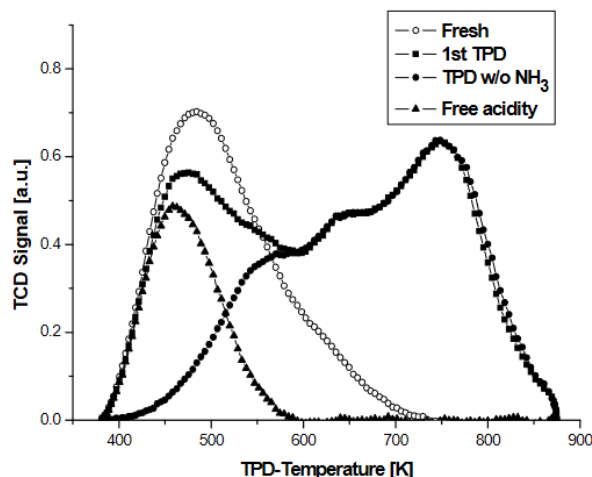


**Figure 2.2.** Determination of free acidity of deactivated USHY zeolite via TPD experiments using  $\text{NH}_3$  as probe molecule (Schmidt *et al.*, 1982) [198].

### 2.1.2. Coke analysis

The following table (Table 2.2) gathers the main different analytical techniques that are used for the study and characterization of coke and deactivating species. Extensive research has been carried out to understand the phenomenon of coke formation, aiming to determine the involved mechanisms and kinetics thanks to one or a combination of these analytical techniques.

**Table 2.2.** Principal analytical techniques used for the analysis of deactivating species over solid catalysts.

Desired information	Analytical technique
C, H, N, S contents H/C ratio	Elemental analysis
Global coke content, H/C ratio Coke reactivity and optimal oxidation temperature	Temperature-Programmed Oxidation (TPO)
Coke nature: aliphatic, aromatic Coke effect on active sites	FTIR, Raman
Coke nature: unsaturated compounds	UV-Vis
Coke nature and location Structural degradation	NMR and XRD
Chemical nature of coke Distribution of coke components	Coke extraction + analysis (see Figure 2.4)
Coking and deactivation kinetics	Tapered Element Oscillating Microbalance (TEOM)
Coke amount and thermal degradation products	Thermogravimetric Analysis (TGA)

### 2.1.2.1. Nature and composition

Elemental analysis is the first approach to characterize coke in order to obtain a rough composition of species causing deactivation. Commonly used elemental study is carried out by combustion of deactivated catalyst with CHN elemental analysis and provides C, H, N and S contents. Therefore, this technique determines the H/C ratio, which is the principal characteristic giving indication of the average nature of coke. Elemental analysis is also used to determine regeneration process efficiency via calculating carbon removal proportion. Richard *et al.* used this criterion to evaluate the influence of ozonation operating parameters for the regeneration of industrial coked zeolites and achieved a maximum of 74.3% carbon removal [9]. The main limitation to this analysis is the potential presence of hydroxyl groups or water molecules within the catalyst that may distort the actual coke composition [207]. Moreover, obtained data is only an average value while coke nature and content may vary alongside the catalyst bed or even within a single pellet because of diffusion limitations.

Temperature-Programmed Oxidation (TPO) analysis provides important data on coke nature showing successive steps during coke combustion [116]. This experiment consists in exposing deactivated catalyst to oxygen flow at varying temperatures. Thanks to mass loss, determined by microgravimetry, and to formed products during oxidation, commonly analyzed in-line via GC-MS, it is possible to extract information about coke nature. Some data concerning global oxidation mechanisms are also available from TPO curves, typically showing distinct oxidation peaks for hydrogen (H<sub>2</sub>O firstly observed) and carbon removal (mixed CO/CO<sub>2</sub>) [117]. Chen *et al.* used TPO experiments to characterize coke formed over Y-zeolite during catalytic pyrolysis of PE and observed, from the deconvolution curves (dash lines) represented on Figure 2.3, two types of coke: external coke with a peak temperature at 400-433°C and internal coke oxidized at 464-488°C [79]. TPO analysis is a very widespread method in the field of catalyst deactivation as it



provides very complete data concerning coke (global content and H/C ratio) determined from the oxidation products. Even though this technique does not offer precise characterization of coke nature, it is widely used to determine the optimal temperature for regenerative treatments via oxidation. While oxygen is the most common molecule used, using other molecules is possible and are referred to as Temperature-Programmed Surface Reaction (TPSR) [201].

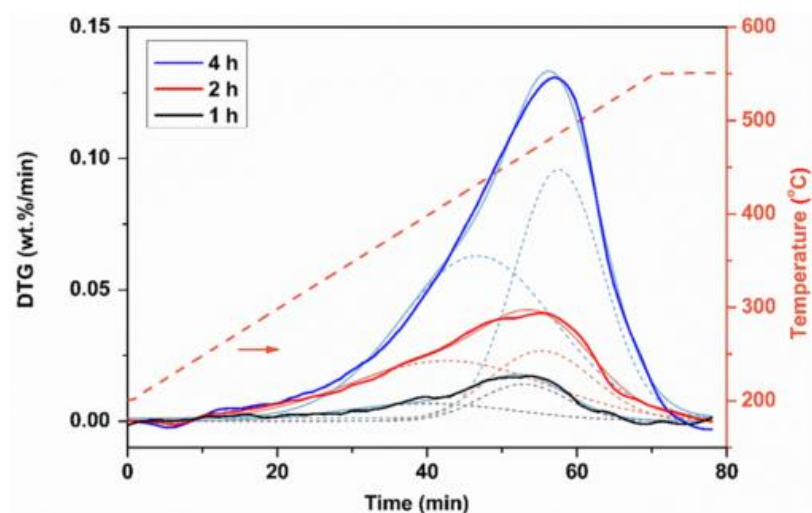


**Figure 2.3.** TPO curves and deconvoluted peaks of Y-zeolite coked during catalytic pyrolysis of PE at different TOS (Chen *et al.*, 2021) [79].

Different analytical techniques are relevant for in situ characterization of coke, for which being non-destructive methods are a main advantage, providing successive analysis for a single sample. IR and UV-Vis spectroscopy, XRD and NMR techniques are commonly used to further investigate coke molecule nature and location. Implementation of operando analysis is very interesting as it becomes possible to monitor simultaneously reaction advancement and modifications of catalyst due to coke formation [202]. Guisnet *et al.* developed a very complete method, presented in Figure 2.4, to determine the chemical nature and distribution of coke compounds on deactivated catalysts [90]. This method

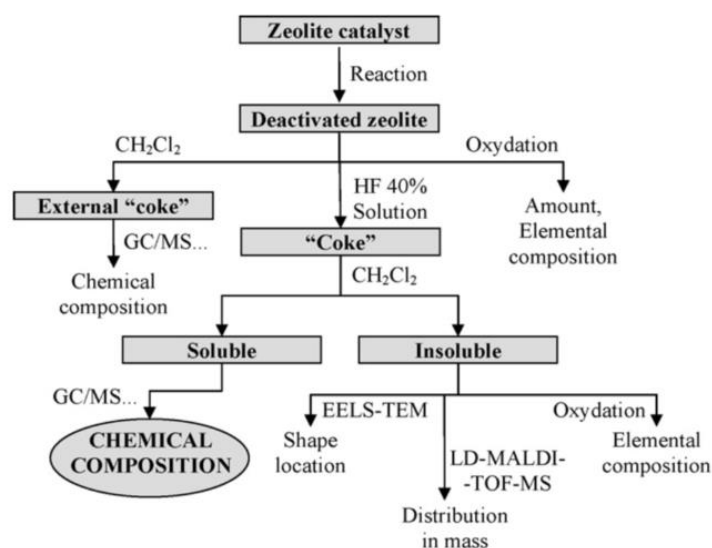


**Figure 2.4.** Method for determination of zeolite coke nature and composition developed by Guisnet *et al.* (graphical abstract from Guisnet *et al.*, 2009) [89].

relies on the partial solubility of coke in  $\text{CH}_2\text{Cl}_2$  and on its absence of reactivity with hydrofluoric acid to separate coke from zeolite structure without modifying chemical nature of molecules. Soluble coke is afterwards characterized by further analysis such as gas-chromatography coupled with mass spectrometry (GC/MS) or other relevant techniques. However, the heavier fraction of coke may remain insoluble in  $\text{CH}_2\text{Cl}_2$  and analysis is limited to elemental composition and shape location within catalyst pores.

### **2.1.2.2. Reactivity and kinetics**

Kinetic study of coke formation is challenging due to the complexity of coke formation mechanisms and competing reactions. Therefore, they are not easily determined thanks to analytical methods. The main approach reported in literature is to decompose the overall coke formation into single elementary steps in order to develop precise kinetic models. However, this approach is only a modelling method and is not observable with analytical techniques. Operando mass measurements on microbalance versus time are usually used to determine the overall reaction rate of coke formation. The mass increase of catalyst during reaction can be related to a reaction rate when reported to a time unit. Conventional microbalance coupled with the reactor are conceivable for *in situ* monitoring (microgravimetry), but use of Tapered Element Oscillating Microbalance (TEOM) provides more precise measurements thanks to the detection of oscillation frequency variation of the plate caused by sample mass increase [208]. Using this apparatus, Gomm *et al.* investigated the *in situ* deactivation of various zeolites during conversion of 2-propanol and were able to correlate the change of reactivity due to coking with mass changes of the catalyst [209].

A similar approach is adopted when using Thermo Gravimetric Analysis (TGA) as a continuous-flow microreactor to monitor coke levels with coupled on-line GC to measure activity [210]. A mathematical model, the Constant-Coke Arrhenius Plot (CCAP), has been modified and used to determine the active site suppression and pore choking during REY zeolite deactivation used in cumene cracking. This method investigates the direct influence of coke formation over catalytic activity. Some experiments transposed this coupled analysis to investigate the evolution of coke levels during catalyst regeneration thanks to a combined TPO-TGA analysis with on-line product analysis [211]. The data obtained by this coupled analysis gave information on the type of carbons obtained at different oxidation temperatures: either amorphous carbons (oxidation at  $<600^\circ\text{C}$ ) or filamentous carbons (oxidation at  $>600^\circ\text{C}$ ). Kinetic modelling is often based on TPO spectrum modelling using a linear combination of kinetic power-law expressions and monitoring carbon oxide concentration evolutions ( $\text{CO}_2/\text{CO}$  ratio). These models integrate variable input parameters such as oxygen concentration or heating rate influencing oxidation kinetics. Kinetic parameters are determined using models that best fit experimental data [117, 122].

## **2.2. Experimental material and methods**

### **2.2.1. Products and chemicals**

#### **2.2.1.1. Polyethylene**

Plastic feedstock used during pyrolysis experiments is virgin low-density polyethylene (LDPE, CAS n°9002-88-4), provided by Sigma-Aldrich (ref. 428043-1KG) in the form of



spherical pellets ( $\approx 3\text{-}4\text{ mm}$ ) as illustrated in the picture (Figure 2.5). Material density is given at  $925\text{ kg}\cdot\text{m}^{-3}$  with a melt index value of  $25\text{ g}/10\text{min}$ . Polymer is used as received without any treatment prior to loading in pyrolysis reactor. TGA curves for different heating rates are presented in Appendix 1.



Figure 2.5. Polyethylene used as plastic feedstock for pyrolysis experiments.

### 2.2.1.2. Zeolite catalysts

Catalysts used in this work are commercial HZSM-5 zeolites provided by Tosoh Company (ref. HSZ-822HOD1A) in the form of cylindrical pellets. The provided material has a  $\text{SiO}_2/\text{Al}_2\text{O}_3$  molar ratio of 23.9 with  $\text{H}^+$  as compensating cation. Zeolite crystals are shaped into cylindrical pellets using alumina binder. Given diameter is  $1.5\text{ mm}$  and grains length repartition is between  $2$  and  $8\text{ mm}$  with an average value of  $4\text{ mm}$  (Figure 2.6). Bulk density is provided by the furnisher while pellet density has been experimentally approximated by measuring the mass with a precision balance and evaluating the dimensions, thus the volume, with digital caliper of limited number of pellets (2 to 5, measurements repeated twice). Measurements and calculations for the determination of pellet density are presented in Appendix 2. Given poured density of the catalyst in bulk is  $680\text{ kg}\cdot\text{m}^{-3}$  and the calculated pellet density is rounded to  $1300\text{ kg}\cdot\text{m}^{-3}$ . Prior to catalytic degradation experiments (Section 2.2.3.2.a), fresh zeolites are placed in an oven during 24h at  $120^\circ\text{C}$  to remove adsorbed water from zeolite material, and are then stored in a dry atmosphere. Otherwise, for all other experiments, catalysts are used as received without any crushing or pretreatment step.



Figure 2.6. ZSM-5 catalysts for deactivation (pyrolysis) and regeneration (ozonation) studies.

### 2.2.1.3. Chemicals and gases

The list of chemicals and products used in this work during the different steps of experimental methodology, from the catalytic pyrolysis of LDPE to the ozonation of spent catalysts as well as the required analytical techniques, are presented in Table 2.3. The respective application is indicated for each product.

**Table 2.3.** Specifications of supplementary gases and chemicals used in experimental section.

Product	Application
<b>Gases</b>	
Nitrogen (on-site generator)	Inerting and sweeping in pyrolysis reactor
Oxygen ( $\geq 99.5$ vol.%, Linde B50)	Ozonation pilot feed
Oxygen and dry air	Characterization of zeolite
Liquid nitrogen	Characterization of zeolite
<b>Chemicals</b>	
Dichloromethane	Extraction of soluble coke
Pyridine	Characterization of zeolite
Heptane	Dilution of pyrolysis oils for GC-MS analysis

## 2.2.2. Catalytic pyrolysis of polyethylene

### 2.2.2.1. Experimental setup

Catalytic pyrolysis experiments were carried out in a bench scale semi-batch reactor designed and built during the first year of the PhD in collaboration with LGC technical service (referring technician: Thomas Ménager). Relevant schematic diagrams are given in Appendix 3 (reactor, condensers, etc.). The resulting experimental pilot is illustrated in Figure 2.7 (photographs) and presented in Figure 2.8 (PID of the installation). The different elements of the setup, presented in the following paragraphs, are divided in two principal blocks connected to each other with insulated stainless steel tubing (ID: 4 mm, ED: 6 mm). All the sensors in the installation, which are connected to a control panel and recording device, are summarized in Table 2.4.

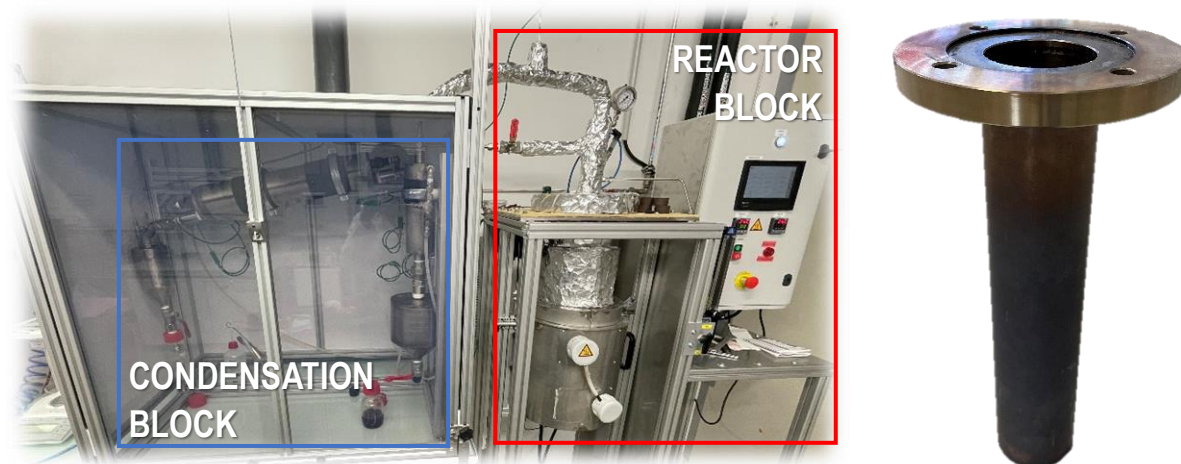


**Figure 2.7.** Photographs of the pyrolysis experimental pilot with the main different blocks, and bottom part of the reactor where feedstock is loaded.

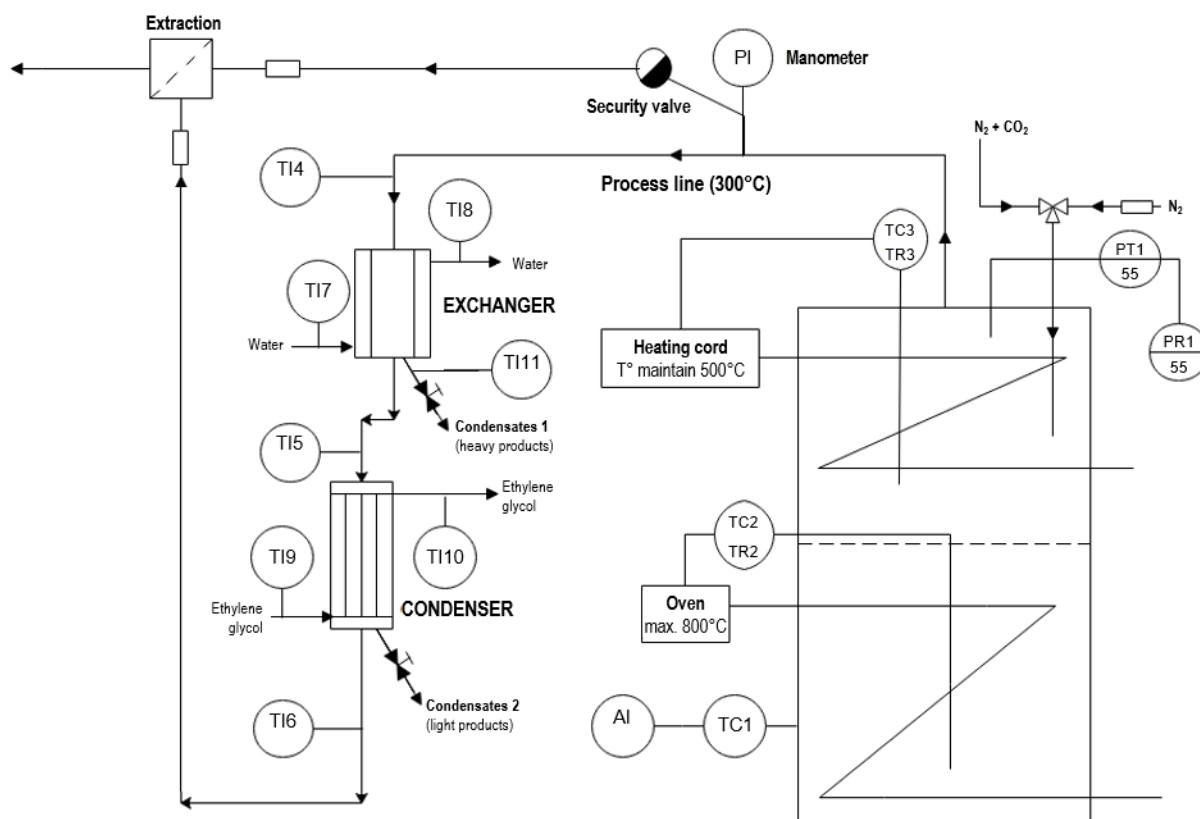


Figure 2.8. PID scheme of pyrolysis experimental setup.

Table 2.4. Temperature (T) and pressure (P) sensors of the installation.

Sensor reference	Location and use
TC1	External surface of the reactor, close to heating shells. Placed in a thimble and has to be placed just above the reactor wall.
TC2, TR2	Internal reactor temperature (pyrolysis stage). Regulation for target temperature is based on this sensor.
TC3, TR3	Internal reactor temperature (reforming stage). Maintained with 375 W heating cord (close to regulated target).
TI4	Process line (between reactor and condenser n°1). Maintained with 125 W heating cord (resulting temperature around 300°C).
TI5	Process line (between condenser n°1 and condenser n°2).
TI6	Process line (between condenser n°2 and extraction).
TI7	Demineralized water inlet (condenser n°1).
TI8	Demineralized water outlet (condenser n°1).
TI9	Ethylene glycol inlet (condenser n°2).
TI10	Ethylene glycol outlet (condenser n°2).
TI11	External surface of the 1 <sup>st</sup> guard (after condenser n°1). Maintained to condenser n°1 cooling fluid temperature with heating cord.
PT1, PR1	Internal reactor pressure sensor and regulation for security alarm if P is superior to 5 bar abs.

*a. Reactor unit*

The reactor block is a stainless steel column of internal dimensions 70 mm (diameter) and 500 mm (height). Corresponding internal volume capacity is approximately 2 L. External diameter is 110 mm. The column can be separated in two parts to allow reactor loading, referred respectively as the pyrolysis stage (bottom) and reforming stage (top). Junction and sealing between the two levels is ensured by 4 bolt, washer and nut assemblies and a high-temperature resistance gasket. The pyrolysis stage is inserted in two regulated shells containing high-voltage electric resistance meant for heating the reactor. In order to maintain the temperature in the upper part of the reactor, the reforming stage is circled by a heating cord (max. 375 W) and wrapped with insulating wool. The reactor ceiling is drilled with two stitchings: for nitrogen (and/or carbon dioxide) feed and for products circulation. The first, equipped with a check valve, is used to inert the reacting media and to generate a flushing for products. Nitrogen injected for inerting is generated on-site. The second line, referred as the process line, allows the circulation of gases to the condensation stages. The process line is also insulated and equipped with a heating cord (max. 125 W) to maintain the temperature (around 300°C) during the transition to first condensation stage.

*b. Condensation unit*

The condensation block consists in two successive stages with different temperatures intended for products fractioning. These two stages have been designed to separate heavy products with a “low-performance” (LP) exchanger and light products with a “high-performance” (HP) condenser. The first condensation level is a double envelope stainless steel heat exchanger (internal diameter 30 mm). Demineralized water circulates through the envelope (from bottom to top, see Figure 2.8) at a chosen temperature between 20 and 80°C thanks to a thermostatic bath. Condensates are collected in a 1 L guard placed downstream and equipped with a valve allowing operator to sample the desired amount of products at any time. While in the guard, products are maintained to the first condenser temperature thanks to adequate insulation and heating cord around the container. Stitching drilled in guard ceiling allows remaining gases to circulate through insulated process line to the second condensation stage. The second condenser is a high performance heat exchanger with double envelope for increased contact surface. Cooling fluid (ethylene glycol) entry is connected to a refrigerated unit allowing a temperature range between 0 and 50°C. Similarly to the first stage, condensates are collected in a valve-equipped guard (0.5 L) with an adequate fitting for the operator to place a bottle. This second guard is not insulated and stitching in its ceiling allows incondensable gases to circulate to extraction.

**2.2.2.2. Operating procedure**

During a typical pyrolysis experiment, 200 g of polyethylene are loaded in the reactor with 20 g of zeolite (fresh, spent or regenerated). This 10:1 mass ratio is identified in the literature as a commonly used value, and integrated in our protocol for comparison purposes [93, 197]. In this work, polymer pellets and zeolites were loaded in two different ways to study the potential influence of initial mixing. Additionally to the schematic representation of pyrolysis pilot, Figure 2.9 represents the different loading methods: either the 20 g of zeolites are simply poured over the plastic pellets (called “top” experiments) or they are placed in successive layers of 50 g LDPE / 5 g HZSM-5 starting

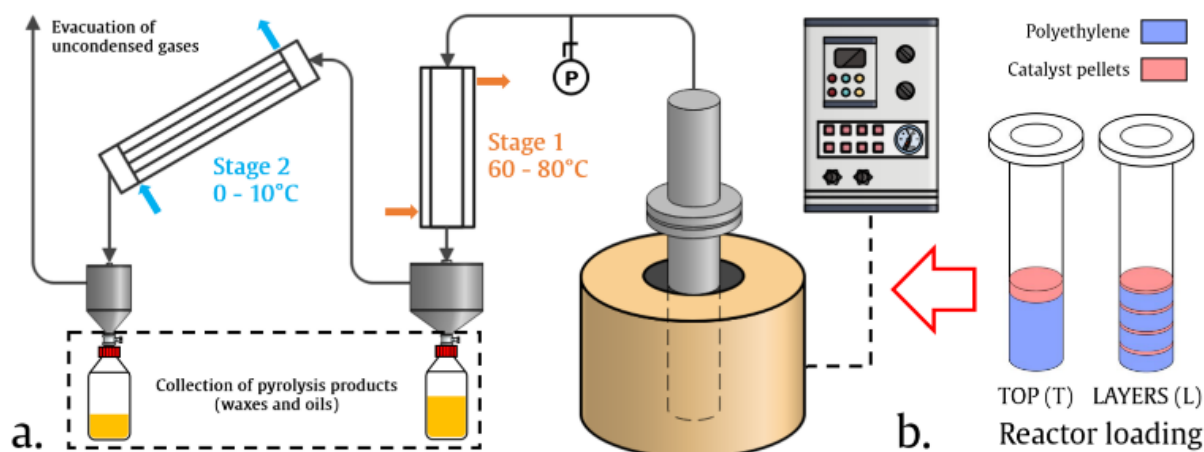


**Figure 2.9.** Scheme of (a) experimental setup for pyrolysis of polyethylene and (b) reactor loading methods. Figure extracted from submitted article presented in Chapter 3.

by 50 g of LDPE at the bottom of the reactor (called “layers” experiments). After sealing the reactor and inerting the atmosphere,  $N_2$  flushing is turned off and the reactor is heated up to 450°C during 40 min. It should be noted that the current PID regulation of the pilot implies an important heating rate of 40°C/min, very superior to the classic value of 20°C/min found in the literature, which leads to an overshoot of 30°C over the target temperature. Maximal temperature observed in the reactor during typical run is therefore 480°C before stabilization. After 40 min,  $N_2$  circulation is turned back on with a flow-rate of 2 L.min<sup>-1</sup> to flush the decomposition components remaining in the reactor. After going through the reforming stage, the gases formed during the catalytic cracking flow through the two successive stages of condensation. The cooling-down temperatures at each stage are respectively 80°C (water) and 0°C (ethylene glycol). The condensed vapors are subsequently collected as pyrolysis waxes and oils for analysis, while the uncondensed products are evacuated to extraction. After appropriate waiting time for natural cool down (around 6 h), used catalysts are recovered and collected for characterization. No other solid residues are found on top of coked zeolites showing complete LDPE conversion.

In order to study the deactivation of ZSM-5 catalysts during these pyrolysis experiments, catalysts were used up to 5 successive times in top or layers experiments without any treatment between pyrolysis runs. For characterization purposes, 100 mg of zeolites were sampled between each experiment. For each experiment, three samples are collected for analysis (see analytical techniques in Section 2.2.4): two fractions of pyrolysis products corresponding to the two condensing stages and spent zeolites. For some experiments, products were only collected at the first collecting point because no products were obtained at the second condensation stage. Notation of samples and journal of pyrolysis experiments carried out during the PhD work are summarized with corresponding labelling in Appendix 4.

### 2.2.2.3. Results exploitation

In this work, catalytic pyrolysis is used as a model reaction to study the deactivation and regeneration of used ZSM-5. Their catalytic activity is assessed based on the results of GC-MS analysis of pyrolysis products. According to the identification of molecules based on chromatogram peak attribution (Section 2.2.4.1), proportions of products are determined thanks to their respective peak area. Identified products are furtherly sorted

based on their number of carbons and aromaticity character to evaluate the evolution of cracking and reforming capacities of the catalysts used in pyrolysis. Molecules are categorized in three fractions corresponding to their nature and potential use: gasoline (C7-C9), kerosene (C10-C14) and waxes (C15+). Aromatic compounds proportion is evaluated both in global content and in each fraction. The products proportions for the different categories are calculated as follows (Equation (2.1)):

$$P_{\alpha} = \sum_{i=1}^n \frac{\text{Peak area of identified product } i}{\text{Total chromatogram area}} \quad (2.1)$$

Where  $\alpha$  is the category of interest (C7-C9, C10-C14, C15+, aromatic or not),  $i$  is an identified molecule included in this category and  $n$  the total number of peaks concerned. Unfortunately, quantitative analysis of pyrolysis yield is not possible, as mass balance was not achieved for the initial experiments due to deposition of waxes in the process lines and to evacuation of incondensable gases. As determining the repartition of these losses was not achievable, the choice was made of doing a semi-quantitative study based on the comparison of GC-MS results between experiments. Pyrolysis yields were not calculated as it was estimated that such material balance would not be accurate since the gas fraction is not collected and a loss of condensed products is observed in the conducts. Catalytic efficiency is measured by following the evolution of pyrolysis condensed products nature. The term of catalytic selectivity is consequently preferred to catalytic activity in this work. Proportion of aromatics and repartition of molecules according to their number of carbon in the oils are used as a descriptor of catalytic performance during pyrolysis. The exploitation of pyrolysis results therefore presents some gaps, caused by the recent development of the pilot, that could be corrected in future studies with methodology and pilot improvements.

### 2.2.3. Ozonation of coked catalysts

#### 2.2.3.1. Experimental setup

Ozonation experiments were carried out in a glass reactor in which zeolites are loaded as a fixed-bed. Two reactor configurations have been used in this work with different zeolite loading capacities: tubular reactor ( $\approx 1.5$  g) and syringe reactor ( $\approx 10$  g). The principal characteristics for each configuration are summarized in Table 2.5.

**Table 2.5.** Catalytic bed and gas stream characteristics for the two different reactor configurations of ozonation experimental setup.

Characteristic	Tubular reactor	Syringe reactor
Catalytic bed		
<i>Mass capacity (g)</i>	1.5	10
<i>Diameter (mm)</i>	4	14
<i>Height (mm)</i>	200	90
<i>Porosity <math>\varepsilon</math> (-)</i>	$0.54 \pm 0.02$	$0.54 \pm 0.01$
Gas stream		
<i>Volumetric flowrate <math>Q_V</math> (<math>L.h^{-1}</math>)</i>	50 to 150	
<i>Ozone concentration <math>C_{O_3}</math> (<math>g.Nm^{-3}</math>)</i>	0 to 80	
<i>Ozone mass flowrate <math>Q_{O_3}</math> (<math>g_{O_3}.h^{-1}</math>)</i>	0 to 6	
<i>Superficial velocity <math>u_0</math> (<math>m.s^{-1}</math>)</i>	1.1 to 3.3	0.1 to 0.3
<i>Residence time <math>\tau</math> (s)</i>	0.18 to 0.06	0.90 to 0.30



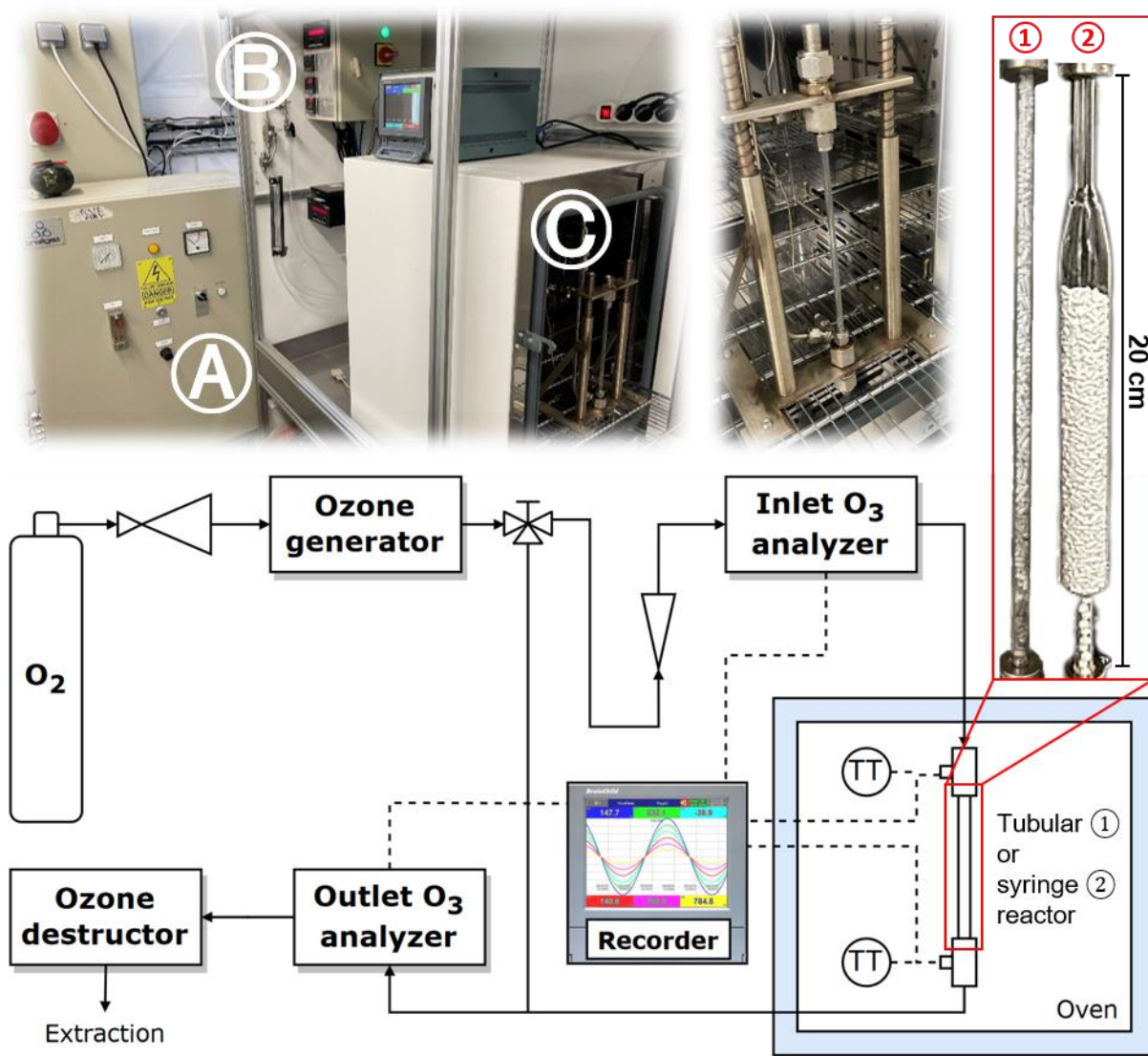


**Figure 2.10.** Photographs and scheme of experimental ozonation setup with tubular and syringe reactor configurations. A, B and C elements correspond to the following paragraphs.

Photographs and scheme of the experimental pilot and reactors are presented in Figure 2.10. The different elements of the installation, presented in the following paragraphs following the same letter notation as in the scheme in logical order from feed to extraction, are connected to each other with Swagelock<sup>®</sup> fittings and 4/6 mm tubing (internal/external diameter) made of stainless steel when exposed to heat and of plastics material otherwise. Thermocouples and analyzers are linked to a display and recording device (Brainchild PR2006).

On top of mandatory personal protection equipment (PPE) use during the experiments for security purposes, the laboratory room is equipped with two ozone detectors (Dräger Company), one in the gas extraction conduct and the other in the room. These sensors are set to detect ozone leaks by activating an alarm and automatically cutting gas circulation when fixed limit is exceeded (0.1 ppm). To avoid such problem occurrence, potential leaks on the setup are checked on the different junctions of the setup before any manipulation by flowing pure oxygen without any ozone production.



*a. Ozone generator and inlet gas stream*

The catalytic bed was exposed to an ozone-enriched gas flow where O<sub>3</sub> is produced onsite by a lab-scale ozone generator (Trailgaz Labo 76) from pure and dry oxygen bottle (B50 Linde, purity > 99.5 vol.%) with high-voltage electric discharge. The required feed pressure for ozone generator is 1.7 bar abs. Oxygen feed therefore goes through two pressure reducers before ozone generator inlet: a first level decreasing from bottle pressure (initial 200 bar abs) to 5 bar abs, and a second from 5 to 2 bar abs. A built-in needle valve in the ozone generator allows to make the final feed pressure adjustment to 1.7 bar abs. Maximal gas flowrate is limited by the important pressure loss generated by the catalytic bed (atmospheric pressure at the outlet). The range of volumetric flowrate allowed by this limitation is 50 to 150 L.h<sup>-1</sup>. Gas flowrate is set downstream of the generator and upstream of inlet ozone analyzer with a volumetric manual rotameter. The production of ozone is dependent of both oxygen flowrate and applied electric power. The maximal applicable power for this apparatus is 150 W, generating ozone concentration up to 80 g/Nm<sup>3</sup> at lower flowrates (50 L.h<sup>-1</sup>). Calibration of inlet ozone concentration depending on volumetric flowrate and electric power is plotted in Appendix 5.

*b. Ozone analyzers and thermocouples*

The experimental setup is equipped with two thermocouples and ozone analyzers (BMT 964) placed in full-flow mode (in-line) to measure reactor inlet and outlet temperatures and O<sub>3</sub> concentrations. Ozone content is determined in the analyzer with a UV photometer using the particular ozone absorption band at a wavelength of 254 nm where clear oxygen and air do not produce any extinction [212]. Ozone concentration is determined based on the degree of extinction of the radiation generated by a mercury lamp, that is to say the difference between the electric signals of the “clean” radiation and after passage through the gas sample. The analyzed gas flows through a quartz cuvette which dimensions define the range of analysis. Inlet O<sub>3</sub> analyzer pressure and concentration ranges go respectively up to 2 bar abs and 100 g/Nm<sup>3</sup>, while outlet analyzer maximal analyzable pressure is 1.15 bar abs. The constructor gives an approximation of ± 0.5 g/Nm<sup>3</sup> due to the conversion to normalized volume. Thermocouples are located inside the oven of reactor unit (see next paragraph), therefore indicating system inlet and outlet temperatures and not directly gas temperatures.

*c. Reactor unit*

As illustrated in Figure 2.10, the reactor unit is placed in a controlled oven (Heratherm OGS60). Maximal target temperature is 250°C. However, the temperature range investigated in this work is between ambient temperature up to 200°C. The 20 cm-high glass reactor, whatever the configuration, is placed in a stainless steel jaw structure with springs maintaining sufficient constraint to hold the reactor. Adequate fittings with Teflon<sup>®</sup> gaskets ensure tightness at the junctions. The presence of grid-shaped flow distributor allows the homogeneous repartition of gas stream at the reactor inlet. As the gas speed is superior to fluidization velocity, gas circulation in the reactor is set downstream (from top to bottom) for practical reasons. To fill the dead volume located between flow distributor and bottom junction of the reactor, zirconium beads (3 mm diameter) are placed under the catalytic bed. In syringe reactor configuration, supplementary beads are added to also occupy the thin part of the reactor before the wide section (14 mm diameter), so that all catalytic bed is exposed to same gas velocity.

Zirconium material was chosen due to inert behavior or limited reactivity regarding ozone. Glass reactor is replaced after 10 experiments or when broken because of too important constraint, causing gas leaks. Eventually, after being analyzed at the outlet, gas stream is evacuated to an ozone destructor, consisting in a high-temperature activated carbon column, in order to degrade residual ozone before being vented to the atmosphere.

### 2.2.3.2. Operating procedures

#### *a. Thermal and catalytic degradation experiments*

Experiments on the degradation of ozone in thermal and catalytic conditions were conducted to evaluate the contribution of each mechanism. Only tubular reactor configuration is used in this procedure. For thermal recombination study, no catalyst were loaded in the reactor and only the zirconium beads were placed to use these results as a “blank”. For catalytic degradation experiments, particles of fresh zeolites were loaded as fixed bed ( $1.50 \pm 0.05$  g). The system was then heated under nitrogen flow circulating at the desired flowrate (between 50 and 150 L.h<sup>-1</sup>) until target temperature was reached. Studied temperature varied from 20 to 200°C. Prior to send the gas stream through the reactor, the ozone concentration was set and stabilized at desired value (50 g/Nm<sup>3</sup>) thanks to the 3-way valve allowing to by-pass the reactor unit. The gas flow was then switched to dry O<sub>2</sub>/O<sub>3</sub> mixture. Inlet and outlet concentrations were afterwards measured in real-time by O<sub>3</sub> analyzers. After steady-state was reached (less than a minute), [O<sub>3</sub>]<sub>in</sub> and [O<sub>3</sub>]<sub>out</sub> were monitored, being respectively the concentrations at reactor inlet and outlet. In order to avoid possible deactivation considerations, catalytic bed was replaced for each experimental conditions.

#### *b. Ozonation of coked zeolites*

The regeneration of coked zeolites has been carried out using the different reactor configurations of experimental setup according to the need: tubular reactor is preferred for parametric study while syringe reactor is used to obtain bigger quantities of regenerated catalysts for pyrolysis reuse. Different initial coked samples were used in these experiments: the initial carbon content and coke nature is dependent of number of pyrolysis successive reuses and mixing method. Coked pellets appear as black grains, traducing carbon deposition when compared to fresh white particles. Visually, coking seems homogeneous both on the outer surface and inside pellets (Figure 2.11). Carbon repartition considerations are discussed in Section 2.2.4.4. Whatever the reactor configuration, operating protocol remains identical. Similarly to previous procedure, coked samples are first loaded in the reactor as a fixed bed and system is heated up until desired

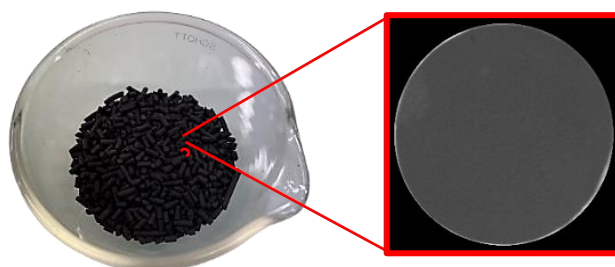


**Figure 2.11.** Illustration of coked zeolites with corresponding pellet cross-section.

temperature. The investigated range for ozonation is between 50 and 150°C. No gas circulation was here set during the time of temperature stabilization to avoid over consumption. Once target temperature is reached, dry O<sub>2</sub> stream is directed through the reactor and recording is launched. After feed pressure and flowrate adjustment, ozone production is started and inlet concentration is stabilized at desired value using power potentiometer (up to 80 g/Nm<sup>3</sup>). Time of exposure for the ozonation experiments is varied between 15 min and 8 h.

During the unloading step of tubular reactor, zeolite samples are split in three roughly even heights/volumes (around 6-7 cm), corresponding to the respective position in the reactor of the different fractions as represented opposite (H high, M middle, B bottom). The occupied height in the reactor of each fraction is annotated and samples are stored for characterization (see analytical methods in Section 2.2.4). To summarize, three samples are collected for analysis after each experiment, being different fractions of regenerated or partially regenerated zeolites according to their position in the reactor. For some experiments, only two fractions (H high and B bottom) were collected because of the difficulty to unload precise quantity. Notation of samples and journal of ozonation experiments carried out during the PhD work are summarized with corresponding labelling and operating conditions in Appendix 6.



The regeneration of coked zeolites reused in pyrolysis (R48 and R8, 20 g each, see in Chapter 3) was carried out using syringe reactor configuration in different batches of 10 g. Batches with identical operating conditions were mixed after regeneration. The first samples, labelled REG1 and REG2 in Appendix 6, were ozonated at 80 and 100°C with an ozone-enriched gas stream (100 L/h) containing between 55 and 80 gO<sub>3</sub>/Nm<sup>3</sup> during cumulatively 48 h (8 runs of 6 h for safety reasons). Different conditions were investigated in this first batch to apprehend the behavior of ozone consumption in this configuration and to achieve complete coke removal. Between each ozonation run, catalytic bed was removed from the reactor, mixed and reloaded in order to favor homogeneity. Combination of the obtained batches corresponds to sample R48. The objective for this series of experiment was to achieve complete coke removal for further reuse in pyrolysis and to apprehend the behavior of ozonation process by increasing the mass of catalytic bed compared to tubular reactor. Observations and comparison between the configurations are presented in Section 4.3. The second batch of samples, labelled REG3 and REG4 in Appendix 6, were mixed together to form R8 sample. Initial mix of coked samples containing between 4.0 and 6.5 wt.%C were exposed to an ozone-enriched gas stream (55 gO<sub>3</sub>/Nm<sup>3</sup>, 100 L/h) during a single run of 8 h with a feed temperature of 75°C.

### 2.2.3.3. Results exploitation

#### a. Thermal and catalytic degradation experiments

Based on the inlet and outlet concentrations values extracted from the experiments presented in Section 2.2.3.2.a, the experimental data were first displayed as the observed ozone degradation calculated as follows (Equation (2.2)):

$$\text{Ozone degradation (\%)} = \frac{[\text{O}_3]_{\text{in}} - [\text{O}_3]_{\text{out}}}{[\text{O}_3]_{\text{in}}} \times 100 \quad (2.2)$$

Where  $[\text{O}_3]_{\text{in}}$  and  $[\text{O}_3]_{\text{out}}$  are the inlet and outlet ozone concentrations (in g.Nm<sup>-3</sup>) respectively. This exploitation allowed apprehending ozone degradation behavior without

any exposition to coke for different temperatures, volumetric flowrates and inlet concentrations. Determination of pseudo-kinetic constants for the respective degradation mechanisms have been successfully carried out in this work. Thermal recombination constant ( $k_{th}$ ) was evaluated by integrating Equation (2.3), while combined degradation integral (Equation (2.4)) was used to determine catalytic degradation constant ( $k_{cat}$ ).

$$\frac{-d[O_3]}{dt} = k_{th}[O_3]^a \quad (2.3)$$

$$\frac{-d[O_3]}{dt} = \varepsilon k_{th} [O_3]^a + (1 - \varepsilon) k_{cat} [O_3]^b \quad (2.4)$$

Where a and b are the orders of reaction regarding ozone for thermal recombination and catalytic degradation respectively. Different values were investigated for a and b and results are presented in Chapter 4 with related experimental data and supporting information placed in Appendix 7.

### *b. Ozonation experiments*

Carbon content obtained by elemental analysis (Section 2.2.4.3.a) was used as an indicator of remaining deposited coke after ozonation treatment. Process efficiency was therefore calculated by evaluating coke removal percentage during the experiment. Carbon removal for a single sample, corresponding to one of the three collected fractions, is calculated using relative comparison between initial and final carbon content (Equation (2.5)). In order to compare experiments for parametric study, global coke removal and process efficiency is calculated for each experiment (Equation (2.6)). This formula considers the different collected samples for one experiment by determining the pondered average of coke removal of each fraction in the reactor based on their respective occupied volume.

$$\text{Sample \%C wt. removal} = \frac{C_{\text{initial}} - C_{\text{final}}}{C_{\text{initial}}} \times 100 \quad (2.5)$$

$$\text{Global \%C wt. removal} = \frac{C_{\text{initial}} - (\alpha_H \cdot C_H + \alpha_M \cdot C_M + \alpha_B \cdot C_B)}{C_{\text{initial}}} \times 100 \quad (2.6)$$

Where  $C_{\text{initial}}$  is the initial weight carbon content of the coked sample,  $C_{\text{final}}$  is the final weight carbon content of the regenerated sample,  $\alpha_i$  describes the occupied volume for each collected samples (ratio between the fraction height and the total reactor length of 20 cm) and  $C_H$ ,  $C_M$ ,  $C_B$  are the final carbon content after ozonation for respectively the high, middle and bottom fractions. The results of this exploitation are also presented in Appendix 6 alongside the journal of ozonation experiments.

### **2.2.4. Analytical techniques**

Based on the contextual knowledge provided by the analytical review in Section 2.1, the different analytical techniques used in this study are summarized in Table 2.6 with their respective application. The material and analysis conditions are subsequently detailed for each method in the following paragraphs.

**Table 2.6.** Summary of analytical methods used in this work with their acronyms and applications.

Analytical technique	Application
Gas chromatography coupled with mass spectrometry detection (GC-MS)	Catalytic activity evaluation: analysis of liquid pyrolysis products
N <sub>2</sub> adsorption/desorption measurement	Zeolite textural properties analysis (specific surface, porosity)
Infrared spectroscopic study of pyridine adsorption (FTIR-Pyridine)	Zeolite chemical properties analysis (catalytic acidity)
Elemental analysis (CH analysis)	Quantification of carbon and hydrogen content (destructive)
Thermogravimetric analysis coupled with infrared spectroscopy (TGA-FTIR)	Qualitative and semi-quantitative analysis of carbonaceous deposits
Cross-polarization magic-angle spinning nuclear magnetic resonance of carbon (CP-MAS <sup>13</sup> C NMR)	Determination of coke molecules nature
Scanning electron microscopy coupled with energy dispersive X-ray spectroscopy (SEM-EDX)	Morphology and elemental analysis over pellet cross-section
Scanning electron microscopy coupled with field emission gun microprobe (SEM-FEG)	Elemental analysis over pellet section after cross-polisher preparation
Optic microscope	Photographs of pellet cross-section

### 2.2.4.1. Pyrolysis products

In order to study the evolution of catalytic activity during the successive pyrolysis runs, the liquid fractions of the products are analyzed by gas-chromatography coupled with mass spectrophotometry (GC-MS). To complete determination of chemical composition of pyrolysis products, gas chromatograph Thermo Trace 1300 was used coupled with a TSQ 8000 Evo quadrupole detector. The GC was equipped with a capillary column of dimensions 30 m long, 0.25 mm internal diameter and 1.4 μm thickness of diphenyl/dimethyl polysiloxane film (Rtx-502.2). Samples were diluted in heptane with a 1:20 volume ratio before analysis. The initial oven temperature was 40 °C and was increased up to 150 °C (24 °C.min<sup>-1</sup> ramp, held 1 min), then to 250 °C (12 °C.min<sup>-1</sup> ramp, held 20 min). The split injection temperature was applied at 250°C. The transfer line and ion source temperatures were 240 °C and 250 °C respectively. Mass data was acquired in full-scan mode between 30 and 600 m/z. Molecules were attributed to corresponding peak using National Institute of Standards and Technology database (NIST).

### 2.2.4.2. Zeolite characterization

#### a. N<sub>2</sub> adsorption/desorption measurement

Textural properties of fresh, deactivated and regenerated zeolite samples are obtained with N<sub>2</sub> adsorption/desorption measurement under vacuum (10<sup>-4</sup>-10<sup>-5</sup> Pa) at -196°C using a BELSORP-Max apparatus (BEL Japan). From the complete adsorption isotherms, main

results are determined based on different methods. Brunauer-Emmet-Teller (BET) equation is used for surface area and global porosity. Mesoporosity and microporosity data are obtained respectively by applying Barret, Joyner and Halenda (BJH) and Horvath-Kawazoe (HK) methods [213, 214].

#### *b. FTIR-Pyridine*

Acidic properties of zeolites are determined by FTIR spectroscopy with pyridine as probe molecule. Samples were pressed ( $10^9$  Pa) into self-supported discs ( $2\text{cm}^2$  area,  $7\text{-}10\text{ mg}\cdot\text{cm}^{-2}$ ) and placed in a quartz cell equipped with KBr windows. A movable quartz sample holder permitted adjustment of the pellet in the infrared beam for spectral acquisition and placement into a furnace at the top of the cell for thermal treatments. The cell was connected to a vacuum line for evacuation, calcination steps ( $P_{\text{residual}}=10^{-3}\text{-}10^{-4}$  Pa) and for the introduction of probe molecules (pyridin vapour phase at  $150^\circ\text{C}$ ). Spectra were recorded at room temperature in the  $4000\text{-}400\text{ cm}^{-1}$  range, with  $4\text{ cm}^{-1}$  resolution, on a Nicolet Nexus spectrometer equipped with an extended KBr beam splitting device and a DTGS detector. Quantification of both Brønsted and Lewis acid sites are determined by integration of IR spectra bands and by using molar absorption coefficients of pyridine commonly accepted in literature:  $1.67\text{ cm}^2/\mu\text{mol}$  for the Brønsted sites band ( $1545\text{ cm}^{-1}$ ) and  $2.22\text{ cm}^2/\mu\text{mol}$  for the Lewis sites band ( $1455\text{ cm}^{-1}$ ) [215].

#### **2.2.4.3. Coke analysis**

##### *a. Elemental CH analysis*

Elemental analysis is performed by combustion at  $1100^\circ\text{C}$  using Perkin Elmer 2400 Series II Flash Combustion Analyzer to determine the carbon and hydrogen content. The results, given in weight percentage with a  $\pm 0.1\text{ wt.}\%$  precision, are used as indicator of deposited coke as it is the only source of carbon in the samples (no carbon at all was detected on fresh zeolite sample). Hydrogen content is used to calculate the H/C molar ratio (Equation (2.7)), giving an indication on coke nature. As a reminder, H/C values superior to 1 denotes a light coke mainly composed of aliphatic structures while H/C values inferior to 1 indicated heavy coke embedding polyaromatic molecules. A decreasing ratio shows the progression of coke condensation degree.

$$\text{H/C ratio (mol/mol)} = \frac{M_{\text{C}}}{M_{\text{H}}} \times \frac{\text{wt. \%H}}{\text{wt. \%C}} \quad (2.7)$$

Where  $M_{\text{C}}$  and  $M_{\text{H}}$  are the molar masses ( $\text{g}\cdot\text{mol}^{-1}$ ) of carbon and hydrogen respectively. This calculated value must be treated with caution as coke might not be the only species containing hydrogen in the zeolites (Brønsted sites for example).

##### *b. TGA-FTIR*

Thermogravimetric analysis is used to get information on coke repartition and nature. Combination of this technique with an online gas detection, such as FTIR, helps qualifying nature of carbonaceous compounds by analyzing the formed gases at the same time as monitoring coke weight loss. This analysis was performed using DSC1 Mettler Toledo TGA apparatus coupled with ThermoScientific IS10 Nicolet FTIR spectrometer. Crushed coked samples ( $\approx 15\text{ mg}$ ) are loaded in the microbalance cell and exposed to air or nitrogen

atmosphere. Different temperature programs, illustrated in Figure 2.12, have been used in this work to investigate the possible weight losses induced by thermal damages. Samples are heated at 10°C/min and maintained at 120°C during 60 min for program 1 or 30 min for program 2 to remove physisorbed water. Heating ramp of 10°C/min is then reactivated: in first program, temperature goes up to 1000°C with this rate while it plateaus at 500°C for the second program. IR spectra are acquired in the constructor measurement range between 4000 and 400 cm<sup>-1</sup>.

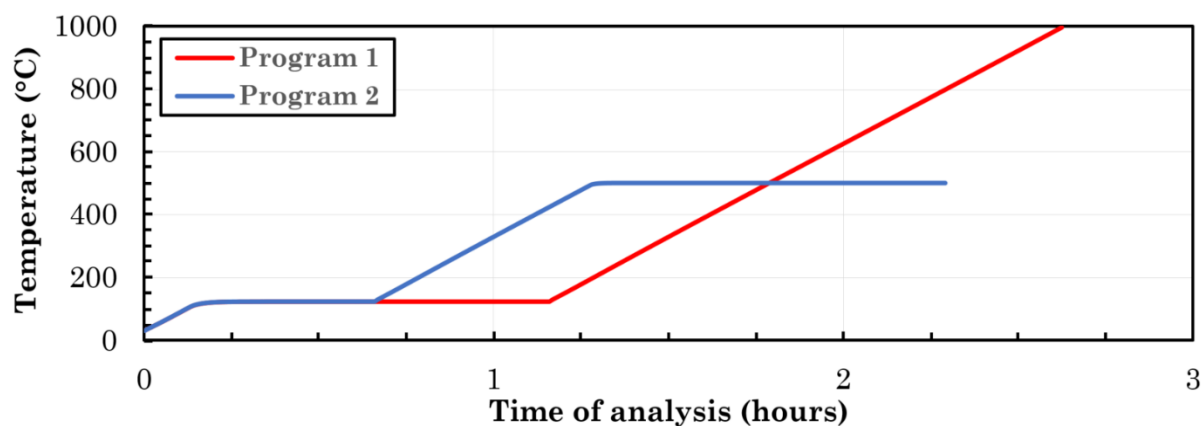


**Figure 2.12.** Different temperature programs for TGA-FTIR analysis of coked samples under air or nitrogen atmosphere.

### c. CP-MAS <sup>13</sup>C NMR

Comprehensive insight of coke molecules nature and structure is given by solid-state <sup>13</sup>C cross-polarization magic-angle spinning (CP-MAS) NMR analysis. Spectra are recorded at ambient temperature in a Bruker Avance III HD 400 (9.4T) spectrometer. Crushed coked zeolite samples were placed in 4 mm zirconia rotors with a MAS rotation speed of 10 kHz. Quantitative acquisition is made with 10 periods of cross-polarization with a contact time of 1.1 ms separated with a repolarizing time <sup>1</sup>H of 0.5 s [216]. The recycling time is set at 1.5 s. The carbon species present over the coked zeolites are identified with a simplified multi Gaussian deconvolution (6 peaks). Each chemical shift was attributed based on literature research to particular carbon environment [217-219]. Integration data of the deconvoluted peaks are used to determine their respective proportions and condensation degree similarly to Chen *et al.* work [79]. Data is normalized based on carbon content obtained by elemental analysis to get quantitative approximation.

#### 2.2.4.4. Pellet cross-section radial carbon profile

The acquisition of radial carbon profile over pellet cross-section presented one of the major analytical challenges of this work. In order to trigger a combined experimental and numerical approach on diffusion-reaction mechanisms during ozonation, this problematic was of main interest to connect the different main axes of the PhD work: ozonation experimental and modelling approaches (presented in Chapters 4 and 5). Due to the microporosity of zeolite material and the difficulty to properly analyze carbon, being a light compound, very few analytical techniques were found to obtain spatial carbon repartition. Similar challenges are encountered in the literature with different deactivating reactions using zeolites or other acid catalysts [8, 94, 220]. However, most of these methods only present a qualitative approach and there is a need of developing new quantitative method.



In this work, an innovative method for quantitative acquisition of radial carbon repartition over zeolite pellet, consistent with elemental analysis, is developed in collaboration with “Centre de microcaractérisation Raimond Castaing” (UAR3623). This paragraph details the approach, thought process and development of this new analytical technique.

According to previous studies, qualitative analysis is possible using SEM coupled with EDX analysis over a definite surface or line [8]. The first tests were therefore conducted in LGC with SEM-EDX analysis (Jeol JSM 7100F coupled with EDX Oxford ASDD X-Max 50mm<sup>2</sup>) over some elected partially regenerated samples visually presenting carbon variation over their radius. Despite observation of a carbon gradient, these primary results presented two main issues: (1) carbon analysis with EDX acquisition over a single line resulted in a very noisy profil due to irregularity of surface topography and carbon repartition (hidden in porosity); (2) obtained carbon contents (in wt.%C) were far superior to actual amount determined with elemental analysis. The first idea to reduce noise over the profiles was to average multiple EDX lines, as presented Figure 2.13. In this figure, optic photographs are added by transparency over corresponding analyzed pellet to show the visual apparition of carbon on the samples. Indeed, SEM images are not a visual but a topographic representation of the sample. Despite several attempts, averaging up to 60 profiles, the resulting carbon repartition remained heavily unstable. Quantitative analysis also remained unexploitable with this modification.

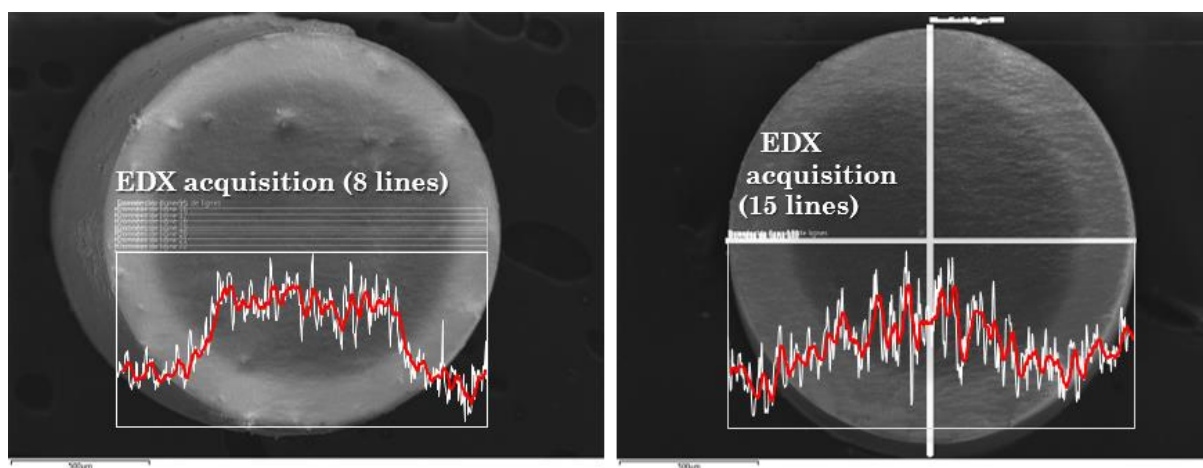


**Figure 2.13.** Superposed optic and SEM pictures for two partially regenerated samples with corresponding EDX acquisition to illustrate carbon profiles obtained with SEM-EDX method.

The following methods were developed in collaboration with S. Gouy and P. De Parseval (Centre Castaing) to overcome the encountered challenges. Acquisition of carbon radial profiles over zeolite pellet cross-sections was successfully achieved with electronic FEG microprobe after adequate sample preparation. In order to remove any topographic irregularities which may alter the measure (noisy profile, altered carbon content), samples were exposed to an ionic argon beam at 6 kV during 8 h using a Cross Polisher Jeol (IB-19510 CP). Acquisition of radial profile was then carried out using microprobe Cameca SXFiveFE with a 10 kV accelerating voltage and 10 nA current. The beam was defocused at 10 µm to limit damages on the material. Two different approaches for acquisition were developed, referred as mapping and scanning methods. Typical SEM-FEG results for a single sample using these methods are illustrated in Figure 2.14.

- ↪ Mapping method was used to obtain precise quantitative values of carbon content (0.1-0.2 wt.%C precision). After calibration with a carbon standard, carbon content was measured during 1 min over each of 20 or 30 equidistant points along the pellet radius (35 or 25  $\mu\text{m}$  steps). Before each quantitative experiment, a blank measurement was carried out over a cross-polished fresh zeolite to evaluate the carbon pollution on the samples. It was observed that during successive analysis, even though sample is placed under important vacuum, carbon content over the fresh sample tended to increase. This pollution is attributed to the remaining carbon species in air or to products generated by the limited, yet present, reactivity between coke compounds and electron beam.
- ↪ The scanning method is meant to provide a qualitative result representing the image of a radial profile, therefore with a reduced acquisition time (1 s) but an increased number of points (roughly 250 points, 3  $\mu\text{m}$  steps). Acquisition is given in detected carbon photons in coups per second (cps). No conversion in carbon content was carried out for this method.

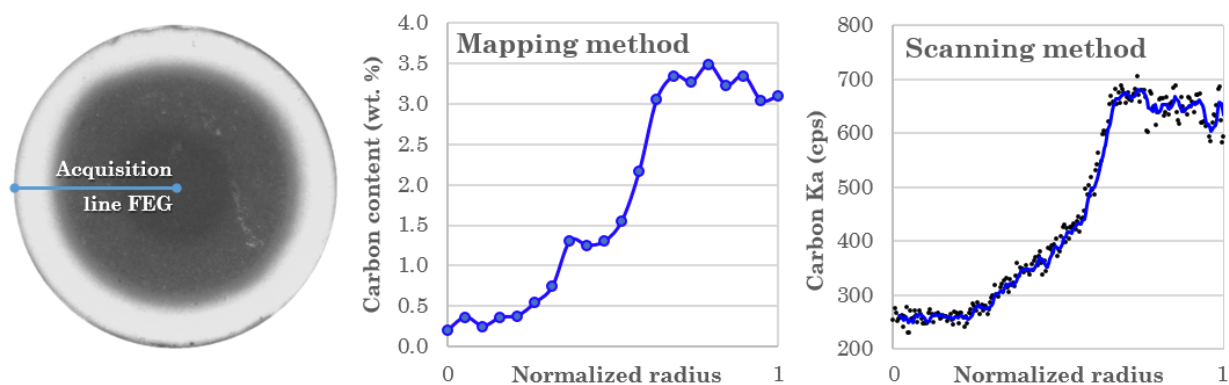


**Figure 2.14.** Results obtained with innovative SEM-FEG technique for one cross-section of a partially regenerated sample, with different obtained profiles based on the acquisition method used for analysis (mapping or scanning).

The obtained profiles were satisfying as the two main aforementioned issues were corrected: (1) noise is strongly reduced as topographic irregularities are removed by cross-polishing treatment; (2) obtained carbon content (given in wt.%C) is consistent with elemental analysis. Only irregularities induced by carbon hindering in microporosity is remaining and generating some noise. For accurate quantitative analysis, progressive carbon pollution during analysis over fresh sample has to be considered and subtracted to acquired value. For visual representation, a cross-section image of single pellet in each collected fraction is acquired with microscope Morphologi G3S (Malvern Instruments). Optic magnification of 2.5 is used. These photographs are then processed with a Matlab<sup>®</sup> post-treatment routine before exploitation (see in Chapter 5).

## 2.3. Conclusion and key takeaways

This chapter presented the analytical and practical background necessary to approach the experimental aspect of the research project. The analytical review provided insight to better understand the chosen techniques and challenges faced in this work. Material, procedures and methods were developed for the two main experimental axes of this study: catalytic pyrolysis of polyethylene and regeneration of so-coked catalysts via ozonation. Global experimental methodology is schematically summarized in Figure 2.15.

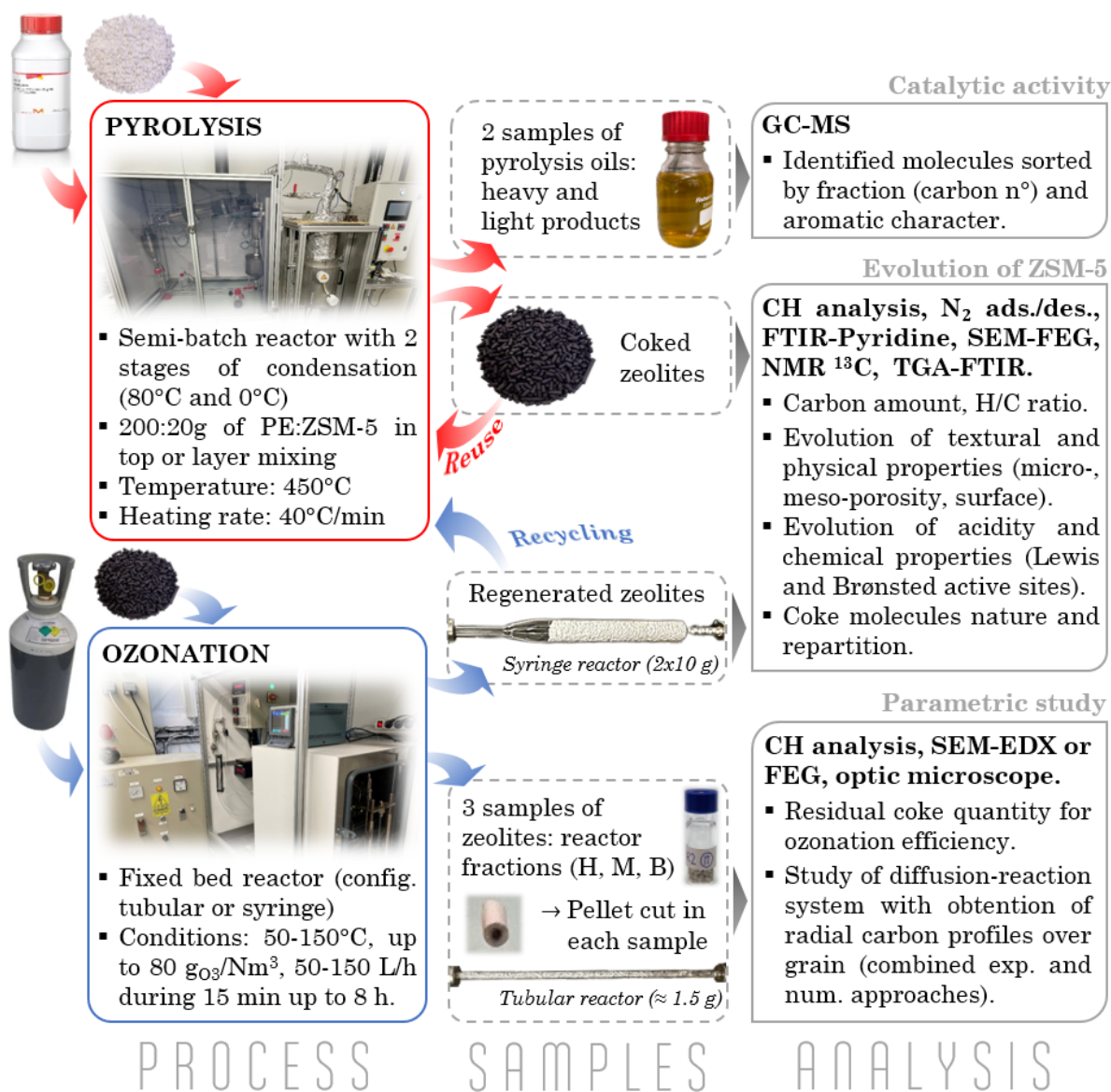


Figure 2.15. Key takeaways of “Chapter 2 – Analytical review and experimental methods”.

# Chapter 3

# Deactivation of catalysts by pyrolysis of LDPE

This chapter focuses on the experimental use of catalysts during pyrolysis of polyethylene. This work is the result of a collaboration with Laboratoire Catalyse et Spectrochimie in Caen (LCS – UMR6506). After briefly reminding the context and process of thoughts of this work (Section 3.1), the obtained results and corresponding discussion are presented in Section 3.2. Additional investigated considerations, such as pyrolysis repeatability and influence of mixing, are presented in Section 3.3 before discussing the conclusions and perspectives of this study in a last paragraph (Section 3.4).

## 3.1. Introduction and presentation of work context

Previous studies regarding deactivation during catalytic pyrolysis have been carried out using different catalysts and reactor geometries [91, 93, 113]. Due to the important operating temperature of pyrolysis (400-500°C), coke formed over the catalysts is mostly composed of polyaromatic heavy coke [79, 112]. This deposition of carbonaceous compounds leads to the loss of textural and chemical characteristics of catalysts [8, 85]. Different studies investigated the influence of catalytic deactivation over the obtained products during pyrolysis, showing an important evolution of oils and gases repartition, as illustrated in Figure 3.1, and composition [85, 93, 221]. However, most of these studies focused on a single use of catalysts in pyrolysis and the study of progressive deactivation during successive reuses at pilot scale was not found in the literature.

Catalytic pyrolysis of polyethylene was elected as deactivating reaction for this PhD work due to its high research interest, its relative ease of implementation and its existing investigations available for comparison. The optimal operating conditions used in this work were therefore identified in the literature as 450°C with a feedstock mass ratio of 10:1 LDPE:ZSM-5 [13]. During the research project, different innovative aspects that were not investigated before (successive reuses of catalysts and effect of initial feedstock mixing in the reactor) were integrated in this chapter. The first aspect investigated in this work is an intensive study of the deactivation occurring via coke formation during catalytic pyrolysis of polyethylene. Catalysts were used in pyrolysis up to five successive runs to study and quantify their progressive deactivation. The evolution of zeolite characteristics

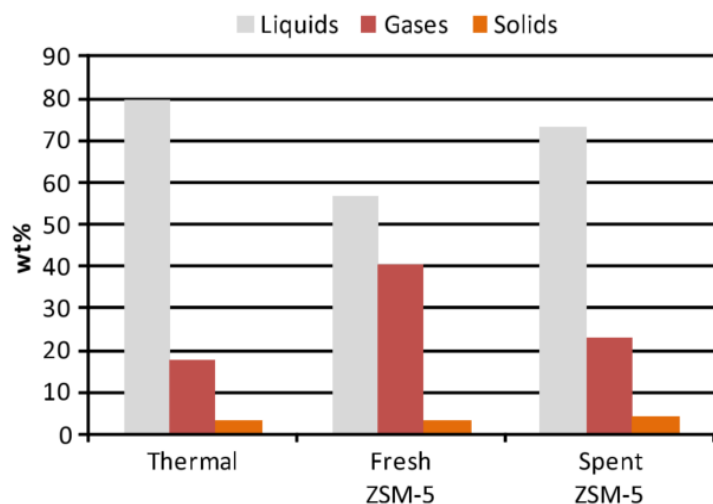


**Figure 3.1.** Illustration of pyrolysis yields evolution for thermal and catalytic pyrolysis of plastic wastes experiments (López *et al.*, 2011) [93].

are compared with the catalytic activity assessed by following the evolution of pyrolysis products. This work intends to provide a deep understanding of coking deactivation prior to furtherly use the spent samples in the study of ozonation process for coke removal and catalysts regeneration.

Different papers in the literature investigated the reuse of coked catalysts in pyrolysis after regeneration by coke combustion process with oxygen over 400°C, showing that catalytic activity could successfully be recovered after coke oxidation [92, 93, 222]. Despite partial recovery of initial catalyst textural and chemical properties using ozonation at 95°C during 4h, Khangkham *et al.* collected products similar to those obtained with fresh catalysts when reusing ozonated samples during PMMA degradation as illustrated in Figure 3.2 [8]. No other studies were found in which ozonated catalysts are reused in initial process. Consequently, the second aspect aimed in this chapter is to assess the ability of the ozonation process to achieve total recovery efficiency at lower temperatures than classic coke combustion process with oxygen. Based on the promising results obtained

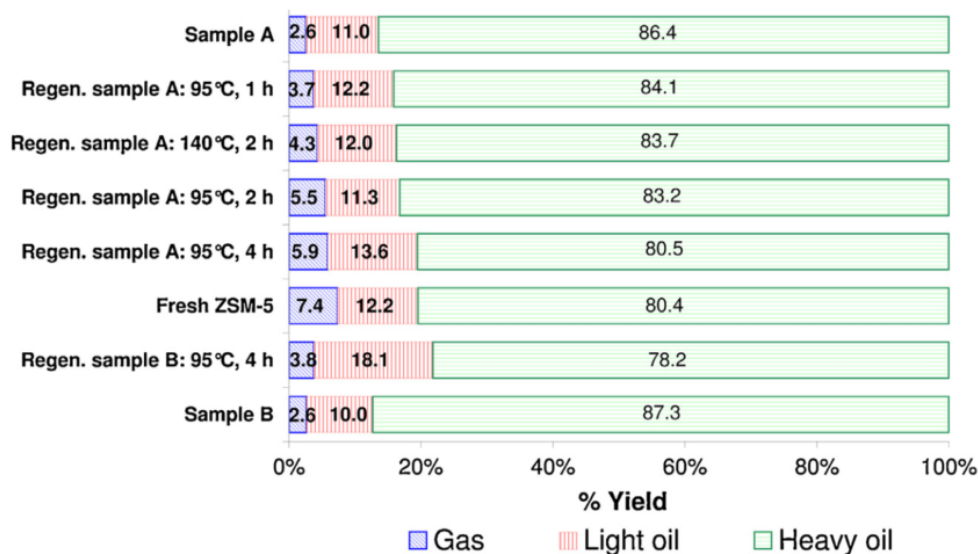


**Figure 3.2.** Illustration of the PMMA degradation yields evolution using fresh, spent and ozonated ZSM-5 industrial catalysts (Khangkham *et al.*, 2013) [8].

by Khangkham *et al.*, ZSM-5 extrudates are here recycled in pyrolysis of polyethylene after regeneration treatment via ozonation. As mentioned previously, due to the relatively high operating temperatures during pyrolysis, coke formed on the catalysts is mainly composed of heavy and stable molecules [79, 89, 90]. Consequently, if ozonation is efficient on such coked samples, its range of applications could be extended to a wide number of processes where operating conditions form lighter coke [89, 123, 124].

The work presented in this chapter therefore contains two main axes: deactivation and regeneration of catalysts used in innovative processes. The authors identified catalytic pyrolysis as an easy-to-use reaction for the revalorization of plastic wastes whose industrial development is restrained by the important coke deactivation [57, 81]. Up to now, most of the studies related to deactivation during pyrolysis of plastics are limited to a single use of spent catalysts in the reaction. The aim of this work is to reuse spent industrial catalysts more than once to reach a better understanding of coke formation during pyrolysis and to conclude about the possibility to reuse extensively spent catalysts before removing them for regeneration. Use of ozonation as an alternative method for coke removal intends replacing classic coke combustion for regeneration by operating at lower temperatures, thus reducing thermal degradation risks and process energy consumption.

### 3.2. Results and discussion

#### 3.2.1. Catalytic deactivation during pyrolysis

Fresh catalyst characteristics and main properties are presented in Table 3.1. The Si/Al ratio of diluted zeolites in binder was experimentally determined by NMR of  $^{27}\text{Al}$  and  $^{29}\text{Si}$  around 18. The proportion of alumina binder in the pellets is thus evaluated around 22%.

**Table 3.1.** Properties and characteristics of industrial ZSM-5 catalysts given by supplier or experimentally determined (pellet density and binder proportion).

<b>HSZ-822HOD1A (Tosoh). Lot n°TZ-200805.</b>	
<b>Binder</b>	Alumina
<b>Shape</b>	Extrudate
<b>Size (diameter x length) (mm)</b>	1.5 x 2-6
<b>Bulk density (kg/m<sup>3</sup>)</b>	680
<b>Pellet density (kg/m<sup>3</sup>)</b>	~ 1300
<b>Alumina binder proportion (%)</b>	22
<b>Zeolite powder</b>	
SiO <sub>2</sub> /Al <sub>2</sub> O <sub>3</sub> (mol/mol)	23
Na <sub>2</sub> O (wt.%)	0.05

As illustrated in Section 2.2.2.2, catalyst pellets are initially placed in layers (labelled L) in the reactor. In order to study the evolution of deactivation and progressive formation of coke, pyrolysis experiments were performed in five successive runs where catalysts are reused without any intermediate treatment. Coked catalysts indicated as L' and L'' are experiments conducted with identical conditions to study the repeatability of coking during catalytic pyrolysis. The number added after this indicative letter corresponds to the number of reuses in pyrolysis. As an example, L4 experiment is the fourth reuse of ZSM-5 catalysts in pyrolysis. Collected samples (spent catalysts and pyrolysis products) are named after this experiment indicator.



### 3.2.1.1. Evolution of pyrolysis products selectivity

The compositions of pyrolysis products collected after the first condenser (Stage 1 on Figure 2.9) are presented in Table 3.2 for the successive experiments (L1 to L4). Wax and oil fraction are there collected as a unique homogeneous phase at 80 °C, which then turns solid by cooling down until ambient temperature. Proportion of aromatics and fractions of molecules according to their number of carbons are used as a descriptor of catalytic performance in the oils during pyrolysis. Peak area percentages were extracted from the total chromatogram to determine the distribution of the products. The different fractions of obtained molecules presented in Figure 3.3 are sorted as follows: C7 to C9, corresponding to gasoline, C10 to C14, representing kerosene components, and C15+ molecules, often mentioned in the literature as heavy oils or waxes [223-225]. The proportion of aromatics is also presented for each fraction as well as the main products of interest: toluene and xylenes. Complete list of identified products during pyrolysis using fresh catalysts is provided in supporting information with corresponding peak area.

**Table 3.2.** Composition of pyrolysis oils analyzed by GC-MS for spent catalysts.

Condensed products distribution (%)		Thermal	Fresh	L1	L2	L3	L4
<b>Identified</b>		96.5	98.5	97.4	95.0	93.6	95.0
<b>Aromatics</b>		0.2	91.9	77.3	55.8	30.6	27.5
<b>C7-C9 (Gasoline)</b>	Total	40.1	94.9	88.8	77.2	69.5	69.8
	Aromatics	0.0	91.5	76.6	55.5	30.6	27.4
<b>C10-C14 (Kerosene)</b>	Total	38.2	3.1	8.0	15.8	20.4	23.1
	Aromatics	0.2	0.4	0.7	0.3	n.d.	n.d.
<b>C15+ (Heavy oils)</b>		18.2	0.5	0.7	2.0	3.6	2.1
<b>Main products</b>	Toluene	-	26.8	28.8	20.8	17.1	15.4
	Xylenes	-	59.4	40.4	26.5	8.2	6.3

Compared to thermal pyrolysis of plastics, the addition of catalysts is known to enhance the cracking of polymers and to allow the formation of aromatic products via mechanisms of rearrangement, cyclization and H-transfer [65, 226]. The use of ZSM-5 zeolites has been extensively studied due to their shape selectivity leading to the important formation of light products and aromatics [227]. Such behavior is confirmed in this study as the fraction of light oil (C7-C9) and aromatics is more important using fresh catalysts compared to thermal pyrolysis [13, 93]. Therefore, this enhanced cracking and rearrangement performances due to the use of zeolite catalysts is here observed for the initial experiment. Thermal pyrolysis only presents 0.2% of aromatics and 40.1% of C7-C9 molecules, while same experiment with fresh zeolites presents aromatics proportion of 91.9%, and a light oil fraction (C7-C9) of 94.9%. Aromatics formed during pyrolysis of polyethylene are mainly molecules containing 7 or 8 carbon atoms, therefore part of the aforementioned light fraction. No aromatic products are identified in the wax fraction (C15+). As observed in Table 3.2, the repartition of obtained pyrolysis products changes during the successive reuses of catalysts. The total proportion of aromatics decreases drastically, from 91.9% to



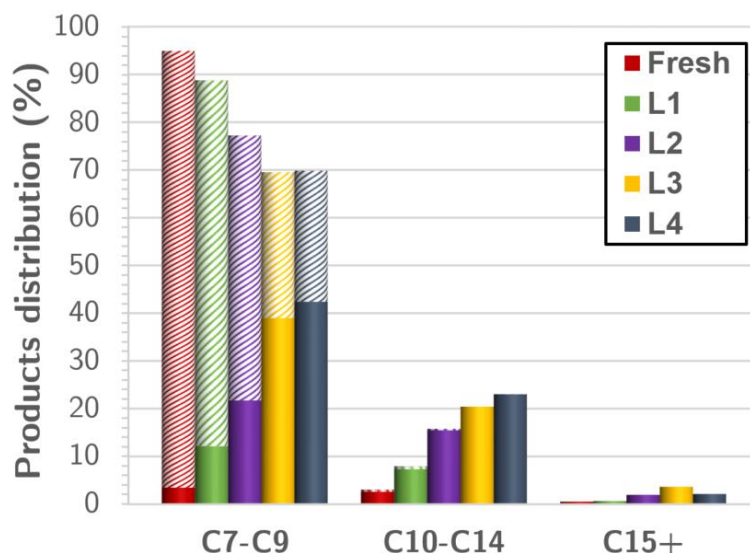


**Figure 3.3.** Evolution of pyrolysis products repartition after successive reuses of catalysts. Hatched area represents aromatic molecules proportion.

27.5% after five successive pyrolysis reuses. This evolution traduces the progressive loss of catalytic performances, and especially the diminution of zeolite rearrangement capacity. The cracking potential of ZSM-5 is also affected by this decrease of catalytic performance as illustrated in Figure 3.3. It appears that, while the C15+ fraction remains globally constant, lower concentrations of light oil products (C7-C9) is formed after successive reuses. On the other hand, the proportion of kerosene products (C10-C14) increases showing that polymer chains are being less cracked during the catalytic reaction. The carbon-number distribution of molecules obtained during pyrolysis is a typical indicator of catalytic performances for cracking [228]. A shift towards higher carbon number is usually obtained when catalytic activity decreases [197]. This tendency is expected here as the catalysts are being gradually deactivated when reused in pyrolysis, therefore reducing its cracking performances. An important decrease of the light fraction (C7-C9) is indeed observed during the five successive reuses as its proportion drops from 94.9% to 69.8%. The evolution of monocyclic molecules content in this fraction is mostly responsible of the global decrease of aromatic products as an important loss of toluene and xylenes production is observed. After the fifth catalysts reuse, the nature of obtained products remains quite different from the composition of thermal pyrolysis oils, suggesting that catalysts remain chemically active despite an important loss of initial selectivity.

### 3.2.1.2. Influence of coking on catalysts characteristics

Textural and chemical properties of spent catalysts are given in Table 3.3 alongside the evolution of carbon content and H/C ratio during successive pyrolysis. These samples correspond to the used ZSM-5 catalysts collected after each pyrolysis run presented in Section 3.2.1.1. The properties are compared to fresh industrial ZSM-5 characteristics to evaluate deactivation caused by coke deposition.

The formation of coke is illustrated by the apparition of carbon on the catalysts with an increasing content as zeolites are reused and furtherly deactivated. Carbon content is expected to increase after each reuse, but a different tendency appears. Whereas carbon content reaches 8.2 wt.% after a single pyrolysis run (L1), its value fluctuates around 9 wt.%C with a maximum of 10.3 wt.%C from the second to the fifth use. As illustrated on

**Table 3.3.** Textural and chemical properties of fresh and spent catalysts after successive runs.

Property	Fresh	L1	L2	L3	L4	L5
Carbon content (wt. %)	-	8.2	6.5	8.3	10.3	9.9
H/C ratio (-)	-	1.6	1.1	0.6	0.8	0.5
BET surface area ( $\text{m}^2\cdot\text{g}^{-1}$ )	369.6	231.7	138.9	49.1	42.6	43.3
Total pore volume ( $\text{cm}^3\cdot\text{g}^{-1}$ )	0.38	0.29	0.23	0.13	0.18	0.16
Microporous volume $V_{\text{micro}}$ ( $\text{cm}^3\cdot\text{g}^{-1}$ )	0.17	0.11	0.07	0.03	0.02	0.02
Mesoporous volume $V_{\text{meso}}$ ( $\text{cm}^3\cdot\text{g}^{-1}$ )	0.21	0.18	0.16	0.10	0.16	0.14
Brønsted acid sites ( $\mu\text{mol}\cdot\text{g}^{-1}$ )	294	191	103	31	10	4
Lewis acid sites ( $\mu\text{mol}\cdot\text{g}^{-1}$ )	193	76	66	33	27	25

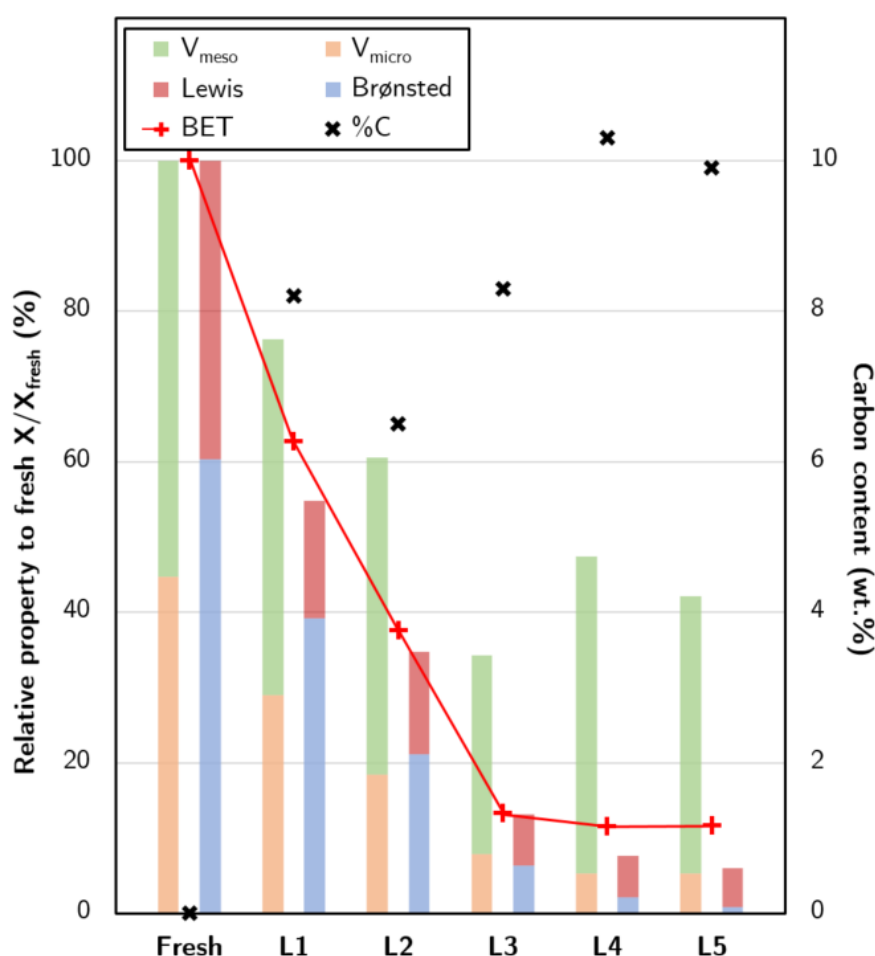
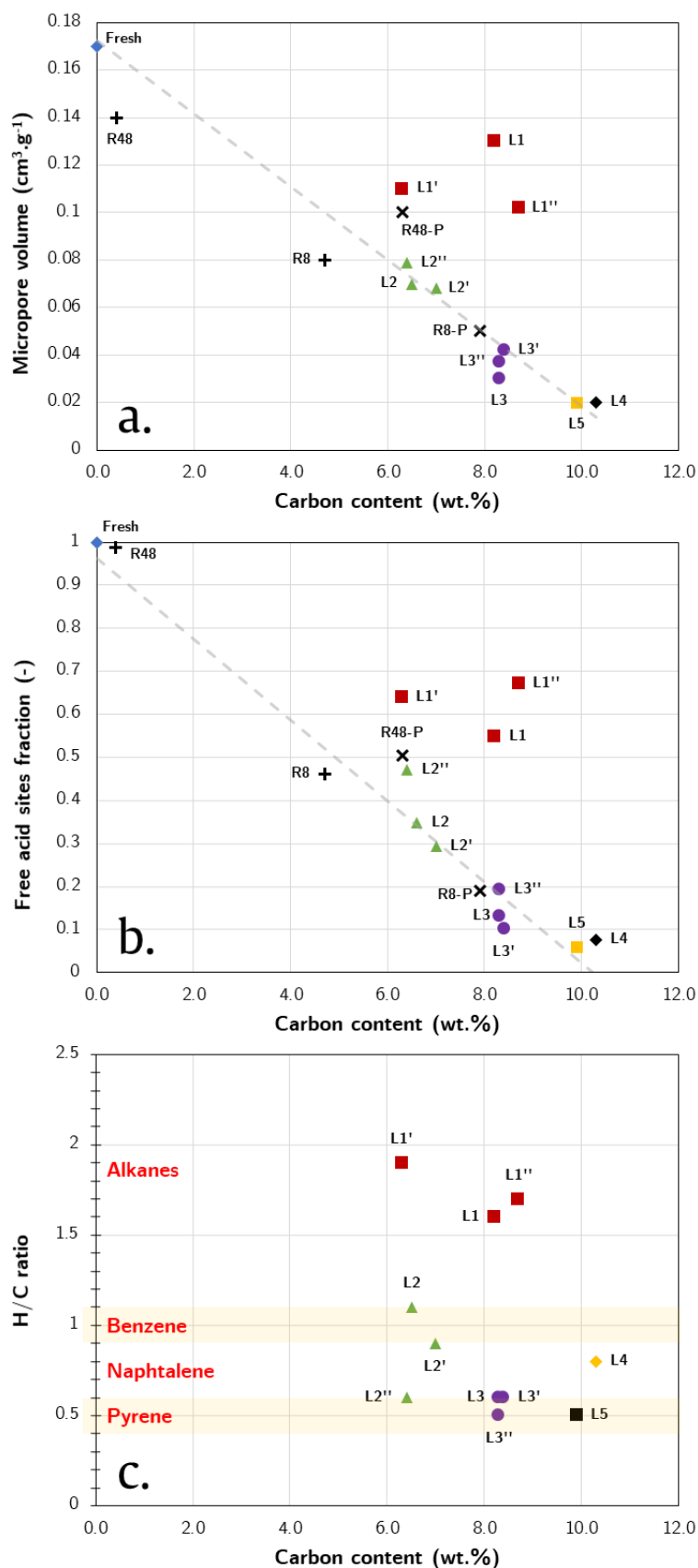
**Figure 3.4.** Evolution of catalysts textural and chemical properties due to coke deposition during several successive runs of pyrolysis of LDPE.

Figure 3.4, carbon deposition and coke formation greatly affect specific surface area, global porosity and acid sites concentration. The evolution of total porosity takes into account the diminution of both meso- and micro-pores volumes. Based on the results presented in Table 3.3, microporosity is the most impacted with a 90% loss after five successive uses (compared to only 33% diminution for mesoporosity). This difference is mainly due to the various deactivating pathways: on top of coke micropore volume occupancy, micropores are also subject to pore blocking. The location of carbon deposits formed during pyrolysis are furtherly discussed in Section 3.2.1.3.

The evolution of acidity is decreasing accordingly to the textural properties: Brønsted sites, mostly located in zeolite microporosity, is heavily impacted with a 99% loss after five pyrolysis. Due to their high reactivity, Brønsted sites are subject to important deactivation as coke precursors are susceptible to react over such acid sites [229]. On the other hand, Lewis sites are little impacted as they are mostly located on the external surface of the crystals and alumina binder, thus in mesopores [230]. Brønsted sites are known to be the most chemically reactive locations during pyrolysis, for either molecule aromatization (H-transfer) but also cracking (protolytic mechanism), while Lewis acidity only promotes cracking ( $\beta$ -scission) at a lower extent [227, 231]. The important loss of Brønsted sites is correlated with the decrease of aromatics proportion in the pyrolysis oils (Section 3.2.1.1) while the smaller diminution of Lewis sites explains the mitigated decrease of cracking performances. Despite complete loss of Brønsted acidity after the fifth experiment, catalysts remain chemically active as products remain different from thermal pyrolysis. Further reuse of the catalysts is expected to lead to a complete deactivation, where catalysts become chemically inert, leading to products similar to thermal pyrolysis.

In order to investigate the influence of coke deposits over catalytic characteristics, the evolution of main properties is plotted as a function of carbon load in Figure 3.5 (a, b). All the aforementioned samples are here presented as well as L' and L'' repeatability experiments. As expected from typical deactivation behavior, a gradual loss of both microporous volume and acidity with carbon load increase is observed. While correlation is almost linear for important number of pyrolysis, suggesting a proportionality relation between coke content and properties, the initial experiments (L1, L1' and L1'') appear out of the tendency as their carbon content is abnormally high regarding the evolution of textural properties. This rapid initial carbon deposition is attributed to the direct contact with molten polyethylene, suggesting an important carbon deposition around the catalysts. These deposits are suggested to form a thin envelope composed of molten polymer chains around the pelletized catalysts chains or around zeolite crystals. This hypothesis could also explain the heterogeneity between the samples used once in pyrolysis. The loading method used in these experiments generates differences of exposition between the layers of catalysts: while three layers are mixed with LDPE, the top layer fraction is located above the plastics (Figure 2.9). It is suggested that the three bottom fractions are dipped into molten polymers during the reaction while the top layer is not exposed to liquid polyethylene by staying at its surface. A different series of experiment which was not presented here, consisting in placing catalysts on top of LDPE, presented lower carbon content (3.3 wt.%C after one pyrolysis). The important external carbon deposition is not likely to occur for the top layer. The grains of this fraction are therefore exposed mainly to pyrolysis vapors. As gas molecules are smaller, their diffusion in the binder/zeolite is easier, the carbon deposition is decreased and its repartition through the catalyst grain is more homogeneous. The different layers cannot be collected separately at the end of each pyrolysis experiment and elemental analysis is carried out on a fraction of the 20 g of spent catalysts. The elemental analysis is consequently possibly biased by the different expositions and the heterogeneity of coking between samples obtained during the reaction. However, the more the number of pyrolysis increases, the more the repeated samples (L, L' and L'') are presenting similar characteristics. Between each run, catalysts are recovered and loaded for reuse regardless their position in the reactor. The difference of exposition and heterogeneity between catalysts is consequently mitigated at each reuse. After using the catalysts for the fourth and fifth times, zeolite materials seem to be saturated with coke, as carbon content, porosity and specific surface



**Figure 3.5.** Correlation between the analyzed carbon content with (a) microporosity, (b) free acid sites and (c) H/C ratio of all catalysts samples (fresh, spent, regenerated and reused). H/C ratio values superior to 1.5 are attributed to aliphatic coke. Benzene, naphthalene and pyrene-like coke structures have an H/C ratio around 1.0, 0.8 and 0.6 respectively.

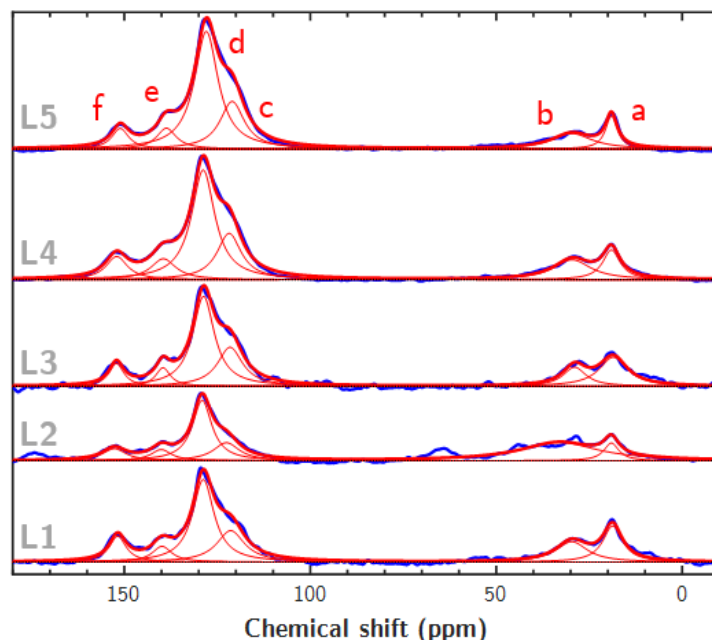
remain globally constant. This observation suggests that industrial ZSM-5 are completely deactivated during semi-batch pyrolysis of polyethylene at 450°C after 3-4 uses in these conditions. Characteristics of L4 and L5 samples are very close: while their carbon content fluctuates around 10.0 wt.%, microporous volume and acidity remain constant. Indeed, microporosity is completely either occupied or blocked, preventing any access to Brønsted acid sites. Consequently, further coke deposition could only occur in mesoporous volume by reacting with previous coke structures or remaining Lewis sites. Detailed considerations about coke location during deactivation by pyrolysis of polyethylene, as well as nature of carbonaceous structures, are discussed in the following paragraph.

### 3.2.1.3. Nature and location of coke

A first approach for the determination of coke nature is provided in Figure 3.5.c. The evolution of H/C ratio obtained by elemental analysis shows progressive condensation of coke structures as its value decreases when pyrolysis number increases. While H/C is around 2 for the first runs, indicating an important fraction of aliphatic coke, condensation occurs for further reuses, forming benzene-like coke ( $H/C \approx 1$ ), followed by naphthalene and pyrene-like molecules ( $H/C \approx 0.5$ ). A more precise determination of coke nature formed over ZSM-5 catalysts is determined by  $^{13}\text{C}$  NMR analysis. Obtained spectra for spent samples are presented in Figure 3.6. The attribution of different observed peaks with corresponding deconvolution exploitation are presented in Table 3.4.

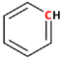
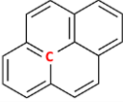
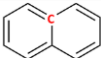
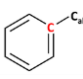
All samples present similar chemical shifts with two main domains: 18-35 ppm and 120-153 ppm. These zones are identified in the literature as aliphatic and aromatic carbons respectively [217-219]. The aromatic carbon area is the main domain observed on the NMR spectra. As sensed due to the high operating temperature of pyrolysis (450°C), coke formed is mainly heavy coke containing condensed carbons forming clusters of polyaromatics. Indeed, the two peaks attributed to ring junction (128-132 ppm and 138-140 ppm), which is the most condensed possible form of carbon as there is no hydrogen remaining, represent the majority of aromatic carbons. The average coke structure formed is mainly an agglomeration of condensed rings. During the successive reuses of catalysts, the condensation degree of aromatic carbons, or in other words the proportion of 2 and 3-ring junction carbons, tends to increase due to the growth mechanisms of initial coke. Chen *et al.* obtained similar behavior during the catalytic pyrolysis of PE over Y-zeolite industrial catalysts in a fixed-bed [79]. The challenge of this work resides in the fact that the successive pyrolysis runs are not considered as a continuous process. It is therefore required to consider at the same time the growth of structures initially formed and the additional deposition of coke. On top of the condensed coke molecules, every sample also presents a significant fraction of aliphatic coke (between 17.7% and 43.4%). This light coke consists in linear and branched alkanes or alkenes, such as partially cracked polymers or intermediate reactants that did not undergo aromatization. During PE cracking in a conical spouted bed reactor, Castaño *et al.* obtained similar mix of aliphatic and aromatic coke over HZSM-5 catalysts [112]. While initial light coke is condensed into heavy coke during successive pyrolysis, additional soft coke is deposited. These deposits will also undergo further condensation, participating to heavy coke growth and lowering the aliphatic compounds proportion after each run. The progressive decrease of aliphatic to aromatic ratio for layer samples illustrates this tendency for three and more reuses. Surprisingly, aliphatic coke load proportion of samples used twice for both mixing methods is more important than after the first run, suggesting that the initial deactivation after the first use modified chemical interactions and coke formation. It is important to remind

that NMR analysis are considering all coke structures regardless of their location. Indeed, coke nature and/or size is susceptible to be different according to its location within the porous matrix. Micropores are sterically limiting coke development while its growth is not restrained in mesoporous volume [232]. Location considerations therefore need to be considered to gain better insights of coke formation during pyrolysis.



**Figure 3.6.** Normalized  $^{13}\text{C}$  NMR spectra of the different coked samples (blue line: initial spectrum; thin red lines: deconvoluted peaks; thick red: deconvoluted spectrum; black line: baseline).

**Table 3.4.** Nature and composition of coke structures formed during pyrolysis determined by CP-MAS  $^{13}\text{C}$  NMR analysis.

% NMR Deconvoluted Peak Area		L1	L2	L3	L4	L5
<b>Aliphatic carbon</b>		<b>28.4</b>	<b>43.4</b>	<b>26.1</b>	<b>21.1</b>	<b>17.7</b>
a. Methyl (18-22 ppm)	$-\text{CH}_3$	14.9	7.0	17.0	8.7	6.8
b. Linear alkane (25-35 ppm)	$-\text{CH}_2-$	13.5	36.4	9.1	12.4	10.9
<b>Aromatic carbon</b>		<b>71.6</b>	<b>56.6</b>	<b>73.8</b>	<b>78.9</b>	<b>82.3</b>
c. Non-substituted (120-128 ppm)		18.4	12.2	20.5	18.8	20.3
d. 3-ring junction (128-132 ppm)		37.5	30.9	40.6	43.0	48.7
e. 2-ring junction (138-140 ppm)		6.5	6.0	5.7	8.8	7.2
f. Substituted (151-153 ppm)		9.2	7.5	7.1	8.3	6.1
Ratio aliphatic/aromatic		0.40	0.77	0.35	0.27	0.22
Condensation degree <sup>a</sup>		0.61	0.65	0.63	0.66	0.68

<sup>a</sup> The condensation degree is calculated as the ratio of ring junction and total aromatic carbons.

Determining the repartition between internal and external coke, i.e. determining coke contained in microporous zeolite crystals and in alumina binder mesoporous volume, is a complex challenge even up to date. The external coke content is usually obtained by difference between total coke load and microporous coke. The latter is determined by correlating micropores volume loss and an approximation of coke density. However, this method approximates that all lost micro-volume is actually occupied by coke molecules which may be untrue as pore blocking can occur, especially in microporous zeolites. In this deactivation pathway, only pore mouth is covered by coke and its volume becomes inaccessible while it is not occupied by deactivating species. In this work, the authors intended to evaluate the contribution between actual occupancy and pore blocking in microporosity loss. The average density of coke for each sample is determined with the H/C ratio using equation given by Kuwata *et al.* to consider the important fluctuation of coke nature confirmed by NMR analysis [233]. Calculated coke density range for all samples is between 0.84 g.cm<sup>-3</sup> (L1') and 1.32 g.cm<sup>-3</sup> (L5). This range is in accordance with the value of 1.22 g.cm<sup>-3</sup>, often used in the literature as value for average coke density [109, 234]. Using the respective calculated coke density for each sample, the actual volume occupied by coke is determined. The proportion of pore blocking is then calculated from the difference between this value and the apparent microporosity loss. Complete results obtained using this method are presented in Table 5. No pore blocking is observed after one pyrolysis but its contribution appears after two or more uses of catalysts (between 40 and 50%). While L5 sample shows an 88% loss of microporosity relatively to fresh zeolite, half is due to pore blockage (49.8%). It is important to remind that this calculation considers that all coke is located in micropores. Volume occupied by mesoporous coke is here neglected due to its limited evolution. However, previous results showed that external coke has an important role in the mechanisms of coke growth and should also be considered for perfect accuracy.

**Table 3.5.** Determination of pore blocking contribution in porous volume loss for coked samples.

Property	L1	L2	L3	L4	L5	L1'	L2'	L3'	L1''	L2''	L3''
Carbon load (wt.%)	8.2	6.5	8.3	10.3	9.9	6.3	7	8.4	8.7	6.4	8.3
H/C ratio (-)	1.6	1.1	0.6	0.8	0.5	1.9	0.9	0.6	1.7	0.6	0.5
Coke density (g.cm <sup>-3</sup> )	0.91	1.05	1.26	1.16	1.32	0.84	1.12	1.26	0.88	1.26	1.32
Apparent occup. (cm <sup>3</sup> )	0.06	0.10	0.14	0.15	0.15	0.07	0.10	0.13	0.08	0.09	0.13
Actual occup. (cm <sup>3</sup> )	0.09	0.06	0.07	0.09	0.08	0.07	0.06	0.07	0.10	0.05	0.06
Pore blocking (%)	-	40.0	52.9	41.0	49.8	-	38.8	47.9	-	44.2	52.6

#### 3.2.1.4. Conclusion on catalytic deactivation

Based on all the results, considerations and observations mentioned in this study, a comprehensive multi-step approach is proposed to describe coke formation over catalysts. Figure 3.7 summarizes and illustrates this suggested deactivation pathway of ZSM-5 catalysts during pyrolysis of LDPE. The initial deactivation after the first use of catalysts in pyrolysis presents an important fraction of coke deposited at the surface of zeolite crystals (external coke). Consequently, the microporous volume and acid sites are less impacted than expected considering the coke content (Figure 3.5.a and b). The high H/C ratio suggests that these deposits are mainly aliphatic compounds. The heavy coke formed during pyrolysis and exposed by NMR analysis is expected to be mostly formed in zeolite



crystals (internal coke). Elordi *et al.* demonstrated similar behavior when conducting cracking of polyethylene with HZSM-5 in a conical spouted bed reactor [221]. When reusing the catalysts, further coke is deposited and carbon load increases as sensed from typical deactivation behavior. Mechanisms of coke growth appears on both internal and external coke: initial coke deposited in the micropores or over the surface condensates to form polyaromatic structures. The development of internal coke causes the apparition of pore blocking as molecules are more likely to cover pore entry without occupying the volume. Moreover, additional light coke is deposited on the crystals surface with the deposition of partially cracked polymers. This phenomenon is particularly observed for the second pyrolysis run where reduced catalytic activity generates an important aliphatic coke formation. Initial coke is suggested to act as coke precursors, which enhances coke formation. Further reuses show typical behavior of coke growth with a gradual condensation of coke structures, surface hindering and porosity loss. At advanced stages of deactivation, the formation of a heavy coke envelope around the crystals is suggested, blocking all access to microporosity and Brønsted acid sites. In this work, actual micropore occupancy by coke molecules have been evaluated to 50-60% while the complement appears to be inaccessible because of pore blocking. A part of Lewis acid sites remains available in mesoporous volume but as zeolite crystals are responsible for most of the reactivity, catalytic selectivity decreases importantly. When all zeolite crystallinity is saturated, cracking and rearrangement capacities are heavily impacted due to the important contribution of Brønsted acidity, but the catalysts remain chemically active as mentioned in Section 3.2.1.1, due to the remaining Lewis acidity. In order to recover catalytic performances, coke has to be removed with a proper regenerating treatment. In the following section, the capacity of the ozonation process to restore catalytic performances in pyrolysis and characteristics is discussed.

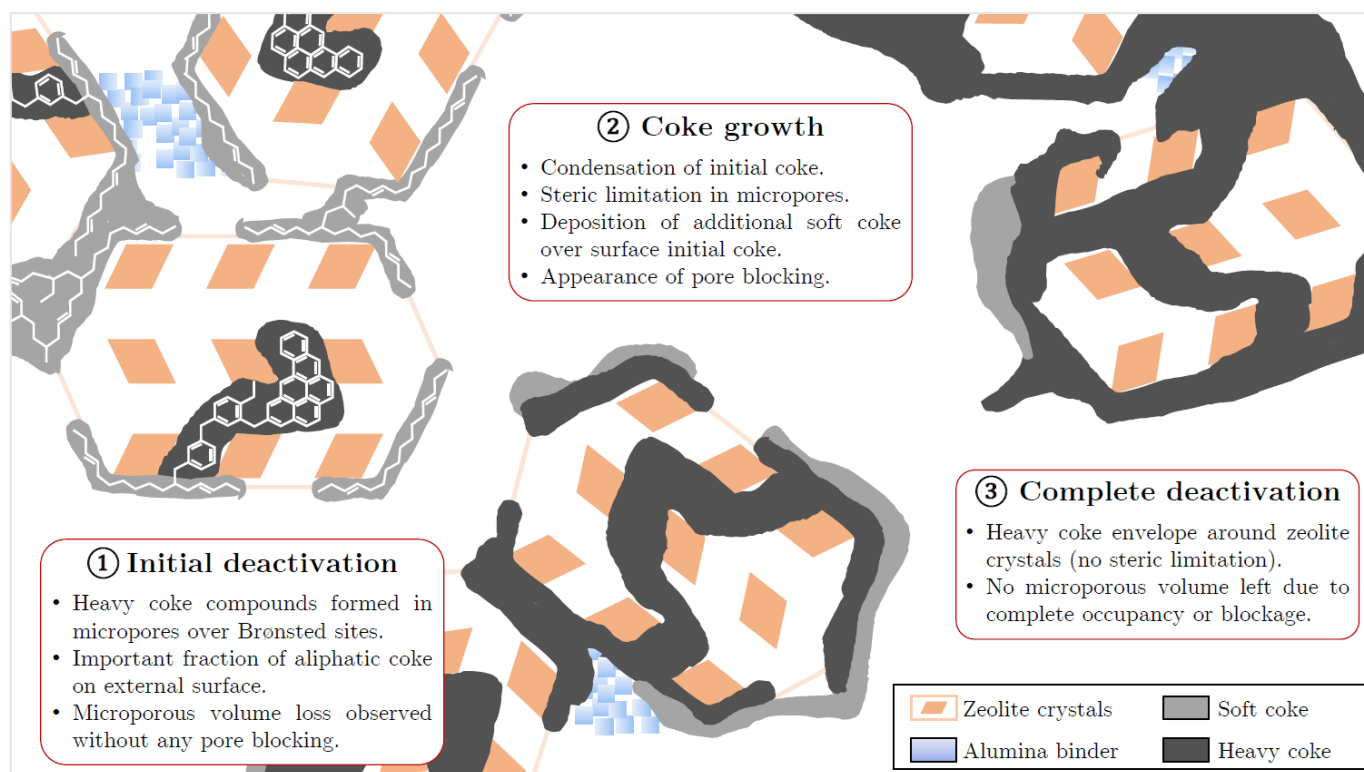


**Figure 3.7.** Schematic representation of coke formation process in industrial ZSM-5 during successive reuses in pyrolysis of LDPE.

### 3.2.2. Ozonated catalysts efficiency and properties

Coke removal was carried out by ozonation in a fixed-bed reactor (complete study in next chapter). First regenerated sample has been obtained by exposing L5 sample (9.9 wt.%C) to an ozone-enriched gas stream at 100 °C during 8 h (R8) to assess the ability of ozonation to remove highly condensed coke. Intending to achieve complete coke removal, ozonation in identical conditions was conducted during 48 h (R48) from a coked sample containing 5.3 wt.%C. The ozonated catalysts (R8 and R48) were analyzed to measure their properties. These regenerated samples were then recycled in two separate pyrolysis runs using the same operating conditions as the first pyrolysis to assess catalytic selectivity recovery. Pyrolysis products and reused zeolites were collected after reaction for analysis (R8-P and R48-P).

#### 3.2.2.1. Study of regenerated catalysts selectivity

The compositions of pyrolysis condensed products collected after reuse of ozonated catalysts are presented in Table 3.6 alongside thermal and fresh experiments for comparison. Similarly to Section 3.2.1.1, the repartition of obtained oils and waxes is discussed according to their fraction (C7-C9, C10-C14 and C15+) as well as their aromaticity. The evolution of main products, toluene and xylenes, is also presented.

**Table 3.6.** Composition of pyrolysis oils analyzed by GC-MS for regenerated catalysts.

Condensed products distribution (%)		Thermal	Fresh	R8	R48
<b>Identified</b>		96.5	98.5	95.9	96.6
<b>Aromatics</b>		0.2	91.9	78.7	91.4
<b>C7-C9 (Gasoline)</b>	Total	40.1	94.9	87.9	92.2
	Aromatics	0.0	91.5	78.2	89.6
<b>C10-C14 (Kerosene)</b>	Total	38.2	3.1	6.1	3.3
	Aromatics	0.2	0.4	0.5	1.8
<b>C15+ (Heavy oils)</b>	Total	18.2	0.5	1.9	1.2
<b>Main products</b>	Toluene	-	26.8	15.3	18.5
	Xylenes	-	59.4	52.1	61.8

The regenerating treatment applied during 8 h allowed to obtain important recovery of cracking and rearrangement performances when compared to spent catalysts capacity (L4 experiment), showing that an important part of initial catalytic selectivity is restored. While the L4 experiment presented only 27.5% of aromatics and 69.8% of light products (C7-C9), pyrolysis using R8 catalysts led to regained formation of aromatics (78.7%) and gasoline fraction (87.9%). Consequently, as illustrated in Figure 3.8, the 8 h ozonation treatment allowed a partial recovery of catalytic performances. The obtained composition is close to pyrolysis products of L1 experiment, where used catalysts were coked once, suggesting that 8 h of ozonation exposition is not sufficient to remove all deposited coke. Indeed, the lower proportions of aromatic products and C7-C9 fraction, compensated by a

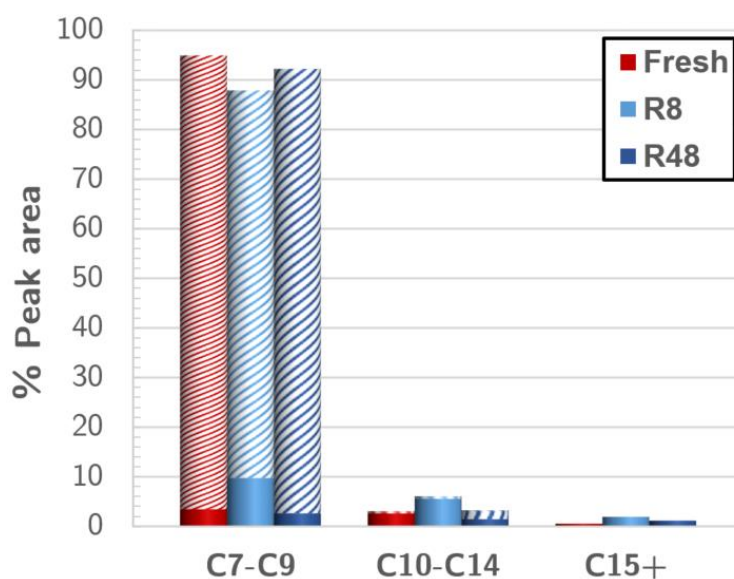


**Figure 3.8.** Comparison of pyrolysis products between fresh and regenerated catalysts. Hatched area represents aromatic molecules.

more important C10-14 content, traduces the incomplete regeneration of active sites. Nevertheless, the reuse of R48 catalysts led to the formation of pyrolysis oils having identical composition to initial catalytic pyrolysis, suggesting that catalytic efficiency is entirely recovered. Both aromatics and light fraction proportions are similar to the experiment conducted with fresh catalysts: 91.4% of aromatic and 92.2% of gasoline products with R48 catalysts. The ozonation treatment during 48 h therefore almost allowed fully restoring initial catalytic selectivity. Similarly to regeneration with combustion, complete regeneration of catalysts is difficult to achieve and require important process times. Results obtained in this work with ozonation show similar behavior as a long time of exposure is required to approach initial catalytic selectivity. Moreover, assessment of restored catalytic selectivity after reasonable regeneration time (8 h) already provides important performances recovery. For industrial application, an optimization of the recovery efficiency gain as a function of process time and energy consumption would be relevant. The characteristics of regenerated catalysts after the different investigated ozonation treatments are discussed in Section 3.2.2.2 in order to assess the recovery of textural and chemical properties leading to the observed restored catalytic efficiency.

### 3.2.2.2. Catalytic properties recovery and evolution

Textural and chemical properties of regenerated and reused samples are presented in Table 3.7. Fresh and L5 samples characteristics are reminded for comparison purposes, being the departing samples before pyrolysis and regeneration respectively. Regenerated (R8 and R48) and reused samples (R8-P and R48-P) are included in the graphic correlation comparing microporous volume and free acid sites fraction as a function of carbon content (Figure 3.5.a, b).

After the 8 h oxidative treatment, 53% of the initial coke is removed. Obtained retrieved characteristics are between those of L1 and L2 samples, such as microporous volume ( $0.08 \text{ g.cm}^{-3}$ ) or Brønsted acidity ( $135 \text{ } \mu\text{mol.g}^{-1}$ ) for instance. Exposition time was therefore not sufficient to recover all active sites but ozonation allowed a 45% recovery for Brønsted

**Table 3.7.** Textural and chemical properties of regenerated and reused catalysts.

Property	Regenerated samples*				Reused in pyrolysis	
	Fresh	L5	R8	R48	R8-P	R48-P
Carbon content (wt. %)	-	9.9	4.7 (53%)	0.4 (92%)	7.9	6.3
BET surface area (m <sup>2</sup> .g <sup>-1</sup> )	369.6	43.3	174.3 (35%)	315.6	86.8	215.3
Total pore volume (cm <sup>3</sup> .g <sup>-1</sup> )	0.38	0.16	0.27 (29%)	0.32	0.22	0.28
Microporous volume V <sub>micro</sub> (cm <sup>3</sup> .g <sup>-1</sup> )	0.17	0.02	0.08 (35%)	0.14	0.05	0.10
Mesoporous volume V <sub>meso</sub> (cm <sup>3</sup> .g <sup>-1</sup> )	0.21	0.14	0.19 (24%)	0.18	0.17	0.18
Brønsted acid sites (μmol.g <sup>-1</sup> )	294	4	135 (45%)	294	50	192
Lewis acid sites (μmol.g <sup>-1</sup> )	193	25	90 (34%)	187	43	54

\* Fraction of removed coke and known recovery rates are indicated in (%) for regenerated samples. Initial coked samples properties before R48 were unknown except carbon content.

sites and 34% of Lewis acidity. Recovery rate of mesoporous volume (24%) is less important than microporous retrieval (35%). Ozone preferentially reacts with coke located over strong acid sites in micropores. Indeed, as mentioned in Section 3.2.1.3, external coke for extensively coked catalysts is made mostly of very stable polyaromatic clusters while the steric limitation leads to the formation of smaller internal coke molecules. Being less stabilized by important condensation, these molecules react more easily with oxidizing agents. A difference of oxidation rate appears depending on the various structures and natures of coke molecules. The partial recovery of textural and chemical properties does not linearly correlate with the catalytic performance discussed in Section 3.2.2.1. Indeed, despite incomplete acid sites recovery, reuse of R-8h sample conducted to an important catalytic efficiency of 86% regarding products aromaticity. However, residual coke is blocking a fraction of active sites preventing complete recovery of catalytic performances. As the ozonation process follows the shrinking-core model, much longer exposition time could allow remaining coke to be oxidized [235]. The ozonation regenerative treatment was thus applied for 48 h at 100 °C intending to achieve complete coke removal (sample R48). A coke removal of 92% is obtained, corresponding to 0.4 wt.% of residual carbon. Despite few coke remaining, acidity has been entirely recovered as both Brønsted and Lewis sites concentrations retrieved their initial value. Nevertheless, the residual carbon causes partial recovery of specific surface and porosity. The fact that chemical properties are completely retrieved while textural characteristics remains impacted by residual coke suggests that ozone and/or hydroxyl radicals have a selective reactivity during oxidation. Coke located over acid sites are suggested to be more reactive and favorably attacked by oxidizing agents. Remaining coke is therefore mainly deposited on the binder. This effect is also enhanced by the higher stability of external coke as previously discussed. Fraction of residual coke is also located in the microporosity as only 83% of microporous volume is recovered. Ozonation process being a diffusion-reaction process as investigated by Daligaux *et al.* [235], these coke molecules are suggested to be inaccessible to oxidizing agents due to competing reactivity and diffusion limitations, and therefore difficult to remove. However, the high coke removal efficiency with the corresponding catalysts properties recovery achieved via ozonation allowed to obtain pyrolysis products similar to fresh zeolites when reusing so-regenerated catalysts as mentioned in Section 3.2.2.1.

After reuse of regenerated samples in pyrolysis, coked catalysts were collected to compare the relative deactivation rates of regenerated samples with those of initial experiments. The evolution of catalytic properties after reuse in pyrolysis is presented in Figure 3.9. A complete cycle is here represented: starting from fresh catalysts, followed by spent material (L5), then corresponding regenerated sample (R8) and finally after being reused in same conditions as initial pyrolysis (R8-P). The sample R48-P, obtained by reuse of R48 in pyrolysis, is also plotted for comparison and shows properties close to L1 spent catalysts. Completely regenerated and fresh catalysts therefore appear to present similar deactivation behavior. Diminution of Brønsted acid sites is identical while Lewis acidity, porosity and specific surface loss is slightly more important. Similar decrease is observed for R8-P sample, which coke content before reuse is not null (4.7 wt.%C). It is expected that remaining coke favor the formation of new deposits as it acts as precursors, amplifying deactivation when recycling regenerated samples with residual carbon compounds. Brønsted acidity loss between R8 and R8-P is 29% while it would be expected around 26.5% by interpolation between the samples with similar characteristics (L1 and L2). However, comparison of relative deactivation rates is more complex and samples with exact initial characteristics would be required for accurate comparison in order to draw any conclusions. Based on our results, deactivation observed when reusing ozonated catalysts does not present a different rate when compared to the initial coke formation discussed in Section 3.2.1.2. The combined results of catalytic selectivity and zeolite

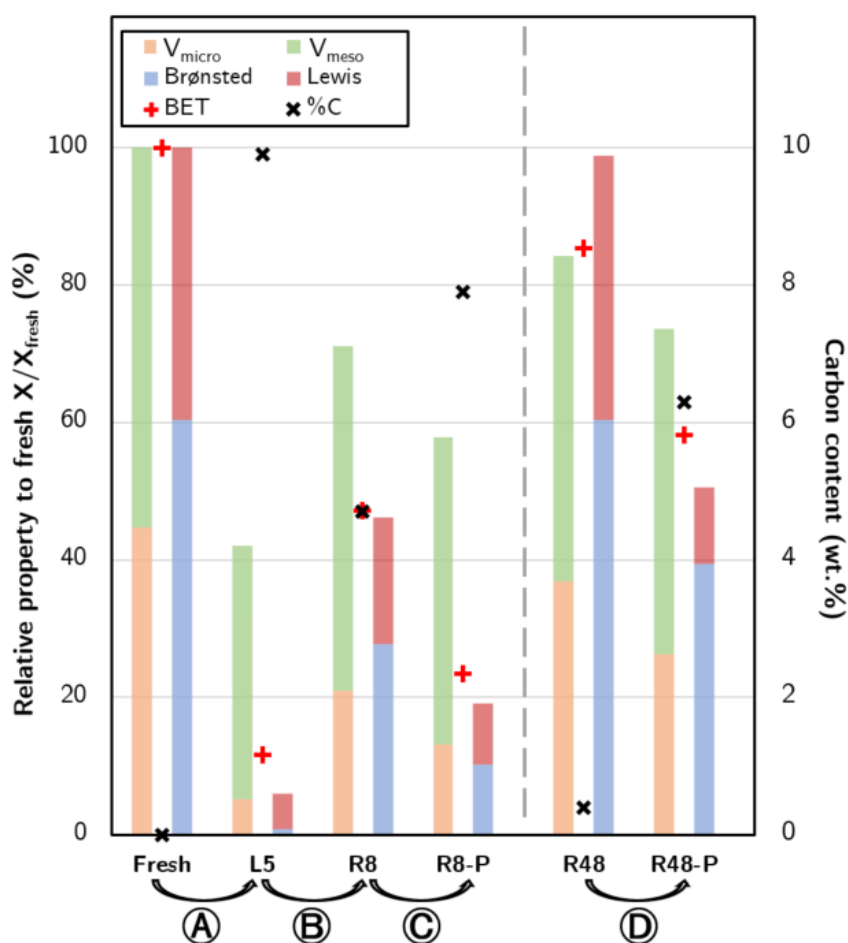


**Figure 3.9.** Evolution of textural and chemical properties of catalysts samples during one cycle of pyrolysis, regeneration with different exposition times and reuse. (A: five successive pyrolysis; B: 8 h ozonation at 100 °C; C and D: reuse in pyrolysis).

material properties in this work show that ozonation is efficient in one reuse cycle. Influence of repeated regenerations, similarly to Kassargy *et al.* [197] who studied catalyst regeneration efficiency up to 14 cycles with combustion, will be investigated using ozonation and presented in a future study.

### 3.3. Additional considerations

#### 3.3.1. Repeatability of coking during pyrolysis

Deactivation via coke formation is a complex phenomenon due to the diversity of formed deposits. Such reactivity is expected to be variable when repeating the process due to the multiple possible pathways in this diffusion-reaction system. A repeatability study was conducted during three successive uses of catalysts in layers. The characteristics of coked samples are presented in Table 3.8.

**Table 3.8.** Textural and chemical properties of spent catalysts for repeatability study.

Property	L1	L1'	L1''	L2	L2'	L2''	L3	L3'	L3''
Carbon content (wt. %)	8.2	6.3	8.7	6.5	7.0	6.4	8.3	8.4	8.3
H/C ratio (-)	1.6	1.9	1.7	1.1	0.9	0.6	0.6	0.6	0.5
BET surface area (m <sup>2</sup> .g <sup>-1</sup> )	231.7	217.7	203.6	138.9	135.8	162.5	49.1	78.6	73.2
Total pore volume (cm <sup>3</sup> .g <sup>-1</sup> )	0.29	0.29	0.26	0.23	0.25	0.26	0.13	0.21	0.20
Microporous volume V <sub>micro</sub> (cm <sup>3</sup> .g <sup>-1</sup> )	0.11	0.10	0.09	0.07	0.07	0.08	0.03	0.04	0.04
Mesoporous volume V <sub>meso</sub> (cm <sup>3</sup> .g <sup>-1</sup> )	0.18	0.19	0.17	0.16	0.18	0.18	0.10	0.17	0.16
Brønsted sites (μmol.g <sup>-1</sup> )	191	249	233	103	94	143	31	36	49
Lewis sites (μmol.g <sup>-1</sup> )	76	63	94	66	49	86	33	14	45

The investigated samples present the expected tendency of global textural and chemical properties loss during successive uses in pyrolysis. Sample L3 appears as an outlier regarding its textural properties. Such gap might be caused by a lack of homogeneity within a single coked sample. As discussed in Section 3.2.1.2, the exposition of catalysts to deactivation varies depending on the layer's initial position in the reactor. When sampling the spent pellets for analysis, it is possible that the collected fraction is not fully representative of the sample. Samples L1, L1' and L1'' therefore present an important variation of carbon content while samples after three uses (L3, L3' and L3'') have a similar carbon content. The heterogeneity of coke deposition is indeed mitigated after several catalysts reuses as the different layers are mixed randomly for each reactor loading. The evolution of textural and chemical properties presented in Table 3.8 is nevertheless not correlated with carbon content as was previously plotted in Figure 3.5. Despite important variation of coke content, catalyst characteristics remain close for each series of successive pyrolysis, especially microporosity and Brønsted acidity. Similar pore blocking contribution are also found in L' and L'' series by using the aforementioned method: pore blocking is not observed after first use, contributes to around 40% of microporosity loss



after second use and 50% after the final pyrolysis run. Coking deactivation is then repeatable despite its complexity and the variations of exposition. Initial heterogeneity of carbon deposition is compensated during further reuses. The obtained results confirm the consistency of the applied operating protocol.

### 3.3.2. Influence of initial mixing on deactivation

Deactivation of industrial ZSM-5 catalysts was also investigated during up to three successive reuses during pyrolysis using “top” mixing method (Figure 2.9, p.58). Pyrolysis waxes and oils were collected in separate fractions making impossible the comparison of their composition with layers experiments where the two fractions were completely mixed. However, oil fraction for these experiments were analyzed by GC-MS using identical method to assess the evolution of their composition. Collected spent catalysts are characterized using same analytical techniques. Results can be exploited to compare the relative deactivation with the two different mixing methods. Using similar notation to layers samples, top experiments are identified with the letter T followed by the number of successive pyrolysis without intermediate treatment.

#### 3.3.2.1. Catalytic selectivity

The composition and distribution of pyrolysis oils collected after successive reuses of catalysts with top mixing are presented in Figure 3.10. The repartition of obtained products is discussed according to their fraction, corresponding to their number of carbon (C7-C9, C10-C14 and C15+) as well as their aromaticity. The evolution of main products, toluene and xylenes, is also presented.

Condensed products distribution (%)		Fresh	T1	T2
<b>Identified</b>		96.2	95.7	92.3
<b>Aromatics</b>		93.6	91.2	78.3
<b>C7-C9 (Gasoline)</b>	Total	95.1	93.3	85.4
	Aromatics	93.2	90.9	77.7
<b>C10-C14 (Kerosene)</b>	Total	1.0	1.7	4.8
	Aromatics	0.5	0.4	0.7
<b>C15+ (Heavy oils)</b>	Total	0.1	0.7	2.1
<b>Main products</b>	Toluene	40.8	24.0	21.8
	Xylenes	49.3	62.8	48.6

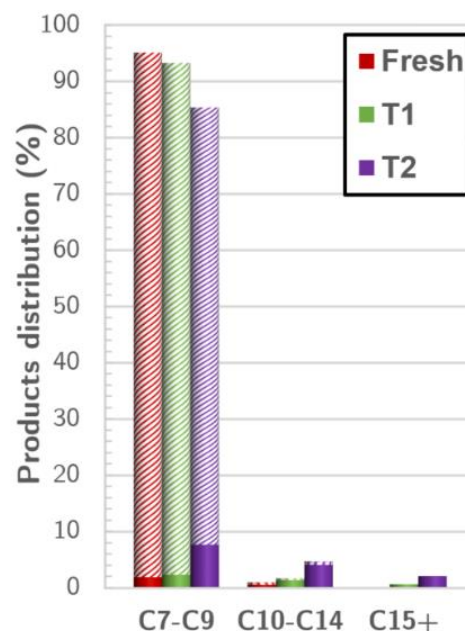


**Figure 3.10.** Evolution of pyrolysis products repartition after successive reuses of catalysts using top mixing method. Hatched area represents aromatic molecules proportion.

As expected as only pyrolysis oils were collected and not waxes, analyzed products present mostly molecules being part of the light fraction (C7-C9). The aromatics proportion using fresh catalysts in top series is however comparable to the one in layers series (93.6% and 91.9% respectively, refer to the “Fresh” column in Table 3.2, p.74). When further



reusing catalysts during top experiments, a slight decrease of aromatic products and increase of heavy fractions is observed. This behavior is expected according to the lowered catalytic performances (cracking, cyclization and rearrangement) discussed in Section 3.2.1.1. The evolution of aromatics proportion from 93.6% to 91.2% after the second use suggests a lowered loss of performances during top series compared to layers experiments but products cannot be compared to assess relative degradation of catalytic efficiency. When further reusing the catalysts (T2 sample), an important catalytic performance loss is observed as obtained aromatics proportion is 78.3% and the C7-C9 fraction drops from 93.3% to 85.4%. Deactivation therefore appears to be more important after the third use in pyrolysis. The related evolution of catalyst textural and chemical properties are discussed in the following paragraph to evaluate the impact of catalysts initial position in the reactor on coke formation.

### 3.3.2.2. Catalysts characteristics

Textural and chemical properties of spent catalysts for this series of experiments are given in Table 3.9, alongside the evolution of carbon content and H/C ratio during successive pyrolysis. The properties of fresh industrial ZSM-5 are reminded for comparison to evaluate deactivation caused by coke deposition.

**Table 3.9.** Textural and chemical properties of fresh and spent catalysts (top experiments).

Property	Fresh	T1	T2	T3
Carbon content (wt. %)	-	3.3	5.8	7.8
H/C ratio (-)	-	2.1	0.8	0.3
BET surface area (m <sup>2</sup> .g <sup>-1</sup> )	369.6	273.6	184.0	115.2
Total pore volume (cm <sup>3</sup> .g <sup>-1</sup> )	0.38	0.31	0.25	0.21
Microporous volume V <sub>micro</sub> (cm <sup>3</sup> .g <sup>-1</sup> )	0.17	0.13	0.09	0.06
Mesoporous volume V <sub>meso</sub> (cm <sup>3</sup> .g <sup>-1</sup> )	0.21	0.18	0.16	0.15
Brønsted acid sites (μmol.g <sup>-1</sup> )	294	211	89	58
Lewis acid sites (μmol.g <sup>-1</sup> )	193	105	54	44

Typical tendency of deactivation by coke deposition similar to previous results is observed on these samples. The increase of carbon content is correlated with a gradual loss of specific surface, porosity and acidity, with a good inclusion in Figure 3.5 tendencies. Coke deposition is traduced by a regular augmentation of carbon content from 3.3 to 7.8 wt.%C. Deposition of carbonaceous compounds appears to be mitigated during top experiments as coke content after one use (3.3 wt.%C) is inferior to the 8.2 wt.%C obtained after single layers use. The almost linear evolution of carbon content during top experiments denotes with the fast increase followed by a stabilization observed for layers series. The evolution of H/C ratio values is however comparable and traduces the condensation progression of coke towards polyaromatic compounds. In order to compare the relative deactivation rates between the different initial mixing methods, samples after three reuses for both series are plotted alongside in Figure 3.11. The decrease of both specific surface and total porosity appears to be more important in layers series. After 3 successive pyrolysis runs, 31.2% of specific area and 55.3% of pore volume are available for top experiments while only 13.3% and 34.2% respectively are remaining using layers mixing method. According to Figure 3.11.b, microporous volume is more impacted than

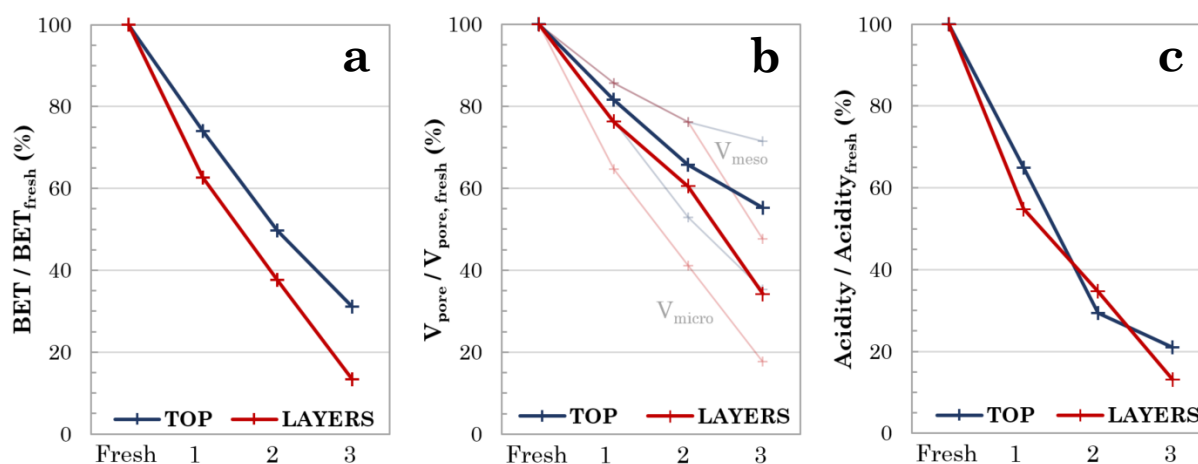
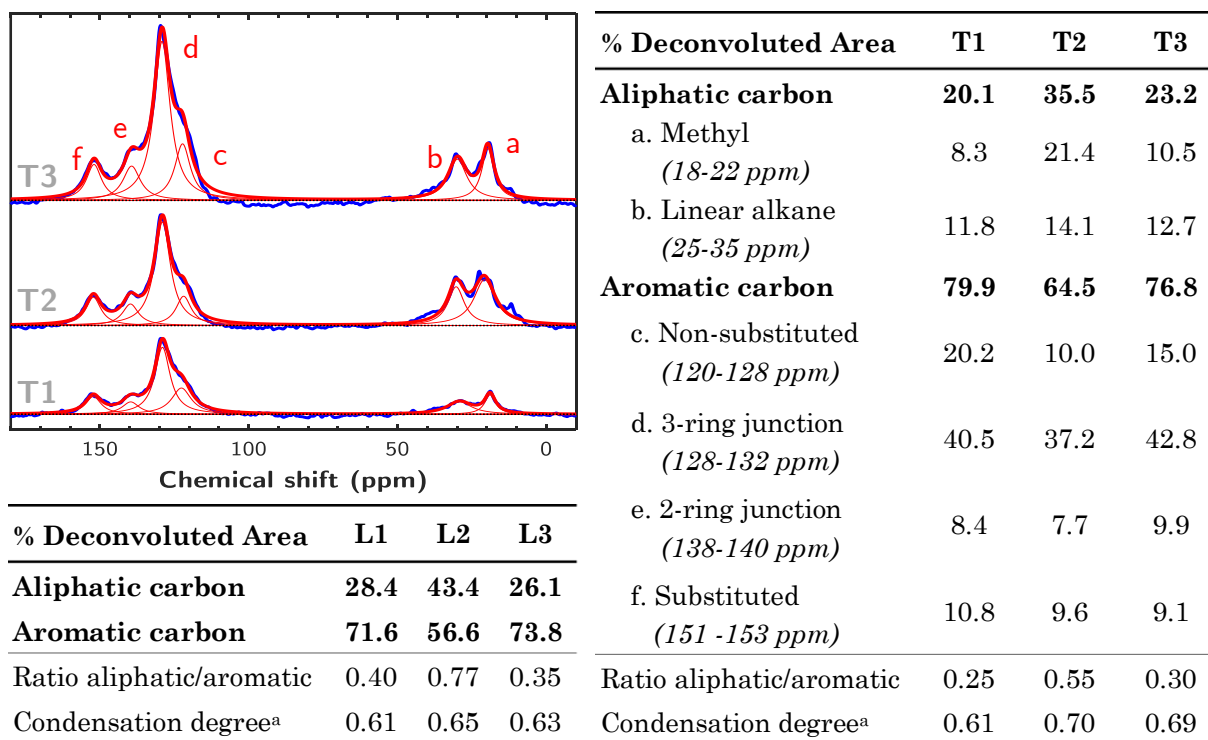


**Figure 3.11.** Comparative evolution of normalized (a) specific surface, (b) porosity and (c) total acidity between the different series of experiments using top and layers mixing.

mesoporous one during top experiments. These results are in accordance with respective carbon contents as the higher coke deposition observed over layers samples is expected to affect more importantly catalyst properties. As previously discussed in Section 3.2.1, catalysts positioned in layers are certainly more exposed to molten polymers generating an increased carbon deposition around the pellets. On the other hand, catalysts during top experiments are suggested to remain at the surface of polyethylene phase due to surface tension, and are therefore mainly exposed to formed vapors. Such molecules being lighter compounds with further cracking, their diffusion in the porous extrudate matrix is eased and formation of external coke is mitigated, limiting deposited carbon content. However, while textural properties show a steeper deactivation when positioning catalysts in layers, the evolution of catalyst acidity suggests a different tendency as both series show similar loss of chemical properties (Figure 3.11.c). The coke formation pathway is therefore likely to be different depending on the mixing method as the different evolutions of textural characteristics are leading to identical active site decrease. This hypothesis is studied in Section 3.3.2.3 by investigating coke nature and location in order to determine potential changes of deactivation pathway depending on catalysts exposition to reactants.

### 3.3.2.3. Coke nature and location

Results of coked samples analysis of top experiments are presented in Figure 3.12. By repeating the study conducted over layer samples, observed coke nature and deactivation tendency is sensibly the same with a mix of aliphatic and aromatic carbons (majority of heavy coke), an increasing condensation degree and coke density (from 0.80 g.cm<sup>-3</sup> for T1 to 1.43 g.cm<sup>-3</sup> for T3), as well as altered reactivity for the second run and apparition of pore blocking. Deactivation via coking in top configuration appears to be very close to layers experiments pathway despite lower observed coke content. As illustrated by the aliphatic to aromatic ratio, the fraction of light coke is lower for top experiments. This observation supports the hypothesis of the deposition of external linear or branched coke molecules over catalysts during layers experiments. Deposition of coke in the pellets during top experiments is suggested to be similar to the deactivation pathway described in Figure 3.7: initial coke formation occurs mainly in zeolite crystals before important deposition of aliphatic compounds around zeolite particles forming a barrier and causing pore blocking. These molecules further condensates following coke growth mechanisms with the deposition of additional soft coke at each reuse until complete deactivation is observed.



<sup>a</sup> The condensation degree is calculated as the ratio of ring junction and total aromatic carbons.

**Figure 3.12.** Normalized  $^{13}\text{C}$  NMR spectra for coked samples after top pyrolysis experiments and deconvolution results for the determination of coke nature and composition. Layers samples are reminded for comparison purposes (refer to Table 3.4 for full results).

The main difference of deactivation by coke formation between the two mixing methods is the enhanced deposition of a layer of molten polymer around the extrudates. Carbon content increases sharply during the first uses while the evolution of zeolite characteristics does not change accordingly. Indeed, both series present similar loss of chemical properties while carbon content is lower for top experiments. The initial position of catalysts in the reactor therefore influences the direct exposition of pellets to reactants. Layers of catalysts located between two loads of polyethylene are dipped into molten plastics while catalysts on top of the material are suggested to remain at the surface, at least until potential mixing generated by ebullition. It is thus suggested that catalysts are exposed to reactants at different stages of the pyrolysis reaction according to their initial position. When placed on top, catalysts are mainly exposed to pyrolysis vapors being small molecules that underwent important cracking. Such molecules can diffuse into zeolite crystallinity to further react and form aromatic products. On the other hand, catalysts dipped into liquid plastics are exposed to reactants during earlier stages of cracking. Molecules diffusing through catalysts pellets are suggested to be longer and heavier, being more susceptible to be sterically blocked around zeolite crystallinity. These carbon compounds therefore do not further react in microporosity and generates a higher proportion of aliphatic coke over catalysts exposed to such conditions. However, configurations of initial position remain close, explaining the many similarities of deactivation despite slight variations. Top mixing method appears to slightly mitigate coke formation due to exposition to lighter reactants. Such behavior is expected as different studies showed lowered deactivation when placing catalysts as a fixed bed in a separate reforming reactor [14]. Industrial catalytic pyrolysis unit could most likely feature different levels of reactors to increase selectivity and mitigate deactivation [236]. However, coke formation cannot be avoided in this process as many of the products or intermediates are precursors.

### 3.4. Conclusions and key takeaways

Catalytic pyrolysis of polyethylene was successfully implemented in this work with the conception and operation of a pilot-scale semi-batch reactor (450°C). This process was used as a model reaction for the study of catalytic deactivation via coke formation. Industrial catalysts were used during five successive pyrolysis runs, showing important carbon deposition ( $\approx 10$  wt.%C) and drastic decrease of product selectivity. A comprehensive study of coke formation during pyrolysis was conducted to gain better insight of involved coke species and deactivation pathways (pore blocking). Such deactivated catalysts were successfully regenerated using ozonation at 100°C in a fixed bed reactor (capacity 10 g). The different times of exposition (8 h and 48 h) both presented an important recovery of catalytic selectivity even though residual coke remains deposited over the pellets. The 48 h regeneration even allowed restoring almost completely the porous volume and the acidity of zeolite material, proving the ability of the ozonation process to remove efficiently heavy coke structures. The results presented in this chapter are therefore of high interest to gain a better understanding of coke formation during catalytic pyrolysis of LDPE and can most likely be transferred to other polymeric materials.

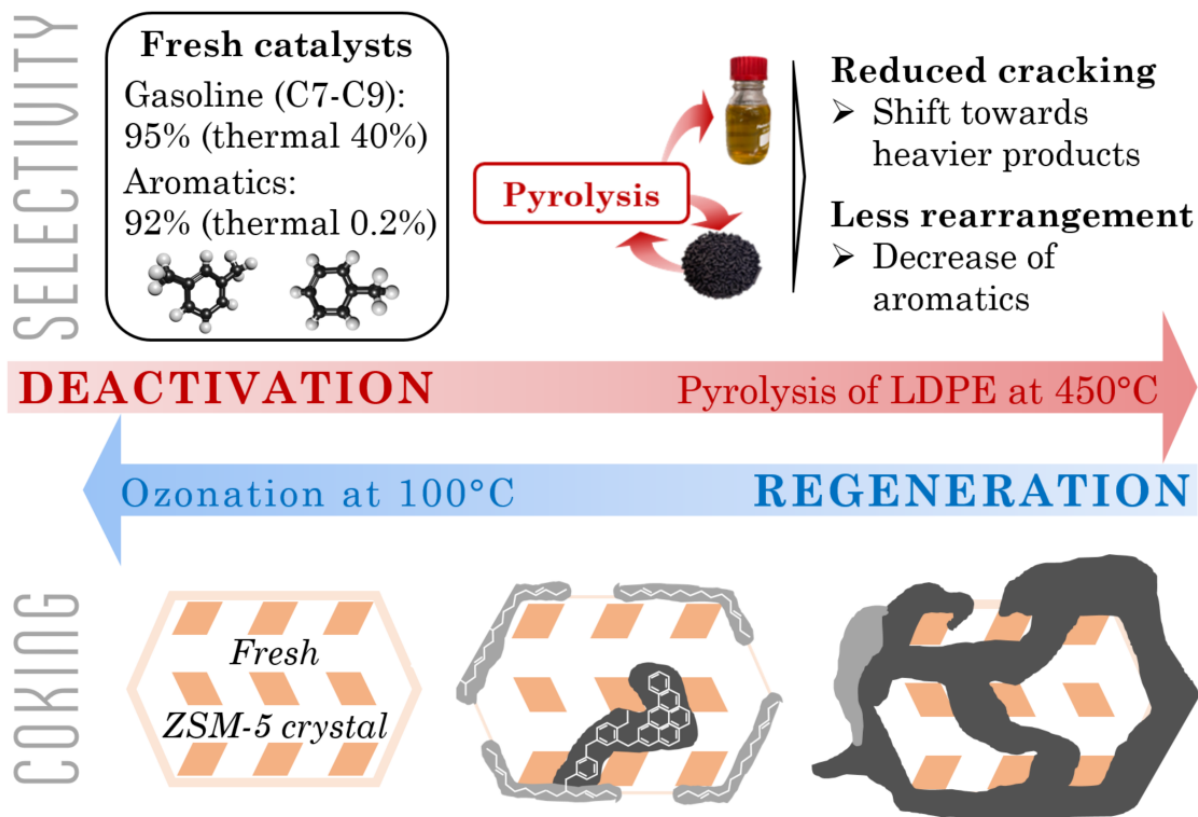
During the work conducted in this chapter, typical behavior of deactivation via coke formation was observed on catalysts during LDPE pyrolysis at 450°C. The apparition of heavy coke molecules, traduced by an increase of carbon content, was correlated with an important loss of catalyst textural and chemical characteristics. Microporous volume was more impacted than mesopores due to steric limitation of coke growth and apparition of pore blocking. Deactivation via coking during this process is described in a multi-step pathway leading to final complete deactivation. Coke deposition during the early stages is mostly occurring in micropores with the formation of condensed cyclic coke molecules. A fraction of external aliphatic coke is also observed mostly around zeolite crystals. This external coke is furtherly growing due to additional soft coke deposition, leading to the formation of a barrier around crystals causing pore blocking and supplementary microporous volume loss. Brønsted acidity is heavily impacted, as mostly located in microporosity but a decrease of Lewis acid sites concentration is also observed. Similar deactivation behavior is observed for the two mixing methods (top and layers). Loss of catalytic performances and properties occurs rapidly after more than two successive runs in both cases. The main difference between the different series is the increased deposition of aliphatic external coke during layer experiments, attributed to the variation of catalysts exposition to reactants during the process. Thus, slight changes in the deactivation pathway are observed even though the global tendency remains identical. The evolution of catalysts properties influences the nature of obtained pyrolysis products as it lowers catalytic performances. As catalytic deactivation progresses, a significant drop of aromatic products and light fraction molecules (C7-C9) is observed in the collected oils, traducing the loss of respectively rearrangement and cracking capacity of the catalysts. The use of ozonation process allowed to retrieve similar catalysts characteristics and pyrolysis products composition after reuse of regenerated catalysts. Conditions of ozonation used in this study was based on the work regarding the optimal parameters for coke removal conducted simultaneously (refer to Chapter 4). Ozonation appears as a promising alternative method to coke combustion with oxygen to achieve coke removal and catalytic regeneration. As coke formed during pyrolysis is mainly composed of heavy and stable structures, these results are promising regarding the use of ozonation in a wide range of deactivating processes with less severe deactivation conditions. During the ozonation

treatment, oxidizing agents reacted preferentially with microporous coke due to its lower stability compared with external polyaromatic clusters. This selectivity allows recovering important proportions of initial characteristics from heavily coked sample with limited time of exposition (8 h). However, complete coke removal is difficult to achieve because of ozone diffusion limitations in micropores. Indeed, despite complete acidity recovery (Lewis and Brønsted sites), the initial textural properties (specific surface and global porosity) are not completely retrieved. Residual coke is suggested to act as precursors and intensify deactivation rate when reusing regenerated catalysts. Principal conclusions and key takeaways of this chapter are summarized in Figure 3.13.



A research paper inspired by this chapter was submitted in *Applied Catalysis B: Environmental* (Elsevier) on 9<sup>th</sup> of October 2023.

“Deactivation by coking of industrial ZSM-5 catalysts used in LDPE pyrolysis and regeneration by ozonation process – Pilot scale studies” – V. Daligaux, R. Richard, M. Marin Gallego, V. Ruaux, L. Pinard, M.-H. Manero



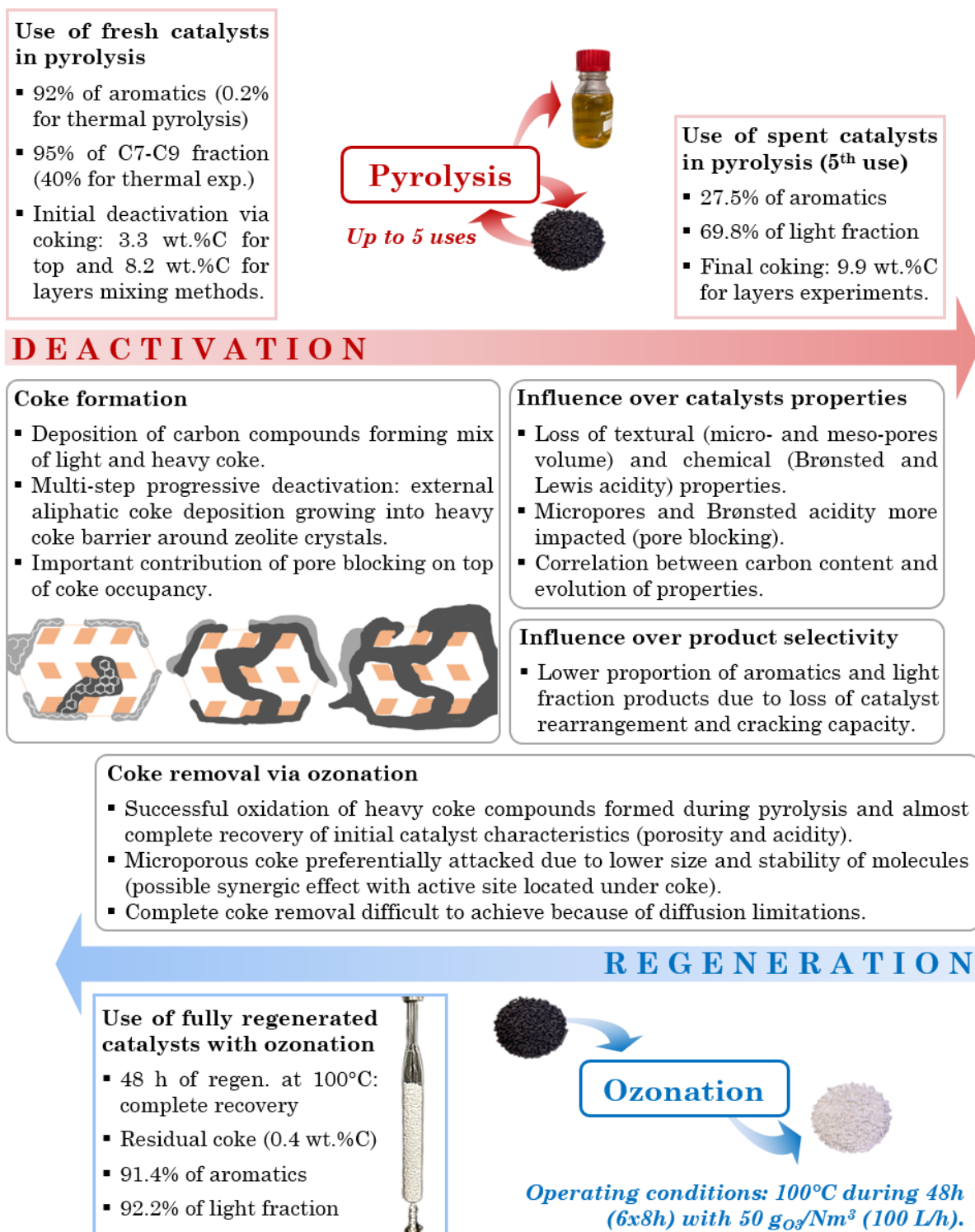


Figure 3.13. Key takeaways of “Chapter 3 – Deactivation of catalysts by pyrolysis of LDPE”.



# Chapter 4

# Regeneration of zeolites by ozonation

This chapter focuses on the experimental aspect of the ozonation process for regeneration of coked zeolites. After presenting the context and previous studies regarding this aspect of the PhD research (Section 4.1), obtained results and corresponding discussion are presented in Section 4.2. First insights on process scale-up are presented in Section 4.3 with a comparison between tubular and syringe reactors configuration. Conclusions of this study are discussed in Section 4.4.

## 4.1. Introduction and context based on previous studies

Previous studies on ozonation showed promising results in terms of coke removal efficiency and catalytic performance recovery [8, 9]. Results presented in Chapter 3 of this work confirmed the ability of ozonation to restore completely both initial zeolite characteristics and catalytic activity. As mentioned in the previous chapter (Section 3.1), operating conditions for ozonation of coked samples aimed for reuse were arbitrary chosen based on the optimal conditions sensed from the work conducted in this chapter.

While the process capacity to allow catalysts recycling has been demonstrated, many aspects of ozonation remain to be understood, such as the contribution of each competing reaction mechanisms (thermal recombination, catalytic degradation and coke oxidation) in ozone consumption and the influence of operating parameters on the diffusion limitations occurring in zeolite pellets during regeneration. This chapter intends to provide better insight on these two principal axes of work with an experimental approach. The conducted parametric study aims to pursue the preliminary works of LGC team with coked catalysts from another deactivating reaction. As illustrated in Figure 4.1, time of exposure (a) and temperature (b) were the most influencing parameters over coke removal. Rapid oxidation was observed at early stages of the process while coke removal was slower after longer times of ozonation. A temperature optimum was also observed with a maximal efficiency between 100 and 150°C depending on gas feed nature. Similar studies were conducted here by evaluating the coke removal efficiency varying the four investigated operating parameters. The use of different coked samples with known characteristics brought new considerations regarding the effect of initial coke load and nature on



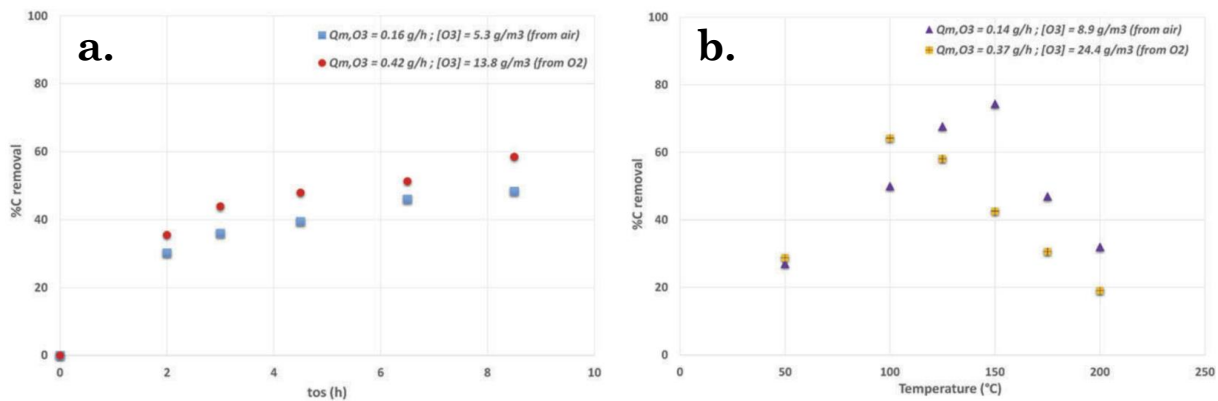


**Figure 4.1.** Influence of (a) time-on-stream (TOS) and (b) temperature over carbon removal efficiency during ozonation (Richard *et al.*, 2017) [9].

regeneration efficiency. The ozonation parametric study was carried out in a fixed-bed reactor (tubular configuration). The influence of different operating parameters on regeneration process was investigated: temperature, ozone inlet concentration, flowrate and time of exposure. Moreover, mass transfer aspects were heavily investigated in this work to better understand the involved effect of operating parameters on process physics. First considerations of diffusion limitations were discussed in Khangkham *et al.* work. The observation of visual differences between pellet cross-sections (black core or regular grey) hinted that different regeneration regimes are occurring during ozonation depending on the process conditions. Innovative SEM-FEG application is used in this work to investigate these different behaviors known in the literature as shrinking-core and homogeneous regimes.

The second aspect investigated in this chapter (Section 4.2.2) is the study of competing consumption mechanisms of ozone at reactor scale. Catalytic degradation is expected to have a major contribution in ozone reactivity as catalytic materials are often used to remove ozone in air treatment processes. The influence of thermal recombination is therefore expected to be of less influence in presence of zeolites, as illustrated in Figure 4.2. Due to ozone instability and complex reactivity, very limited work can be found concerning the determination of its kinetic parameters. The lack of information for such data is an important barrier for further understanding of the ozonation process.

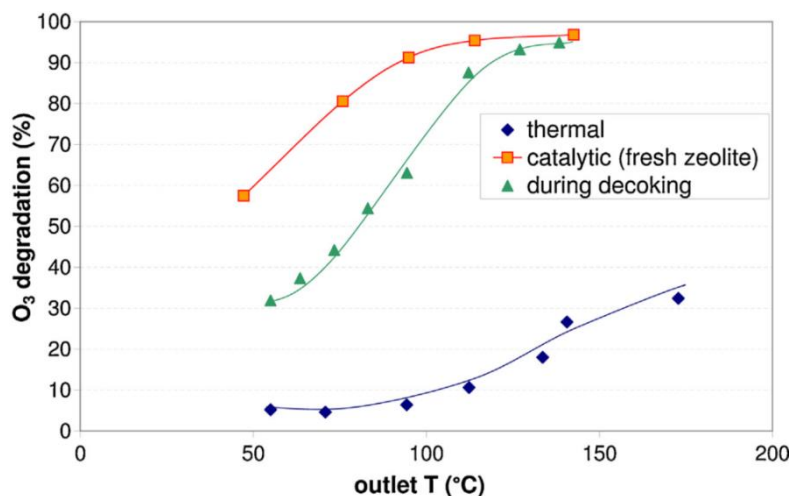


**Figure 4.2.** Evolution of the different pathways of ozone degradation (thermal, catalytic and decoking) for different reactor temperatures (Khangkham *et al.*, 2013) [8].

Consequently, in order to achieve experimental determination of these parameters, robust analytical techniques have to be developed in order to overcome the challenges related to the characterization of coke and the ozone reaction mechanisms with such molecules. In this work, an experimental study was conducted using tubular reactor configuration to determine pseudo-kinetic constants in our system. Experimental outlet concentrations are exploited to calculate the constant values, which are then plotted using Arrhenius equation in order to extract pre-exponential factors and activation energies. The main challenge is that the different mechanisms cannot be investigated separately during decoking as they are occurring simultaneously. Thermal recombination study is conducted in the empty tubular reactor while combination of thermal and catalytic mechanisms is investigated using fresh zeolite catalytic bed. With the addition of coke oxidation, global  $O_3$  reactivity and its evolution during decoking is eventually discussed, providing complete overview of ozone consumption during ozonation.

## 4.2. Results and discussion

### 4.2.1. Parametric study at pellet scale

#### 4.2.1.1. Time of exposure

Regeneration kinetics were first examined for different coked samples by varying the time of ozone exposure. Table 4.1 summarizes used coke samples in this study alongside their carbon load, number of pyrolysis and global textural properties. Samples Cok1 (3.3 wt.%C) and Cok2 (8.3 wt.%C) were used for these experiments. The temperature was set at 100 °C and spent zeolites were exposed to a gas flowrate of 50 L/h containing 50 g/Nm<sup>3</sup> of ozone, resulting in a mass flowrate  $Q_{m,O_3}$  of 2.5 g/h. For each experiment, an optical picture of a pellet cross-section from the upper fraction of the reactor is presented (Figure 4.3.a). Figure 4.3.b represents the evolution of ozonation efficiency up to 8 h.

**Table 4.1.** Summary of coked samples used as initial samples for regeneration via ozonation.

Sample notation (Chapter 3 notation)	Fresh	Cok1 (T1)	Cok2 (L3 <sup>''</sup> )	Cok3 (T3)	Cok4 (T2)	Cok5 (L3')	Cok6 (N/A)
Carbon content (wt.%)	0.0 %C	3.3 %C	8.3 %C	7.8 %C	5.8 %C	8.4 %C	6.0 %C
Number of successive pyrolysis runs (-)	-	1	3	3	2	3	2
Surface area (m <sup>2</sup> .g <sup>-1</sup> )	370	274	73	115	184	79	ND <sup>a</sup>
Total pore volume (cm <sup>3</sup> .g <sup>-1</sup> )	0.38	0.31	0.20	0.21	0.25	0.21	

<sup>a</sup> Not Determined

As expected, process efficiency, indicated by carbon removal, tends to increase as it is longer exposed to ozone stream. While an important kinetic of oxidation is observed during the first hour of ozonation, an asymptotic behavior seems to appear for higher exposition times. Indeed, oxidation kinetics for the less-coked sample (Cok1) reaches a plateau after approximately 4.5 h, corresponding to a coke removal around 80%. This value corresponds to a 0.5 wt.% residual carbon content which appears to be the minimal coke content achievable in these conditions. Using the zeolite sample with a higher initial coke content (Cok2), a coke removal of 78% is achieved (1.8 wt.% final carbon content). The expected plateau does not seem to be reached and longer time-on-stream (TOS) could allow to

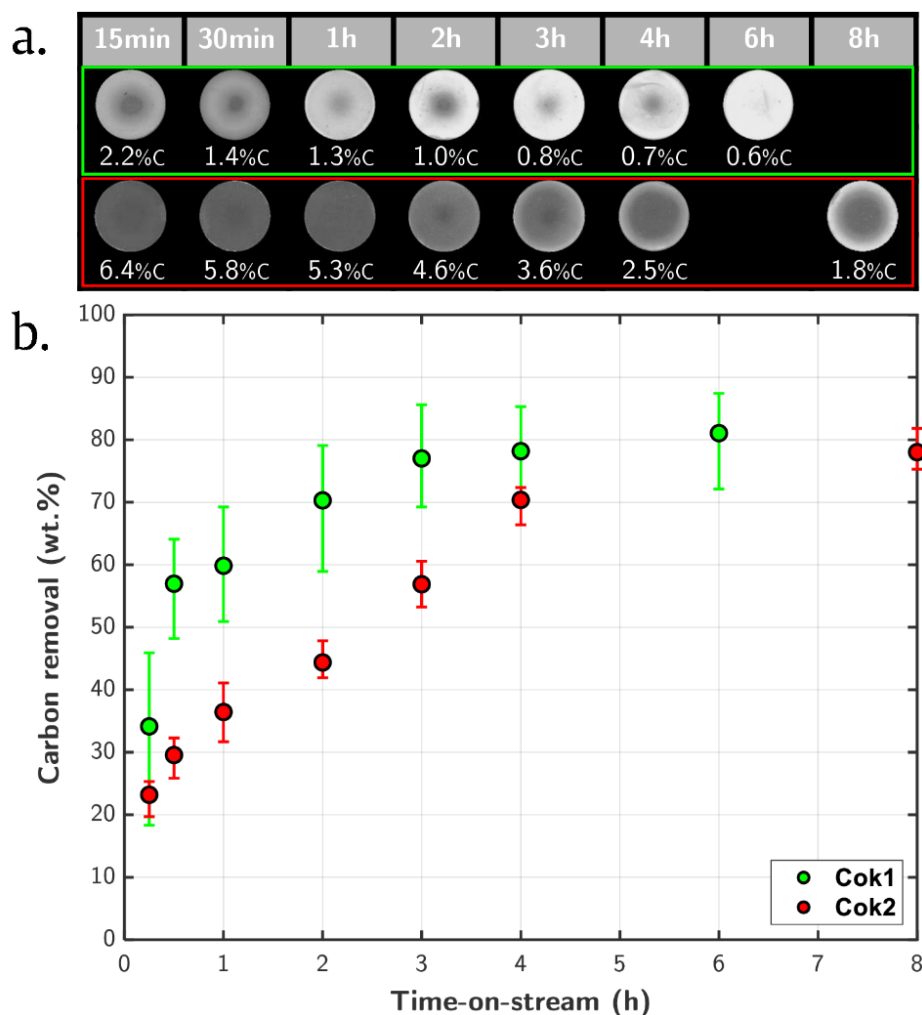


**Figure 4.3.** Optical images of catalyst pellet cross-sections (a) and evolution of corresponding carbon removal efficiency (b) for different times of ozonation. Regeneration conditions: 2.5 gO<sub>3</sub>/h (50 L/h and 50 g/Nm<sup>3</sup>) at 100 °C.

remove more coke. It is also observed that, due to the higher coke content, oxidation kinetics is slower for Cok2 at the beginning of the reaction. For both samples, the important coke removal observed in the early stages of ozonation is attributed to the oxidation of external and easily accessible carbon compounds, potentially located in the mesoporosities. On the other hand, coke located at the center of the pellet and/or in the microporosities is more difficult to reach due to ozone diffusion limitations through the pellet. This phenomenon results in a progressive coke oxidation from the external surface towards the center of the pellet, which is known in the literature as the shrinking-core model [125].

The optical images presented above for this set of experiments are a good illustration of shrinking-core behavior as the coke core visible on the pellet cross-sections appears smaller as time of exposure increases. This diffusion-reaction regime is expected from a system with reactivity in a porous media and is similar to coke combustion with oxygen, which has been highly investigated over the years [124-127]. The main difference of ozonation compared to combustion in terms of mass transfer is the appearance of competing reactions due to the instability of ozone [147, 237]. It is known that molecular ozone naturally reforms into dioxygen because of its higher stability [238]. Ozone also reacts with catalytic material to form oxygenated molecules and radicals with high

oxidative potentials. Previous studies have shown the important catalytic degradation of ozone occurring over HZSM-5 zeolites [184]. Even though catalytic degradation is desired as it allows the formation of highly reactive species for coke removal, ozone reactivity is consequently the result of three competitive reactions: thermal decomposition, catalytic degradation and coke oxidation. During ozonation reaction, O<sub>3</sub> mass transfer through the pellet to reach unreacted coke is therefore not only driven by diffusion limitations, as it is the case for O<sub>2</sub>, but also possibly limited by thermal and catalytic reactions. Indeed, ozone is degraded over active sites, whose concentration increases with time as coke is removed. If ozone is entirely degraded by these competing mechanisms, carbon compounds are not oxidized and steady-state is reached. Such phenomenon is observed at high temperatures resulting in a lowered maximal coke removal. This explains the asymptotic value of 62% (corresponding to 1.3 wt.%C) observed after 6 h at 150 °C, compared to 80% at 100 °C, with identical concentration and flowrate conditions using PY1 as initial sample. In such process, after rapid external coke removal, all ozone is catalytically degraded over the outer pellet edge before being able to react with coke, which thus cannot be furtherly oxidized while steady-state is reached. Consequently, while time of exposure presents important influence over ozonation efficiency, temperature is also sensed to be a significant parameter in this process and will be discussed in the next section.

#### 4.2.1.2. Temperature

The influence of temperature on ozonation has been investigated in the range from 50 to 150 °C. Similarly to time of exposure, two series of experiments were conducted with the same coked samples as in Section 4.2.1.1: Cok1 and Cok2. Zeolites were exposed to an ozone mass flowrate of 2.5 g/h (inlet concentration 50 g/Nm<sup>3</sup>, volumetric flowrate 50 L/h) during 3 h for the Cok1 sample, and 4 h for the Cok2 sample to reach higher coke removal. Figure 4.4 represents the cross-section images of a pellet collected in the upper fraction of the reactor for each experiment (Figure 4.4.a) alongside the corresponding evolution of carbon removal (ozonation efficiency) presented in Figure 4.4.b.

The figure shows optimal efficiency between 100 and 125 °C. The highest efficiency for the less-coked sample is obtained at 100 °C (77% of coke removal, corresponding to 0.8 wt.% as final carbon content). Moreover, a maximal coke removal of 78% is obtained for the high-coked sample at 125 °C, corresponding to a final carbon load of 2.5 wt.%. The apparition of an optimal temperature corresponds to a good compromise between efficient oxidation kinetics and limited O<sub>3</sub> degradation, both thermal and catalytic. The shift of optimal temperature is attributed to the different coking between the samples: as expected from coke growth mechanisms, carbonaceous compounds tend to progressively form polyaromatic structures [89, 113]. Consequently, Cok2 sample not only has a bigger carbon content but contains heavier coke. These more stable coke molecules require higher activation energy, thus temperature, to be oxidized. It should also be noted that coke distribution over the pellet radius is not necessarily homogeneous as there is also a diffusion of cracked polymer organic molecules into the catalyst porosity. Similar challenges are encountered in the literature with different deactivating reactions using zeolites or other acid catalysts [94, 220]. In our study, profiles of carbon distribution along the pellet radius are obtained with microprobe analysis for particular coked and partially regenerated samples. The obtained results are presented in Figure 4.5. A complete summary of SEM-FEG results for the determination of carbon radial profiles is presented in Appendix 8. Based on elemental analysis, the investigated coked sample (Cok3) had an expected carbon content of 7.8 wt.%. Its radial carbon distribution, represented in

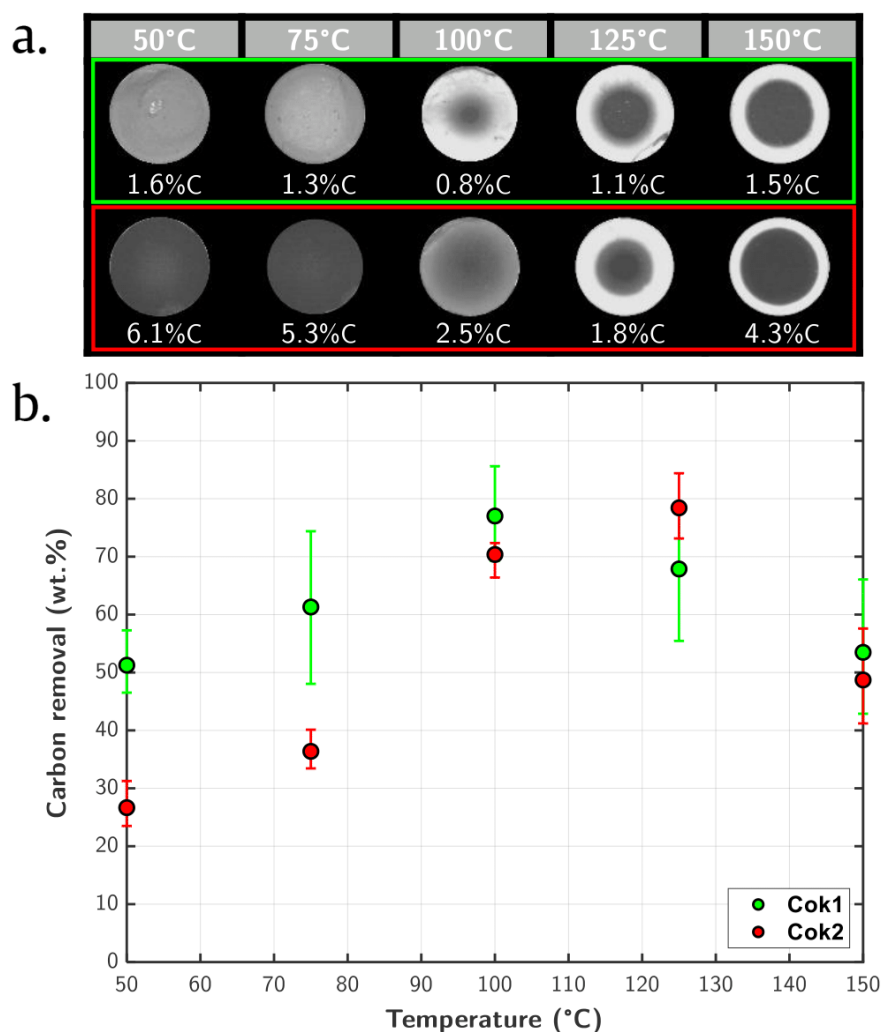


**Figure 4.4.** Optical images of catalyst pellet cross-sections (a) and evolution of corresponding carbon removal efficiency (b) for different ozonation temperatures. Regeneration conditions: 2.5 g<sub>03</sub>/h (50 L/h; 50 g/Nm<sup>3</sup>) during 3 h for Cok1 and 4 h for Cok2.

Figure 4.5.a, can be considered as homogeneous as no strong variation is observed over the radius. This Cok3 catalyst was ozonated during 3 h at 125 °C, resulting in R1 sample. The latter was also analyzed using micr oprobe alongside four other partially regenerated samples (R2, R3, R4, R5) obtained from a different coked sample (Cok1). Ozonation conditions for regenerating experiments are detailed in the legend of Table 4.2. In order to compare the results with elemental analysis, the carbon load determined with microprobe for each sample is calculated as the average carbon content over its radius (axisymmetric system). A comparison table between the techniques is also presented in Table 4.2. While carbon content is consistent between elemental and microprobe for partially regenerated samples, there is an important gap for this coked sample (7.8 wt.%C with elemental, 3.5 wt.%C with microprobe). This might be due to the presence of a thin layer with important carbon content on the outer edge of the extrud ate as observed in the literature for industrial extrudates [8, 220]. Such carbonaceous content are suggested to be polymer chains dispersed over the catalyst surface that did not diffuse into the porous matrix, due to steric blockage (partial cracking) or insufficient reaction time [226]. Consequently, sample with high carbon content has a more important fraction of coke around the extrudate. This easily accessible coke is not subject to diffusion limitations as it is located outside or at the outer range of the catalyst pellet and is therefore more easily

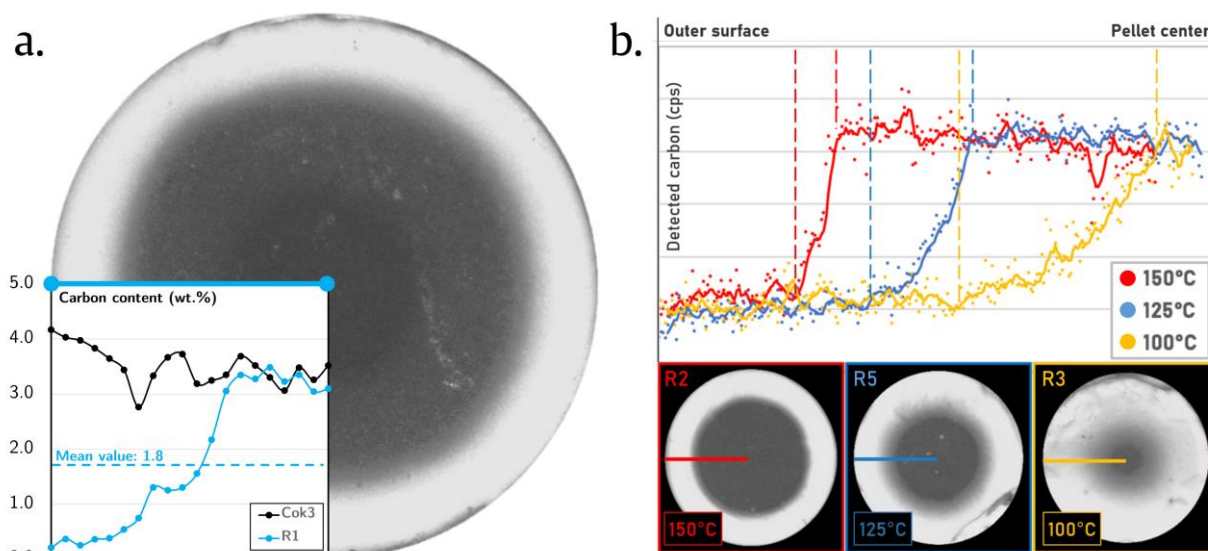


**Figure 4.5.** (a) Radial carbon profiles for Cok3 and R1 samples (mapping method) and (b) for R2, R3 and R5 samples (scanning method) with corresponding pellets cross-sections.

**Table 4.2.** Comparison between carbon contents obtained with elemental and microprobe analytical techniques. Regeneration conditions: R1 (3 h; 125 °C; Cok3), R2 (3 h; 150 °C; Cok3), R3 (3 h; 100 °C; Cok1), R4 (6 h; 150 °C; Cok1) and R5 (3 h; 125 °C; Cok1). For all samples: 2.5 g<sub>o</sub>/h (50 g/Nm<sup>3</sup> and 50 L/h).

	Elemental (wt.%C)	Microprobe (wt.%C)
Cok3	7.8	3.5
R1	1.9	1.8
R2	1.2	1.2
R3	0.6	0.6
R4	1.1	1.1
R5	0.8	0.9

removed at high temperature as oxidation kinetics is the only limitant factor. However, while increasing the temperature allows efficient coke removal at the outer edge due to high oxidation rate, it probably also inhibits coke removal at the center of the pellet. Indeed, as mentioned in the previous section, all competing reaction rates are increased at important temperatures meaning that ozone is susceptible to be entirely consumed by catalytic degradation on the active sites on the regenerated outer edge before diffusing and oxidizing unreacted coke located at the center of the pellet. To achieve complete or maximal coke removal, temperature has to be set so that ozone can reach the center of the pellet, keeping a balance between diffusion and oxidation, catalytic and thermal degradation kinetics.

This diffusion-reaction balance leads to the apparition of different regimes of regeneration depending on the temperature: homogeneous or shrinking-core regimes. At low temperatures, reaction kinetics are slow thus diffusion is preponderant, meaning that ozone diffuses through the whole pellet and oxidizes coke with a uniform conversion (homogeneous regime). At high temperatures, reactivity is dominant as reaction rates are high: ozone reacts as soon as the species are in contact with a coke molecule or an acid site. The optical images presented Figure 4.4.a perfectly illustrate the two regimes with homogeneous coke removal at 50 °C and the ideal coke core obtained at 150 °C.

Intermediate temperatures present a mix between these two extreme behaviors. Figure 4.5.b represents the evolution of carbon radial profiles at different temperatures when a core is observed. All of the aforementioned scanning acquisitions present three main domains of interest: an outer range with really low carbon content (assumed to be fully regenerated), a zone presenting a carbon gradient where coke partially reacted and finally, an unreacted coke core at the center of the pellet. Depending on the temperature and the discussed diffusion limitations, a difference of profile shape is observed. At 150 °C, the gradient zone is thin with an important slope as ozone reacts quickly with coke, while it is wider and less steep at 100 °C as oxidizing agents are able to diffuse further in the pellet. The regime of regeneration can be determined by using the initial Thiele's modulus, given by the following formula:

$$\Phi = \sqrt{\frac{\text{reaction rate}}{\text{diffusion rate}}} = \frac{V_p}{A_p} \sqrt{\frac{k_{\text{Oxi}} L_C \rho_p}{D_{\text{O}_3, \text{eff}}}} \quad (4.1)$$

Where  $V_p/A_p$  is the catalyst particle volume to external surface ratio ( $\text{m}^3 \cdot \text{m}^{-2}$ ),  $k_{\text{Oxi}}$  is the oxidation rate constant ( $\text{m}^3 \cdot \text{kg}_C^{-1} \cdot \text{s}^{-1}$ ),  $L_C$  is the initial carbon content ( $\text{kg}_C \cdot \text{kg}_{\text{cat}}^{-1}$ ),  $\rho_p$  is the catalyst particle density ( $\text{kg}_{\text{cat}} \cdot \text{m}^{-3}$ ) and  $D_{\text{O}_3, \text{eff}}$  is the effective diffusion coefficient of ozone in ZSM-5 zeolite ( $\text{m}^2 \cdot \text{s}^{-1}$ ). Regeneration will follow an homogeneous regime if  $\Phi$  is inferior to 1, while a shrinking-core mode appears when  $\Phi$  is significantly higher to 1. However, as very few studies were carried out with ozone in gas phase, there is a lack of experimental data regarding kinetics and diffusion coefficients. Therefore, Thiele's number cannot be calculated here to validate the visual change of regime which seems to occur between 75 and 100 °C for the first series of experiments (with Cok1 sample) and between 100 and 125 °C for the second set (with Cok2 sample).

#### 4.2.1.3. Inlet $\text{O}_3$ concentration

The ozone concentration at the reactor inlet was ranged from 20 to 80  $\text{g}/\text{Nm}^3$  to study the influence of this parameter. The volumetric flowrate was set at 50 L/h, resulting in a mass flowrate from 1 to 4  $\text{g}_{\text{O}_3}/\text{h}$ . These conditions were applied to two different series of experiments whose resulting optical pictures of pellet cross-section from the upper reactor fraction and corresponding coke removal are presented in Figure 4.6 (a,b). The ozonation experiments for the first series have been carried out during 2 h at 100 °C from Cok4 sample. For the second series, Cok5 sample was exposed to the ozone gas stream during 4 h at 125 °C. To provide an energetic insight to these experiments, the electric power set on the ozone generator for this concentration range corresponds to 15 W for 20  $\text{g}/\text{Nm}^3$  and to 150 W for 80  $\text{g}/\text{Nm}^3$  for a 50 L/h volumetric flowrate.

Based on the results presented in Figure 4.6.b, no optimal ozone concentration is observed. However, an increase of coke removal efficiency appears as the concentration rises. A maximal coke removal of 75% for the first series and of 78% for the second is obtained at 80  $\text{g}/\text{Nm}^3$ . Process efficiency seems to increase linearly with respect to ozone concentration but the impact of this parameter is lower than temperature or time of exposure. This trend makes sense as an increase of ozone concentration means that more oxidizing agents are available for coke oxidation. However, the reactivity of thermal recombination and catalytic degradation are also increased as there is a higher probability of contact. Depending on the order of the three competing reactions, the weight of each mechanism can vary depending on the ozone concentration. From the optical images of the



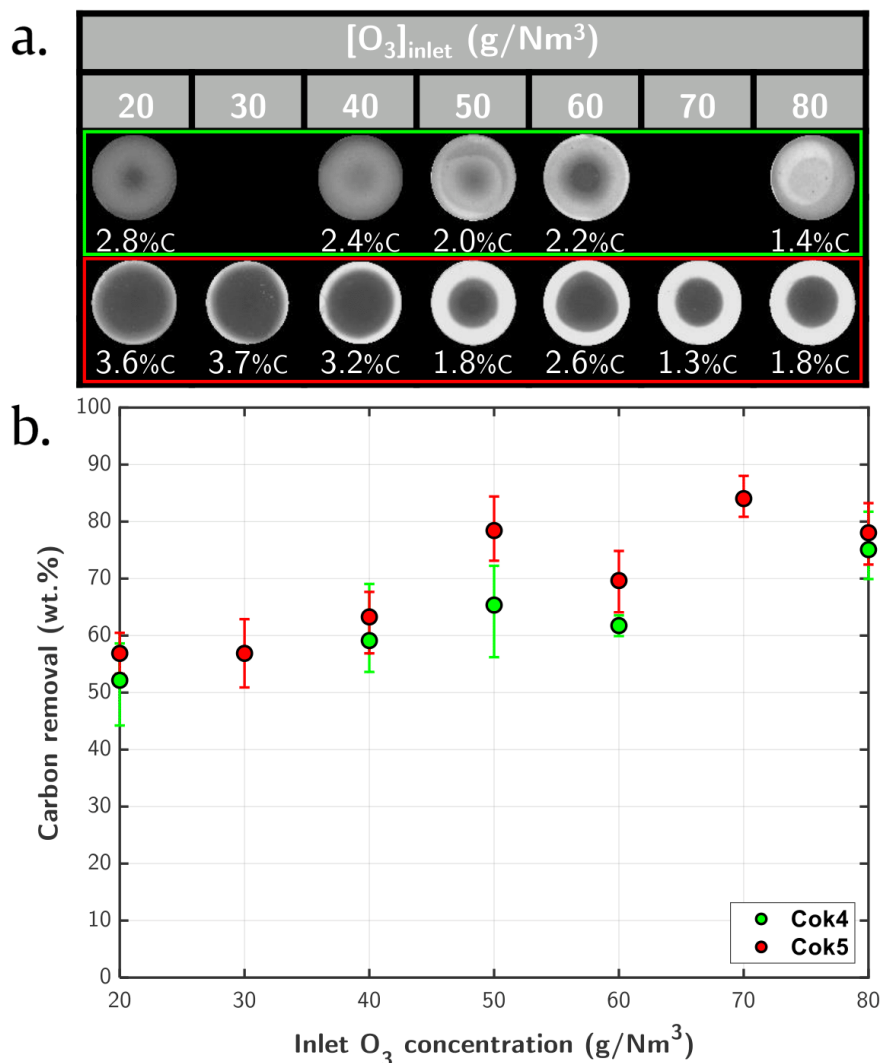


**Figure 4.6.** Catalyst pellet cross-sections (a) and evolution of carbon removal efficiency (b) for different inlet ozone concentrations. Regeneration conditions: 50 L/h during 2 h at 100 °C for Cok4 and 4 h at 125 °C for Cok5.

pellet cross-sections for these series of experiments, despite the slight increase of coke removal, inlet ozone concentration also seems to impact diffusion behavior. Low content allows diffusion through the pellet and reaching the center (homogeneous regime) while coked cores appear for higher ozone contents (shrinking-core regime). Two different explanations or a combination of both can explain this observation. First, at low concentrations, oxidation is quite slow because of the limited presence of oxidizing species. Thus, internal porosity remains heavily coked and catalytic degradation is consequently minimized as active sites remain hindered. On the other hand, at high concentrations, coke oxidation is fast, starting by the outer ring, where active sites are recovered and catalytic degradation rapidly increases, limiting ozone diffusion towards the center. Secondly, for high concentrations, collision frequency between ozone molecules is increased, enhancing thermal recombination, while at low concentrations, thermal recombination is therefore mitigated and only coke oxidation occurs [150, 239]. The contribution of the different ozone consumption mechanisms (thermal recombination, catalytic degradation and coke oxidation) therefore varies depending on the operating conditions. Determination of pseudo-kinetic parameters have been achieved at the reactor scale to have a better understanding of this repartition and is discussed in Section 4.2.2.

#### 4.2.1.4. Volumetric and mass flowrate

The influence of volumetric flowrate has been investigated in the range allowed by the important pressure drop generated by the catalytic bed, between 50 and 200 L/h. From different initial coked samples, volumetric flowrate was varied in this range while the other parameters were fixed (time of exposure, temperature and O<sub>3</sub> concentration). The coke removal efficiencies for the three series are presented in Figure 4.7.a.

From these results, it appears that volumetric flowrate influence over ozonation efficiency is not significant in the studied range. With the reactor geometry used (L = 20 cm, ID = 4 mm), corresponding superficial velocity is 1.1 to 4.4 m/s. The resulting residence time is 0.2 to 0.05s, which is really short. To characterize the hydrodynamic flow in the reactor, the packed-bed Reynolds is determined using the following formula:

$$Re^* = \frac{\rho_{O_2} \cdot u_s \cdot D_p}{\mu_{O_2} \cdot (1 - \varepsilon_{bed})} \quad (4.2)$$

Where  $\rho_{O_2}$  and  $\mu_{O_2}$  are oxygen density and dynamic viscosity (kg/m<sup>3</sup> and kg/m.s respectively),  $u_s$  is gas superficial velocity (m/s),  $D_p$  is the equivalent diameter of catalyst pellet (m) and  $\varepsilon_{bed}$  is the bed voidage (adimensional number). For the investigated range

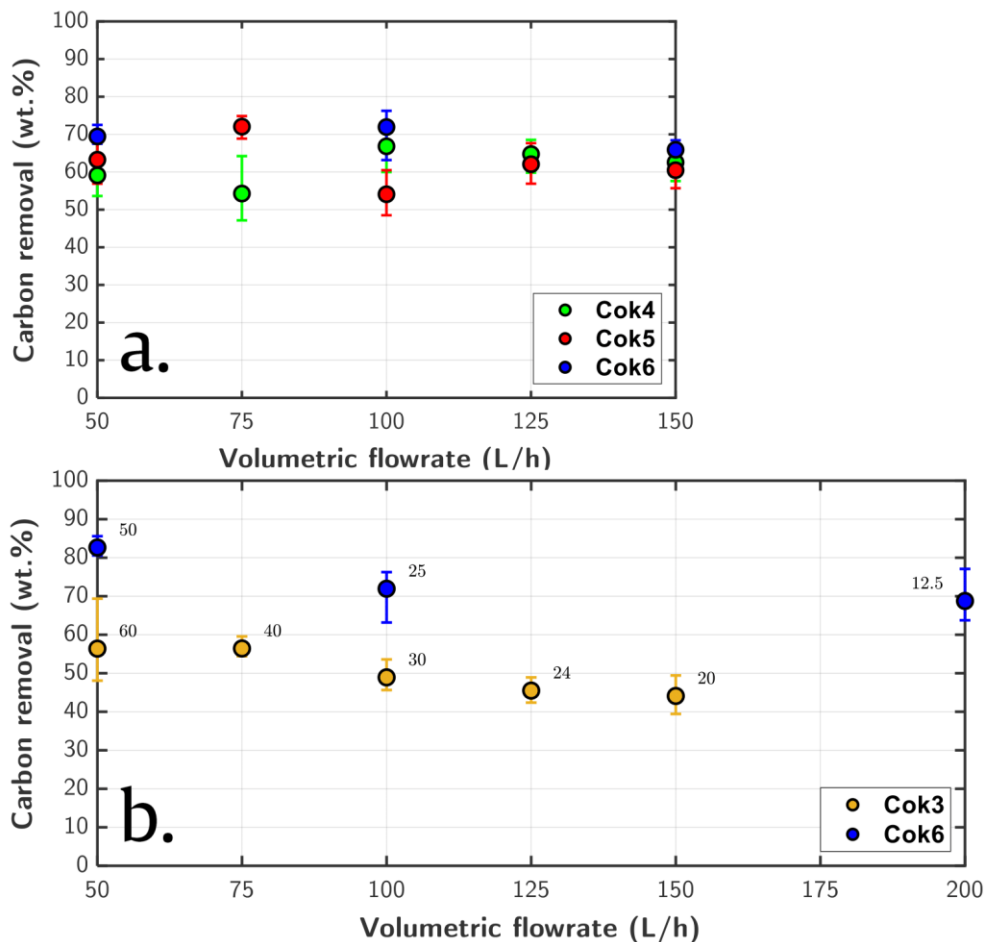


**Figure 4.7.** Evolution of coke removal efficiency for (a) different volumetric flowrates of ozone with (b) constant ozone mass flowrate. Regeneration conditions: (a) (2h; 100 °C; 40 g<sub>O<sub>3</sub></sub>/Nm<sup>3</sup>) for Cok4; (4 h; 125 °C; 40 g<sub>O<sub>3</sub></sub>/Nm<sup>3</sup>) for Cok5; (3h; 100 °C; 25 g<sub>O<sub>3</sub></sub>/Nm<sup>3</sup>) for Cok6. (b) (3 h; 125 °C; 3.0 g<sub>O<sub>3</sub></sub>/h) for Cok3; (3 h; 100 °C; 2.5 g<sub>O<sub>3</sub></sub>/h) for Cok6. Inlet ozone concentrations for ozone mass flowrate conservation are indicated as labels in g<sub>O<sub>3</sub></sub>/Nm<sup>3</sup>.

of volumetric flowrate,  $Re^*$  is between 200 and 1000, corresponding to a transitional regime. At fixed ozone concentration, the mass flowrate increases when volumetric flowrate raises. It is therefore not intuitive that coke removal does not increase with flowrate as the sample is exposed to more ozone. However, only the inlet  $O_3$  concentration seems to have an impact on coke removal efficiency. It is theorized that the aforementioned hydrodynamic conditions eliminate external mass transfer limitations as the almost turbulent regime reduces boundary layer thickness. Internal diffusion would then be the only limitant factor.

In order to validate this hypothesis, a last set of experiments have been carried out on coked samples with different initial carbon contents keeping a constant mass flowrate by adjusting volumetric flowrate and ozone concentrations accordingly. Figure 4.7.b represents the results obtained for these experiments: one with a fixed  $Q_{m,O_3}$  of 2.5 g/h (using Cok6) and the other one was set at 3.0 g/h (using Cok3). The effect of ozone concentration alone is observed as the experiments with higher  $O_3$  content and lower volumetric flowrate present higher coke removal efficiency. This observation confirms that, in the investigated system and range, volumetric flowrate is not a significant parameter. To limit oxygen consumption, further experiments were conducted with a 50 L/h volumetric flowrate.

#### 4.2.2. Ozonation study at reactor scale

##### 4.2.2.1. Thermal and catalytic degradation of ozone

To evaluate the weight of each ozone consumption mechanism, determination of apparent kinetic parameters in the experimental setup have been carried out. Tubular glass reactor was considered as an ideal plugflow reactor to evaluate respective reaction rates. The study was carried out at 50 L/h, corresponding to a residence time ( $\tau$ ) of 0.18 s. Due to the small reactor internal diameter (4 mm) and the important mixing generated by the turbulent flowing conditions, radial distribution in the reactor is considered as homogeneous: channeling and wall effects are therefore neglected. During the different experiments, inlet and outlet  $O_3$  concentrations were noted after system stabilization. Values of thermal decomposition ( $k_{th}$ ) and catalytic degradation ( $k_{cat}$ ) kinetic constants were then calculated following the reaction order (equations are presented in). Arrhenius plot allows to extract the activation energy and the pre-exponential factor for each mechanism. Different reaction orders were examined and only the best fit is presented here. The outcomes and limitations of the obtained kinetic constants are discussed in this section. Details of results and calculations which were not included in the article are placed in Appendix 7.

##### *a. Thermal decomposition*

The study of thermal ozone recombination has been carried out in the empty reactor between 100 and 200 °C. Thermal ozone degradation is here considered as the only occurring mechanism. Very small decomposition was observed at lower temperatures. Based on the experimental results, second order reaction is the best fit ( $R^2 = 0.9965$ ) compared to the first order ( $R^2 = 0.9879$ ). While the fit difference is not significant, second-order reaction was elected based on these results with the support of literature references [150, 240]. Indeed, this reaction order was historically often used to approach ozone thermal recombination mechanism even though more complex reactivities have been

investigated during the last decades [239]. With the corresponding Arrhenius equation, which plot is presented Figure 4.8, the apparent kinetic of thermal decomposition is given by the following equation:

$$k_{th} = 2.47 * 10^{10} * \exp\left(\frac{-81375}{8.314 * T}\right) \quad (2^{nd} \text{ order: } k_{th} \text{ in } L \cdot mol^{-1} \cdot s^{-1}) \quad (4.3)$$

This pseudo-kinetic constant generates really low ozone decomposition at ambient temperature as expected both from experimental observations (no decomposition under 100 °C) and from literature where ozone half-life at 20 °C is reported to be around 3 days [212]. Consequently, the very low residence time in the system is not sufficient to observe ozone consumption from decomposition. However, the observed ozone consumption is much more important than rates provided in the literature. While half-life time of 1.5 h is given at 120 °C, approximately 80% of ozone is already consumed in our system at this temperature. It is important to remind that these kinetic parameters are proper to this experimental setup and should not be used in another context. The gap between these values might be attributed to the hydrodynamics in the reactor as mixing and probability of contact is improved when the regime is not laminar in a continuous flow reactor. The concentration conditions are also far from those investigated when focusing on ozone decomposition in atmosphere. For high concentrations, thermal recombination is also increased due to the higher load of ozone molecules.

#### *b. Catalytic degradation over fresh ZSM-5*

Determination of catalytic degradation of ozone over ZSM-5 zeolite is conducted between 50 and 150 °C with a catalytic fixed-bed mass around 1.5 g. Complete ozone depletion is obtained for higher temperatures. Both thermal and catalytic degradation are occurring during these experiments. The equation used for the evaluation of the catalytic degradation kinetic parameter ( $k_{cat}$ ) is presented in Table 4.3 (Equation (4.6)). To consider the combined reactivity, it has been hypothesized that thermal decomposition only occurs in bed voidage while catalytic degradation takes place in the space occupied by pellets. The value of  $k_{cat}$  for each temperature is determined by using a solver so that the left member of the equation approaches residence time. The obtained value is then divided by the catalytic bed mass to express the reaction rate by second and mass of catalyst ( $s^{-1} \cdot g_{cat}^{-1}$ ). From this exploitation, first order reaction is the best fit for Arrhenius plot (Figure 4.8) with a  $R^2$  coefficient of 0.9983 (whereas second order reaction gave  $R^2 = 0.9599$ ). The corresponding apparent kinetic parameter for ozone degradation over ZSM-5 zeolite is given by the following equation:

$$k_{cat} = 4.37 * 10^5 * \exp\left(\frac{-34481}{8,314 * T}\right) \quad (1^{st} \text{ order: } k_{cat} \text{ in } s^{-1} \cdot g_{cat}^{-1}) \quad (4.4)$$

The activation energy is lower for catalytic compared to thermal degradation (34 kJ/mol vs 81 kJ/mol). Interaction with active acid sites favours molecular ozone decomposition into oxygenated species and/or radicals. Some studies have investigated the capacity to remove ozone from air, which concluded that zeolite materials have good abatement efficiency [241]. Use of the equation with combined thermal and catalytic reactivities provides good results matching the experimental tests and can be furtherly used as a background ozone consumption when coke oxidation is also competing in the system. However, the fact that only fresh zeolites were used for catalytic degradation kinetic study

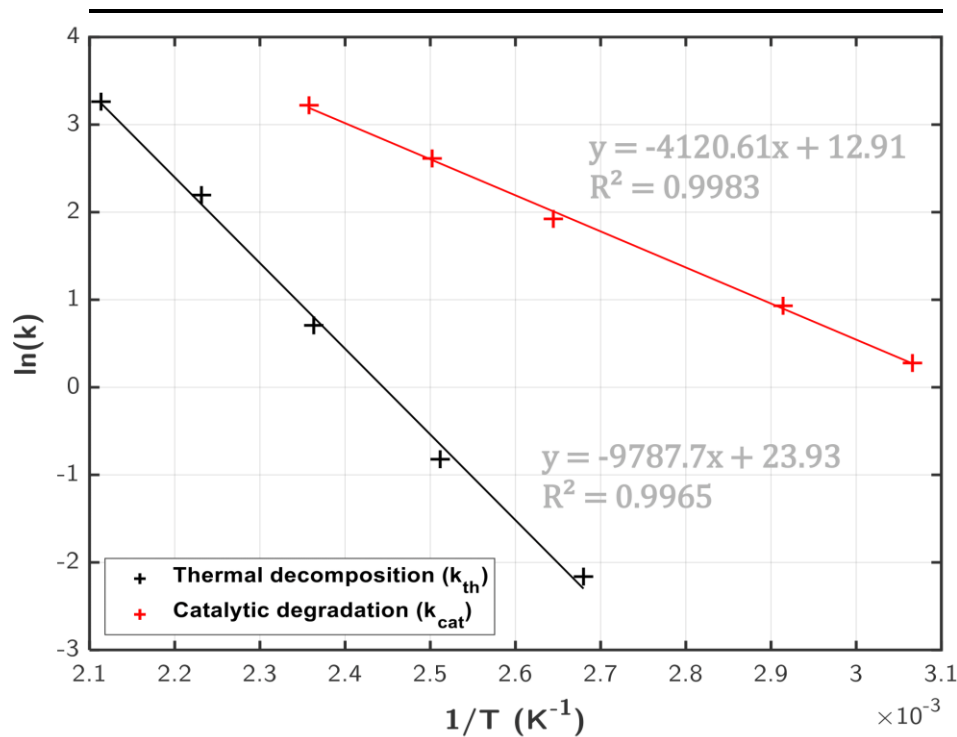
**Table 4.3.** Equations for kinetic constants determination from inlet/outlet O<sub>3</sub> concentrations.**Thermal decomposition: 2<sup>nd</sup> order (R<sup>2</sup> = 0.9965)**

$$\frac{-d[\text{O}_3]}{dt} = k_{\text{th}} [\text{O}_3]^2 \rightarrow k_{\text{th}} = -\frac{1}{\tau} \cdot \left( \frac{1}{[\text{O}_3]_{\text{in}}} - \frac{1}{[\text{O}_3]_{\text{out}}} \right) \quad (4.5)$$

**Catalytic degradation: 1<sup>st</sup> order (R<sup>2</sup> = 0.9983)**

$$\text{Hypothesis: } \frac{-d[\text{O}_3]}{dt} = \varepsilon k_{\text{th}} [\text{O}_3]^2 + (1 - \varepsilon) k_{\text{cat}} [\text{O}_3] \rightarrow$$

$$\frac{1}{(1 - \varepsilon) k_{\text{cat}}} * \ln \left( \frac{[\text{O}_3]_{\text{out}} (\varepsilon k_{\text{th}} [\text{O}_3]_{\text{in}} + (1 - \varepsilon) k_{\text{cat}})}{[\text{O}_3]_{\text{in}} (\varepsilon k_{\text{th}} [\text{O}_3]_{\text{out}} + (1 - \varepsilon) k_{\text{cat}})} \right) = -\tau \quad (4.6)$$

**Figure 4.8.** Experimental Arrhenius plots of thermal decomposition and catalytic degradation of ozone over HZSM-5 zeolite.

means that all active sites are available for molecule adsorption. It is not the case with coked catalysts, in which active sites are partially hindered and blocked by carbon deposition, so catalytic degradation is lowered. On top of that, Brodu *et al.* showed that some oxygenated species can remain adsorbed during catalytic degradation and therefore also hinder a fraction of acid sites [241]. Experimental observations going in this direction will be discussed in next section. Consequently, more complex kinetic laws would be more appropriate to follow the catalytic degradation mechanisms suggested in the literature [152]. First order reaction remains a good approximation of catalytic ozone degradation in our system. The addition of a parameter  $\theta$  representing the fraction of free

acid sites allows to consider the evolution of active sites and correlated reactivity. The following equation is used for combined thermal and catalytic ozone consumption:

$$\frac{-d[\text{O}_3]}{dt} = \varepsilon k_{\text{th}} [\text{O}_3]^2 + (1 - \varepsilon) m_{\text{cat}} k_{\text{cat}} \theta [\text{O}_3] \quad (4.7)$$

Where  $\theta = 1$  when catalyst is fresh (all active sites available). This parameter can be evaluated for coked samples by comparing acidities between fresh and spent sample. Based on this equation and on the determination of apparent kinetic parameters, the repartition between thermal and catalytic mechanisms will be discussed in the next section (Section 4.2.2.2).

#### 4.2.2.2. Combined degradation and zeolite deactivation

The complexity of the ozonation process is mainly due to the competing reactions, constantly evolving during the reaction. Using the aforementioned equation and the kinetic parameters determined experimentally in the previous section, the total ozone degradation as well as the repartition of thermal and catalytic mechanisms during exposition of a ZSM-5 zeolite bed at different temperatures between 50 and 150 °C are presented in Figure 4.9. Total degraded ozone fast increases with temperature and reaches almost complete decomposition (95%) at 150 °C. The influence of thermal mechanism in the total degradation appears to be negligible with a maximal impact of 0.9% of the total consumption (at 125 °C). At 50 °C, ozone degradation is almost entirely catalytic (> 99%) as expected from the very low reaction rate for thermal degradation under 100 °C.

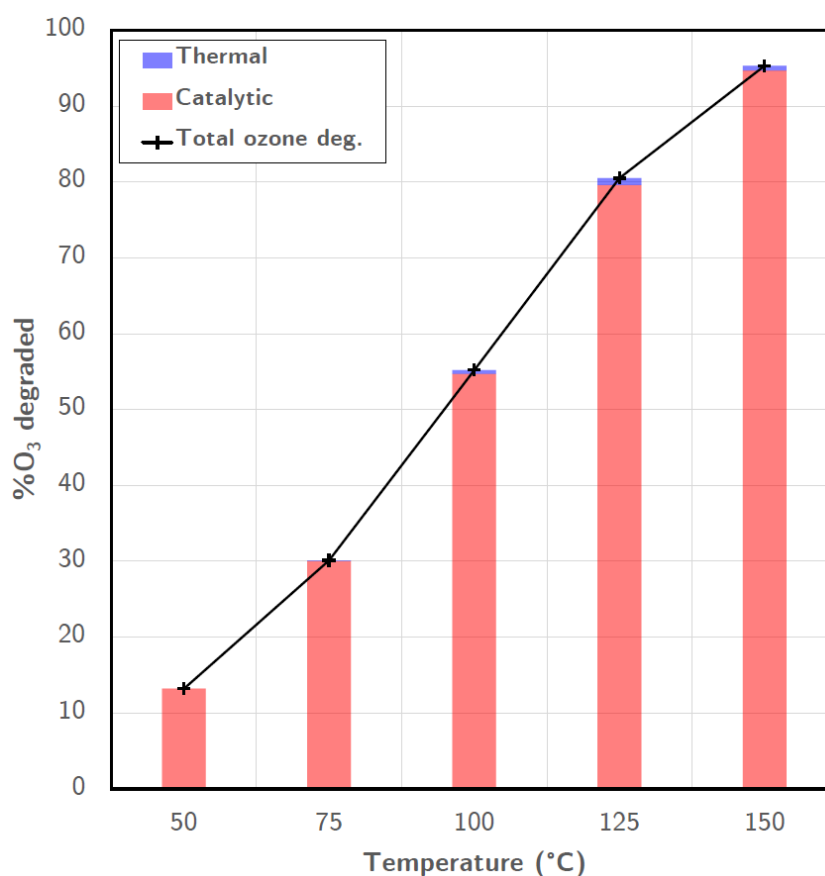


**Figure 4.9.** Evolution of ozone decomposition depending on the temperature with repartition of thermal decomposition and catalytic degradation based on apparent reaction rates.

However, catalytic degradation is considered as optimal ( $\theta = 1$ ) for these results. As mentioned earlier, the fraction of free active sites is susceptible to decrease due to an adsorption rate of oxygenated species superior to the desorption rate ( $r_{\text{ads}} > r_{\text{des}}$ ), leading to the progressive deactivation of zeolite and to the mitigation of catalytic degradation.

In order to evaluate this loss of performance, a fresh zeolitic bed was exposed during 30 min at 150 °C to an ozone-enriched gas flow. The evolution of inlet and outlet concentrations with the corresponding ozone degradation is presented in Figure 4.10. Initial ozone degradation (94%) is consistent with the results obtained previously. However, an important decrease of decomposed ozone is observed after 5 min of exposition and leads to a stabilization at the end of the experiment around 72%. This behavior could mean that a steady state is achieved after this duration with an equilibrium of adsorption and desorption of species resulting in a constant rate of ozone degradation. This decomposition performance corresponds to a free accessible active sites fraction of 0.43, meaning that 57% of active sites would be occupied by unreactive oxygenated species. However, it is important to remember that due to diffusion limitations, active sites are not available all at once and a part of this unavailable fraction is not necessarily deactivated. Diffusion considerations will be included when discussing coke oxidation at the reactor scale in the following section.

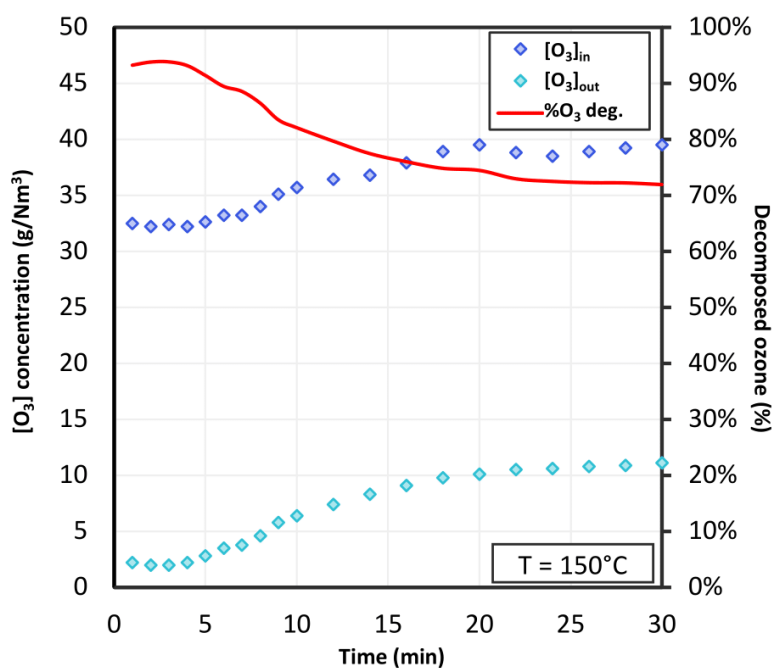


**Figure 4.10.** Evolution of ozone degradation efficiency for a catalytic bed (fresh HZSM-5 zeolite) exposed to an ozone-enriched stream.

#### 4.2.2.3. Coke oxidation in zeolite catalytic bed

Study of coke oxidation via ozonation is conducted using the same experiments presented in Section 4.2.1. This previous paragraph focused on the pellet scale for the upper part of the reactor while the whole reactor and the three collected fractions (higher part at the reactor inlet H, in the middle of the reactor M and at the bottom for the reactor outlet B) are now considered. As expected from typical fixed-bed reactor behavior, process efficiency is not homogeneous due to reactants consumption along the catalytic bed leading to a concentration gradient, and therefore different efficiencies. The implementation of the



ozonation process at industrial scale for the regeneration of coked catalysts during pyrolysis could involve a FCC-type process with a fluidized bed regenerator to overcome this challenge. Coke removal efficiency would therefore be homogeneous and improved in the regenerator due to increased mass transfer and reaction kinetics in a fluidized bed. During the fixed bed experiments conducted in this work, as reactor inlet (H zone) is exposed to higher ozone concentrations than the outlet part (B zone), coke removal is expected to be more important in this H zone. This phenomenon is amplified for ozonation reaction as  $O_3$  is not only consumed by coke oxidation but is also degraded thermally and even more by catalytic decomposition. In this section, typical observations during ozonation are discussed to provide a better comprehension of the process for further modelling or optimization.

Experiments with a varying time of exposure and temperature, being the most significant operating parameters, are presented in Figure 4.11. Optical pictures of a pellet cross-section from each of the collected fractions (H, M, B) are presented in Figure 4.11.a and b with their corresponding carbon content. This carbon load obtained with CH analysis is assumed as the average content of the fraction and corresponding coke removal is calculated. An exponential tendency curve was added to provide an illustration of coke removal profile, thus ozonation efficiency, along the reactor (Figure 4.11.c and d). A difference in terms of carbon content is observed according to the position in the reactor, as sensed, due to the gradient of  $O_3$  concentration. Despite longer time-on-stream (Figure 4.11.c), carbon removal difference between inlet and outlet samples is maintained

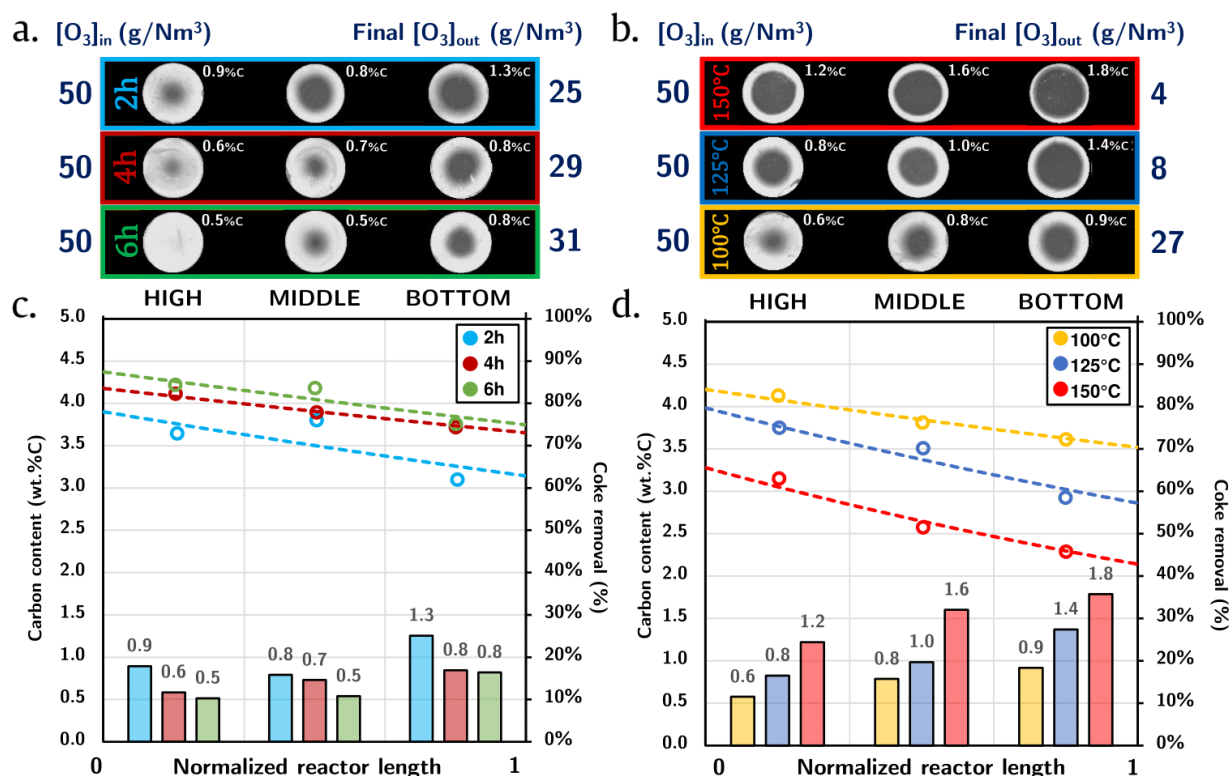


**Figure 4.11.** Optical images of zeolite pellet cross-sections for distinct collected fractions of catalytic bed (high, middle and bottom) to illustrate the influence of time of exposure (a) and temperature (b) of ozonation at reactor scale. Corresponding carbon contents and coke removal are presented with tendencies of coke removal efficiency along the reactor (c,d). Regeneration conditions: (a,c) 100 °C; 2.5 g<sub>O<sub>3</sub></sub>/h and (b,d) 3 h; 2.5 g<sub>O<sub>3</sub></sub>/h. Cok1 was used as initial coked sample for all experiments.

(0.2-0.4%). The whole coke removal efficiency profile in the reactor moves upwards with time, rapidly for short times of exposure, and then slower because of the asymptotic behavior observed in Section 4.2.1.1. Estimated efficiency reactor profiles for 4 h and 6 h are consequently really close one from another. However, as illustrated on Figure 4.11.d, the gap between high and bottom samples is more important at higher temperatures as the aforementioned gradient of concentration is more pronounced. As an indicator, final outlet concentration is given for each of the experiments: while bottom fraction is exposed to  $27 \text{ g/Nm}^3$  at  $100 \text{ }^\circ\text{C}$ , the outlet concentration at  $150 \text{ }^\circ\text{C}$  is only of  $4 \text{ g/Nm}^3$ . The carbon removal efficiency gap between the samples for the  $100 \text{ }^\circ\text{C}$  experiment is therefore less important. Even though concentration does not heavily impact coke removal efficiency, this difference explains the noticeable gap of efficiency. Moreover, it is important to keep in mind that the gradient of concentration is not constant and is constantly evolving during the reaction due to the change of reactivity balance. The evolution of outlet concentration for a typical ozonation run is presented in Figure 4.12. The observed trend presents a maximum at  $35 \text{ g/Nm}^3$  while the final outlet concentration is down to  $7 \text{ g/Nm}^3$ . Indeed, catalytic degradation is initially really low as a part of the active sites are covered by coke deposition (small  $\theta$ ). In the early stages of the reaction, ozone consumption is mainly attributed to coke oxidation while, as the reaction progresses, coke is removed and active sites recovered ( $\theta$  increases). Thus, catalytic degradation influence grows while coke oxidation weight decreases during the process. The constant balance and evolution between thermal, catalytic and oxidation mechanisms is responsible for the evolution of outlet  $\text{O}_3$  concentration. Moreover, Figure 4.12 also shows an evolution of temperature during the experiment. This temperature increase is attributed to the exothermicity of coke oxidation, also observed during coke combustion with oxygen [115]. Consequently, catalytic bed presents a gradient of both  $\text{O}_3$  concentration and temperature impacting

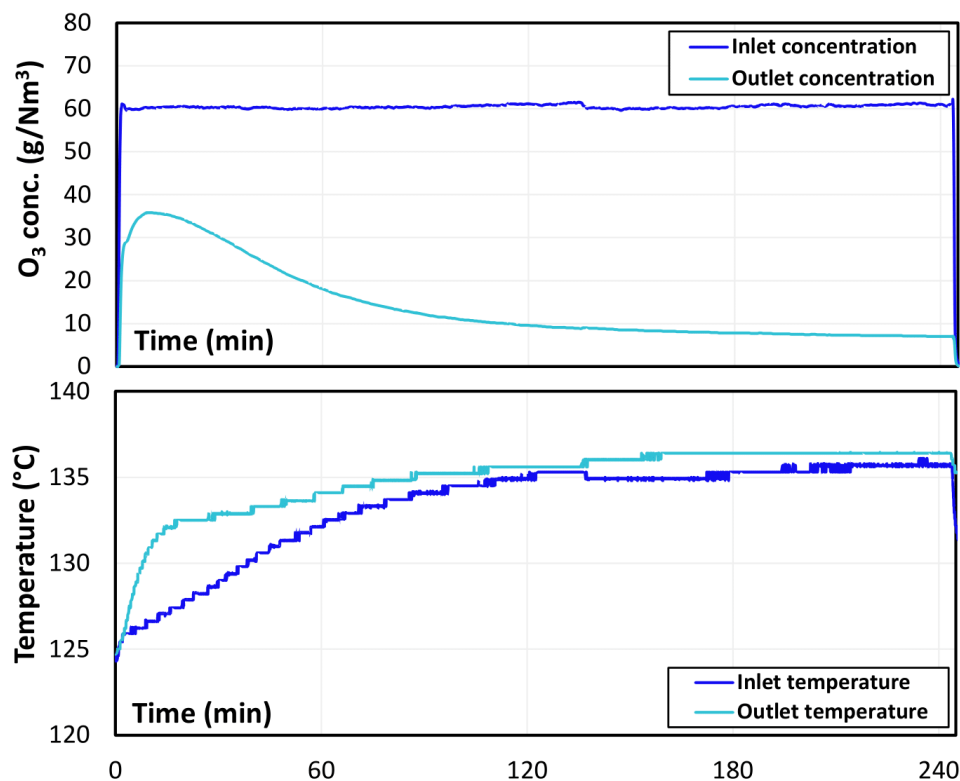


**Figure 4.12.** Recording of inlet/outlet  $\text{O}_3$  concentrations and temperatures for a typical ozonation experiment. Regeneration conditions: (4 h;  $125 \text{ }^\circ\text{C}$ ;  $3.0 \text{ gO}_3/\text{h}$ ) from Cok5 ( $8.4 \text{ wt.}\% \text{C}_{\text{init}}$ ).

diffusion and reactions at the pellet scale as presented in Section 4.2.1. Based on the previous work of kinetic parameters determination at the reactor scale for thermal and catalytic decomposition, rate of oxidation has been added in the following equation describing global ozone consumption:

$$\frac{-d[O_3]}{dt} = \varepsilon_{\text{bed}} k_{\text{th}} [O_3]^2 + (1 - \varepsilon_{\text{bed}}) (k_{\text{cat}} \theta [O_3] + k_{\text{oxi}} [LC]^a [O_3]^b) \quad (4.8)$$

Where [LC] is the carbon content of coked sample (wt.%), a and b are the orders of oxidation reaction regarding carbon and ozone respectively, and  $k_{\text{oxi}}$  is the oxidation kinetic parameter ( $L^{b-1} \cdot \text{mol}^{1-b} \cdot \text{s}^{-1}$ ).

Despite different attempts to include coke oxidation in a global ozone consumption rate, no reaction order was found to describe the process due to the complexity and constant evolution of reactivity balance. Moreover, apparent ozone decomposition rate needs to take into account the challenges related to diffusion in catalyst pellets. When considering these phenomena, the equation describing ozone consumption has to imply an effective reactivity depending on the diffusion of ozone in the ZSM-5 catalysts. It is also interesting to notice that the effective diffusion is correlated with coke load, as is the fraction of free acid sites  $\theta$ , since it impacts porosity and tortuosity of the catalyst, therefore media resistance to ozone circulation. Modelling the reaction, both at pellet and reactor scale, requires a much more complex set of equations in order to describe the complexity of a constant change in a diffusion-reaction system. Similar studies have been carried out with different processes, including coke combustion, and could be adapted to the ozonation process in the future [124, 127, 242].

### 4.3. Comparison tubular/syringe reactor experiments

The experiments using syringe reactor were conducted simultaneously with the parametric study presented in previous section in order to collect regenerated samples for reuse in pyrolysis. The operating conditions used for these manipulations (detailed in Section 2.2.3.2) were elected based on the sensed optimal parameters. Visual tendencies observed using the syringe reactor confirmed previous results with tubular reactor. As a fixed catalytic bed with no intermediate unloading, regeneration efficiencies between top and bottom fractions are expected to be heterogeneous. Indeed, previous results in tubular reactor confirmed higher coke removal closer to reactor inlet due to higher ozone concentrations (Section 4.2.2.3). This behavior, expected as a classic tendency for all fixed bed reactors, is visually illustrated for the ozonation process in Figure 4.14.

The progression of decoking with downstream circulation of gas stream appears from top to bottom. Rapid coke removal is observed in early stages of the reaction while visual evolution does not change much after 4 h, reminding the asymptotic behavior discussed in Section 4.2.1.1. It is important to notice that these photographs allow observing external coke deposited around the grain but not internal compounds. A lower coke oxidation, traduced by a black zone, is observed on top of the catalytic bed for REG2 batch. This phenomenon is attributed to the difference of volumetric flowrate between the experiments: the more important flowrate led to decreased hydrodynamics repartition as no flow distributor was placed after reactor section enlargement. Moreover, oxidation reactivity is enhanced by the temperature rise caused by the important exothermicity of ozonation at the top of the catalytic bed.

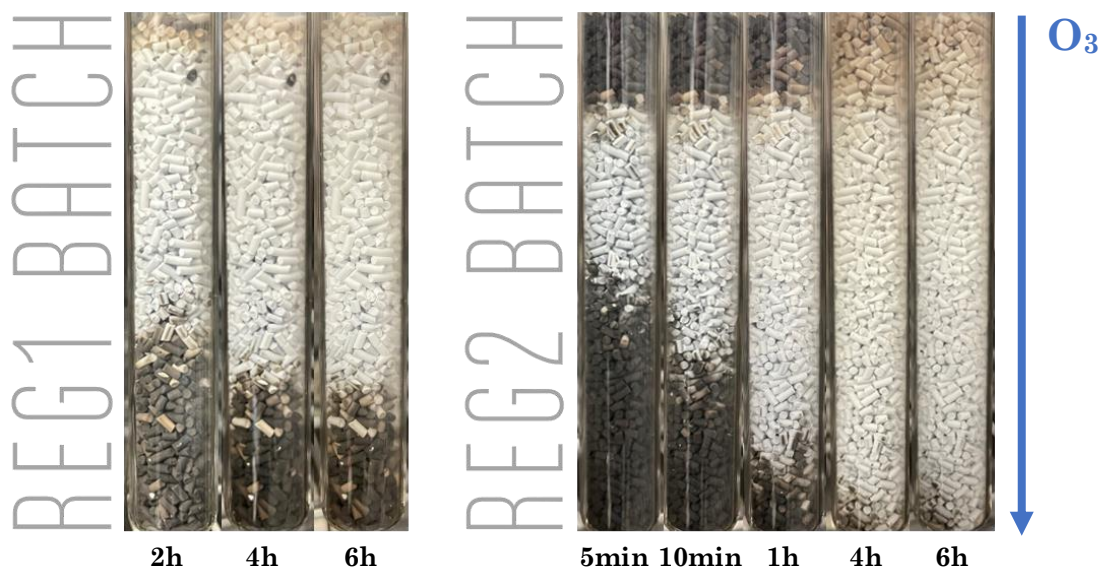


**Figure 4.13.** Visual evolution of catalytic bed during ozonation first run of REG1 and REG2 batches in syringe configuration. Regeneration conditions: REG1 (100°C; 60 g<sub>O<sub>3</sub></sub>/Nm<sup>3</sup>; 50 L/h) from 5.4 wt.%C coked sample and REG2 (100°C; 60 g<sub>O<sub>3</sub></sub>/Nm<sup>3</sup>; 100 L/h) from average 5.3 wt.%C mixed coked samples.

The main challenge of these experiments was to adapt accordingly the operating conditions from the practical knowledge based on tubular configuration experiments. Due to the increase of catalytic material quantity, ozone consumption by catalytic degradation and coke oxidation increased importantly. Operating conditions had to be set so that all catalytic bed is exposed to ozone despite inevitable strong gradient of concentration. For this reason, as outlet concentration was null during the first runs, flowrate was increased from 50 to 100 L/h to decrease residence time and allow ozone reaching the reactor outlet. However, concentration gradient remained very important (from 55 g<sub>O<sub>3</sub></sub>/Nm<sup>3</sup> at the top to 5 g<sub>O<sub>3</sub></sub>/Nm<sup>3</sup> at the bottom) and sample homogeneity was not ensured. The other key point was the choice of inlet temperature. Parametric study in tubular configuration showed that optimal temperature combining good oxidation rate and diffusion is around 100°C. However, while temperature rise due to coke oxidation was limited in tubular configuration, the higher quantity of coked zeolites highly increased the induced exothermicity. The evolution of temperature difference between reactor inlet and outlet during different runs of REG2 batch is represented in Figure 4.14.a. An increase of up to almost 30°C is observed for the outlet temperature during the first run, being the one with most coke removed. During subsequent runs, temperature rise remains important but tends to decrease gradually as kinetics of coke oxidation are slower (less accessible due to diffusion limitations). This factor needs to be considered when choosing the process temperature: initial 100°C will become 130°C or more where ozone could not be able to reach catalyst pellet center. After first runs at 100°C, initial temperature was then set at 80°C in order to anticipate this temperature rise and try to mitigate concentration gradient. As catalytic bed is exposed to high temperatures, ozone consumption by combined mechanisms is very important during the reaction leading to complete degradation in the case of “Run 1” (Figure 4.14.b). For subsequent runs, the limited temperature rise mitigates degradation and ozone is observed at reactor outlet. In such conditions, despite different conditions according to the position in the reactor, all catalytic bed is exposed to oxidizing gas.

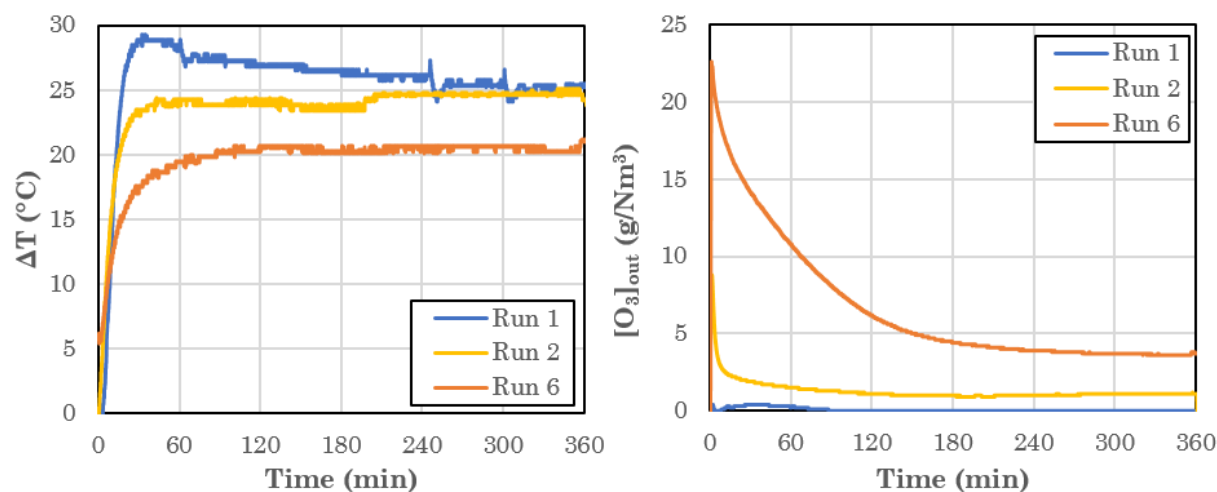


**Figure 4.14.** Evolution of (a) temperature difference and (b) outlet ozone concentration during ozonation experiments in syringe reactor. Regeneration conditions: batch REG2 runs 1, 2 and 6 (100°C; 55 g<sub>O<sub>3</sub></sub>/Nm<sup>3</sup>; 100 L/h) during 6h.

#### 4.4. Conclusions and key takeaways

Ozonation reaction in a fixed bed reactor was successfully implemented in this work. During a parametric study conducted in tubular reactor (ID 4 mm, length 20 cm, capacity 1.5 g), coke removal up to 81% from spent ZSM-5 zeolites was achieved after ozonation during 6 h at 100°C (50 g/Nm<sup>3</sup>). Higher coke removal efficiency can be achieved with longer exposition. Time of exposure and temperature were found to be the most significant operating parameters. A temperature optimum was identified between 100 and 125°C depending on carbon content and coke nature of initial spent zeolites. Experiments using syringe reactor (ID 14 mm, length 20 cm, capacity 10 g) demonstrated the feasibility of complete oxidation of coke deposited during pyrolysis of polyethylene. Indeed, coke removal of 98% is achieved from coked zeolites (5.3 wt.%C<sub>init.</sub>) after a 48h-regeneration at 100°C (50 g<sub>O<sub>3</sub></sub>/Nm<sup>3</sup>), allowing complete recovery of textural and chemical properties as well as catalytic activity (refer to Chapter 3).

Experimental results and observations confirm that ozonation is a diffusion-reaction process, similarly to coke combustion with O<sub>2</sub>, and follows well-known regeneration regimes depending on the operating conditions: either homogeneous or shrinking-core. On the one hand, homogeneous regime occurs at low temperatures and/or concentrations where ozone diffuses through the catalyst pellet, resulting in a uniform coke removal (flat radial carbon profile). On the other hand, shrinking-core regime occurs at high temperature and/or concentrations. In such conditions, reaction rate is more important than diffusion and ozone is consumed before being able to reach the center of the pellet (vertical or sharp radial carbon profiles). The strong influence of catalytic degradation as a competing mechanism with coke oxidation reinforces these limitations: at high temperatures, ozone might be fully degraded over the recovered active sites before interacting with any coke molecule. Choice of temperature is therefore a crucial aspect of this process as balance is needed between oxidation rate and mass transfer. The innovative analytical technique used in this work, consisting in using microprobe after adequate sample preparation, allowed illustrating this balance between reactivity and diffusion at pellet scale for intermediate regimes, with the apparition of varying coke core and gradient zone sizes on the radial carbon profiles. Detailed discussion about the



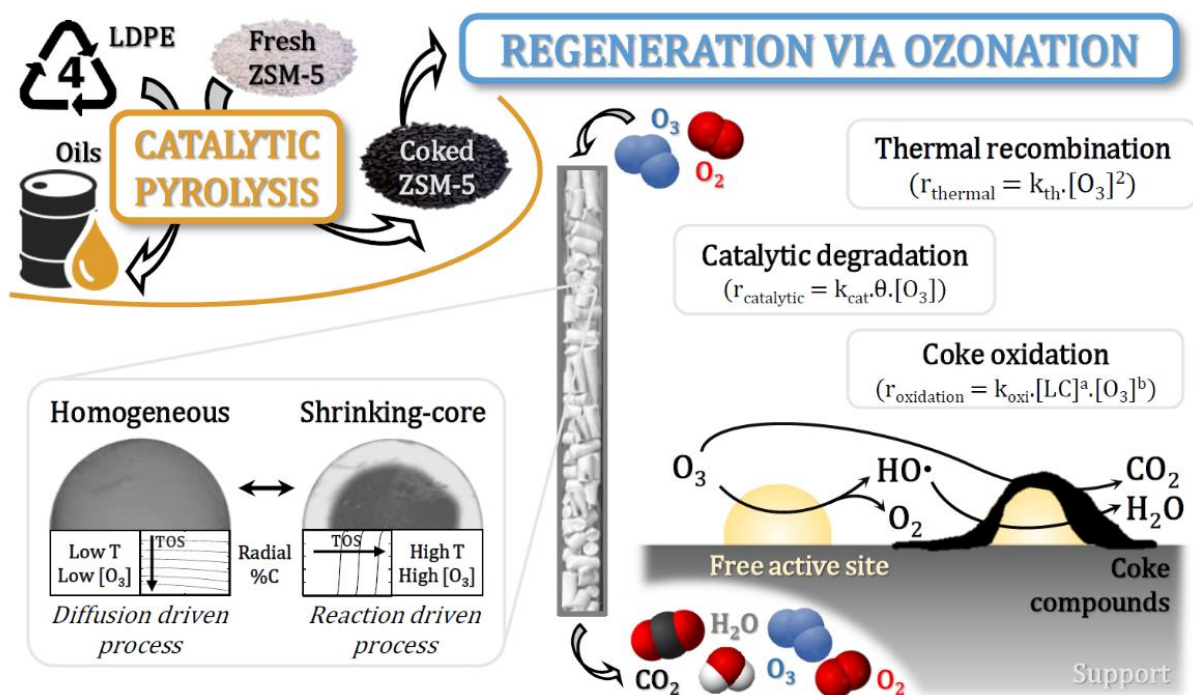
development of the method and complete results obtained using this analysis are presented in Appendix 8. Despite thrilling results showing consistency of this technique with elemental analysis, a critical discussion is also conducted to evaluate the limitations of this method as well as the perspectives of future improvement. Due to the competition of coke oxidation (direct/indirect) with thermal and catalytic degradation, ozonation is more complex than coke combustion. Kinetic study in the reactor allowed to determine that thermal recombination of ozone has a limited impact on global  $O_3$  consumption. Catalytic degradation and coke oxidation are the main reactions occurring during ozonation. Different efficiencies were observed in the reactor due to the use of a fixed-bed, but also because of the constant evolution of available active sites (correlated with coke content), ozone concentration and temperature gradients alongside the catalytic bed. Principal conclusions and key takeaways of this chapter are summarized in Figure 4.15.



A research article based on this chapter results was published in *Chemical Engineering Journal* (Elsevier) on 15<sup>th</sup> of November 2023 (Volume 476).

“Regeneration of coked catalysts via ozonation: experimental study of diffusion-reaction mechanisms at pellet and reactor scales” – V. Daligaux, R. Richard, M.-H. Manero

Access: <https://doi.org/10.1016/j.cej.2023.146446>



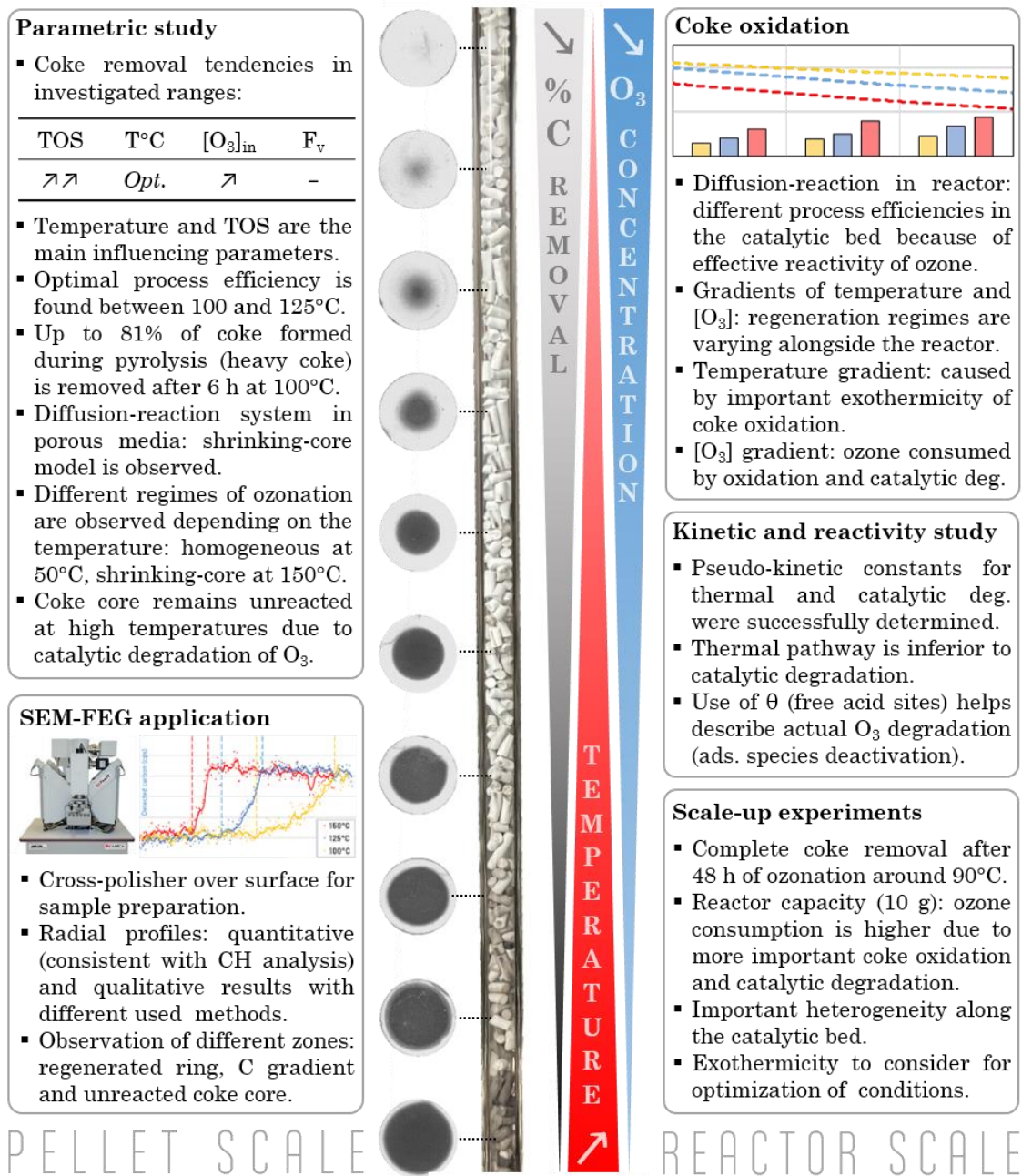


Figure 4.15. Key takeaways of "Chapter 4 – Regeneration of coked zeolites by ozonation".



# Chapter 5

## Modelling approach to ozonation reaction



The numerical approach for ozonation process presented in this work was conducted in parallel with the experimental results discussed in previous chapters. Matlab® software was used in this work and all relevant codes are given in Appendix 10 to 12. A 3-month MEng degree internship dedicated to this topic was supervised during the PhD period (Callum Murray, Strathclyde University). Based on this primary work, further collaboration has been engaged with Dr. Jean-Marie BUCHOT, IMT (Institut de Mathématiques de Toulouse) to pursue these considerations.

---

This chapter focuses on the numerical aspect of the ozonation process for regeneration of coked zeolites. After introducing the work (Section 5.1), theoretical and literature background is provided for the mathematic resolution of diffusion-reaction equations at pellet scale in a real system (Section 5.2). Assumptions are made for initial problem simplification in order to present the first approach to ozonation modelling. Methods used in this combined numerical and experimental approach, from image processing to curve fitting tool development and partial differential equations (PDEs) resolution, are detailed in Section 5.3. Obtained results are then presented and discussed (Section 5.4) before concluding and discussing future work on this problematic (Section 5.4.2). Nomenclature is given p.143 summarizing all used terms and symbols with their corresponding unit.

### 5.1. Introduction and presentation of work

Regenerating processes for coked solid catalysts involve both chemical reactivity and mass transfer: reacting molecule must be transported by external mass transfer before diffusing within the porous material towards internal coke compounds. According to previous studies but also to obtained results during this PhD work, role of pore diffusion is determinant for coke removal efficiency, leading to different regeneration regimes according to the process parameters [243]. The complexity of these diffusion-reaction systems often requires mathematical modelling to reach a better understanding of involved phenomena. Numerical simulation also allows avoiding extensive experiments, either lab or full-scale, and is nowadays heavily used to solve fundamental or technical

problems in the domain of heterogeneous catalytic processes [244]. Coke combustion with oxygen, being the most common method for coked catalysts regeneration in industry, is the only one of the aforementioned processes which was investigated in different studies using computational simulations [124, 127, 245]. This type of research is conducted both at single particle level and catalytic bed for process optimization purposes to determine safe and efficient conditions of coke burn-off. Even though those industrialization considerations are not topical yet for ozonation, a numerical approach is expected to provide better comprehension of complex reactivity occurring within zeolite porosity.

The different studies carried out on simulation of coke combustion with  $O_2$  at pellet scale showed the expected two extreme behaviors: homogeneous and shrinking-core regimes [127]. Coke removal is slow and uniform in all pellet for the first, leading to a flat carbon profile over the radius, while it is immediate and heterogeneous for the second, causing the apparition of a coke core (Figure 5.1). Kern *et al.* demonstrated such behavior between  $350^\circ\text{C}$  and  $650^\circ\text{C}$  using simplified coke reactivity as simple reaction of carbon with oxygen (1<sup>st</sup> order reaction). Such assumption is possible as hydrogen oxidation rate is higher than for carbon, the latter being therefore considered as the limiting factor for complete coke removal. In recent work, complex mechanisms were implemented by Yazovtseva *et al.*, considering multi-step oxidation with the different atoms contained in coke structure [245]. This approach allowed to obtain a spatial repartition of the different reactants and products. On top of its chemical reactions, transport of oxygen is also evaluated using effective diffusion coefficient. This key parameter of the process is constantly evolving during the reaction as it is correlated with porosity and tortuosity for instance, which are changing with coke content, but also temperature. The simulation of diffusion-reaction system at reactor scale must therefore include the notion of effective reactivity induced by diffusion limitations during the process [124, 127, 246]. These investigations provide practical insights for final regeneration time optimization and gradients of temperature and concentration observed along the catalytic bed [247]. Based on the experimental results obtained in Chapter 4, ozonation process presents many similarities with coke combustion as an oxidative regenerating treatment over porous material. Modelling of coke removal via ozonation could thus be inspired by the numerous studies carried out on combustion, requiring implementation of some additional features, such as mechanisms of ozone catalytic degradation for instance.

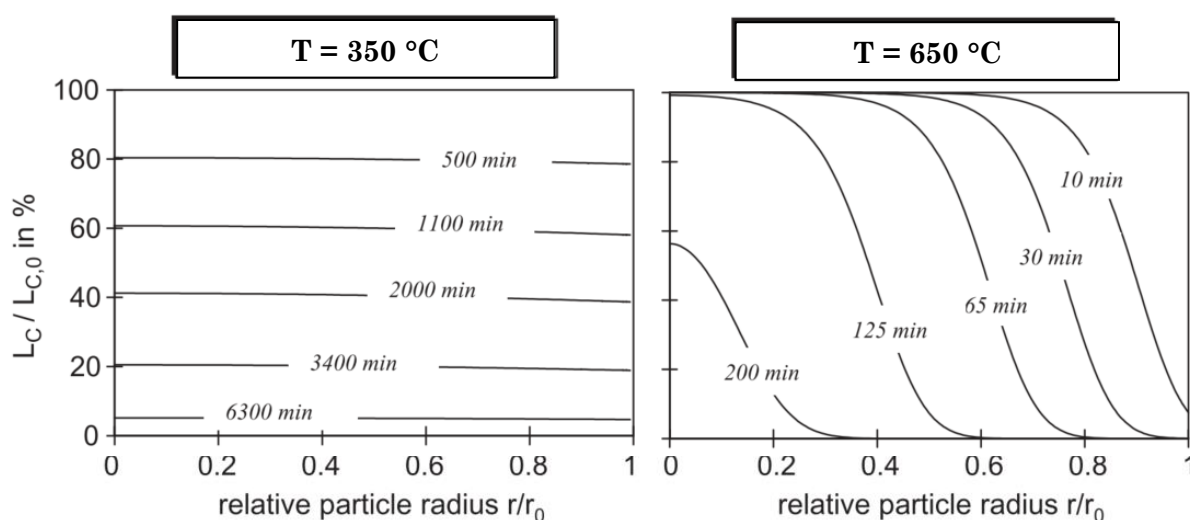


**Figure 5.1.** Radial profiles of carbon content over a single cylindrical catalyst particle for different regeneration regimes (Kern *et al.*, 2005) [127].

In this work, numerical resolution of diffusion-reaction system at single pellet level is applied to ozonation including simplified reactivity (oxidation and catalytic degradation). Using a curve optimization tool, triplets of key parameters (diffusion coefficient and intrinsic kinetic constants) are determined by approaching experimental radial carbon profiles. Such data were obtained beforehand using SEM-FEG results presented in Chapter 4, pellet cross-sections optic photographs and a Matlab® image processing routine. Complete methodology is described in Section 5.3.2. This combined experimental and numerical approach is a thrilling opportunity to conduct a parametric identification for ozonation based on these results. Such methodology could provide first approximations of missing information in the literature while obtaining a better understanding of the process and involved phenomena.

## 5.2. Model of ozonation at pellet scale

### 5.2.1. Global approach: diffusion-reaction system

The set of equations for the ozonation process has to describe the evolution of ozone and carbon content in the zeolite cylindrical pellet. As discussed in Chapter 1, extrudates are agglomerated zeolite crystals shaped with alumina binder. The resulting particle presents both meso- and micro-porosity, usually attributed to the binder and to the crystals respectively. Ozone is here the oxidizing agent which concentration in the particle is initially null. Coke is the other reactant which concentration in the particle is assumed to be homogeneous over the radius at the beginning of the process. This hypothesis appeared to be confirmed by the SEM-FEG analysis of Cok3 sample (Appendix 8). During the regeneration, ozone repartition in the pellet is therefore described by both diffusion and reaction terms while coke evolution only requires the term related to oxidation as no carbon mass transfer is involved. Using mass conservation principle, second Fick's law with the addition of a reaction term can be used to describe spatial evolution of ozone with time in the catalyst particle:

$$\varepsilon_p \frac{\delta C_{O_3}}{\delta t} = \nabla^2 (D_{O_3, \text{eff}} C_{O_3}) + R_{O_3} \quad (5.1)$$

$$\frac{\delta C_{\text{Coke}}}{\delta t} = R_{\text{Coke}} \quad (5.2)$$

The particle porosity ( $\varepsilon_p$ ) is placed as factor since ozone only diffuses and reacts in the porous volume of the grain. As it is evolving with time and space, the effective diffusion coefficient is included in the nabla operator contrary to usual diffusion systems. Because of the high thermal conductivity of solid phase, thermal gradients are neglected and only mass balances are described using Equations (5.1) and (5.2). Cylindrical coordinates are used in our system due to the shape of catalyst pellets. Their dimension ( $L_p/D_p \approx 4$ ) allows neglecting gradients of axial gradients ( $\theta$  and  $z$ ). Equation (5.1) therefore becomes:

$$\varepsilon_p \frac{\delta C_{O_3}}{\delta t} = \frac{d}{r dr} \left( D_{O_3, \text{eff}} r \frac{\delta C_{O_3}}{\delta r} \right) + R_{O_3} \quad (5.3)$$

The effective diffusion coefficient and the reaction term are depending on several factors that are discussed in the following sections to understand the involved phenomena necessary for their evaluation.

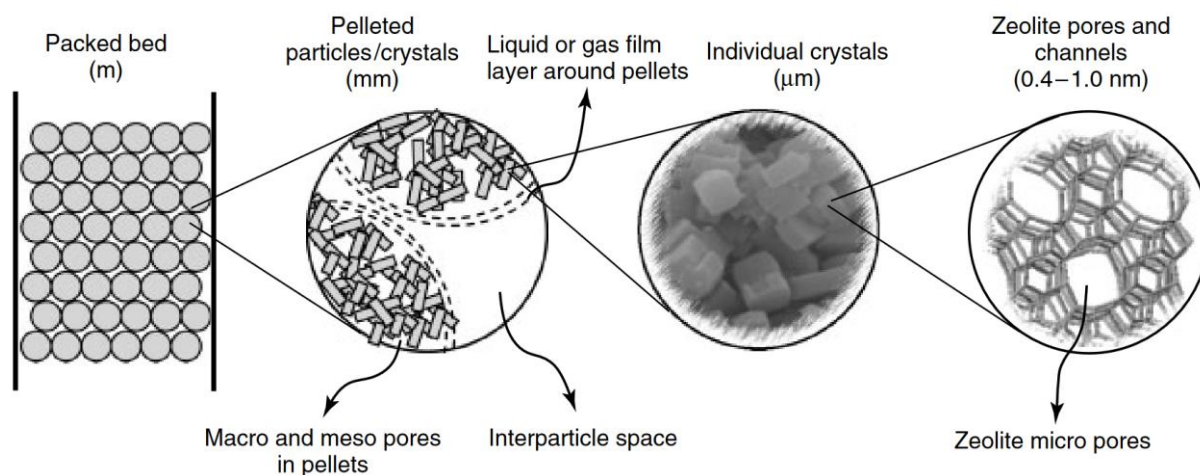


**Figure 5.2.** Ozone diffusion pathway from catalytic bed level to zeolite crystals active sites located in microporosity (Cejka *et al.*, 2010) [19].

### 5.2.2. Effective diffusion in zeolites

When exposing the catalytic bed to ozone-enriched gas stream, mass transfer occurs during different steps according to the different scales of diffusion (Figure 5.2). Ozone molecules first circulate in the bed void towards the surface of the pellets before mass transfer occurs through boundary layer around the material. The efficiency of this transfer is directly linked with this layer width, itself correlated with flow turbulence (Reynolds number). Ozone then diffuses through the mesoporosity, where it either reacts with external coke or transports further into microporosity of zeolite crystals before interacting with internal coke or active sites. The external mass transfer through the boundary layer drives the actual concentration of ozone diffusing in the porous material. Numerous correlations have been developed considering the influence of Sherwood number, particle size and molecular diffusivity [248]. The width of boundary layer, and therefore the efficiency of external transfer, is mostly driven by the hydrodynamic conditions of the system. The inlet concentration diffusing in the porous catalyst is therefore not necessarily identical to the surrounding gaseous stream content. The internal diffusion in porous volume is explained in the literature with three mechanisms: molecular diffusivity, Knudsen diffusivity and surface diffusivity as illustrated in Figure 5.3 [249].

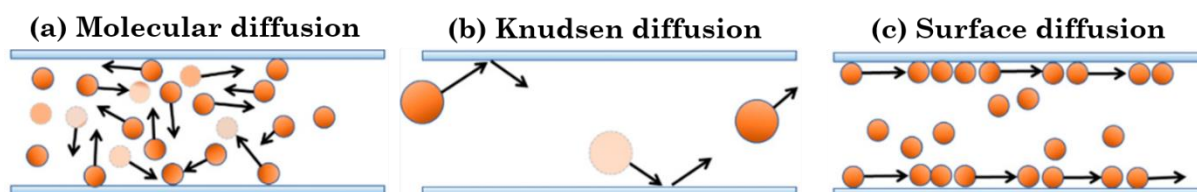


**Figure 5.3.** Different diffusion mechanisms for molecular transport in a porous volume. Adapted from Ratnakar *et al.* (2022) [252].

In mesoporosity, the molecular diffusivity drives molecular transport when pore diameter is superior to 100 nm while Knudsen diffusion pathway influence is added when pores are between 100 and 10 nm [19]. Surface diffusivity corresponds to the molecule ability to migrate from one active site to another by remaining adsorbed on the surface. In the case of coked zeolites, the partial hindering of active sites lowers surface diffusion. During coke combustion, surface diffusion does not occur as oxygen has no interactions

with active sites while it should be considered for ozonation because of catalytic reactivity of ozone. While molecular diffusivity ( $D_{\text{mol}}$ ) can be determined using semi-empirical correlations, such as Chapman and Enskog theory [250], Knudsen diffusion coefficient ( $D_k$ ) is calculated with the following formula:

$$D_k = \frac{d_{\text{pore}}}{3} \sqrt{\frac{8RT}{\pi M_{\text{O}_3}}} \quad (5.4)$$

The combined contributions of molecular and Knudsen diffusivities are often considered in series to obtain the global pore resistance to diffusion ( $D_{\text{po}}$ ) as follows:

$$D_{\text{po}} = \left( \frac{1}{D_{\text{mol}}} + \frac{1}{D_k} \right)^{-1} \quad (5.5)$$

The effective diffusion coefficient considers that only a portion of the catalyst is permeable using its porosity ( $\epsilon_p$ ) and that the path followed by molecules is random and tortuous thanks to its tortuosity ( $\tau_p$ ). Then, the effective diffusion coefficient of ozone used in Equation (5.3) is therefore given by:

$$D_{\text{O}_3, \text{eff}} = \frac{\epsilon_p}{\tau_p} D_{\text{O}_3, \text{po}} \quad (5.6)$$

This factor  $\epsilon_p/\tau_p$  is changing with coke content during the regeneration as volume occupancy and pore mouth blocking are decreasing with carbon compounds removal. Effective diffusion of ozone is therefore different depending on the spatial repartition of coke over the radius, itself evolving during time. This parameter should therefore be included inside the derivative of the partial differential equation (PDE) describing radial evolution of ozone. Porosity and tortuosity having values proper to the catalyst geometry, their correlation with coke content needs to be experimentally determined for each particular application.

### 5.2.3. Ozone and coke reactivity

The reactivity of ozone and coke, respectively  $R_{\text{O}_3}$  and  $R_{\text{Coke}}$ , present complex mechanisms already discussed in Section 1.4.2.2. Ozone is consumed via three different pathways: thermal recombination (Equations (1.15) and (1.16)), catalytic degradation (Equations (1.17) to (1.22)) and coke oxidation (Equation (1.23)). Thermal recombination of ozone occurs with a third molecule (M), being  $\text{O}_2$ ,  $\text{O}_3$ ,  $\text{CO}_2$ ,  $\text{N}_2$ , He or other gaseous body. Ozone is also degraded catalytically over active sites (\*) into oxygenated adsorbed species leading to the formation of molecular dioxygen but also hydroxyl radicals. Direct and indirect oxidation mechanisms are involved during coke removal: oxidation with molecular ozone and with hydroxyl radicals. Moreover, coke molecules are composed of various structures having different stabilities and therefore reactivity. In the case of catalytic pyrolysis of polyethylene, coke contains only carbon and hydrogen as there is no heteroatoms. Carbon and hydrogen atoms are embedded in either aliphatic or aromatic coke molecules. Coke rates are often simplified by assuming that oxidative species are attacking atoms one at a time, thus reacting with deposits noted as solid hydrogen ( $\text{H}_s$ ) and carbon ( $\text{C}_{\text{aromatic}}$  or  $\text{C}_{\text{aliphatic}}$ ).

The following set of equations is suggested to summarize the different reactions rates that are involved in the consumption of ozone and coke considering all discussed mechanisms:

*Thermal recombination ( $r_{th}$ ):*



*Catalytic degradation ( $r_{deg}$ ):*



*Hydroxyl radicals formation ( $r_{OH}$ ):*



*Coke oxidation ( $r_{oxi}$ ):*



Where a to l exponents are the reaction orders regarding each reacting species and the greek symbols are the stoichiometric coefficients for coke reactivity. This combination of reaction rates is expected to provide a realistic approximation of ozone and coke reactivity with their different mechanisms. However, many simplifications are already made in these equations: the difference of reactivity between Lewis and Brønsted acid sites is not considered, the rates of oxidation (Equations (5.12) and (5.13)) will vary according to the nature of coke (ratio Y/X corresponds to the H/C molar ratio), etc. Indeed, the different atoms contained in coke molecules present different oxidation rates. Hydrogen is the first to react while reaction rate of aromatic carbons ( $C_{ar}$ ) is lower than aliphatic carbon ( $C_{al}$ ) due to their higher stability generated by the condensed rings. Moreover, the real mechanisms of coke molecules oxidation by molecular ozone and hydroxyl radicals generate oxygenated reaction intermediates (ketones, aldehydes, etc). The variety of functional groups present in these structures makes impossible to describe the real multistep reactions occurring during coke removal. By combining the previous set of equations, the respective reaction terms for ozone and coke are given by:

$$R_{O_3} = r_{th} + r_{deg} + r_{oxi} = -(r_1 + r_2) - (r_3 + r_4) - r_6 \quad (5.14)$$

$$R_{Coke} = r_{oxi} = -(r_6 + r_7) \quad (5.15)$$

However, different kinetic studies were conducted with coke combustion showing that simplified pseudo-reaction rates, using often 1<sup>st</sup> order reaction rates, provide a good approximation of the real system. These assumptions for problem simplification are discussed in the next paragraph.

### 5.2.4. Simplifications and final PDEs

In this work, many hypotheses have been made in order to simplify the complexity of the problem. Some assumptions are classic and often used in literature, while other simplifications were carried out to provide a first approach of the system before envisaging further improvements. All the hypotheses that were made in this study are listed below before presenting the problem as it was investigated in the following sections:

- i. **Constant diffusion coefficient.** Effective diffusion coefficient is here considered as constant for initial problem solving. This is expected to be the most impacting simplification due to the aforementioned importance of the diffusion resistance evolution during coke removal (Section 5.2.2).
- ii. **Ideal external mass transfer.** External molecular transport of ozone is considered as ideal because of the hydrodynamic conditions in tubular configuration. Important flowrate generates an important turbulence and a thin boundary layer. The ozone concentration entering the pellet is assumed equal to the gaseous phase content.
- iii. **Thermal recombination neglected.** Reaction rate related to the thermal recombination of ozone is neglected based on the experimental results (Chapter 4) showing very limited contribution facing catalytic degradation.
- iv. **Use of experimental catalytic degradation rate.** The overall reaction rate determined in Chapter 4 using first order reaction and free fraction of acid sites ( $\theta$ ) is used for numerical solution. No adsorption or desorption considerations are implemented. The kinetic constant experimentally determined ( $k_{\text{cat}}$ ) is however not used in order to compare with numerical solution values.
- v. **Coke assimilation to carbon.** Due to the more important oxidation rate of hydrogen, carbon is considered as the limiting factor of coke removal. The evolution of coke in the system is consequently assimilated to carbon reactivity. Concentration of coke ( $C_{\text{coke}}$ ) is therefore replaced by carbon load ( $L_C$ ), joining the experimental results where coke removal is evaluated by carbon content analysis.
- vi. **Overall coke oxidation rate.** Direct and indirect mechanisms of coke oxidation are not differentiated. Consequently, the concentration of hydroxyl radicals is not determined and coke removal is considered as being entirely due to molecular ozone. The overall coke oxidation rate is considered as a first order reaction regarding both ozone and carbon load.

According to the assumptions (iii) to (vi), the reaction terms presented in Equations (5.14) and (5.15) are modified as follows:

$$R_{O_3} = r_{\text{deg}} + r_{\text{oxi}} = -(k_{\text{deg}}\theta [O_3] + \rho_p k_{\text{oxi}} [L_C][O_3]) \quad (5.16)$$

$$R_C = r_{\text{oxi}} = -k_{\text{oxi}} [L_C][O_3] \quad (5.17)$$

Ozone concentration and carbon load are expressed in  $\text{kg}_{O_3} \cdot \text{m}^{-3}$  and in  $\text{kg}_C \cdot \text{kg}_{\text{cat}}^{-1}$  to match experimental data. The density of the zeolite  $\rho_p$  ( $\text{kg}_{\text{cat}} \cdot \text{m}^{-3}$ ) is introduced to maintain unit balance. Equations (5.2) and (5.3), which were the initial statements describing the spatial and temporal evolution of ozone and coke over catalyst pellet radius, are adapted by using the aforementioned assumptions and simplifications. Notations are also changed to alleviate the equations:  $[O_3]$  becomes  $C$ ,  $[L_C]$  becomes  $L_C$  and  $D_{O_3, \text{eff}}$  becomes  $D$ .



The following mass balances for the gas and solid phase arise as final PDEs system:

$$\varepsilon_p \frac{\delta C}{\delta t} = D \frac{d}{dr} \left( r \frac{\delta C}{\delta r} \right) - (k_{deg} \theta C + \rho_p k_{oxi} L_C C) \quad (5.18)$$

$$\frac{\delta L_C}{\delta t} = - k_{oxi} L_C C \quad (5.19)$$

The boundary conditions for the differential equation resolution are as follows:

$$\frac{\delta C}{\delta r} = 0 \quad \text{for } r = 0 \text{ (particle center)} \quad (5.20)$$

$$C = C_{O_3,G} \quad \text{for } r = r_p \text{ (particle surface)} \quad (5.21)$$

The axis formed by pellet center is considered as an impermeable boundary, leading to a null flux of transferring species at this point (Equation (5.20)). Boundary condition at the pellet external surface (Equation (5.21)) was set according to assumption (ii). The initial conditions for ozone and carbon radial repartition are stated by the following equations based on experimental knowledge:

$$C = 0 \quad \text{for } 0 < r < r_p \quad \text{at } t = 0 \quad (5.22)$$

$$L_C = L_{C,0} \quad \text{for } 0 < r < r_p \quad \text{at } t = 0 \quad (5.23)$$

Where  $L_{C,0}$  is the initial carbon load of the catalyst pellet. Radial carbon repartition is considered as homogeneous over the particle radius.  $L_{C,0}$  will therefore be in most cases a single value. If initial radial carbon profile is found to be heterogeneous,  $L_{C,0}$  can possibly be a vector representing carbon load analyzed over the radius. Numerical methods for system resolution are presented in the following paragraph (Section 5.3).

### 5.3. Numerical methods

In this section, the computational methods used in this work for the combined experimental and numerical approach are presented. The resolution of partial differential equations and curve optimization present many possibilities due to the high number of existing numerical approaches. Even though different existing software with embedded methods are available, we chose to use homemade Matlab® codes in this work. Despite important code development and higher computational time, this choice allowed to acquire deeper knowledge of simulation domain by understanding the mathematical background of these methods. On top of this training aspect, developing original codes provide full control over its content for implementation of future additional features. The approach in this work consists in three aspects: acquire numerical profiles by numerical resolution (Section 5.3.1), obtain experimental profiles by image processing (Section 5.3.2) and combine these two aspects with a curve fitting tool developed to determine triplets of physical parameters optimizing the difference between the profiles (parameters identification, Section 5.3.3). Numerical methods and equations are detailed in this section by presenting the discretization scheme and algorithm of coupled PDEs resolution, the image processing routine and eventually the parameters optimization algorithm. Respective codes are placed in Appendix 10 to 12. The results obtained thanks to this methodology and to the developed codes are presented in Section 5.4.

### 5.3.1. PDEs resolution

#### 5.3.1.1. Crank-Nicolson discretization

Crank-Nicolson algorithm is often used to solve one-dimensional diffusion equation. Based on the finite difference principle, this implicit method is unconditionally stable and has the advantage of being second-order in both time and space. The stencils representing the points used during the resolution for each of the different methods are illustrated in Figure 5.4. For each variable, “i” represents the spatial steps and “n” stands for the temporal steps.

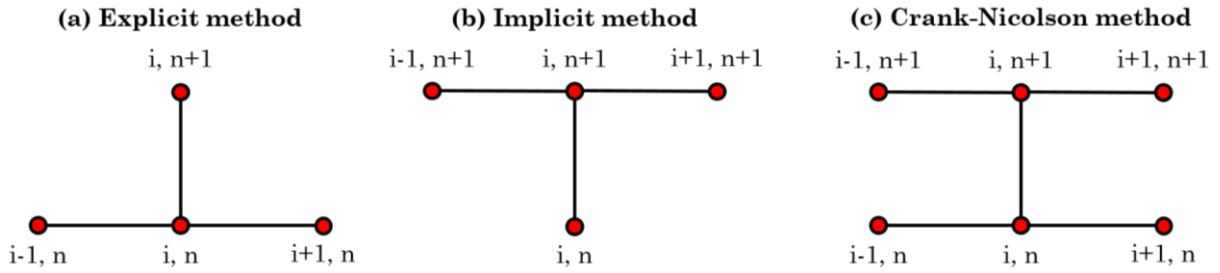


Figure 5.4. Different methods for the resolution of second-order derivative equations.

As departing stage, Equation (5.18) and (5.19) are discretized using second order centered scheme for the spatial derivative. For clarity of equations and ease of read, ozone concentration and diffusion coefficient symbols become a single  $C$  and  $D$ . Spatial step  $i$  is subscripted and time step  $n$  is superscripted for each variable:

$$\varepsilon_p \frac{C_i^{n+1} - C_i^n}{\Delta t} = D \frac{C_{i+1}^n - 2C_i^n + C_{i-1}^n}{\Delta r^2} + \frac{D}{r_i} \cdot \frac{C_{i+1}^n - C_{i-1}^n}{2\Delta r} - (k_{\text{deg}} \theta_i^n C_i^n + \rho_p k_{\text{oxi}} C_i^n Lc_i^n) \quad (5.24)$$

$$\frac{Lc_i^{n+1} - Lc_i^n}{\Delta t} = -k_{\text{oxi}} C_i^n Lc_i^n \quad (5.25)$$

In Crank-Nicolson method, the temporal derivate is evaluated at the center point between time steps ( $t_{n+1/2}$ ), corresponding to the average of spatial derivative evaluated at  $t_n$  and  $t_{n+1}$ . By sorting the terms for each stencil point, we have:

$$\begin{aligned} -\left(\alpha - \frac{\beta}{r_i}\right) C_{i-1}^{n+1} + (1 + 2\alpha + \gamma_i^{n+1}) C_i^{n+1} - \left(\alpha + \frac{\beta}{r_i}\right) C_{i+1}^{n+1} \\ = \left(\alpha - \frac{\beta}{r_i}\right) C_{i-1}^n + (1 - 2\alpha - \gamma_i^n) C_i^n + \left(\alpha + \frac{\beta}{r_i}\right) C_{i+1}^n \end{aligned} \quad (5.26)$$

$$(1 + \zeta C_i^{n+1}) Lc_i^{n+1} = (1 - \zeta C_i^n) Lc_i^n \quad (5.27)$$

With:

$$\alpha = \frac{\Delta t. D}{2\varepsilon_p \Delta r^2} \quad (5.28)$$

$$\beta = \frac{\Delta t. D}{4\varepsilon_p \Delta r} \quad (5.29)$$

$$\zeta = \frac{\Delta t. k_{\text{oxi}}}{2} \quad (5.30)$$

$$\gamma_i^{t=n \text{ or } n+1} = \frac{\Delta t}{2\varepsilon_p} (k_{\text{deg}} + \rho_p k_{\text{oxi}} \text{LC}_i^t) \quad (5.31)$$

While  $\alpha$ ,  $\beta$  and  $\zeta$  are constants, the term  $\gamma$  is depending on the carbon load and its radial repartition is therefore evolving at each time step. In these equations,  $\alpha$  and  $\beta$  are representing the diffusion term and  $\zeta$  and  $\gamma$  describe the reaction term. Equations (5.26) and (5.27) are then transformed into a matrix equation for the determination of the profiles at  $t_{n+1}$  from precedent results  $t_n$  (initial conditions if  $n = 0$ ). For representation, only four radial steps are here considered ( $i = 1$  to  $4$ ):

$$A. \begin{bmatrix} C_1^{n+1} \\ C_2^{n+1} \\ C_3^{n+1} \\ C_4^{n+1} \end{bmatrix} = \begin{bmatrix} (1 - 2\alpha - \gamma_1^n) C_1^n + 2\alpha C_2^n \\ (\alpha - \beta/r_2) C_1^n + (1 - 2\alpha - \gamma_2^n) C_2^n + (\alpha + \beta/r_2) C_3^n \\ (\alpha - \beta/r_3) C_2^n + (1 - 2\alpha - \gamma_3^n) C_3^n + (\alpha + \beta/r_4) C_4^n \\ C_{O_3,G} \end{bmatrix} \quad (5.32)$$

$$\begin{bmatrix} 1 + \zeta C_1^{n+1} \\ 1 + \zeta C_2^{n+1} \\ 1 + \zeta C_3^{n+1} \\ 1 + \zeta C_4^{n+1} \end{bmatrix}^T \cdot \begin{bmatrix} \text{LC}_1^{n+1} \\ \text{LC}_2^{n+1} \\ \text{LC}_3^{n+1} \\ \text{LC}_4^{n+1} \end{bmatrix} = \begin{bmatrix} (1 - \zeta C_1^n) \text{LC}_1^n \\ (1 - \zeta C_2^n) \text{LC}_2^n \\ (1 - \zeta C_3^n) \text{LC}_3^n \\ (1 - \zeta C_4^n) \text{LC}_4^n \end{bmatrix} \quad (5.33)$$

With A tridiagonal matrix defined as:

$$A = \begin{bmatrix} 1 + 2\alpha + \gamma_1^{n+1} & -2\alpha & 0 & 0 \\ -\left(\alpha - \frac{\beta}{r_2}\right) & 1 + 2\alpha + \gamma_2^{n+1} & -\left(\alpha - \frac{\beta}{r_2}\right) & 0 \\ 0 & -\left(\alpha - \frac{\beta}{r_3}\right) & 1 + 2\alpha + \gamma_3^{n+1} & -\left(\alpha - \frac{\beta}{r_3}\right) \\ 0 & 0 & 0 & 1 \end{bmatrix} \quad (5.34)$$

The boundary conditions coefficients were calculated based on the Equations (5.20) and (5.21) using the discretized formula. This matrix system is used for the numerical resolution of the two initial equations to find the profiles at next time step ( $C^{n+1}$  and  $\text{LC}^{n+1}$ ) based on the previous profiles ( $C^n$  and  $\text{LC}^n$ ). In most systems with only a diffusion term, the tridiagonal matrix (A) needed for the resolution is constant. However, due to the addition of the reaction term, the principal diagonal ( $A_p$ ) is changing at each time step, requiring new calculation of A for each iteration. Diffusion-reaction system is therefore more intensive in terms of calculation and the Crank-Nicolson method may present long calculation times.

### 5.3.1.2. Newton method for resolution coupling

Newton method is often used for the resolution of non-linear systems and allows to combine the resolution of different PDEs linked with each other [251]. The principle of this method is to find the solution vector for which a given function  $F$  cancels itself. In the case of the investigated system, this vector is the combination of the two radial profiles at the following time step ( $C$  and  $Lc$ ). The two cancelling functions involving these variables are obtained by doing the difference of the left and right members of Equation (5.26) for  $f_2$  and Equation (5.27) for  $f_1$ . The problem is presented as follows:

$$\vec{F}([Lc_1 \dots Lc_r \ C_1 \dots C_r]) = \vec{F}([Lc \ C]) = \vec{F}(\vec{x}) = 0 \quad \leftrightarrow \quad \begin{cases} f_1(Lc, C) = 0 \\ f_2(Lc, C) = 0 \end{cases} \quad (5.35)$$

This method requires an initial approximation of the system solution, noted  $C^0$  and  $Lc^0$ , in order to determine a correction ( $\delta$ ) applied to the initial vector (Equation (5.36)). For each iteration  $k$ , the corrected vector is then used as input value for the evaluation of the new error.

$$\vec{x}^{k+1} = \vec{x}^k + \vec{\delta x} \quad (5.36)$$

Where  $\vec{\delta x}$  is the correction column, calculated using the following matrix system as detailed by Fortin *et al.* (2006):

$$J_F(\vec{x}^k) \cdot \vec{\delta x} = -\vec{F}(\vec{x}^k) \quad \leftrightarrow \quad \begin{bmatrix} \frac{\partial f_1}{\partial Lc} & \frac{\partial f_1}{\partial C} \\ \frac{\partial f_2}{\partial Lc} & \frac{\partial f_2}{\partial C} \end{bmatrix} \begin{bmatrix} \delta Lc \\ \delta C \end{bmatrix} = - \begin{bmatrix} f_1(\vec{x}^k) \\ f_2(\vec{x}^k) \end{bmatrix} \quad (5.37)$$

The Jacobian matrix  $J_F$  coefficients are the partial derivatives of the non-linear equations by the variables. Their values are changing and are evaluated for each Newton iteration. The following set of equations is obtained from Equations (5.26) and (5.27) for the iterative calculation of  $J_F$  quarters (top-left TL, top-right TR, bottom-left BL and bottom-right BR):

$$J_F(\text{TL}) = \frac{\partial f_1}{\partial Lc} = 1 + \zeta C^k \quad (5.38)$$

$$J_F(\text{TR}) = \frac{\partial f_1}{\partial C} = \zeta Lc^k \quad (5.39)$$

$$J_F(\text{BL}) = \frac{\partial f_2}{\partial Lc} = \frac{k_{\text{oxi}} \Delta t \rho_p}{2\varepsilon_p} C^k \quad (5.40)$$

$$J_F(\text{BR}) = \frac{\partial f_2}{\partial C} = 1 + 2\alpha + \frac{\Delta t}{2\varepsilon_p} (k_{\text{deg}} + \rho_p k_{\text{oxi}} Lc^k) = 1 + 2\alpha + \gamma_1^{n+1} = A_p \quad (5.41)$$

Each of the Jacobian portions is therefore a diagonal matrix of spatial step dimensions. The principal diagonal of the tridiagonal matrix (Equation (5.34)) is reused for the bottom-right quarter to save computational time. The algorithm converges if the correction vector norm is inferior to a tolerance set by the user. A maximal number of iterations is usually also chosen to exit the loop if the resolution does not converge. With a proper initialization, convergence in the developed code usually occurred in two to three Newton

iterations. This algorithm is called for each time step of the global resolution and is included in another loop incrementing time. The final output of this numerical resolution is the carbon and ozone internal concentration profiles over the pellet radius at a final time  $T_f$  corresponding to the experimental time of exposure. Profiles at intermediate times can be saved to show their evolution during the resolution. Normalization of results is possible afterwards for plotting or comparing with experimental profiles obtained via the image processing routine presented in the following section.

### 5.3.2. Image processing

#### 5.3.2.1. Raw image preparation

The first step of image processing is the preparation of the image from the raw microscope photograph obtained using Morphology G3S (Section 2.2.4.4). The different steps are illustrated in Figure 5.5. The initial objective is to automatically identify the circular zone corresponding to the catalyst pellet. The edges on typical raw images (a, e) are not easily detected by the computer even though it is visible to the naked eye. The picture is treated with binary function (b) or edge detection (f) to facilitate circle detection. If no circle is automatically found after these methods with different thresholds and sensitivities, two diameters are drawn manually. Once the pellet zone is detected or entered if applicable, its coordinates are saved and image is cropped (c, g) and background is removed (d, h) to obtain the image further used for radial profile acquisition.

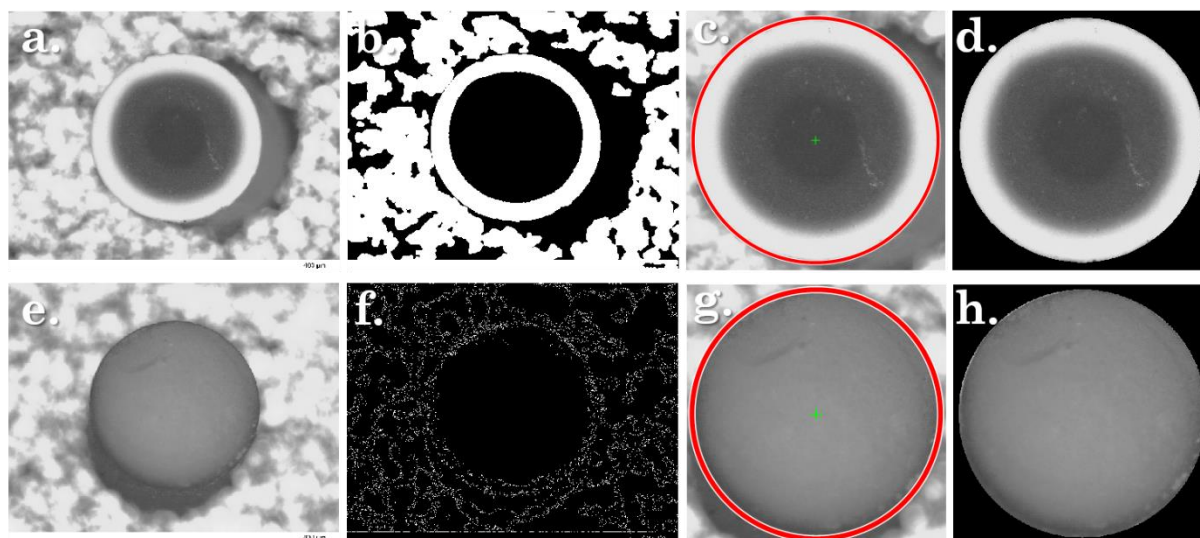


**Figure 5.5.** Different steps of photographs treatment by pellet zone detection with developed Matlab® routine, from raw pictures (a, e) to processed images (d, h).

#### 5.3.2.2. Profile acquisition

In order to obtain experimental radial carbon profiles from image processing, the idea was to use the grey level variations corresponding to the different carbon contents over pellet cross-sections. The different steps of profile acquisition and processing are illustrated in Figure 5.6. From the images acquired after raw image preparation (a, e), grey level intensity, from 0 for black to 255 for white, is acquired over different radii of the pellet. Center point of the circle and polar coordinates are used to command the acquisition of several profiles, which are subsequently averaged to obtain the mean greyscale radial

profile of the pellet (b, f). Number of acquired profiles on a single pellet is set by the user from 1 to 360 (one per degree). Averaging a high number of profiles allows smoothing the irregularities and imperfections of the pellet cut. The conversion from grey intensity (GI) to carbon load (Lc) is calibrated using the SEM-FEG quantitative results presented in Appendix 8. The correlation between these two values, plotted in Appendix 9, is best approached by second-order exponential function ( $a \cdot \exp(bx) + c \cdot \exp(dx)$ ) with a  $R^2$  value of 0.8924. Very few carbon content (0.1 wt.%) is sufficient to visually observe dark color and therefore low grey intensity. The raw profile (c, g) is smoothed using moving average function (window size: 10) to obtain the final carbon profile (d, h).

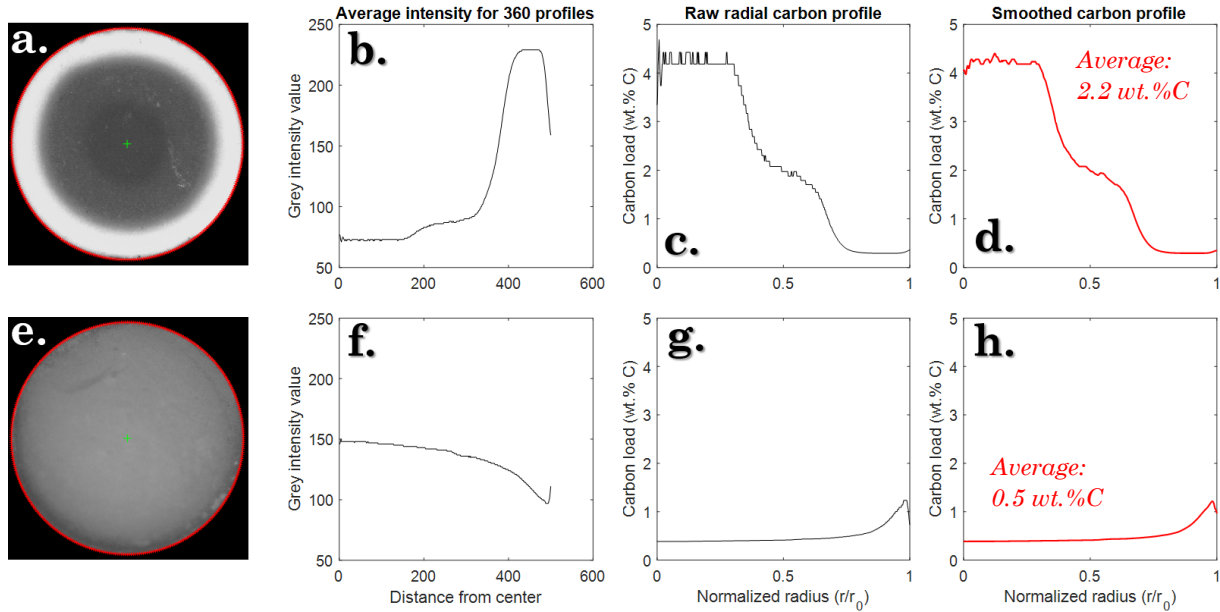


**Figure 5.6.** Different steps for the acquisition of radial carbon profiles via grey intensity reading, from processed images (a, e) to smoothed profile (d, h).

To verify the consistency of the obtained carbon profile, its average value over the radius is compared with the carbon content obtained by elemental analysis. In the case of the two check samples presented above, a difference is observed: 2.2 wt.%C instead of 1.9 for one and 0.5 for the second while CH analysis gave 1.7 wt.%C. This gap is due to the combined incertitude of luminosity and reflection variation depending on the pictures but also to the error induced by the calibration of the grey-to-carbon scale. As presented in Table 5.1, a difference is observed also for the various calibration samples. It is therefore necessary to correct the profiles obtained by image processing to keep consistency with other profile acquisition techniques and mitigate the error of this method. Correction and normalization of radial carbon profile for comparison with numerical results is discussed in the next paragraph.

**Table 5.1.** Comparison between carbon contents obtained with elemental, microprobe and image processing methods. Adapted from Table 4.2.

	Elemental (wt.%C)	Microprobe (wt.%C)	Image process (wt.%C)
R1	1.9	1.8	2.2
R2	1.2	1.2	1.0
R3	0.6	0.6	0.3
R4	1.1	1.1	1.0
R5	0.8	0.9	0.8

### 5.3.2.3. Data normalization

Profiles obtained with the developed image-processing tool are post-treated to allow the comparison with those obtained by numerical resolution. Carbon load was therefore normalized following different strategies depending on the profile appearance. Profiles presenting a flat zone at the outer edge of the pellet are suggested to be entirely regenerated: the minimum value is therefore shifted to 0. If a plateau appears at the center of the pellet, the pellet features an unreacted coke core which normalized value is 1. For the profiles that are not presenting any of these two particular behaviors, carbon load values found by image processing are artificially corrected to match elemental analysis result by using a multiplying factor. As an example, the profile obtained in Figure 5.6.h is multiplied by 3.4 to obtain the experimental 1.7 wt.%C. The profile is subsequently normalized using the initial carbon load considered as homogeneous along the radius. Initial carbon load for the presented example is 3.3 wt.%C. These two strategies cover all possible scenario and provide carbon profiles normalized in both radial and concentration dimensions. These final profiles are then compared with the numerical simulation results as presented in the following section.

### 5.3.3. Profiles fitting optimization

This section presents the fitting tool developed in collaboration with Dr. Jean-Marie Buchot (IMT) to approach the obtained experimental carbon profiles (Section 5.3.2) with the numerical resolution presented in Section 5.3.1. The optimization of numerical profile is based on the variation of three unknown parameters: the effective diffusion coefficient ( $D$ ) and the kinetic constants of catalytic degradation and coke oxidation ( $k_{deg}$  and  $k_{oxi}$ ). The difference between the two profiles is evaluated with the residual sum of squares function (RSS) as cost function:

$$J = \sum (y_{exp} - y_{num})^2 \quad (5.42)$$

Where  $y_{exp}$  and  $y_{num}$  are the experimental and numerical profiles respectively. This cost function  $J$  is minimized using Newton method. Finding cost function minimum is equivalent to find the numerical profile for which the derivative of  $J$  is null. The Newton problem is therefore set as follows:

$$\vec{F}(D, k_{deg}, k_{oxi}) = \vec{F}(X) = \vec{\nabla}J(X) = 0 \quad \leftrightarrow \quad \begin{cases} f_1 = \frac{\partial J}{\partial D} = 0 \\ f_2 = \frac{\partial J}{\partial k_{deg}} = 0 \\ f_3 = \frac{\partial J}{\partial k_{oxi}} = 0 \end{cases} \quad (5.43)$$

For each iteration, a new triplet of parameters  $[D, k_{deg}, k_{oxi}]$ , called  $X^{k+1}$ , is calculated from the previous values ( $X^k$ ) with a correction term  $\delta X$  similarly to Equation (5.36). This error is evaluated using the following matrix system:

$$H_J(\vec{X}^k) \cdot \delta \vec{X} = -\vec{F}(\vec{X}^k) \quad (5.44)$$

Where  $H_J$  is the Hessian matrix of the cost function, whose coefficients are by definition the second-order partial derivatives of  $J$ .



The condensed matrix system described in Equation (5.44) can be developed as follows:

$$\begin{bmatrix} \frac{\partial^2 J}{\partial D^2} & \frac{\partial^2 J}{\partial D \partial k_{\text{deg}}} & \frac{\partial^2 J}{\partial D \partial k_{\text{oxi}}} \\ \frac{\partial^2 J}{\partial k_{\text{deg}} \partial D} & \frac{\partial^2 J}{\partial k_{\text{deg}}^2} & \frac{\partial^2 J}{\partial k_{\text{deg}} \partial k_{\text{oxi}}} \\ \frac{\partial^2 J}{\partial k_{\text{oxi}} \partial D} & \frac{\partial^2 J}{\partial k_{\text{oxi}} \partial k_{\text{deg}}} & \frac{\partial^2 J}{\partial k_{\text{oxi}}^2} \end{bmatrix} \begin{bmatrix} \delta D \\ \delta k_{\text{deg}} \\ \delta k_{\text{oxi}} \end{bmatrix} = - \begin{bmatrix} \frac{\partial J}{\partial D} \\ \frac{\partial J}{\partial k_{\text{deg}}} \\ \frac{\partial J}{\partial k_{\text{oxi}}} \end{bmatrix} \quad (5.45)$$

The coefficients of the Hessian matrix and of the gradient column of J (right member of Equation (5.45)) are evaluated with finite difference method. Expression of each coefficient is equivalent to the evaluation of the cost function variation according to each parameter, calling numerical resolution at different set of  $[D \pm \Delta D; k_{\text{deg}} \pm \Delta k_{\text{deg}}; k_{\text{oxi}} \pm \Delta k_{\text{oxi}}]$ . According to these calculations, one Newton iteration for the curve optimization tool requires 25 numerical resolution (1 initial, 6 for the gradient and 18 for the Hessian matrix) leading to quite important calculation times. Considering that one resolution takes in average 4 to 5 s ( $dt = 10$  s), one iteration for triplet parameter correction takes a bit less than 2 minutes. The algorithm loops until norm of cost function gradient is inferior to the set tolerance. The final output is the triplet  $[D, k_{\text{deg}}, k_{\text{oxi}}]$  that fits the most the experimental profile. Even though numerical profile cannot fit perfectly due to image processing limitations and initial simplifications of the problem, this tool is used to provide a first approximation of key parameters during ozonation. This general approach with the simultaneous variation of the three parameters can be simplified by removing adequate matrix coefficients to optimize separately one or two parameters by fixing the other(s).

## 5.4. Results and discussion

### 5.4.1. Influence of key parameters on numerical resolution

#### 5.4.1.1. Coke oxidation kinetic constant

The kinetic constant of oxidation ( $k_{\text{oxi}}$ ) is the most important term in the reaction term as it describes the reactivity of ozone with coke allowing carbon removal from the catalysts. As discussed in Chapter 4, the balance between diffusion and reaction governs the regeneration regime leading to different carbon repartition profiles. These behaviors are illustrated in Figure 5.7 using the developed numerical resolution. During these simulations, the effective diffusion coefficient D of ozone in the catalyst grain is fixed at  $4 \cdot 10^{-7} \text{ m}^2 \cdot \text{s}^{-1}$ , corresponding to typical magnitude found in the literature for the diffusion of oxygen in catalysts [127]. The catalytic degradation kinetic constant of ozone  $k_{\text{deg}}$  is set at  $1 \cdot 10^{-2} \text{ s}^{-1}$ . For such value, the contribution of this mechanism is limited and can be considered as null since it was experimentally found in Chapter 4 that it physically fluctuates between  $10^0$  and  $10^2$  magnitudes. The profiles presented in Figure 5.7 therefore illustrate the influence of the variation of oxidation contribution without any competition with catalytic degradation.

The results obtained with  $k_{\text{oxi}} = 1$  (Figure 5.7.a) illustrate the typical behavior of regeneration following shrinking-core regime: carbon profiles present a sharp gradient zone with an unreacted coke core located at the center of the catalyst pellet. In such conditions, ozone reacts with carbon before being able to diffuse through the pellet. The

$O_3$  concentration profiles show that the center of the catalyst grain is never exposed to ozone after 8h of reaction. In this case, ozone is entirely consumed by coke oxidation. As expected from the shrinking-core model, the completely regenerated ring ( $LC = 0$ ) is progressing with time as the coke core shrinks. The homogeneous regime regeneration is observed in Figure 5.7.c for lower oxidation rate ( $k_{oxi} = 1.10^{-4}$ ). The reactivity of ozone with carbon is the limiting factor in such conditions: ozone is therefore able to diffuse through the pellet and reach its center before reacting. Coke removal is consequently homogeneous

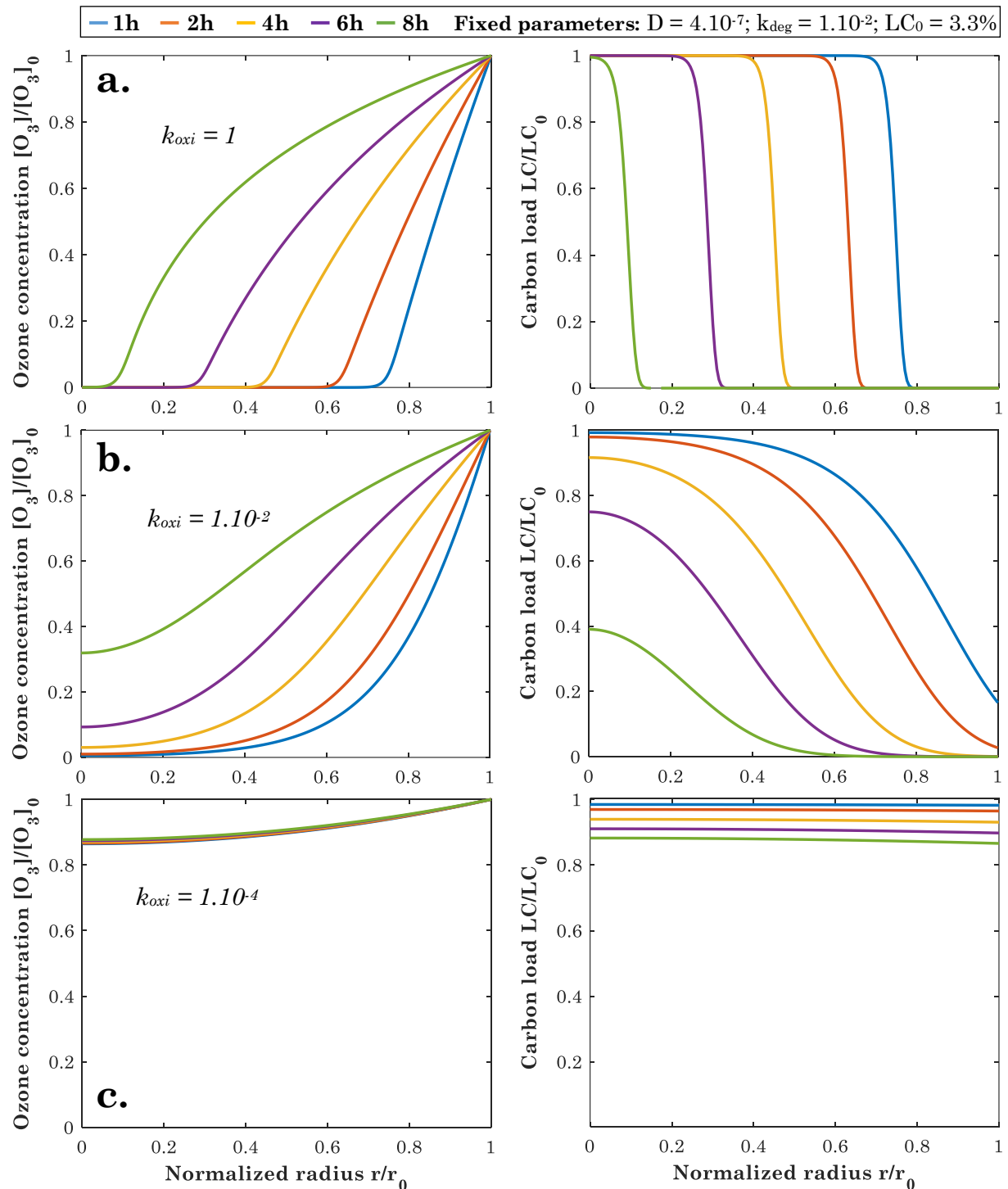


**Figure 5.7.** Radial profiles of  $O_3$  content (relative to the gas phase) and carbon load (relative to the initial content) alongside a single catalyst pellet at different process times with varying oxidation kinetic constant  $k_{oxi}$  ( $m^3.kg^{-1}.s^{-1}$ ).

over the radius but is really slow. In Figure 5.7.b ( $k_{\text{oxi}} = 1.10^{-2}$ ), intermediate behavior is obtained similarly to experimental results: a wide gradient zone of carbon is observed showing a good balance between diffusion and reactivity. The numerical resolution of the diffusion-reaction system is consequently able to describe the range of experimental behaviors obtained in Chapter 4. The oxidation kinetic constant is therefore expected to be between  $10^{-4}$  and  $10^0$  magnitudes in the investigated temperature range and will be determined using the optimization tool in Section 5.4.2.

#### 5.4.1.2. Effective diffusion coefficient

The diffusion coefficient of ozone in the catalysts is the parameter governing the mass transfer within the porous matrix. To illustrate its influence over carbon removal, the resolution with different values of  $D$  are presented in Figure 5.8. The kinetic constants  $k_{\text{deg}}$  and  $k_{\text{oxi}}$  are both fixed at  $1.10^{-2}$  for these simulations. The two sets of profiles obtained can therefore be compared with Figure 5.7.b whose diffusion coefficient ( $D = 4.10^{-7}$ ) is included between the values represented below. A smaller diffusion coefficient leads to decreased mass transfer in the catalyst: the progression of ozone through the center of the pellet is therefore limited (Figure 5.8.a). On the other hand, ozone easily reaches the center of the grain with an increased value ( $D = 1.10^{-6}$ , Figure 5.8.b). Similarly to  $k_{\text{oxi}}$ , these fluctuations govern the diffusion-reaction balance, thus the regeneration regime.

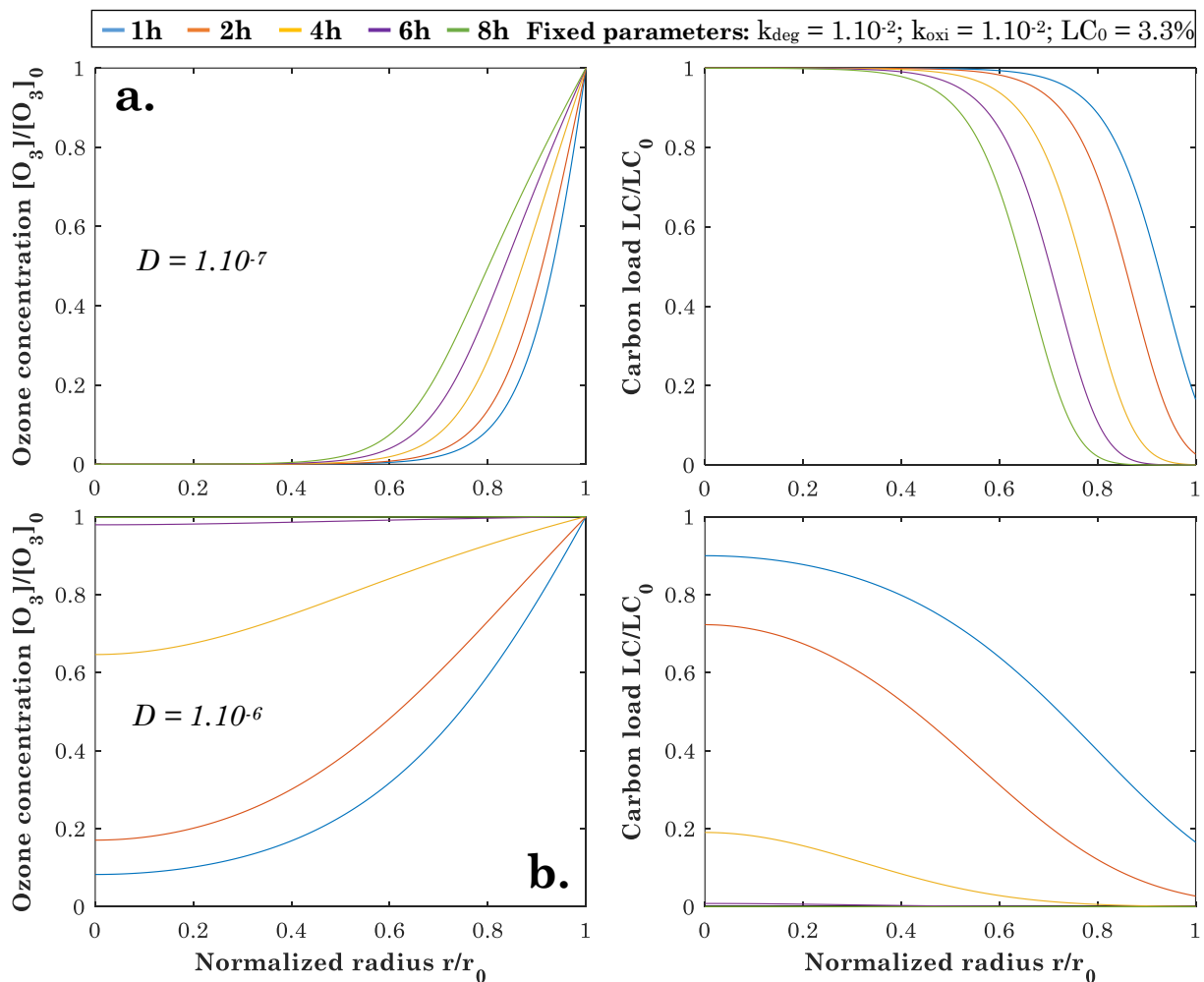


**Figure 5.8.** Profiles of  $O_3$  concentration and carbon content over catalyst radius at different times with varying diffusion coefficient  $D$  ( $\text{m}^2.\text{s}^{-1}$ ).

The effective coefficient represents the resistance of the porous material to the diffusion of ozone within the catalyst. As mentioned earlier, industrial zeolite catalysts are a complex three-dimensional network embedding mesoporous but mostly microporous volumes. The pore size of these volumes being different, the diffusion coefficient is different according to the location. Zhokh *et al.* demonstrated an important difference of diffusion coefficient of C6 cyclic hydrocarbons in ZSM-5 from  $10^{-16}$  to  $10^{-10}$  between zeolite crystal and pellet [252]. Due to the smaller molecular size, the diffusion coefficient of ozone is expected to be more important and values around  $10^{-9}$  are found in the literature for the diffusion of molecules with similar sizes in ZSM-5 crystals [253]. The coefficient  $D$  used in the numerical resolution is the global apparent diffusion coefficient, and is consequently lower than the effective diffusivity in microporous network. The magnitude  $10^{-7}$  initially elected from the diffusion of oxygen in pelletized catalysts appears as a relevant value for the physical meaning of the simulation.

### 5.4.1.3. Catalytic degradation kinetic constant

The kinetic constant of catalytic degradation  $k_{deg}$  represents the competing mechanism in the reaction term of the process. In the model, ozone either reacts with coke or is degraded over catalytic active sites. A global oxidation rate regarding molecular ozone is observed and indirect oxidation mechanism via radical species is not considered. Catalytic

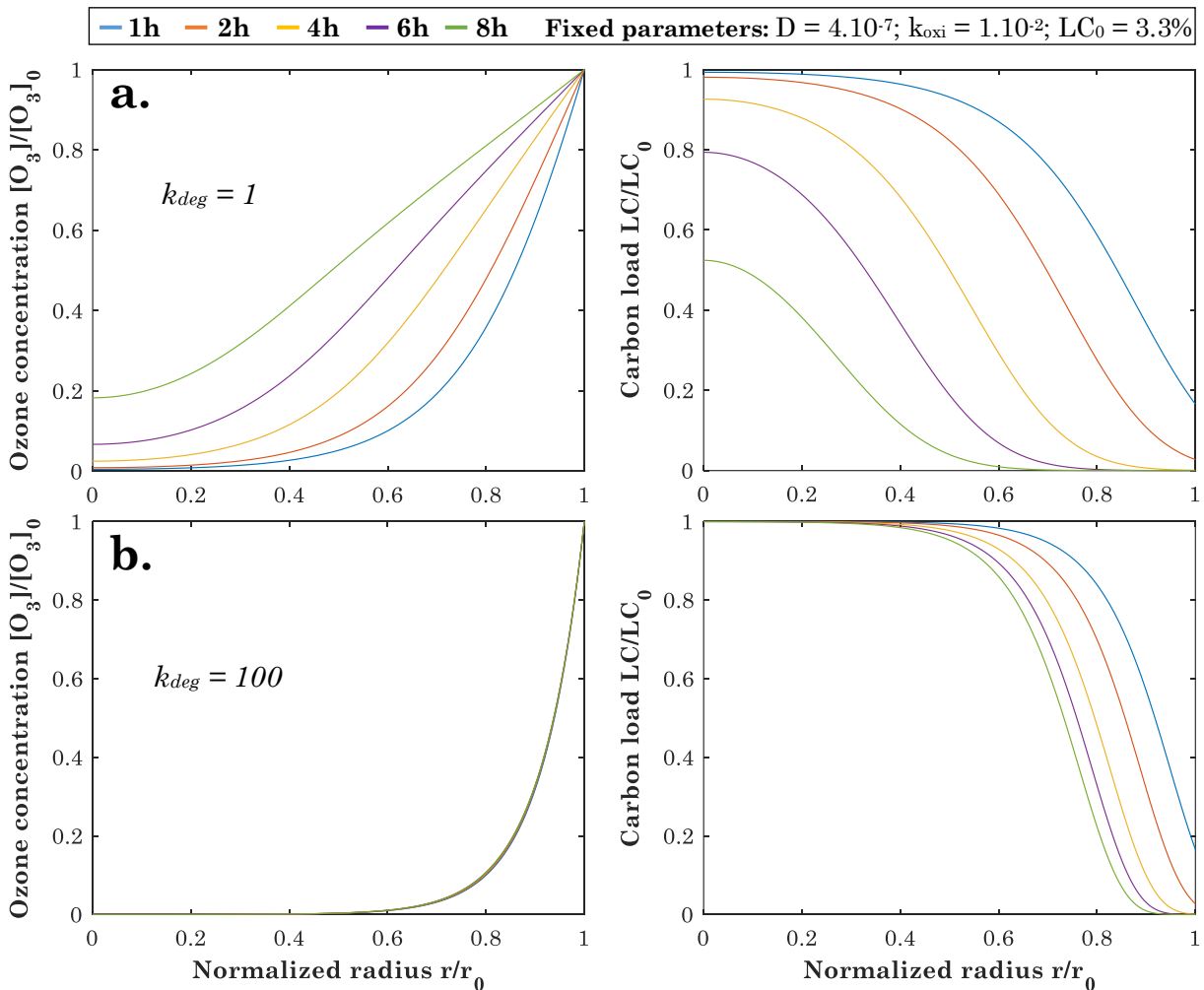


**Figure 5.9.** Profiles of  $O_3$  concentration and carbon content over catalyst radius at different times with varying catalytic degradation kinetic constant  $k_{deg}$  ( $s^{-1}$ ).

degradation rate is consequently not directly involved in coke removal efficiency but affects the concentration of ozone remaining for oxidation. The influence of  $k_{deg}$  variation on the obtained numerical profiles is illustrated in Figure 5.9. While the contribution of this mechanism was negligible for previous resolutions ( $k_{deg} = 1.10^{-2}$ ), it is fixed at  $1.10^0$  and  $1.10^2$  for the following profiles (Figure 5.9.a and b). These extreme values include the experimental set of data found in the investigated temperature range. For these simulations, diffusion coefficient was fixed at  $4.10^{-7} \text{ m}^2.\text{s}^{-1}$  and  $k_{oxi}$  at  $1.10^{-2} \text{ m}^3.\text{kg}^{-1}.\text{s}^{-1}$  and can therefore be compared with Figure 5.7.b to evaluate the influence of  $k_{deg}$  parameter in the process.

The increasing contribution of catalytic degradation in ozone reactivity impacts strongly the ozone and carbon radial profiles evaluated at different exposition times. As a competing mechanism with coke oxidation, the important consumption of ozone by catalytic degradation leads to lowered carbon removal efficiency. Consequently, relative carbon content after 8 h of process is slightly higher for  $k_{deg} = 1.10^0$  (Figure 5.9.a) compared to the final carbon profile obtained in Figure 5.7.b ( $k_{deg} = 1.10^{-2}$ ). However, for higher  $k_{deg}$  values, the contribution of this mechanism can become dominant. In such configuration, ozone is likely to be entirely degraded before diffusing and reacting with coke. This behavior, observed experimentally in Chapter 4, is illustrated in Figure 5.9.b. The evolution of the ozone concentration profiles shows that steady state is already achieved after 1 h of process time: due to the important catalytic degradation, only the first half of the pellet radius is exposed to ozone. In such conditions, coke core size will not vary anymore whatever the exposition time of catalysts to ozone gaseous stream. The influence of  $k_{deg}$  parameter is also related to the parameter  $\theta$ , representing the fraction of available active sites for ozone degradation. This factor is dependent of the carbon load deposited over the catalysts. When the pellet is heavily fouled, catalytic degradation contribution is weak as acid sites are covered by coke. However, as coke is removed and active sites recovered, the influence of  $k_{deg}$  in the reaction term grows. The resolution therefore also depends on the initial carbon load as discussed in the following paragraph.

#### 5.4.1.4. Initial carbon load

The initial quantity of coke deposited on the fouled catalysts is expected to mostly influence the reaction term of the resolution as it is involved directly in oxidation rate and indirectly in catalytic degradation rate. Different simulations with increasing initial carbon load are presented in Figure 5.10. The elected values are representing the highest coke content obtained in this work ( $LC_0 = 10 \text{ wt.\%C}$ ) and also typical value for spent catalysts of  $20 \text{ wt.\%C}$  found in the literature [127]. These graphs can be compared with Figure 5.9.a ( $LC_0 = 3.3 \text{ wt.\%C}$ ) to evaluate the influence of initial carbon load in the process. The three key parameters [ $D$ ;  $k_{deg}$ ;  $k_{oxi}$ ] were fixed for these simulations.

The variation of initial carbon load contributes to the oxidation regime as the slope of radial carbon profiles appears to be impacted. Indeed,  $LC_0$  is included in the initial Thiele's modulus  $\Phi_0$  and therefore influences the regeneration regime. However, the contribution of  $LC_0$  to the catalytic degradation mechanism through  $\theta$  does not visually appear on the profiles presented in Figure 5.10. It is suggested that this mechanism is not significant compared to the contribution of  $k_{oxi}$  using this set of parameters. The importance of initial carbon load would be more pronounced if the model embedded the variation of diffusion coefficient with coke content. A difference of effective diffusivity would then be observed between regenerated zones of the pellet and heavily coked parts, leading to an evolution of diffusion-reaction balance along the radius.

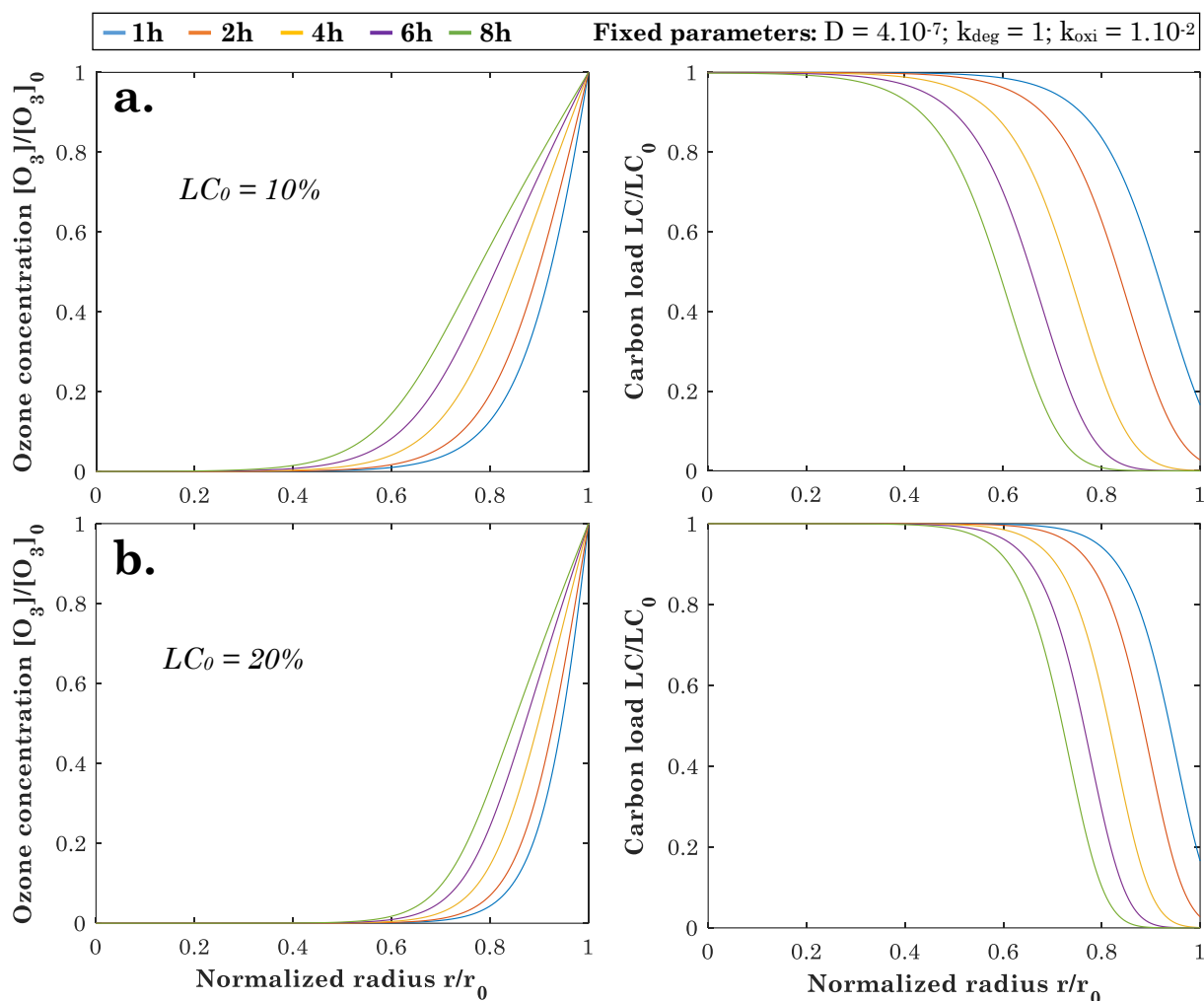


**Figure 5.10.** Profiles of  $O_3$  concentration and carbon content over catalyst radius at different times with varying initial carbon load  $LC_0$  (weight %).

According to the different observations conducted in Sections 5.4.1.1 to 5.4.1.4, the numerical resolution developed in this work is able to describe the different behaviors observed during the experimental investigations. The diffusion coefficient  $D$  and the kinetic constant of oxidation  $k_{oxi}$  appears as the most impacting factors for coke removal efficiency. The variation of regeneration regimes induced by the balance between these parameters generates different profile behaviors approaching the expected shrinking-core and homogeneous regimes. Even though it does not affect coke oxidation directly, the influence of the catalytic degradation constant  $k_{deg}$  is significant as its ozone consumption competes with carbon removal. The influence of initial carbon load  $LC_0$  is not significant in the investigated range of coke content despite high values, especially as the variation of  $D$  with  $LC$  is not described in the model. During these different simulations, conducted to obtain a better apprehension of the physical meaning of the model, the different parameters were treated as separate variables. However, the three key parameters [ $D$ ;  $k_{deg}$ ;  $k_{oxi}$ ] are evolving simultaneously in the system and their values are changing according to the operating conditions during ozonation. The kinetic constants are for instance correlated with temperature. In the following section, the model is confronted to experimental results by optimization in order to quantify the evolution of these parameters. Obtained values and tendencies are then injected in the initial numerical resolution to assess and discuss the physical accuracy and limitations of the model.

### 5.4.2. Parametric identification by profile optimization

In this section, the developed optimization tool for curve fitting was used with two variable parameters,  $D$  and  $k_{\text{oxi}}$ , while  $k_{\text{deg}}$  was fixed using the experimental value found in Chapter 4 (Equation (4.4)). While it was initially planned to optimize the numerical profile with three varying parameters, no convergence could be obtained without fixing one of the unknown values. Further numerical development could allow complete optimization of the triplet  $[D; k_{\text{deg}}; k_{\text{oxi}}]$ . Following results present the current work as it stands at the end of the PhD thesis period: pending questions, limitations and future possible improvements are discussed in Section 5.5.

#### 5.4.2.1. Arrhenius correlation for $k_{\text{oxi}}$

The curve optimization code was used on the different samples where ozonation was conducted at different temperatures from 50 to 150°C. The obtained values of  $k_{\text{oxi}}$  are extracted and analyzed to determine a tendency. Results of optimization are illustrated in Figure 5.11 and 5.12 with the representation of experimental and numerical profiles for the different investigated samples. Extracted parameters are summarized in Table 5.2.

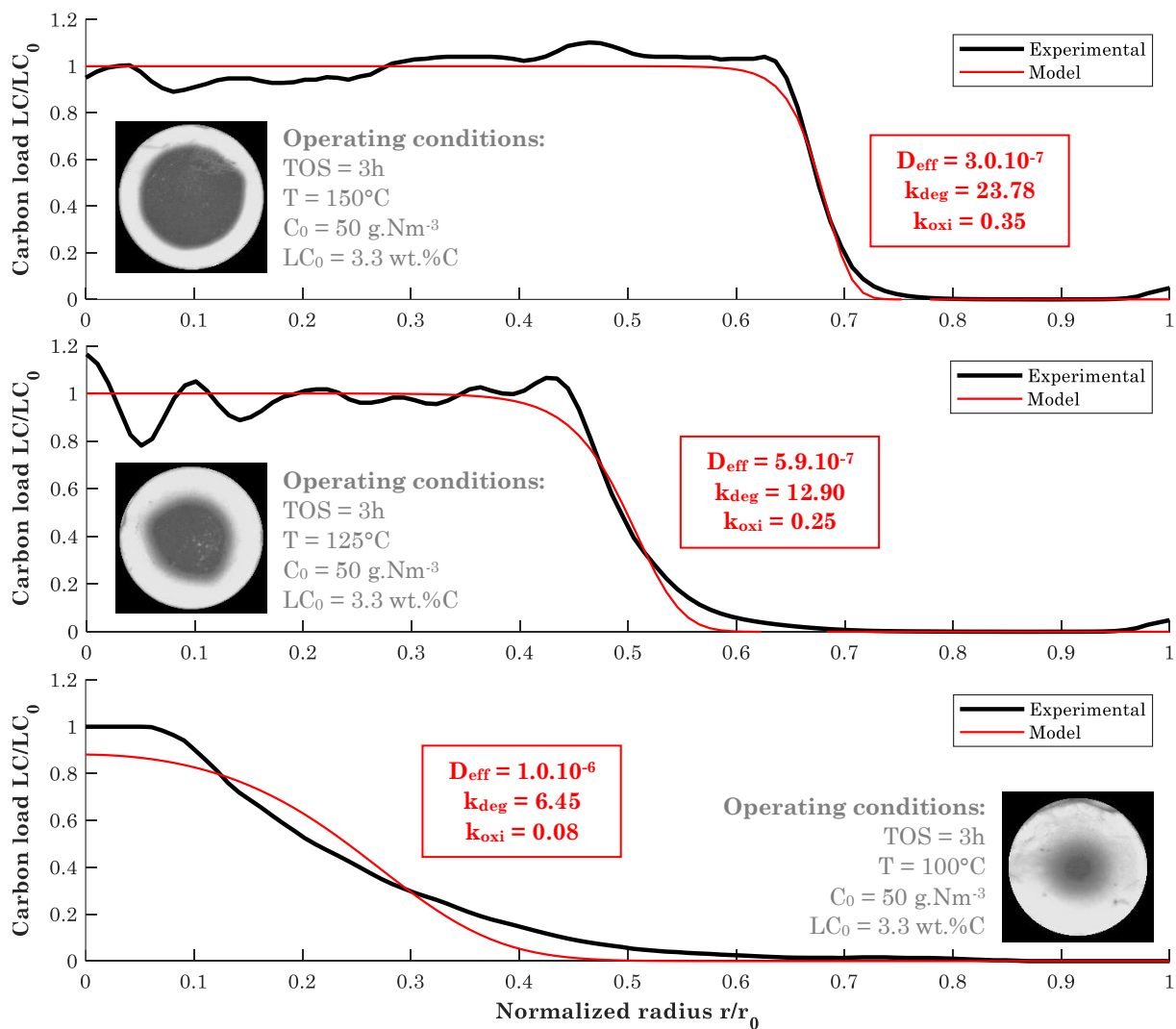


**Figure 5.11.** Curve optimization for the determination of diffusion coefficient and oxidation kinetic constant by comparison with experimental profiles at high temperatures (100 to 150°C).



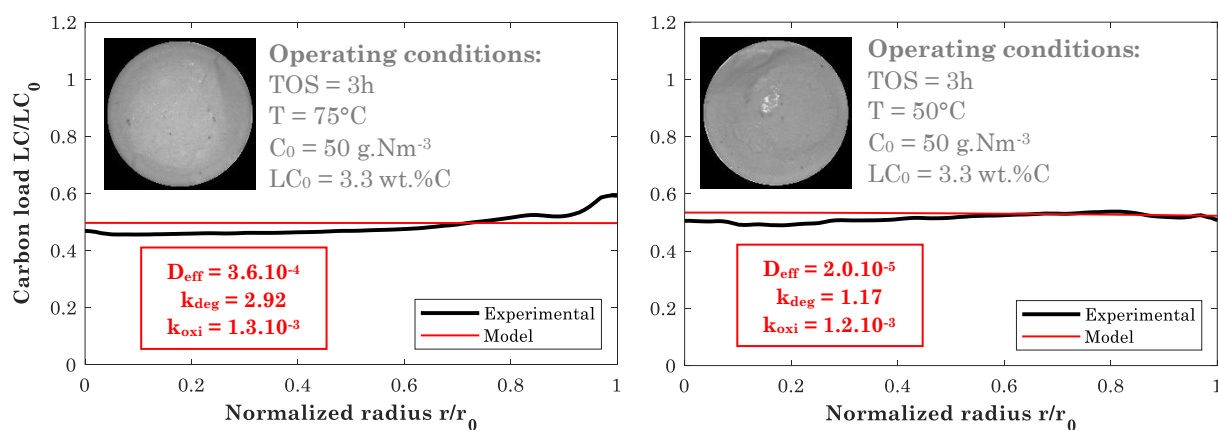


**Figure 5.12.** Curve optimization for the determination of diffusion coefficient and oxidation kinetic constant by comparison with experimental profiles at low temperatures (50 to 75°C).

The optimization results for the higher part of the temperature range present a good fit with the experimental profile (Figure 5.11). The profile with a thin gradient zone (150°C) is particularly accurate. As expected from typical kinetics behavior, the value of  $k_{oxi}$  decreases with temperature, going from 0.35 to 0.08 between 150 and 100°C. For samples at 125 and 100°C, the match between experimental and numerical profiles remains decent, but the model appears not being able to describe precisely wide gradient zones. For such samples, the contribution of diffusion and its gradient along the pellet radius in the system is expected to be significant. For samples ozonated at lower temperatures (Figure 5.12), oxidation rate is the limiting factor leading to a homogeneous regeneration regime. The obtained  $k_{oxi}$  values for the samples treated at 50 and 75°C are in accordance with this observation being close to zero.

Kinetic constants obtained are represented in an Arrhenius plot (Figure 5.13) to evaluate the activation energy and pre-exponential factor of  $k_{oxi}$ . The tendency including the five points is not approached by a linear correlation ( $R^2 = 0.8841$ ). The samples obtained at lower temperatures can be considered as outliers, especially the  $k_{oxi}$  value obtained at 75°C. Different hypotheses are possible to explain the lack of precision of such methodology to determine kinetic constants. The main expected reason is suggested to be the error generated by the normalization step for the samples without carbon gradient. While entirely regenerated and unreacted coke zones are easily normalized (to 0 and 1 respectively), the normalization for flat profiles is entirely artificial in order to match elemental analysis results. Such post-treatment might be responsible of an important shift of the profile and consequently of the extracted parameters. Moreover, for all the samples, the initial carbon load  $LC_0$  remains uncertain: even though the microprobe analysis showed homogeneous repartition along the radius for catalysts used three times in

**Table 5.2.** Extracted values of oxidation kinetic constant and effective diffusion coefficient obtained by curve optimization for samples ozonated at different temperatures.

Sample ID	Temperature (°C)	$k_{deg}$ (s <sup>-1</sup> )	$k_{oxi}$ (m <sup>3</sup> .kg <sup>-1</sup> .s <sup>-1</sup> )	$D_{eff}$ (m <sup>2</sup> .s <sup>-1</sup> )
R3-H	50	1.17	0.0012	1.97E-5
R8-H	75	2.92	0.0013	3.62E-4
R2-H	100	6.45	0.0788	1.02E-6
R7-H	125	12.90	0.2472	5.89E-7
R1-H	150	23.78	0.3528	3.01E-7

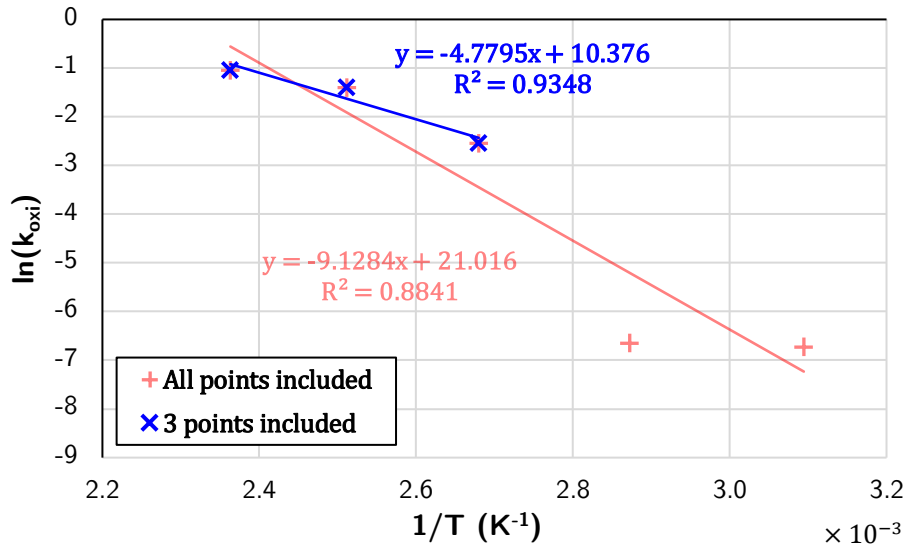


**Figure 5.13.** Arrhenius plots of oxidation rate of coke deposited on HZSM-5 obtained by combined numerical and experimental approach.

pyrolysis, the actual inner carbon content was not consistent with CH analysis. The hypothesis of a carbon-rich thin envelope around the pellets is susceptible to influence highly the use of numerical resolution as the internal initial carbon content would be decreased. Otherwise, when considering the three samples ozonated between 100 and 150°C, the linear tendency appears being more accurate ( $R^2 = 0.9348$ ). The exponential expression of  $k_{oxi}$  using Arrhenius law for these three points is presented below in Equation (5.46). Even though this value can be used as a first approximation to obtain its magnitude, further development of the current methodology has to be conducted to determine accurate coke oxidation kinetics.

$$k_{oxi} = 3.21 \times 10^4 \times \exp\left(\frac{-39737}{8.314 \times T}\right) \quad (5.46)$$

Based on these results, the activation energy of the apparent rate of coke oxidation is 39.7 kJ.mol<sup>-1</sup>. At ambient temperature ( $T = 293$  K), the apparent oxidation kinetic constant is therefore  $2.64 \times 10^{-3}$  m<sup>3</sup>.kg<sup>-1</sup>.s<sup>-1</sup>. This value corresponds to  $5.26 \times 10^{-23}$  in cm<sup>3</sup>.molecule<sup>-1</sup>.s<sup>-1</sup> for comparison with values found in the literature (refer to Table 1.4). The found value is in accordance with the  $10^{-20}$ - $10^{-24}$  range given by Treacy *et al.* for molecular ozone reactivity with aromatic and alkane carbon [161]. However, this observation has to be treated with caution: the extracted  $k_{oxi}$  value in this work is an effective oxidation rate impacted by diffusion limitations and is therefore underestimating the actual reactivity. Moreover, coke oxidation by radical species is not considered in this study. The variation of  $k_{oxi}$  determined by optimization is also correlated with an important evolution of  $D_{eff}$ . The difference of match between experimental and numerical profiles appears to increase when the contribution of diffusion in the process is growing. The influence of effective diffusion coefficient is discussed in Section 5.4.2.2.

#### 5.4.2.2. Sensibility of effective diffusion coefficient

During the ozonation process, the effective diffusion coefficient is known to have a major influence on coke removal efficiency. Based on the optimization results, an important variation of  $D_{eff}$  is observed according to the temperature. Its value decreases with

temperature increase, traducing diffusion limitations at higher temperatures. However, the  $D_{\text{eff}}$  values determined using the optimization tool have limited physical meaning. This apparent diffusion coefficient can be assimilated to an average value over space and time during the process. Consequently, the values can be used as an indicator of the diffusion phenomena for comparison but are not representing the effective coefficient at any given time in the process (initial or final). This limitation appears as an evidence for samples at 100 and 125°C: considering a constant oxidation rate at a given temperature, the diffusion coefficient is the only parameter impacting the shape and slope of the profile. For the two aforementioned profiles, the model fails to describe the slope variation in the carbon gradient zone. This is the consequence of the hypothesis of a constant  $D_{\text{eff}}$  coefficient for initial problem simplification.

In the real system, effective diffusion coefficient is changing with space and time as it is correlated with carbon load as discussed in Section 5.2.2. Deposited coke is indeed impacting the porosity and tortuosity of the catalysts and consequently the ability of ozone to diffuse through the porous matrix. As coke is removed, resistance to ozone mass transfer decreases and its diffusion coefficient increases. The fluctuation of slope observed in the carbon gradient zones is due to this change: the gradient is sharp close to the unreacted coke core as diffusion resistance is increased by coke while the slope is smooth near the entirely regenerated zone. In a single sample, the diffusion coefficient varies alongside the radius in a range defined by the different carbon loads. The extreme values of this range are approximated in Figure 5.14: using fixed  $k_{\text{oxi}}$  value determined in the previous paragraph,  $D_{\text{eff}}$  is optimized to match the profiles at the gradient zone limits. According to this exploitation, the effective diffusion coefficient of ozone in fresh catalysts is around  $4 \cdot 10^{-6} \text{ m}^2 \cdot \text{s}^{-1}$ . Similar magnitude is found in the literature for molecules with similar molecular diameters [254]. This value decreases down to  $1 \cdot 10^{-7} \text{ m}^2 \cdot \text{s}^{-1}$  when coke is deposited over the catalyst, traducing the evolution of pellet porosity and the tortuous pathway for ozone circulation. These limiting values are identical or similar when the temperature varies as it affects mostly the kinetic constants. As expected from Equation (5.4) (p.121), the influence of the temperature on the diffusion coefficient is not important. The variation of  $D_{\text{eff}}$  during the ozonation process is consequently very important: the current model is therefore not able to describe the process. An empiric correlation between the diffusion coefficient and the carbon load has to be determined to implement a varying  $D_{\text{eff}}$  in the model. Such upgrade would allow removing this coefficient of the unknown parameters in the resolution, and the optimization could be conducted for the different kinetic constants simultaneously.

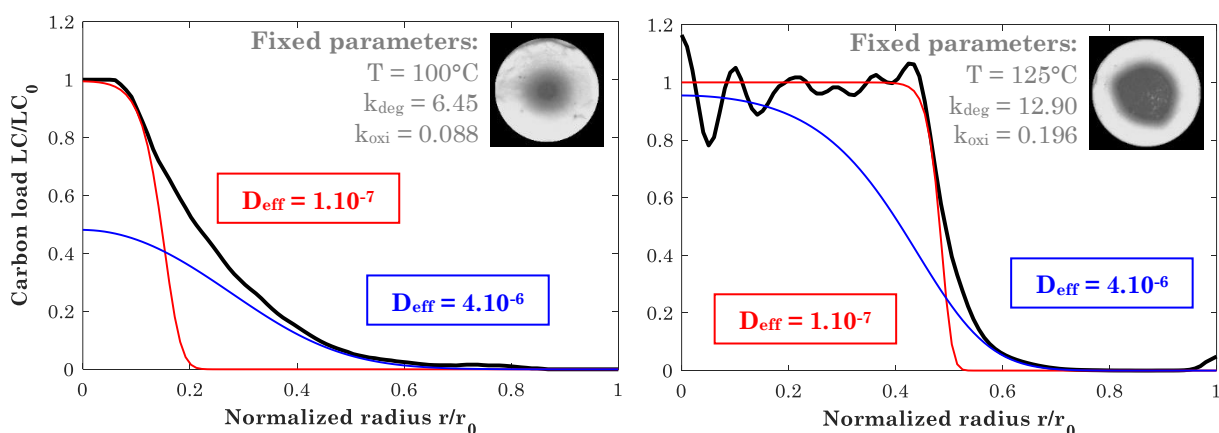


Figure 5.14. Determination of the variation range of effective diffusion coefficient  $D_{\text{eff}}$

## 5.5. Conclusions and key takeaways

The regeneration by ozonation of ZSM-5 catalysts coked at 450°C during pyrolysis of polyethylene was studied in this chapter with a modelling approach of diffusion-reaction phenomena at single catalyst particle level. The coupled resolution of the partial differential equations was successfully solved using Newton algorithm to describe the system of coke oxidation with ozone in a porous catalyst. The physical sense of the model was discussed by observing separately the influence of key parameters on the resolution: diffusion coefficient, kinetic constants of coke oxidation and catalytic degradation, as well as initial carbon load. As expected from the experimental results obtained in Chapter 4,  $D_{\text{eff}}$  and  $k_{\text{oxi}}$  are the parameters changing the shape of the obtained radial carbon profile as the regime of regeneration is affected. The other parameters,  $k_{\text{deg}}$  and  $LC_0$ , are more significant regarding the coke removal efficiency and time of exposure as it influences the quantity of available reactants (ozone and carbon). Balance between chemical reactivity and pore diffusion appears in both experimental and numerical results with observation of different regeneration regimes: homogeneous when diffusion is the limiting factor (at low temperatures) and shrinking-core when process is driven by ozone reactivity (at high temperatures). Experimental radial carbon profiles over pellets cross-section are obtained via SEM-FEG analysis and/or developed image-processing routine. An optimization code was then implemented in order to compare experimental and numerical results and to determine unknown key parameters of ozonation process. This curve-fitting tool optimizes different variable parameters ( $D$ ,  $k_{\text{deg}}$  and  $k_{\text{oxi}}$ ) in the resolution to reduce the cost function between the profiles. Such approach allowed to extract values for crucial parameters of the ozonation process. The coke oxidation kinetic constant was estimated at different temperatures, which resulted in determining activation energy (39.7 kJ.mol<sup>-1</sup>) via Arrhenius law. Moreover, the range of effective diffusion coefficient was found between  $1.10^{-7}$  and  $4.10^{-6}$  m<sup>2</sup>.s<sup>-1</sup>, showing the importance of a varying  $D$  to accurately describe ozonation. Obtained results and correlations are confronted to literature for model limitations and future implementations discussion. Indeed, the developed model for the PDEs system resolution presents some physical limitations as it fails to describe accurately the process when an important gradient of carbon load, thus of diffusion resistance, is present over the radius. The different achievements and conclusions of this chapter are summarized in Figure 5.15.

# NUMERICAL AND EXPERIMENTAL METHODOLOGY

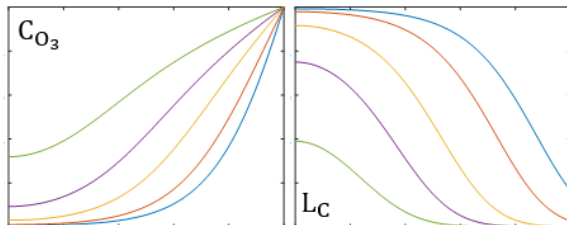
## Resolution of diffusion-reaction system

- Numerical resolution of coupled PDEs using Newton algorithm:

$$\varepsilon_p \frac{\delta C_{O_2}}{\delta t} = D_{O_2,eff} \frac{d}{dr} \left( r \frac{\delta C_{O_2}}{\delta r} \right) - (k_{deg} \theta C_{O_2} + \rho_p k_{oxi} L_C C_{O_2})$$

$$\frac{\delta L_C}{\delta t} = -k_{oxi} L_C C_{O_2}$$

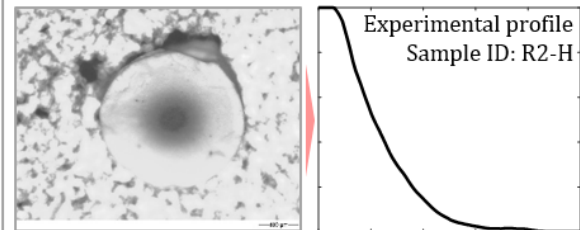
- Validation of the model physical sense with the study of key parameters influence on the obtained profiles



- Effective diffusion coefficient  $D_{eff}$  and coke oxidation kinetic constant  $k_{oxi}$  govern the profile shape, thus the regeneration regime.

## Image processing

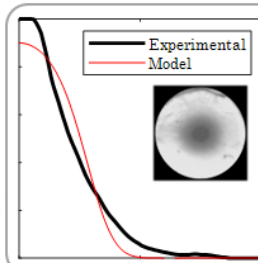
- Acquisition: batch code routine to obtain experimental carbon radial profiles from catalysts cross-section optic images
- Post-treatment: use of greyscale intensity and microprobe analytical results to convert profiles into carbon content
- Normalization: profiles are fixed between 0 and 1 or adapted using CHN analysis results for comparison with numerical data



- Accuracy of post-treatment steps remains questionable (sources of error: image quality, grey-to-carbon scale,  $LC_0$  hypothesis)

## Profile optimization (curve-fitting)

- Minimization of cost function between experimental and numerical profiles by varying parameters [ $D$ ;  $k_{deg}$ ;  $k_{oxi}$ ]
- Determination of key parameters of ozonation process difficult to evaluate experimentally



Approximation of  $k_{oxi}$  with Arrhenius law

Range of  $D_{eff}$  due to the evolution of coke

RESULTS

Coke oxidation rate is entirely due to reactivity with molecular ozone

Hypothesis of constant diffusion coefficient in the numerical resolution

LIMITATIONS

Addition of radical reactivity to describe both direct and indirect mechanisms

Implementation of varying effective diffusion correlated with carbon load

PERSPECTIVES

Figure 5.15. Key takeaways of "Chapter 5 – Modelling approach to ozonation reaction"

## NOMENCLATURE

$C_{O_3}$ or $[O_3]$	Ozone concentration ( $\text{g.Nm}^{-3}$ )
$C_{O_3,G}$	Ozone concentration in the gas phase ( $\text{g.Nm}^{-3}$ )
$D$ or $D_{O_3,eff}$	Effective diffusion coefficient of ozone ( $\text{m}^2.\text{s}^{-1}$ )
$D_k$	Knudsen diffusion coefficient ( $\text{m}^2.\text{s}^{-1}$ )
$D_{mol}$	Molecular diffusion coefficient ( $\text{m}^2.\text{s}^{-1}$ )
$D_{po}$	Porous diffusion coefficient ( $\text{m}^2.\text{s}^{-1}$ )
$d_{pore}$	Mean pore diameter of catalysts (m)
$k_{deg}$	Catalytic degradation kinetic constant ( $\text{s}^{-1}$ )
$k_{oxi}$	Coke oxidation kinetic constant ( $\text{m}^3.\text{kg}^{-1}.\text{s}^{-1}$ )
$L_C$ or $[L_C]$	Carbon load (wt.%, $\text{kgC}/\text{kg}_{cat}$ )
$LC_0$ or $L_{C,0}$	Initial carbon load (wt.%, $\text{kgC}/\text{kg}_{cat}$ )
$M_C$	Carbon molecular weight ( $\text{kg.mol}^{-1}$ )
$M_{O_3}$	Ozone molecular weight ( $\text{kg.mol}^{-1}$ )
$r, dr, \Delta r$	Radial distance and step (-)
$r_p$	Catalyst particle radius (mm)
$r_{th}$	Thermal recombination rate ( $\text{g.Nm}^{-3}.\text{s}^{-1}$ )
$r_{deg}$	Catalytic degradation rate ( $\text{g.Nm}^{-3}.\text{s}^{-1}$ )
$r_{oxi}$	Coke oxidation rate ( $\text{g.Nm}^{-3}.\text{s}^{-1}$ )
$R$	Ideal gas constant ( $8.314 \text{ J.mol}^{-1}.\text{K}^{-1}$ )
$R_{Coke}$	Coke reaction term ( $\text{kgC.k}_{cat}^{-1}.\text{s}^{-1}$ )
$R_{O_3}$	Ozone reaction term ( $\text{g.Nm}^{-3}.\text{s}^{-1}$ )
$t, dt, \Delta t$	Time variable and step (s)
$T$	Temperature of gas phase (K)
$y_{exp}$	Experimental profile (-)
$y_{num}$	Numerical profile (-)
$\theta$	Fraction of free acid sites (-)
$\varepsilon_p$	Catalyst particle porosity (-)
$\tau_p$	Catalyst particle tortuosity (-)
$\rho_p$	Catalyst particle density ( $\text{kg.m}^{-3}$ )





# General conclusion

## (English version)

The research project conducted in this PhD thesis combined the study of two different processes: catalytic pyrolysis of low-density polyethylene and regeneration of coked catalysts via ozonation. While the regeneration process by ozonation was the core motivation for this work due to its innovative aspect, the necessity of a model reaction for catalysts deactivation represented an opportunity to investigate another process in parallel: catalytic pyrolysis of plastic wastes was elected. One of the main challenges of this work was to maintain a proper balance between these different problematics: even though a sufficient comprehension of pyrolysis and deactivation phenomena were required, the ozonation process for the regeneration of coked catalysts had to remain the center of the research project. This diversity represents the wealth and training aspect of this PhD work, covering many scientific domains involving complex phenomena in different processes with combined approaches. Indeed, on top of the experimental aspect very present, the numerical approach for the modelling of the reaction was brought in this project with a will of developing homemade codes and tools that would be useful for the continuity of the research. The presented results consequently cover various scientific aspects and development of new methodologies focused towards an intensive study and a deeper comprehension of the ozonation process.

## Results

The results presented in this PhD thesis provide comprehensive insights regarding the deactivation of industrial ZSM-5 catalysts by coking during pyrolysis of LDPE and the regeneration of so-deactivated material using ozonation.

Deactivation via coke formation was observed on catalysts during LDPE pyrolysis at 450°C in a semi-batch reactor. Deposition and formation of coke over the zeolites at an important rate led to rapid loss of catalytic performances, which was evaluated in this work by a measure of pyrolysis products quality. As catalytic deactivation progresses, a significant drop of aromatic products and light fraction molecules is observed, traducing the loss of respectively rearrangement and cracking capacity of the catalysts. After five successive uses of spent catalysts, pyrolysis oils remained of higher quality than those obtained with purely thermal reaction. Zeolites consequently remained chemically active despite heavy catalytic activity loss and important decrease of their textural and chemical properties. Analyzed carbonaceous molecules presented a major part of heavy stable coke. Deactivation via coking during pyrolysis was described in a suggested pathway leading to

final complete deactivation. Initial coke deposition after first catalyst use mostly occurs in micropores with the formation of condensed cyclic coke molecules. Lighter compounds are also deposited as external coke around zeolite crystals. During successive reuses of the catalysts, mechanisms of coke growth are observed with progressive condensation of coke combined with deposition of additional coke. While microporous coke growth is restrained by steric limitations, external coke progresses importantly due to additional soft coke and forms a coke barrier around zeolite crystals. This phenomenon causes important pore blocking. Microporous volume is therefore more impacted than mesopores, thus the loss of Brønsted acidity is more important compared to Lewis acid sites. The obtained evolution of catalysts properties is well correlated with the decrease of pyrolysis oils quality, thus catalytic performances.

Use of ozonation as an alternative method to combustion to remove coke allowed regenerating ZSM-5 catalysts and obtaining almost complete recovery of fresh catalytic characteristics. While initial acidity is entirely recovered (Lewis and Brønsted sites), textural properties (specific surface and global porosity) remains impacted by residual coke. Nevertheless, ozonation appears to fully restore catalytic efficiency as similar pyrolysis products to fresh catalysts use were obtained when reusing ozonated zeolites. Due to the heavy nature of removed coke molecules, such results are highly promising regarding a wide range of applications for ozonation. During regeneration, important coke removal is observed during the early stages of the reaction while complete oxidation appears difficult to achieve due to diffusion limitations.

A deeper comprehension of the different phenomena involved during the ozonation process was achieved in this work thanks to an intensive parametric study, to the application of a wide range of analytical techniques and to a modelling approach of the reaction. The ozonation process for the regeneration of coked catalysts is a diffusion-reaction system in which the balance of mass transfer and reactivity plays an important role in coke removal efficiency. This work showed that time of exposure and temperature are the most impacting parameters in the process. Rapid oxidation is observed during the early stages of the reaction corresponding to the removal of external easily accessible coke. Process efficiency with time of exposure then has an asymptotic behavior when unreacted coke is subject to ozone mass transfer limitations. Different regeneration regimes are observed depending on the operating conditions: (i) the shrinking-core regime when diffusion is the limiting factor, at relative high temperatures (150°C), or (ii) the homogeneous regime when coke oxidation rate is governing the reaction, observed at lower temperatures (50-75°C).

One of the main challenge for the study of this process is the presence of different competing mechanisms for ozone consumption: thermal recombination, catalytic degradation and coke oxidation. A kinetic study at reactor scale demonstrated that the influence of thermal recombination is negligible facing catalytic degradation. Even though ozone reactivity over zeolite active sites can form hydroxyl radicals favorable to coke oxidation, its major contribution can lower process efficiency: at high temperatures, ozone is fully degraded before being able to diffuse through the pellet and to react with coke. At reactor scale, the exothermic character of coke oxidation and growing competition with catalytic degradation during the reaction (recovery of active sites) generate important gradients of temperature and concentration alongside the catalytic bed. Fixed bed ozonation process therefore presents heterogeneous efficiency depending on the position of catalysts in the reactor.

Optimal regeneration temperature obtained in this work (up to 98% of coke removal) is between 100 and 125°C providing a good balance between oxidation and degradation rates as well as diffusion of oxidative species. Choice of temperature is therefore a crucial aspect of the process. This equilibrium was observed and quantified at single catalyst grain scale with the experimental acquisition of radial coke profiles. Different behaviors were obtained according to the regeneration regime by analyzing coke core and gradient zone sizes over these carbon profiles. These experimental results were successfully confronted to simulations obtained via the resolution in space and time of the ozone and carbon concentrations over catalyst radius.

The modelling approach provided promising results as the different behaviors obtained experimentally are described by solving the PDEs system. Different key parameters of the process, such as effective diffusion coefficient and ozone reaction rates (coke oxidation and catalytic degradation), were extracted by combining experimental and simulation results. The parametric identification allowed approximating key parameters for ozonation, which experimental determination is difficult due to ozone instability. The effective diffusion coefficient of ozone in industrial ZSM-5 catalyst is varying depending on the coke content, from  $4.10^{-6} \text{ m}^2.\text{s}^{-1}$  in fresh catalyst to  $1.10^{-7} \text{ m}^2.\text{s}^{-1}$  in sample containing 3.3 wt.% carbon. The activation energy of apparent coke oxidation is also approximated ( $39.7 \text{ kJ.mol}^{-1}$ ) using Arrhenius law. Obtained results and correlations were confronted to the literature to discuss model limitations and future implementations.

Based on the different results and conclusions of this work, ozonation process for the regeneration of coked catalysts appears as a credible alternative to combustion of coke with oxygen. The ability of this innovative process to oxidize heavy coke compounds and to restore catalytic properties and efficiency around 100°C is promising when compared to the important temperature required for oxidation with oxygen (500°C).

## Perspectives

Following the intensive study and methodology development conducted in this work, different challenges remain due to the complexity of the investigated processes, providing leads for future investigations. Concerning catalytic pyrolysis of plastics, short-term concerns to pursue the development of this research aspect in the lab would be to further develop the experimental setup and to optimize the experimental operating parameters to approach conditions described in the literature. Next pilot upgrade consequently needs to feature a mean to collect and analyze gas fraction of pyrolysis products to conduct material balance. Temperature regulation also has to be improved to have a better control over heating ramp that needs to be around 20°C/min for optimal oil quality. Once pilot robustness is proved, the next relevant aspect for the study of ozonation viability would be to reuse catalysts in successive cycles of deactivation/regeneration to assess the evolution efficiency of regeneration. Moreover, using different geometries of zeolite catalysts could allow studying the influence of shape selectivity on pyrolysis and pursuing investigations regarding coke location (microporous or mesoporous volumes, coke deposited around the pellets). An industrial configuration for catalytic pyrolysis could also be investigated by using different reactors: a cracking reactor followed by a catalytic rearrangement level. Future work with high industrial relevance would be to use real wastes, such as municipal plastics waste, as feedstock for pyrolysis [236].

Future studies on ozonation could concern further optimization of operating conditions to reach maximal coke removal in reduced time. Use of sequential ozonation with different temperature steps during the process would be of high interest for such efficiency improvement: a sequential process could involve a rapid step with important initial temperature to quickly remove external coke, followed by a longer low-temperature step to favor diffusion of oxidizing agents for internal coke removal. Initial tests for process with temperature steps led to 84% of coke removal in tubular reactor (samples R21 and R27 in Appendix 6). In order to facilitate reuse of catalysts in initial process, which is here pyrolysis but all coking reactions can be considered, homogeneity of regeneration efficiency in a sample has to be ensured. Use of fluidized bed reactor could be investigated to overcome this challenge and meet industrial needs. Number of ozonation cycles before degradation of regeneration efficiency as well as energetic comparison are research axis that need to be considered in the future prior to envisage the industrial development of this process.

Coming back to fundamental considerations, some aspects of ozone reactivity and mass transfer could be further investigated, such as the contribution of hydroxyl radicals in indirect oxidation of coke by using radical inhibitors during the reaction. The study of such unstable species reactivity with complex coke molecules in microporous zeolite structures remains challenging to this day. Operando techniques, which are used to monitor coke growth over catalysts in different studies [220, 255], appear as an interesting possibility to investigate experimentally coke oxidation and determine the contribution of direct and indirect mechanisms. If combined with a spatial repartition approach, exciting insight on complex diffusion phenomena would be obtained. Emergence of novel analytical techniques for zeolite-based materials could overcome many of the current barriers for further comprehension of regeneration reactivity during ozonation and more generally of radical reactivity over zeolites [256, 257].

The modelling aspect of this study also provides many thrilling opportunities for future work by adding different bricks of complexity to gain model accuracy: implementation of variable effective diffusion coefficient changing with space and time with carbon load, determination of an empirical correlation between catalyst tortuosity and coke content, addition of a detailed reaction term or more insights on coke nature diversity and complexity of its location could be added to model the reaction at catalyst grain scale. Eventually, the modelling of the ozonation process at reactor scale is also of high interest to achieve deeper comprehension of the reaction. For further industrial development, modelling of the ozonation process in a fluidized bed reactor would be of high relevance.

Complete energetic study over the whole process is required to evaluate the environmental and economic viability of the process. The industrial implementation of ozonation involves additional energy consumption sources other than reactor heating: production of ozone via electric discharge and complete destruction of residual ozone in the effluents. Indeed, ozone is a toxic compound subject to release regulations and therefore needs to be degraded before venting. The industrial application of ozonation is likely to operate in a fluidized bed reactor to avoid the heterogeneity of coke removal efficiency observed in this work. Considering a FCC-type industrial unit with a catalytic bed transferred between process and regenerating reactors, ozonation could be implemented in the regeneration unit. A combined process with catalytic pyrolysis of plastics and regeneration via ozonation, joining the different aspects investigated in this PhD research, could even be imagined in similar industrial units.

# Conclusion générale

## (Version française)

Le projet de recherche mené dans cette thèse de doctorat combine l'étude de deux procédés : la pyrolyse catalytique du polyéthylène à basse densité et la régénération des catalyseurs cokés par ozonation. Bien que le procédé de régénération par ozonation constituait la genèse de cette étude de par son aspect innovant, la nécessité d'avoir une réaction modèle pour la désactivation des catalyseurs s'est présenté comme l'opportunité d'explorer un procédé différent en parallèle : la pyrolyse catalytique des déchets plastiques a été choisie. L'un des principaux défis de cette thèse était de maintenir l'équilibre entre ces différentes problématiques : bien que l'étude de la pyrolyse était requise pour appréhender les phénomènes de désactivation, le procédé d'ozonation pour la régénération des catalyseurs cokés devait demeurer le cœur du projet de recherche. Cette diversité des problématiques abordées représente la richesse et l'aspect formateur de ce doctorat. En effet, de nombreux domaines scientifiques sont couverts, impliquant des phénomènes complexes dans différents procédés avec des approches variées. En plus de l'aspect expérimental très présent dans ce projet, l'approche numérique pour la modélisation de la réaction a été intégrée avec la volonté de développer en interne des codes et des outils qui seraient utiles pour la poursuite du projet. Les résultats obtenus et présentés couvrent donc divers aspects scientifiques ainsi que le développement de nouvelles méthodologies, le tout au service d'une étude approfondie du procédé d'ozonation et d'une meilleure compréhension des phénomènes impliqués.

## Résultats

Les résultats présentés dans cette thèse fournissent à la fois un aperçu global et des considérations locales sur la désactivation des catalyseurs ZSM-5 industriels par formation de coke lors de la pyrolyse du polyéthylène basse densité, ainsi que sur leur régénération par ozonation.

La désactivation par formation de coke a été étudiée lors de la pyrolyse du PE-BD à 450 °C dans un réacteur semi-batch. La formation de coke au cours de la pyrolyse est importante, entraînant une perte rapide des performances catalytiques. Cette évolution a été évaluée dans ce travail par la mesure de la qualité des huiles de pyrolyse : une diminution importante des produits aromatiques et de la fraction de molécules légères a été montrée. Cette évolution indique la diminution des capacités de réarrangement et de craquage du catalyseur. Après cinq utilisations successives de catalyseurs, les huiles collectées restent de meilleures qualités que celles obtenues par pyrolyse purement

thermique. Les zéolithes sont donc toujours actives malgré une forte diminution de leurs performances et une perte significative de leurs propriétés texturales et chimiques. Les dépôts carbonés analysés sont majoritairement composés de coke lourd et stable. Un mécanisme de désactivation est proposé dans cette étude, correspondant à la formation de coke jusqu'à la désactivation complète du matériau catalytique. Le coke formé lors de la première pyrolyse se dépose majoritairement dans les micropores en formant des molécules cycliques condensées. Des composés plus légers sont aussi formés sur et autour des cristaux de zéolithes (coke externe). Au cours des réutilisations successives des catalyseurs, les mécanismes connus de croissance de coke sont observés avec la condensation progressive du coke et un dépôt additionnel. Alors que le coke microporeux est limité stériquement, le coke externe progresse et forme une enveloppe autour des cristaux de zéolithes. Ce phénomène génère un blocage de pores important. Les micropores sont ainsi plus fortement impactés que les mésopores, et par conséquent la perte des sites de Brønsted, est plus importante que celle des sites de Lewis. Une bonne corrélation est observée entre l'évolution des caractéristiques des catalyseurs et la diminution de la qualité des huiles de pyrolyse, et donc de l'activité catalytique.

L'utilisation de l'ozonation comme méthode alternative à la combustion pour oxyder le coke a permis de régénérer les catalyseurs ZSM-5 et de retrouver des propriétés proches des catalyseurs frais. L'acidité initiale est entièrement régénérée (sites de Brønsted et Lewis), les propriétés texturales (surface spécifique et porosité totale) restent légèrement impactées par du coke résiduel. Malgré tout, l'ozonation permet de restaurer entièrement la performance des catalyseurs car la réutilisation des zéolithes ozonées en pyrolyse a permis d'obtenir des produits similaires à ceux collectés après l'utilisation de catalyseurs frais. Ces résultats sont donc très prometteurs pour une gamme d'application plus large du procédé d'ozonation si l'on considère la nature stable du coke lourd oxydé. Alors qu'une rapide oxydation du coke est observée au cours des premiers instants de la réaction, une régénération totale est difficile à cause de limitations de diffusion.

Une compréhension approfondie des phénomènes impliqués au cours de l'ozonation a été acquise par cette thèse grâce à une étude paramétrique importante, à l'utilisation d'une vaste gamme de techniques analytiques et à une approche numérique de la réaction. Le procédé d'ozonation pour la régénération de catalyseurs cokés est un système de diffusion-réaction régi par un équilibre entre le transfert de matière et la réactivité. Ces travaux ont montré que le temps d'exposition et la température sont les paramètres clés du procédé. L'oxydation rapide observée dans les premiers instants de la réaction correspond au nettoyage du coke externe facilement accessible. Le taux de conversion du coke présente ensuite un comportement asymptotique car le coke restant est moins facilement atteignable et est donc sujet à une limitation liée au transfert de matière. Différents régimes de régénération sont observés selon les conditions opératoires : (i) celui du cœur rétrécissant lorsque la diffusion est le facteur limitant, à des températures relativement élevées (150°C), ou (ii) celui du régime homogène si la réaction est régie par la réaction d'oxydation, observé à des températures plus basses (50-75°C).

L'une des difficultés de l'étude de ce procédé est la présence de plusieurs mécanismes réactionnels en compétition pour la consommation d'ozone: la recombinaison thermique, la dégradation catalytique et l'oxydation du coke. Une étude cinétique à l'échelle du réacteur a démontré que la contribution du mécanisme de recombinaison thermique est négligeable comparé à celle de la dégradation catalytique. Bien que ce dernier permette la formation de radicaux hydroxyles favorables à l'oxydation du coke, son importance

contribution entraîne une baisse d'efficacité du procédé dans certaines conditions : à haute température, l'ozone est entièrement dégradé avant de pouvoir diffuser au cœur du grain et de réagir avec le noyau de coke. A l'échelle du réacteur, le caractère exothermique de l'oxydation du coke et sa compétition croissante au cours de la réaction avec la dégradation catalytique de l'ozone (restauration des sites actifs) génèrent d'importants gradients de température et de concentration le long du lit catalytique. La régénération par ozonation en lit fixe présente ainsi une hétérogénéité importante et une efficacité variable selon la position des catalyseurs dans le réacteur.

La température optimale d'ozonation (près de 98% d'élimination de coke) obtenue dans cette étude est entre 100 et 125°C, permettant un bon équilibre entre cinétiques de réaction et diffusion des espèces oxydantes. Le choix de la température est donc un point crucial du procédé. Cet équilibre a été observé et quantifié à l'échelle du grain de catalyseur grâce à l'acquisition expérimentale de profils radiaux de carbone. Les différentes tendances liées aux régimes de régénération ont été mises en évidence en analysant la variation de taille du noyau de coke non-réagi et de la zone de gradient de carbone sur les profils radiaux. Ces résultats expérimentaux ont été confrontés avec succès à des profils issus de simulation du procédé, par la résolution en temps et espace des concentrations d'ozone et de carbone sur le rayon d'un grain de catalyseur.

La modélisation du système a permis d'obtenir des résultats prometteurs permettant de décrire les différentes tendances obtenues expérimentalement grâce à la résolution d'un système d'EDP. Les paramètres clés du procédé d'ozonation, tels que le coefficient de diffusion effectif ou les cinétiques de réaction de l'ozone (oxydation du coke et dégradation catalytique), ont été extraits de cette combinaison des résultats expérimentaux et simulés. L'identification paramétrique a permis d'approcher ces paramètres importants du procédé dont la détermination expérimentale est difficile de par l'instabilité de l'ozone. Le coefficient de diffusion effectif de l'ozone dans un catalyseur ZSM-5 industriel varie, selon l'évolution de la teneur en coke, de  $4 \cdot 10^{-6} \text{ m}^2 \cdot \text{s}^{-1}$  pour un catalyseur vierge à  $1 \cdot 10^{-7} \text{ m}^2 \cdot \text{s}^{-1}$  pour un catalyseur contenant 3.3 wt.% de carbone. L'énergie d'activation apparente de l'oxydation du coke est aussi déterminée ( $39.7 \text{ kJ} \cdot \text{mol}^{-1}$ ) à l'aide de la loi d'Arrhenius. Les résultats et corrélations obtenus ont été comparés à la littérature afin de discuter des limites du modèle et des futures améliorations.

D'après les différents résultats et conclusions présentés dans cette thèse, le procédé d'ozonation pour la régénération de catalyseurs cokés semble donc être une alternative crédible à la combustion par oxygène. Ce procédé innovant a permis d'oxyder des molécules de coke lourd à 100°C sur un catalyseur microporeux et de restaurer entièrement son activité catalytique, montrant un différentiel de température important comparativement au procédé classique (500°C).

## Perspectives

Suite au travail approfondi et au développement de méthodologie conduits dans cette étude, différentes problématiques demeurent au vu de la complexité des procédés étudiés, donnant des pistes intéressantes pour de futurs travaux. Afin de poursuivre le développement de l'axe de recherche pyrolyse au sein du laboratoire, différentes améliorations sont à envisager à court terme afin d'optimiser le protocole expérimental et d'approcher les conditions opératoires optimales identifiées dans la littérature. Une collecte et une analyse de la phase gazeuse des produits de pyrolyse sont ainsi à



implémenter afin de pouvoir réaliser le bilan massique de la réaction. De plus, il est nécessaire d'améliorer la régulation de la température afin d'obtenir une rampe de chauffe de 20°C/min, optimale pour la qualité des huiles. Une fois la robustesse du pilote démontrée, la réutilisation de catalyseurs ozonés sur plusieurs cycles de désactivation/régénération apparaît comme le prochain point à étudier afin d'évaluer l'évolution de la capacité de régénération. D'autre part, l'utilisation de zéolithes avec des géométries variables permettrait de déterminer l'influence de la sélectivité stérique et de poursuivre la recherche sur la localisation du coke (micropores, mésopores et coke déposé autour des grains). Une configuration proche de l'industrie de la pyrolyse catalytique pourrait être envisagée en utilisant différents réacteurs : un réacteur de craquage puis un niveau de réarrangement catalytique. De plus, il serait intéressant de travailler avec des déchets « réels », par exemple l'utilisation de plastiques municipaux qui représentent aujourd'hui un axe de travail potentiel d'un grand intérêt industriel [236].

Concernant le procédé d'ozonation pour la régénération de catalyseurs cokés, la poursuite de l'optimisation des conditions opératoires du procédé pourrait être le sujet de futures études. La mise en place d'un procédé séquencé avec différents paliers de températures semble être une piste d'amélioration : un palier court à haute température (150°C) pour nettoyer rapidement le coke externe suivi d'un temps plus long avec une diminution de la température pour favoriser la diffusion des espèces oxydantes et la réaction avec le coke interne. Des tests préliminaires utilisant cette stratégie en réacteur tubulaire ont mené à un taux d'élimination de 84% du coke (échantillons R21 et R27 en Annexe 6). Afin de favoriser la réutilisation des catalyseurs ozonés dans le procédé d'origine, l'homogénéité de la régénération doit être assurée dans le lit catalytique. Pour répondre à ce besoin industriel, l'utilisation d'un lit fluidisé pourrait faire l'objet d'études pour le procédé d'ozonation. Le nombre de cycles avant une perte d'efficacité ainsi qu'une comparaison énergétique seront donc des axes à étudier dans le futur avant d'envisager un développement industriel de ce procédé.

Concernant les aspects plus fondamentaux de la réaction, l'étude de certains aspects de la réactivité et du transfert de l'ozone pourraient être approfondis. Ainsi, la contribution des radicaux hydroxyles pour l'oxydation indirecte du coke pourrait être étudiée grâce à l'utilisation de molécule inhibitrices de radicaux au cours de la réaction. Le suivi d'espèces chimiques instables et leur réactivité avec des structures de coke complexe au sein d'un matériau microporeux reste à ce jour un défi majeur. Les techniques analytiques operando, utilisées pour suivre la croissance du coke au sein de catalyseurs dans différentes études [220, 255], semble être une possibilité prometteuse pour étudier l'oxydation du coke in situ et déterminer la contribution des mécanismes d'oxydation direct et indirect. Une telle étude avec un suivi spatial de la répartition des espèces permettrait d'acquérir une compréhension approfondie des phénomènes de diffusion complexes impliqués. L'émergence de nouvelles techniques analytiques pour les matériaux zéolitiques devrait permettre de telles avancées pour les procédés de régénération mais plus généralement pour la réactivité des espèces radicalaires sur les zéolithes [256, 257].

L'aspect modélisation de ce travail pourrait être amélioré en complexifiant le modèle actuel avec des briques supplémentaires pour améliorer la justesse du modèle : l'implémentation d'un coefficient de diffusion effectif variable évoluant dans l'espace et le temps en fonction de la teneur en carbone, une corrélation expérimentale liant la tortuosité du grain de catalyseur avec la quantité de coke, l'ajout d'une réactivité plus complète ou l'ajout de notions concernant la diversité de la nature et de la localisation du

coke permettrait une description précise de la réaction à l'échelle du grain. Enfin, pour atteindre une meilleure compréhension de la réaction, la modélisation du procédé d'ozonation à l'échelle du réacteur présente de même un grand intérêt. Dans l'optique d'un développement industriel, la modélisation du procédé en lit fluidisé semble plus pertinent.

Une étude énergétique complète sur l'intégralité du procédé reste nécessaire pour évaluer la viabilité du procédé. L'implémentation industrielle du procédé intègre des sources de consommation d'énergie autres que la chauffe du réacteur : la production d'ozone par décharge électrique et la destruction complète de l'ozone résiduel dans les effluents. En effet, l'ozone est un composé toxique sujet à des réglementations de rejet et doit donc être détruit en sortie d'unité. Etant donné que ce procédé est susceptible d'être opéré en lit fluidisé afin d'éviter l'hétérogénéité de régénération mise en évidence dans ce travail, l'ozonation pourrait être implantée facilement dans des unités industrielles de craquage. Ce type d'installation contient deux unités, l'une pour le craquage catalytique et l'autre pour la régénération des catalyseurs, dans lesquelles le lit catalytique circule. L'opération de pyrolyse catalytique de plastiques combinée à une régénération par ozonation, joignant les différents aspects étudiés dans cette thèse, peut donc être imaginée dans une installation industrielle similaire.



# References

- [1] International Energy Agency, CO2 Emissions in 2022, License: CC BY 4.0 (2023). Access link: <https://www.iea.org/reports/co2-emissions-in-2022>
- [2] H. Ritchie, P. Rosado, M. Roser, Emissions by sector, Our World in Data (2020). Access link: <https://ourworldindata.org/emissions-by-sector>
- [3] J.M. Thomas, Summarizing comments on the discussion and a prospectus for urgent future action, *Philosophical Transactions of the Royal Society A: Mathematical, Physical and Engineering Sciences*, 374 (2016). <https://doi.org/10.1098/rsta.2015.0226>
- [4] Bartholomew, Catalyst Deactivation and Regeneration, in: *Kirk-Othmer Encyclopedia of Chemical Technology*, 2003.
- [5] M. Guisnet, F.R. Ribeiro, *Deactivation and regeneration of zeolite catalysts*. 2011, London: Imperial College Press.
- [6] M. Argyle, C. Bartholomew, Heterogeneous Catalyst Deactivation and Regeneration: A Review, *Catalysts*, 5 (2015). <https://doi.org/10.3390/catal5010145>
- [7] J. Zhou, J. Zhao, J. Zhang, T. Zhang, M. Ye, Z. Liu, Regeneration of catalysts deactivated by coke deposition: A review, *Chinese Journal of Catalysis*, 41 (2020). [https://doi.org/10.1016/S1872-2067\(20\)63552-5](https://doi.org/10.1016/S1872-2067(20)63552-5)
- [8] S. Khangkham, C. Julcour-Lebigue, S. Damronglerd, C. Ngamcharussrivichai, M.-H. Manero, H. Delmas, Regeneration of coked zeolite from PMMA cracking process by ozonation, *Applied Catalysis B: Environmental*, 140-141 (2013). <https://doi.org/10.1016/j.apcatb.2013.04.041>
- [9] R. Richard, C. Julcour, M. Manero, Towards a New Oxidation Process Using Ozone to Regenerate Coked Catalysts, *Ozone: Science and Engineering*, 39 (2017). <https://doi.org/10.1080/01919512.2017.1326005>
- [10] J. Weitkamp, Zeolites and catalysis, in: *Solid State Ionics*, 2000, pp. 175-188.
- [11] R.A. Sheldon, I.W.C.E. Arends, U. Hanefeld, Solid Acids and Bases as Catalysts, in: *Green Chemistry and Catalysis*, 2007, pp. 49-90.
- [12] K. Ragaert, L. Delva, K. Van Geem, Mechanical and chemical recycling of solid plastic waste, *Waste Management*, 69 (2017). <https://doi.org/10.1016/j.wasman.2017.07.044>
- [13] R. Miandad, M.A. Barakat, A.S. Aburiazaza, M. Rehan, A.S. Nizami, Catalytic pyrolysis of plastic waste: A review, *Process Safety and Environmental Protection*, 102 (2016). <https://doi.org/10.1016/j.psep.2016.06.022>
- [14] A. Ochoa, J. Bilbao, A.G. Gayubo, P. Castaño, Coke formation and deactivation during catalytic reforming of biomass and waste pyrolysis products: A review, *Renewable and Sustainable Energy Reviews*, 119 (2020). <https://doi.org/10.1016/j.rser.2019.109600>
- [15] A.W. Chester, E.G. Derouane, *Zeolite characterization and catalysis a tutorial*, in, Springer, Dordrecht, 2009.
- [16] H.v. Bekkum, *Introduction to zeolite science and practice*, 2001.
- [17] Database of Zeolite Structures (2017). <http://www.iza-structure.org/databases/>
- [18] V. Van Speybroeck, K. Hemelsoet, L. Joos, M. Waroquier, R.G. Bell, C.R.A. Catlow, Advances in theory and their application within the field of zeolite chemistry, *Chemical Society Reviews*, 44 (2015). <https://doi.org/10.1039/C5CS00029G>
- [19] J. Cejka, A. Corma, S. Zones, *Zeolites and Catalysis: Synthesis, Reactions and Applications*, in, Wiley, 2010.

- [20] C. Chizallet, C. Bouchy, K. Larmier, G. Pirngruber, Molecular Views on Mechanisms of Brønsted Acid-Catalyzed Reactions in Zeolites, *Chemical Reviews*, 123 (2023). <https://doi.org/10.1021/acs.chemrev.2c00896>
- [21] S.R. Batool, V.L. Sushkevich, J.A. van Bokhoven, Correlating Lewis acid activity to extra-framework aluminum species in zeolite Y introduced by Ion-exchange, *Journal of Catalysis*, 408 (2022). <https://doi.org/10.1016/j.jcat.2022.02.010>
- [22] X. Lv, S. Cai, J. Chen, D. Yan, M. Jiang, J. Chen, H. Jia, Tuning the degradation activity and pathways of chlorinated organic pollutants over CeO<sub>2</sub> catalyst with acid sites: synergistic effect of Lewis and Brønsted acid sites, *Catalysis Science & Technology*, 11 (2021). <https://doi.org/10.1039/D1CY00626F>
- [23] C. Jia, P. Massiani, D. Barthomeuf, Characterization by infrared and nuclear magnetic resonance spectroscopies of calcined beta zeolite, *Journal of the Chemical Society, Faraday Transactions*, 89 (1993). <https://doi.org/10.1039/FT9938903659>
- [24] L. Shirazi, E. Jamshidi, M.R. Ghasemi, The effect of Si/Al ratio of ZSM-5 zeolite on its morphology, acidity and crystal size, *Crystal Research and Technology*, 43 (2008). <https://doi.org/10.1002/crat.200800149>
- [25] N.Y. Chen, W.E. Garwood, F.G. Dwyer, Shape selective catalysis in industrial applications. 1989, New York: M. Dekker.
- [26] A. Dhakshinamoorthy, A.M. Asiri, H. Garcia, Catalysis in Confined Spaces of Metal Organic Frameworks, *ChemCatChem*, 12 (2020). <https://doi.org/10.1002/cctc.202001188>
- [27] S. Mitchell, N.-L. Michels, J. Pérez-Ramírez, From powder to technical body: the undervalued science of catalyst scale up, *Chemical Society Reviews*, 42 (2013). <https://doi.org/10.1039/C3CS60076A>
- [28] J. Hagen, Catalyst Shapes and Production of Heterogeneous Catalysts, in: *Industrial Catalysis*, 2015, pp. 211-238.
- [29] Z. Vajglová, N. Kumar, P. Mäki-Arvela, K. Eränen, M. Peurla, L. Hupa, D.Y. Murzin, Effect of Binders on the Physicochemical and Catalytic Properties of Extrudate-Shaped Beta Zeolite Catalysts for Cyclization of Citronellal, *Organic Process Research & Development*, 23 (2019). <https://doi.org/10.1021/acs.oprd.9b00346>
- [30] J.S.J. Hargreaves, A.L. Munnoch, A survey of the influence of binders in zeolite catalysis, *Catalysis Science & Technology*, 3 (2013). <https://doi.org/10.1039/C3CY20866D>
- [31] L.D. Rollmann, E.W. Valyocsik, *Synthesis of large crystal zeolite ZSM-5 and zeolite so made*. 1981, Mobil Oil Corp.
- [32] Z. Lounis, H. Belarbi, The Nanostructure Zeolites MFI-Type ZSM5, in: S. Claudia Maria Editor *Nanocrystals and Nanostructures*, IntechOpen, Rijeka, 2018, Ch. 3.
- [33] H. Sharbini Kamaluddin, X. Gong, P. Ma, K. Narasimharao, A. Dutta Chowdhury, M. Mokhtar, Influence of zeolite ZSM-5 synthesis protocols and physicochemical properties in the methanol-to-olefin process, *Materials Today Chemistry*, 26 (2022). <https://doi.org/10.1016/j.mtchem.2022.101061>
- [34] X. Liu, J. Shi, G. Yang, J. Zhou, C. Wang, J. Teng, Y. Wang, Z. Xie, A diffusion anisotropy descriptor links morphology effects of H-ZSM-5 zeolites to their catalytic cracking performance, *Communications Chemistry*, 4 (2021). <https://doi.org/10.1038/s42004-021-00543-w>
- [35] ZSM-5 - Zeolite Socony Mobil-5. Access link: <https://www.acsmaterial.com/blog-detail/zsm-5-molecular-seive.html>.
- [36] Y. Jia, Q. Shi, J. Wang, C. Ding, K. Zhang, Synthesis, characterization, and catalytic application of hierarchical nano-ZSM-5 zeolite, *RSC Advances*, 10 (2020). <https://doi.org/10.1039/D0RA06040B>

- [37] N. Rahimi, R. Karimzadeh, Catalytic cracking of hydrocarbons over modified ZSM-5 zeolites to produce light olefins: A review, *Applied Catalysis A: General*, 398 (2011). <https://doi.org/10.1016/j.apcata.2011.03.009>
- [38] C.G.S. Lima, E.Y.C. Jorge, L.G.S. Batinga, T.d.M. Lima, M.W. Paixão, ZSM-5 zeolite as a promising catalyst for the preparation and upgrading of lignocellulosic biomass-derived chemicals, *Nanocatalysis • Special Issue on the Green and Sustainable Chemistry Conference, Berlin, May 2018, 15* (2019). <https://doi.org/10.1016/j.cogsc.2018.08.001>
- [39] A. Marino, A. Aloise, H. Hernando, J. Feroso, D. Cozza, E. Giglio, M. Migliori, P. Pizarro, G. Giordano, D.P. Serrano, ZSM-5 zeolites performance assessment in catalytic pyrolysis of PVC-containing real WEEE plastic wastes, *Catalysis Today*, 390-391 (2022). <https://doi.org/10.1016/j.cattod.2021.11.033>
- [40] M. Lackner, *Bioplastics - Biobased plastics as renewable and/or biodegradable alternatives to petroplastics*, 2015.
- [41] M. van den Oever, K. Molenveld, M. van der Zee, H.t. Bos, *Bio-based and biodegradable plastics : facts and figures : focus on food packaging in the Netherlands. Wageningen Food & Biobased Research. 2017, Wageningen: Wageningen Food & Biobased Research.*
- [42] J. Yeo, J. Muiruri, T. Warintorn, Z. Li, C. He, Recent advances in the development of biodegradable PHB-based toughening materials: Approaches, advantages and applications, *Materials Science and Engineering: C*, 92 (2017). <https://doi.org/10.1016/j.msec.2017.11.006>
- [43] Y. Chen, A.K. Awasthi, F. Wei, Q. Tan, J. Li, Single-use plastics: Production, usage, disposal, and adverse impacts, *Science of the Total Environment*, 752 (2021). <https://doi.org/10.1016/j.scitotenv.2020.141772>
- [44] C. Carroll, J. Sousa, *Plastic Debris in the Ocean. The Characterization of Marine Plastics and their Environmental Impacts, Situation Analysis Report. 2014.*
- [45] N. Hidayah, Syafrudin, A Review on Landfill Management in the Utilization of Plastic Waste as an Alternative Fuel, *E3S Web Conf.*, 31 (2018). <https://doi.org/10.1051/e3sconf/20183105013>
- [46] M. Crippa, B. De Wilde, R. Koopmans, J. Leysens, M. Linder, J. Muncke, A.-C. Ritschkoff, K. Van Doorselaer, C. Velis, M. Wagner, *A circular economy for plastics. Insights from research and innovation to inform policy and funding decisions. 2019: European Commission EC.*
- [47] Z.O.G. Schyns, M.P. Shaver, Mechanical Recycling of Packaging Plastics: A Review, *Macromolecular Rapid Communications*, 42 (2021). <https://doi.org/10.1002/marc.202000415>
- [48] I. Vollmer, M.J.F. Jenks, M.C.P. Roelands, R.J. White, T. van Harmelen, P. de Wild, G.P. van der Laan, F. Meirer, J.T.F. Keurentjes, B.M. Weckhuysen, *Beyond Mechanical Recycling: Giving New Life to Plastic Waste, Angewandte Chemie International Edition*, 59 (2020). <https://doi.org/10.1002/anie.201915651>
- [49] S. Ügdüler, K.M. Van Geem, R. Denolf, M. Roosen, N. Mys, K. Ragaert, S. De Meester, Towards closed-loop recycling of multilayer and coloured PET plastic waste by alkaline hydrolysis, *Green Chemistry*, 22 (2020). <https://doi.org/10.1039/D0GC00894J>
- [50] L.-C. Hu, A. Oku, E. Yamada, Alkali-catalyzed methanolysis of polycarbonate. A study on recycling of bisphenol A and dimethyl carbonate, *Polymer*, 39 (1998). [https://doi.org/10.1016/S0032-3861\(97\)10298-1](https://doi.org/10.1016/S0032-3861(97)10298-1)
- [51] G.P. Karayannidis, A.K. Nikolaidis, I.D. Sideridou, D.N. Bikiaris, D.S. Achilias, *Chemical Recycling of PET by Glycolysis: Polymerization and Characterization of*



- the Dimethacrylated Glycolysate, *Macromolecular Materials and Engineering*, 291 (2006). <https://doi.org/10.1002/mame.200600243>
- [52] A.M. Al-Sabagh, F.Z. Yehia, G. Eshaq, A.M. Rabie, A.E. ElMetwally, Greener routes for recycling of polyethylene terephthalate, *Egyptian Journal of Petroleum*, 25 (2016). <https://doi.org/10.1016/j.ejpe.2015.03.001>
- [53] M.E. Grigore, *Methods of Recycling, Properties and Applications of Recycled Thermoplastic Polymers, Recycling*, 2 (2017). <https://doi.org/10.3390/recycling2040024>
- [54] P. Zahedifar, L. Pazdur, C.M.L. Vande Velde, P. Billen, Multistage Chemical Recycling of Polyurethanes and Dicarbamates: A Glycolysis–Hydrolysis Demonstration, *Sustainability*, 13 (2021). <https://doi.org/10.3390/su13063583>
- [55] C. Gamerith, B. Zartl, A. Pellis, F. Guillamot, A. Marty, E.H. Acero, G.M. Guebitz, Enzymatic recovery of polyester building blocks from polymer blends, *Process Biochemistry*, 59 (2017). <https://doi.org/10.1016/j.procbio.2017.01.004>
- [56] A. Lee, M.S. Liew, Tertiary recycling of plastics waste: an analysis of feedstock, chemical and biological degradation methods, *Journal of Material Cycles and Waste Management*, 23 (2021). <https://doi.org/10.1007/s10163-020-01106-2>
- [57] S.D. Anuar Sharuddin, F. Abnisa, W.M.A. Wan Daud, M.K. Aroua, A review on pyrolysis of plastic wastes, *Energy Conversion and Management*, 115 (2016). <https://doi.org/10.1016/j.enconman.2016.02.037>
- [58] D. Almeida, M.d.F. Marques, Thermal and catalytic pyrolysis of plastic waste, *Polímeros*, 26 (2016). <https://doi.org/10.1590/0104-1428.2100>
- [59] R. Miandad, M. Rehan, M.A. Barakat, A.S. Aburiazaiza, H. Khan, I.M.I. Ismail, J. Dhavamani, J. Gardy, A. Hassanpour, A.-S. Nizami, Catalytic Pyrolysis of Plastic Waste: Moving Toward Pyrolysis Based Biorefineries, *Frontiers in Energy Research*, 7 (2019). <https://doi.org/10.3389/fenrg.2019.00027>
- [60] M. Syamsiro, H. Saptoadi, T. Norsujianto, P. Noviasri, S. Cheng, Z. Alimuddin, K. Yoshikawa, Fuel Oil Production from Municipal Plastic Wastes in Sequential Pyrolysis and Catalytic Reforming Reactors, *Energy Procedia*, 47 (2014). <https://doi.org/10.1016/j.egypro.2014.01.212>
- [61] K.-H. Lee, N.-S. Noh, D.-H. Shin, Y. Seo, Comparison of plastic types for catalytic degradation of waste plastics into liquid product with spent FCC catalyst, *Polymer Degradation and Stability*, 78 (2002). [https://doi.org/10.1016/S0141-3910\(02\)00227-6](https://doi.org/10.1016/S0141-3910(02)00227-6)
- [62] Y. Sakata, M.A. Uddin, K. Koizumi, K. Murata, Thermal degradation of polyethylene mixed with poly(vinyl chloride) and poly(ethyleneterephthalate), *Polymer Degradation and Stability*, 53 (1996). [https://doi.org/10.1016/0141-3910\(96\)00077-8](https://doi.org/10.1016/0141-3910(96)00077-8)
- [63] A. Corma, Inorganic Solid Acids and Their Use in Acid-Catalyzed Hydrocarbon Reactions, *Chemical Reviews*, 95 (1995). <https://doi.org/10.1021/cr00035a006>
- [64] H. Ohkita, R. Nishiyama, Y. Tochiwara, T. Mizushima, N. Kakuta, Y. Morioka, A. Ueno, Y. Namiki, S. Tanifuji, Acid properties of silica-alumina catalysts and catalytic degradation of polyethylene, *Industrial & Engineering Chemistry Research*, 32 (1993). <https://doi.org/10.1021/ie00024a021>
- [65] J. Aguado, D.P. Serrano, J.L. Sotelo, R. Van Grieken, J.M. Escola, Influence of the Operating Variables on the Catalytic Conversion of a Polyolefin Mixture over HMCM-41 and Nanosized HZSM-5, *Industrial and Engineering Chemistry Research*, 40 (2001). <https://doi.org/10.1021/ie010420c>
- [66] N.A. Abdullah, A. Novianti, I.I. Hakim, N. Putra, R.A. Koestoer, Influence of temperature on conversion of plastics waste (polystyrene) to liquid oil using

- pyrolysis process, IOP Conference Series: Earth and Environmental Science, 105 (2018). <https://doi.org/10.1088/1755-1315/105/1/012033>
- [67] A. López, I. de Marco, B.M. Caballero, M.F. Laresgoiti, A. Adrados, Influence of time and temperature on pyrolysis of plastic wastes in a semi-batch reactor, *Chemical Engineering Journal*, 173 (2011). <https://doi.org/10.1016/j.cej.2011.07.037>
- [68] M.D. Hernandez, A. Gomez, A.N. Garcia, J. Agullo, A. Marcilla, Effect of the temperature in the nature and extension of the primary and secondary reactions in the thermal and HZSM-5 catalytic pyrolysis of HDPE, *Applied Catalysis A: General*, 317 (2007). <https://doi.org/10.1016/j.apcata.2006.10.017>
- [69] R. Miandad, M.A. Barakat, M. Rehan, A.S. Aburiazaiza, I.M.I. Ismail, A.S. Nizami, Plastic waste to liquid oil through catalytic pyrolysis using natural and synthetic zeolite catalysts, *Waste Management*, 69 (2017). <https://doi.org/10.1016/j.wasman.2017.08.032>
- [70] K. Murata, K. Sato, Y. Sakata, Effect of pressure on thermal degradation of polyethylene, *Journal of Analytical and Applied Pyrolysis*, 71 (2004). <https://doi.org/10.1016/j.jaap.2003.08.010>
- [71] K.-H. Lee, D.-H. Shin, Characteristics of liquid product from the pyrolysis of waste plastic mixture at low and high temperatures: Influence of lapse time of reaction, *Waste Management*, 27 (2007). <https://doi.org/10.1016/j.wasman.2005.12.017>
- [72] G. Newalkar, K. Iisa, A.D. D'Amico, C. Sievers, P. Agrawal, Effect of Temperature, Pressure, and Residence Time on Pyrolysis of Pine in an Entrained Flow Reactor, *Energy & Fuels*, 28 (2014). <https://doi.org/10.1021/ef5009715>
- [73] L. Quesada, M. Calero de Hoces, M.A. Martín-Lara, G. Luzón, G. Blázquez, Performance of Different Catalysts for the In Situ Cracking of the Oil-Waxes Obtained by the Pyrolysis of Polyethylene Film Waste, *Sustainability*, 12 (2020). <https://doi.org/10.3390/su12135482>
- [74] Y.-H. Seo, K.-H. Lee, D.-H. Shin, Investigation of catalytic degradation of high-density polyethylene by hydrocarbon group type analysis, *Journal of Analytical and Applied Pyrolysis*, 70 (2003). [https://doi.org/10.1016/S0165-2370\(02\)00186-9](https://doi.org/10.1016/S0165-2370(02)00186-9)
- [75] Y. Sakata, M.A. Uddin, A. Muto, Degradation of polyethylene and polypropylene into fuel oil by using solid acid and non-acid catalysts, *Journal of Analytical and Applied Pyrolysis*, 51 (1999). [https://doi.org/10.1016/S0165-2370\(99\)00013-3](https://doi.org/10.1016/S0165-2370(99)00013-3)
- [76] M.S. Abbas-Abadi, M.N. Haghghi, H. Yeganeh, A.G. McDonald, Evaluation of pyrolysis process parameters on polypropylene degradation products, *Journal of Analytical and Applied Pyrolysis*, 109 (2014). <https://doi.org/10.1016/j.jaap.2014.05.023>
- [77] M.S. Renzini, L.C. Lericci, U. Sedran, L.B. Pierella, Stability of ZSM-11 and BETA zeolites during the catalytic cracking of low-density polyethylene, *Journal of Analytical and Applied Pyrolysis*, 92 (2011). <https://doi.org/10.1016/j.jaap.2011.08.008>
- [78] J.M. Saad, M.A. Nahil, P.T. Williams, Influence of process conditions on syngas production from the thermal processing of waste high density polyethylene, *Journal of Analytical and Applied Pyrolysis*, 113 (2015). <https://doi.org/10.1016/j.jaap.2014.09.027>
- [79] Z. Chen, X. Zhang, F. Yang, H. Peng, X. Zhang, S. Zhu, L. Che, Deactivation of a Y-zeolite based catalyst with coke evolution during the catalytic pyrolysis of polyethylene for fuel oil, *Applied Catalysis A: General*, 609 (2021). <https://doi.org/10.1016/j.apcata.2020.117873>



- [80] C. Vasile, H. Pakdel, B. Mihai, P. Onu, H. Darie, S. Ciocâlțeu, Thermal and catalytic decomposition of mixed plastics, *Journal of Analytical and Applied Pyrolysis*, 57 (2001). [https://doi.org/10.1016/S0165-2370\(00\)00151-0](https://doi.org/10.1016/S0165-2370(00)00151-0)
- [81] S. Budsareechai, A.J. Hunt, Y. Ngernyen, Catalytic pyrolysis of plastic waste for the production of liquid fuels for engines, *RSC Advances*, 9 (2019). <https://doi.org/10.1039/C8RA10058F>
- [82] Y.H. Lin, H.Y. Yen, Fluidised bed pyrolysis of polypropylene over cracking catalysts for producing hydrocarbons, *Polymer Degradation and Stability*, 89 (2005). <https://doi.org/10.1016/j.polymdegradstab.2005.01.006>
- [83] A. Marcilla, M.d.R. Hernández, Á.N. García, Study of the polymer–catalyst contact effectivity and the heating rate influence on the HDPE pyrolysis, *Journal of Analytical and Applied Pyrolysis*, 79 (2007). <https://doi.org/10.1016/j.jaap.2006.10.017>
- [84] M.I. Isma, S. Ali, D. Nur, Mixed Plastic Wastes Pyrolysis in a Fluidized Bed Reactor for Potential Diesel Production, *International Journal of Environmental Science and Development*, 6 (2015). <https://doi.org/10.7763/IJESD.2015.V6.666>
- [85] G. Elordi, M. Olazar, G. Lopez, P. Castaño, J. Bilbao, Role of pore structure in the deactivation of zeolites (HZSM-5, H $\beta$  and HY) by coke in the pyrolysis of polyethylene in a conical spouted bed reactor, *Applied Catalysis B: Environmental*, 102 (2011). <https://doi.org/10.1016/j.apcatb.2010.12.002>
- [86] M. Olazar, G. Lopez, M. Amutio, G. Elordi, R. Aguado, J. Bilbao, Influence of FCC catalyst steaming on HDPE pyrolysis product distribution, *Journal of Analytical and Applied Pyrolysis*, 85 (2009). <https://doi.org/10.1016/j.jaap.2008.10.016>
- [87] Eli Ruckenstein, Dady B. Dadyburjor, Sintering and Redispersion in Supported Metal Catalysts, *Reviews in Chemical Engineering*, 1 (1983). <https://doi.org/10.1515/REVCE.1983.1.3.251>
- [88] J. Rostrup-Nielsen, D.L. Trimm, Mechanisms of carbon formation on nickel-containing catalysts, *Journal of Catalysis*, 48 (1977). [https://doi.org/10.1016/0021-9517\(77\)90087-2](https://doi.org/10.1016/0021-9517(77)90087-2)
- [89] M. Guisnet, L. Costa, F.R. Ribeiro, Prevention of zeolite deactivation by coking, *Journal of Molecular Catalysis A: Chemical*, 305 (2009). <https://doi.org/10.1016/j.molcata.2008.11.012>
- [90] M. Guisnet, P. Magnoux, Organic chemistry of coke formation, *Applied Catalysis A: General*, 212 (2001). [https://doi.org/10.1016/S0926-860X\(00\)00845-0](https://doi.org/10.1016/S0926-860X(00)00845-0)
- [91] A. Marcilla, M.I. Beltrán, F. Hernández, R. Navarro, HZSM5 and HUSY deactivation during the catalytic pyrolysis of polyethylene, *Applied Catalysis A: General*, 278 (2004). <https://doi.org/10.1016/j.apcata.2004.09.023>
- [92] A. Marcilla, M.I. Beltrán, R. Navarro, Effect of regeneration temperature and time on the activity of HUSY and HZSM5 zeolites during the catalytic pyrolysis of polyethylene, *Journal of Analytical and Applied Pyrolysis*, 74 (2005). <https://doi.org/10.1016/j.jaap.2004.10.006>
- [93] A. López, I. de Marco, B.M. Caballero, A. Adrados, M.F. Laresgoiti, Deactivation and regeneration of ZSM-5 zeolite in catalytic pyrolysis of plastic wastes, *Waste Management*, 31 (2011). <https://doi.org/10.1016/j.wasman.2011.04.004>
- [94] Y. Gao, S.-L. Chen, Y. Wei, Y. Wang, W. Sun, Y. Cao, P. Zeng, Kinetics of coke formation in the dimethyl ether-to-olefins process over SAPO-34 catalyst, *Chemical Engineering Journal*, 326 (2017). <https://doi.org/10.1016/j.cej.2017.05.158>
- [95] S. Mahamulkar, K. Yin, P. Agrawal, R. Davis, C. Jones, A. Malek, H. Shibata, Formation and Oxidation/Gasification of Carbonaceous Deposits: A Review, *Industrial & Engineering Chemistry Research*, 55 (2016). <https://doi.org/10.1021/acs.iecr.6b02220>

- [96] Y. Ozawa, K.B. Bischoff, Coke Formation Kinetics on Silica-Alumina Catalyst. Analysis, *Industrial & Engineering Chemistry Process Design and Development*, 7 (1968). <https://doi.org/10.1021/i260025a015>
- [97] S. Wauters, G.B. Marin, Kinetic Modeling of Coke Formation during Steam Cracking, *Industrial & Engineering Chemistry Research*, 41 (2002). <https://doi.org/10.1021/ie010822k>
- [98] T.M. Moustafa, G.F. Froment, Kinetic Modeling of Coke Formation and Deactivation in the Catalytic Cracking of Vacuum Gas Oil, *Industrial & Engineering Chemistry Research*, 42 (2003). <https://doi.org/10.1021/ie0204538>
- [99] M. Omidkhah, J. Modarres, J. Towfighi Darian, A. Niaei, Estimation of Kinetic Parameters of Coking Reaction Rate in Pyrolysis of Naphtha, *International Journal of Engineering*, 17 (2004). [http://www.ije.ir/article\\_71541.html](http://www.ije.ir/article_71541.html)
- [100] M. Bjørgen, U. Olsbye, S. Kolboe, Coke precursor formation and zeolite deactivation: mechanistic insights from hexamethylbenzene conversion, *Journal of Catalysis*, 215 (2003). [https://doi.org/10.1016/S0021-9517\(02\)00050-7](https://doi.org/10.1016/S0021-9517(02)00050-7)
- [101] X. Guo, Y. Zheng, B. Zhang, J. Chen, Analysis of coke precursor on catalyst and study on regeneration of catalyst in upgrading of bio-oil, *Biomass and Bioenergy*, 33 (2009). <https://doi.org/10.1016/j.biombioe.2009.07.002>
- [102] M. Ibáñez, P. Pérez-Urriarte, M. Sánchez-Contador, T. Cordero-Lanzac, A.T. Aguayo, J. Bilbao, P. Castaño, Nature and Location of Carbonaceous Species in a Composite HZSM-5 Zeolite Catalyst during the Conversion of Dimethyl Ether into Light Olefins, *Catalysts*, 7 (2017). <https://doi.org/10.3390/catal7090254>
- [103] H. Karimi, B. Olayiwola, H. Farag, K.B. McAuley, Modelling coke formation in an industrial ethane-cracking furnace for ethylene production, *The Canadian Journal of Chemical Engineering*, 98 (2020). <https://doi.org/10.1002/cjce.23619>
- [104] M. Guisnet, P. Magnoux, Coking and deactivation of zeolites: Influence of the Pore Structure, *Applied Catalysis*, 54 (1989). [https://doi.org/10.1016/S0166-9834\(00\)82350-7](https://doi.org/10.1016/S0166-9834(00)82350-7)
- [105] G.A. Doka Nassionou, P. Magnoux, M. Guisnet, Comparative study of coking and regeneration of HEMT and HFAU zeolites, *Microporous and Mesoporous Materials*, 22 (1998). [https://doi.org/10.1016/S1387-1811\(98\)00087-0](https://doi.org/10.1016/S1387-1811(98)00087-0)
- [106] H.S. Cerqueira, P. Magnoux, D. Martin, M. Guisnet, Effect of contact time on the nature and location of coke during methylcyclohexane transformation over a USHY zeolite, in: B. Delmon, G.F. Froment (Eds.), *Studies in Surface Science and Catalysis*, Elsevier, 1999, pp. 105-112.
- [107] P. Magnoux, M. Guisnet, Coking, ageing and regeneration of zeolites: VI. Comparison of the Rates of Coke Oxidation of HY, H-Mordenite and HZSM-5, *Applied Catalysis*, 38 (1988). [https://doi.org/10.1016/S0166-9834\(00\)82836-5](https://doi.org/10.1016/S0166-9834(00)82836-5)
- [108] M.A. Uguina, D.P. Serrano, R. Van Grieken, S. Vènes, Adsorption, acid and catalytic changes induced in ZSM-5 by coking with different hydrocarbons, *Applied Catalysis A: General*, 99 (1993). [https://doi.org/10.1016/0926-860X\(93\)80093-6](https://doi.org/10.1016/0926-860X(93)80093-6)
- [109] D.M. Bibby, N.B. Milestone, J.E. Patterson, L.P. Aldridge, Coke formation in zeolite ZSM-5, *Journal of Catalysis*, 97 (1986). [https://doi.org/10.1016/0021-9517\(86\)90020-5](https://doi.org/10.1016/0021-9517(86)90020-5)
- [110] G.F. Froment, J.D. Meyer, E.G. Derouane, Deactivation of zeolite catalysts by coke formation, *Journal of Catalysis*, 124 (1990). [https://doi.org/10.1016/0021-9517\(90\)90187-0](https://doi.org/10.1016/0021-9517(90)90187-0)
- [111] L.D.T. Câmara, K. Rajagopal, D.A.G. Aranda, The effects of pore structure on catalyst deactivation by coke formation, in: J.J. Spivey, G.W. Roberts, B.H. Davis (Eds.), *Studies in Surface Science and Catalysis*, Elsevier, 2001, pp. 61-68.

- [112] P. Castaño, G. Elordi, M. Olazar, A. Aguayo, B. Pawelec, J. Bilbao, Insights into the coke deposited on HZSM-5, H beta and HY zeolites during the cracking of polyethylene, *Applied Catalysis B: Environmental*, 104 (2011). <https://doi.org/10.1016/j.apcatb.2011.02.024>
- [113] C.A. Mullen, C. Dorado, A.A. Boateng, Catalytic co-pyrolysis of switchgrass and polyethylene over HZSM-5: Catalyst deactivation and coke formation, *Journal of Analytical and Applied Pyrolysis*, 129 (2018). <https://doi.org/10.1016/j.jaap.2017.11.012>
- [114] R. Hughes, M. Parvinian. *Regeneration kinetics of coked silica-alumina catalyst*. 1989. United States.
- [115] J. Santamaría, A. Monzón, M. Berbegal, R. Hughes, Regeneration strategies for coked fixed bed reactors, *Chemical Engineering Science*, 46 (1991). [https://doi.org/10.1016/0009-2509\(91\)80111-B](https://doi.org/10.1016/0009-2509(91)80111-B)
- [116] C.L. Minh, R.A. Jones, Craven, I. E., T. Brown, Temperature-Programmed Oxidation of Coke Deposited on Cracking Catalysts: Combustion Mechanism Dependence, *Energy & Fuels*, 11 (1997). <https://doi.org/10.1021/ef960114p>
- [117] C.L. Minh, C. Li, T.C. Brown, Kinetics of coke combustion during temperature-programmed oxidation of deactivated cracking catalysts, in: C.H. Bartholomew, G.A. Fuentes (Eds.), *Studies in Surface Science and Catalysis*, Elsevier, 1997, pp. 383-390.
- [118] T.J. Keskkitalo, K.J.T. Lipiäinen, A.O.I. Krause, Kinetic Modeling of Coke Oxidation of a Ferrierite Catalyst, *Industrial & Engineering Chemistry Research*, 45 (2006). <https://doi.org/10.1021/ie060521g>
- [119] J. Nováková, Z. Dolejšek, A comment on the oxidation of coke deposited on zeolites, *Zeolites*, 10 (1990). [https://doi.org/10.1016/0144-2449\(90\)90044-R](https://doi.org/10.1016/0144-2449(90)90044-R)
- [120] K. Morley, H.I. De Lasa, On the determination of kinetic parameters for the regeneration of cracking catalyst, *The Canadian Journal of Chemical Engineering*, 65 (1987). <https://doi.org/10.1002/cjce.5450650510>
- [121] H.M. Ngomo, A.A. Susu, THE INFLUENCE OF NATURE OF COKE ON KINETICS OF CATALYST REGENERATION, *Petroleum Science and Technology*, 20 (2002). <https://doi.org/10.1081/LFT-120003703>
- [122] C.A. Querini, S.C. Fung, Temperature-programmed oxidation technique: kinetics of coke-O<sub>2</sub> reaction on supported metal catalysts, *Applied Catalysis A: General*, 117 (1994). [https://doi.org/10.1016/0926-860X\(94\)80158-4](https://doi.org/10.1016/0926-860X(94)80158-4)
- [123] K. Hashimoto, K. Takatani, H. Iwasa, T. Masuda, A multiple-reaction model for burning regeneration of coked catalysts, *The Chemical Engineering Journal*, 27 (1983). [https://doi.org/10.1016/0300-9467\(83\)80074-4](https://doi.org/10.1016/0300-9467(83)80074-4)
- [124] Y. Nakasaka, T. Tago, H. Konno, A. Okabe, T. Masuda, Kinetic study for burning regeneration of coked MFI-type zeolite and numerical modeling for regeneration process in a fixed-bed reactor, *Chemical Engineering Journal*, 207-208 (2012). <https://doi.org/10.1016/j.cej.2012.06.138>
- [125] H.S. Fogler, *The Shrinking Core Model*, in: *Essentials of chemical reaction engineering*, Prentice Hall, Upper Saddle River, NJ, 2011.
- [126] N. Müller, R. Moos, A. Jess, In situ Monitoring of Coke Deposits during Coking and Regeneration of Solid Catalysts by Electrical Impedance-based Sensors, *Chemical Engineering & Technology*, 33 (2010). <https://doi.org/10.1002/ceat.200900380>
- [127] C. Kern, A. Jess, Regeneration of coked catalysts—modelling and verification of coke burn-off in single particles and fixed bed reactors, *Chemical Engineering Science*, 60 (2005). <https://doi.org/10.1016/j.ces.2005.01.024>
- [128] O.V. Dubinets, M.R. Davletova, G.I. Islamova, I.M. Gubaydullin, G.D. Khannanova, I.V. Akhmetov, Simulation of the coke burning process on the

- catalyst grain, *Journal of Physics: Conference Series*, 1368 (2019). <https://doi.org/10.1088/1742-6596/1368/4/042068>
- [129] L. Pinard, A. Astafan, A. Sachse, C. Dupeyrat, Impact of the Framework Type on the Regeneration of Coked Zeolites by Non-Thermal Plasma in a Fixed Bed Dielectric Barrier Reactor, *Catalysts*, 9 (2019). <https://doi.org/10.3390/catal9120985>
- [130] K. Moljord, P. Magnoux, M. Guisnet, Evidence for a participation of zeolite acid sites in the coke removal through oxidative treatment, *Catalysis Letters*, 25 (1994). <https://doi.org/10.1007/BF00815423>
- [131] C.L. Pieck, C.R. Vera, C.A. Querini, J.M. Parera, Differences in coke burning-off from Pt–Sn/Al<sub>2</sub>O<sub>3</sub> catalyst with oxygen or ozone, *Applied Catalysis A: General*, 278 (2005). <https://doi.org/10.1016/j.apcata.2004.05.001>
- [132] Q.N. Dong, J.R. Anderson, T. Mole, Y.F. Chang, R.J. Western, Reaction of benzene and toluene in the presence of oxygen over H-ZSM5 zeolite Aromatic oxygenates in the product, *Applied Catalysis*, 72 (1991). [https://doi.org/10.1016/0166-9834\(91\)85031-P](https://doi.org/10.1016/0166-9834(91)85031-P)
- [133] K. Adachi, K. Hirabayashi, N. Hoshino, S. Inoue, T. Kondoh, T. Murakami, S. Shibata, M. Ueda, *Process for the regeneration of coke-deposited, crystalline silicate catalyst*. 1994, Res Ass for the Utilization Of.
- [134] S.-J. Jong, A.R. Pradhan, J.-F. Wu, T.-C. Tsai, S.-B. Liu, On the Regeneration of Coked H-ZSM-5 Catalysts, *Journal of Catalysis*, 174 (1998). <https://doi.org/10.1006/jcat.1998.1971>
- [135] W.J. Koves, *Apparatus for coke burning in regeneration of hydrocarbon conversion catalyst*. 1989, Uop Inc. Patent n°US4880604A.
- [136] G. Nazarova, E. Ivashkina, T. Shafran, A. Oreshina, G. Seitenova, Prediction of residue coke content and operating modes of regenerator in the catalytic cracking technology, *Petroleum Science and Technology*, (2020). <https://doi.org/10.1080/10916466.2020.1825966>
- [137] T. Sano, N. Yamashita, Y. Iwami, K. Takeda, Y. Kawakami, Estimation of dealumination rate of ZSM-5 zeolite by adsorption of water vapor, *Zeolites*, 16 (1996). [https://doi.org/10.1016/0144-2449\(95\)00161-1](https://doi.org/10.1016/0144-2449(95)00161-1)
- [138] T. Sano, H. Ikeya, T. Kasuno, Z.B. Wang, Y. Kawakami, K. Soga, Influence of Crystallinity of HZSM-5 Zeolite on Its Dealumination Rate, *Zeolites*, 19 (1997). [https://doi.org/10.1016/S0144-2449\(97\)00052-3](https://doi.org/10.1016/S0144-2449(97)00052-3)
- [139] A.A. Nikolopoulos, A. Kogelbauer, J.G. Goodwin, G. Marcelin, Effect of dealumination on the catalytic activity of acid zeolites for the gas phase synthesis of MTBE, *Applied Catalysis A: General*, 119 (1994). [https://doi.org/10.1016/0926-860X\(94\)85025-9](https://doi.org/10.1016/0926-860X(94)85025-9)
- [140] A.G. Gayubo, A.T. Aguayo, A. Atutxa, R. Prieto, J. Bilbao, Deactivation of a HZSM-5 Zeolite Catalyst in the Transformation of the Aqueous Fraction of Biomass Pyrolysis Oil into Hydrocarbons, *Energy & Fuels*, 18 (2004). <https://doi.org/10.1021/ef040027u>
- [141] I.V. Kozhevnikov, S. Holmes, M.R.H. Siddiqui, Coking and regeneration of H<sub>3</sub>PW<sub>12</sub>O<sub>40</sub>/SiO<sub>2</sub> catalysts, *Applied Catalysis A: General*, 214 (2001). [https://doi.org/10.1016/S0926-860X\(01\)00469-0](https://doi.org/10.1016/S0926-860X(01)00469-0)
- [142] C.L. Pieck, R.J. Verderone, E.L. Jablonski, J.M. Parera, Burning of coke on Pt Re/Al<sub>2</sub>O<sub>3</sub> catalyst: Activation energy and oxygen reaction order, *Applied Catalysis*, 55 (1989). [https://doi.org/10.1016/S0166-9834\(00\)82312-X](https://doi.org/10.1016/S0166-9834(00)82312-X)
- [143] T. Furusawa, Y. Miura, Y. Kori, M. Sato, N. Suzuki, The cycle usage test of Ni/MgO catalyst for the steam reforming of naphthalene/benzene as model tar compounds



- of biomass gasification, *Catalysis Communications*, 10 (2009). <https://doi.org/10.1016/j.catcom.2008.10.032>
- [144] P. Lu, Q. Huang, Y. Chi, J. Yan, Coking and Regeneration of Nickel Catalyst for the Cracking of Toluene As a Tar Model Compound, *Energy & Fuels*, 31 (2017). <https://doi.org/10.1021/acs.energyfuels.7b01218>
- [145] J. Chen, C.-Y. Liu, Regeneration of Spent Catalysts with Ozone, *World Academy of Science, Engineering and Technology, International Journal of Environmental, Chemical, Ecological, Geological and Geophysical Engineering*, 7 (2013).
- [146] C.Y.H. Chao, C.W. Kwong, K.S. Hui, Potential use of a combined ozone and zeolite system for gaseous toluene elimination, *Journal of Hazardous Materials*, 143 (2007). <https://doi.org/10.1016/j.jhazmat.2006.08.077>
- [147] S.T. Oyama, Chemical and Catalytic Properties of Ozone, *Catalysis Reviews - Science and Engineering*, 42 (2000). <https://doi.org/10.1081/CR-100100263>
- [148] S. Rakovsky, M. Anachkov, G. Zaikov, N.M. Emanuel. *FIELDS OF OZONE APPLICATIONS*. 2009.
- [149] T. Vijayan, J.G. Patil, High concentration ozone generation in the laboratory for various applications, (2010). <https://doi.org/10.5897/IJSTER>
- [150] S.W. Benson, A.E. Axworthy, Jr., Mechanism of the Gas Phase, Thermal Decomposition of Ozone, *Journal of Chemical Physics*, 26 (1957). <https://doi.org/10.1063/1.1743610>
- [151] K.M. Bulanin, J.C. Lavalley, A.A. Tsyganenko, IR spectra of adsorbed ozone, *Colloids and Surfaces A: Physicochemical and Engineering Aspects*, 101 (1995). [https://doi.org/10.1016/0927-7757\(95\)03130-6](https://doi.org/10.1016/0927-7757(95)03130-6)
- [152] W. Li, G.V. Gibbs, S.T. Oyama, Mechanism of Ozone Decomposition on a Manganese Oxide Catalyst. 1. In Situ Raman Spectroscopy and Ab Initio Molecular Orbital Calculations, *Journal of the American Chemical Society*, 120 (1998). <https://doi.org/10.1021/ja981441+>
- [153] H. Huang, W. Li, Destruction of toluene by ozone-enhanced photocatalysis: Performance and mechanism, *Applied Catalysis B: Environmental*, 102 (2011). <https://doi.org/10.1016/j.apcatb.2010.12.025>
- [154] P. Monneyron, S. Mathé, M.H. Manero, J.N. Foussard, Regeneration of High Silica Zeolites via Advanced Oxidation Processes—A Preliminary Study About Adsorbent Reactivity Toward Ozone, *Chemical Engineering Research and Design*, 81 (2003). <https://doi.org/10.1205/026387603770866371>
- [155] S. Alejandro, H. Valdés, C.A. Zaror, Natural Zeolite Reactivity Towards Ozone: The Role of Acid Surface Sites, *Journal of Advanced Oxidation Technologies*, 14 (2011). <https://doi.org/doi:10.1515/jaots-2011-0201>
- [156] C.V. Rekhate, J.K. Srivastava, Recent advances in ozone-based advanced oxidation processes for treatment of wastewater- A review, *Chemical Engineering Journal Advances*, 3 (2020). <https://doi.org/10.1016/j.ceja.2020.100031>
- [157] P.S. Bailey, The Reactions Of Ozone With Organic Compounds, *Chemical Reviews*, 58 (1958). <https://doi.org/10.1021/cr50023a005>
- [158] R. Criegee, Mechanism of Ozonolysis, *Angewandte Chemie International Edition in English*, 14 (1975). <https://doi.org/10.1002/anie.197507451>
- [159] D.B. Miklos, C. Remy, M. Jekel, K.G. Linden, J.E. Drewes, U. Hübner, Evaluation of advanced oxidation processes for water and wastewater treatment – A critical review, *Water Research*, 139 (2018). <https://doi.org/10.1016/j.watres.2018.03.042>
- [160] S. Khangkham, PhD thesis, *Catalytic degradation of poly(methyl methacrylate) by zeolites and regeneration of used zeolites via ozonation*, in *Institut National Polytechnique de Toulouse*. 2012.

- [161] J. Treacy, M.E. Hag, D. O'Farrell, H. Sidebottom, Reactions of Ozone with Unsaturated Organic Compounds, *Berichte der Bunsengesellschaft für physikalische Chemie*, 96 (1992). <https://doi.org/10.1002/bbpc.19920960337>
- [162] M.E. Jenkin, R. Valorso, B. Aumont, M.J. Newland, A.R. Rickard, Estimation of rate coefficients for the reactions of O<sub>3</sub> with unsaturated organic compounds for use in automated mechanism construction, *Atmos. Chem. Phys.*, 20 (2020). <https://doi.org/10.5194/acp-20-12921-2020>
- [163] R.G. Copperthwaite, G.J. Hutchings, P. Johnston, S.W. Orchard, Regeneration of pentasil zeolite catalysts using ozone and oxygen, *Journal of the Chemical Society, Faraday Transactions 1: Physical Chemistry in Condensed Phases*, 82 (1986). <https://doi.org/10.1039/F19868201007>
- [164] L. Mariey, J. Lamotte, T. Chevreau, J.C. Lavalley, FT-IR study of coked HY zeolite regeneration using oxygen or ozone, *Reaction Kinetics and Catalysis Letters*, 59 (1996). <https://doi.org/10.1007/BF02068119>
- [165] G.J. Hutchings, R.G. Copperthwaite, T. Themistocleous, G.A. Foulds, A.S. Bielowitch, B.J. Loots, G. Nowitz, P. Van Eck, A comparative study of reactivation of zeolite Y using oxygen and ozone/oxygen mixtures, *Applied Catalysis*, 34 (1987). [https://doi.org/10.1016/S0166-9834\(00\)82452-5](https://doi.org/10.1016/S0166-9834(00)82452-5)
- [166] C.A. Querini, Isobutane/butene alkylation: regeneration of solid acid catalysts, *Catalysis Today*, 62 (2000). [https://doi.org/10.1016/S0920-5861\(00\)00415-6](https://doi.org/10.1016/S0920-5861(00)00415-6)
- [167] T. Zhang, Q. Lin, Z. Xue, R. Munson, G. Magneschi, Sinopec Zhongyuan Oil Field Company Refinery CCS-EOR Project, *Energy Procedia*, 114 (2017). <https://doi.org/10.1016/j.egypro.2017.03.1724>
- [168] J. Hunt, A. Ferrari, A. Lita, M. Crosswhite, B. Ashley, A.E. Stiegman, Microwave-Specific Enhancement of the Carbon–Carbon Dioxide (Boudouard) Reaction, *The Journal of Physical Chemistry C*, 117 (2013). <https://doi.org/10.1021/jp4076965>
- [169] C.S. Triantafyllidis, A.G. Vlessidis, N.P. Evmiridis, Dealuminated H–Y Zeolites: Influence of the Degree and the Type of Dealumination Method on the Structural and Acidic Characteristics of H–Y Zeolites, *Industrial & Engineering Chemistry Research*, 39 (2000). <https://doi.org/10.1021/ie990568k>
- [170] L.T.d. Santos, F.M. Santos, R.S. Silva, T.S. Gomes, P.M. Esteves, R.D.M. Pimenta, S.M.C. Menezes, O.R. Chamberlain, Y.L. Lam, M.M. Pereira, Mechanistic insights of CO<sub>2</sub>-coke reaction during the regeneration step of the fluid cracking catalyst, *Applied Catalysis A: General*, 336 (2008). <https://doi.org/10.1016/j.apcata.2007.10.005>
- [171] Y. Zhang, G. Sun, S. Gao, G. Xu, Regeneration Kinetics of Spent FCC Catalyst via Coke Gasification in a Micro Fluidized Bed, *Procedia Engineering*, 102 (2015). <https://doi.org/10.1016/j.proeng.2015.01.312>
- [172] G. Tian, G. Wang, C. Xu, J. Gao, Gasification of the Coke on Spent-Residue-Pretreating Catalysts with Steam and Steam–O<sub>2</sub> Mixtures, *Energy & Fuels*, 28 (2014). <https://doi.org/10.1021/ef402045d>
- [173] F. Ferella, I. D'Adamo, S. Leone, V. Innocenzi, I. De Michelis, F. Vegliò, Spent FCC E-Cat: Towards a Circular Approach in the Oil Refining Industry, *Sustainability*, 11 (2019). <https://doi.org/10.3390/su11010113>
- [174] F. Bauer, H. Ernst, E. Geidel, R. Schödel, Reactivation of Coked H-ZSM-5 by Treatment with Hydrogen and Alkanes, *Journal of Catalysis*, 164 (1996). <https://doi.org/10.1006/jcat.1996.0370>
- [175] P. Marecot\*, S. Peyrovi, D. Bahloul, J. Barbier, Regeneration by hydrogen treatment of bifunctional catalysts deactivated by coke deposition, *Applied Catalysis*, 66 (1990). [https://doi.org/10.1016/S0166-9834\(00\)81636-X](https://doi.org/10.1016/S0166-9834(00)81636-X)

- [176] P.L. Walker, S. Matsumoto, T. Hanzawa, T. Muira, I.M.K. Ismail, Catalysis of gasification of coal-derived cokes and chars, *Fuel*, 62 (1983). [https://doi.org/10.1016/0016-2361\(83\)90186-2](https://doi.org/10.1016/0016-2361(83)90186-2)
- [177] R. Josl, R. Klingmann, Y. Traa, R. Gläser, J. Weitkamp, Regeneration of zeolite catalysts deactivated in isobutane/butene alkylation: an in situ FTIR investigation at elevated H<sub>2</sub> pressure, *Catalysis Communications*, 5 (2004). <https://doi.org/10.1016/j.catcom.2004.02.005>
- [178] R. Klingmann, R. Josl, Y. Traa, R. Gläser, J. Weitkamp, Hydrogenative regeneration of a Pt/La-Y zeolite catalyst deactivated in the isobutane/n-butene alkylation, *Applied Catalysis A: General*, 281 (2005). <https://doi.org/10.1016/j.apcata.2004.11.032>
- [179] A.T. Aguayo, A.G. Gayubo, J. Ereña, A. Atutxa, J. Bilbao, Coke Aging and Its Incidence on Catalyst Regeneration, *Industrial & Engineering Chemistry Research*, 42 (2003). <https://doi.org/10.1021/ie030085n>
- [180] N.S. Gnep, M.L. Martin De Armando, M. Guisnet, TOLUENE DISPROPORTIONATION AND COKE FORMATION OVER FLUORIED ALUMINA AND HYDROGEN-MORDENITE (1980).
- [181] A.G. Alvarez, H. Viturro, R.D. Bonetto, Structural changes on deactivation of ZSM-5. A study by X-ray powder diffraction, *Materials Chemistry and Physics*, 32 (1992). [https://doi.org/10.1016/0254-0584\(92\)90269-E](https://doi.org/10.1016/0254-0584(92)90269-E)
- [182] S. Parsons, *Advanced Oxidation Processes for Water and Wastewater Treatment*. 2005: IWA Publishing.
- [183] Y. Deng, R. Zhao, *Advanced Oxidation Processes (AOPs) in Wastewater Treatment*, *Current Pollution Reports*, 1 (2015). <https://doi.org/10.1007/s40726-015-0015-z>
- [184] N. Brodu, M.-H. Manero, C. Andriantsiferana, J.-S. Pic, H. Valdés, Role of Lewis acid sites of ZSM-5 zeolite on gaseous ozone abatement, *Chemical Engineering Journal*, 231 (2013). <https://doi.org/10.1016/j.cej.2013.07.002>
- [185] S. Alejandro, H. Valdés, M.-H. Manero, C.A. Zaror, Oxidative regeneration of toluene-saturated natural zeolite by gaseous ozone: The influence of zeolite chemical surface characteristics, *Journal of Hazardous Materials*, 274 (2014). <https://doi.org/10.1016/j.jhazmat.2014.04.006>
- [186] S. Alejandro-Martín, H. Valdés, M.-H. Manero, C.A. Zaror, Catalytic Ozonation of Toluene Using Chilean Natural Zeolite: The Key Role of Brønsted and Lewis Acid Sites, *Catalysts*, 8 (2018). <https://doi.org/10.3390/catal8050211>
- [187] I. Polaert, A. Ledoux, L. Estel, R. Huyghe, M. Thomas, Microwave Assisted Regeneration of Zeolite, *International Journal of Chemical Reactor Engineering*, 5 (2007). <https://doi.org/doi:10.2202/1542-6580.1436>
- [188] L.Y. Jia, A. Farouha, L. Pinard, S. Hedan, J.D. Comparot, A. Dufour, K. Ben Tayeb, H. Vezin, C. Batiot-Dupeyrat, New routes for complete regeneration of coked zeolite, *Applied Catalysis B: Environmental*, 219 (2017). <https://doi.org/10.1016/j.apcatb.2017.07.040>
- [189] N. HafezKhiabani, S. Fathi, B. Shokri, S.I. Hosseini, A novel method for decoking of Pt–Sn/Al<sub>2</sub>O<sub>3</sub> in the naphtha reforming process using RF and pin-to-plate DBD plasma systems, *Applied Catalysis A: General*, 493 (2015). <https://doi.org/10.1016/j.apcata.2014.12.041>
- [190] A. Astafan, C. Batiot-Dupeyrat, L. Pinard, Mechanism and Kinetic of Coke Oxidation by Nonthermal Plasma in Fixed-Bed Dielectric Barrier Reactor, *The Journal of Physical Chemistry C*, 123 (2019). <https://doi.org/10.1021/acs.jpcc.9b00743>



- [191] L. Pinard, N. Ayoub, C. Batiot-Dupeyrat, Regeneration of a Coked Zeolite via Nonthermal Plasma Process: A Parametric Study, *Plasma Chemistry and Plasma Processing*, 39 (2019). <https://doi.org/10.1007/s11090-019-09972-x>
- [192] I. Braschi, S. Blasioli, E. Buscaroli, D. Montecchio, A. Martucci, Physicochemical regeneration of high silica zeolite Y used to clean-up water polluted with sulfonamide antibiotics, *Journal of Environmental Sciences*, 43 (2016). <https://doi.org/10.1016/j.jes.2015.07.017>
- [193] A.M. Díez, M.A. Sanromán, M. Pazos, Fenton-based processes for the regeneration of catalytic adsorbents, *Catalysis Today*, 313 (2018). <https://doi.org/10.1016/j.cattod.2017.10.030>
- [194] M.V. Morales, K. Góra-Marek, H. Musch, A. Pineda, B. Murray, S. Stefanidis, L. Falco, K. Tarach, E. Ponomareva, J.H. Marsman, I. Melián-Cabrera, Advanced oxidation process for coke removal: A systematic study of hydrogen peroxide and OH-derived-Fenton radicals of a fouled zeolite, *Applied Catalysis A: General*, 562 (2018). <https://doi.org/10.1016/j.apcata.2018.06.008>
- [195] M. Díaz, E. Epelde, J. Valecillos, S. Izaddoust, A.T. Aguayo, J. Bilbao, Coke deactivation and regeneration of HZSM-5 zeolite catalysts in the oligomerization of 1-butene, *Applied Catalysis B: Environmental*, 291 (2021). <https://doi.org/10.1016/j.apcatb.2021.120076>
- [196] Z. Ma, J.A. van Bokhoven, Deactivation and Regeneration of H-USY Zeolite during Lignin Catalytic Fast Pyrolysis, *ChemCatChem*, 4 (2012). <https://doi.org/10.1002/cctc.201200401>
- [197] C. Kassargy, S. Awad, G. Burnens, G. Upreti, K. Kahine, M. Tazerout, Study of the effects of regeneration of USY zeolite on the catalytic cracking of polyethylene, *Applied Catalysis B: Environmental*, 244 (2019). <https://doi.org/10.1016/j.apcatb.2018.11.093>
- [198] L.D. Schmidt, T. Wang, A. Vacquez, Electron microscopy of catalyst particles, *Ultramicroscopy*, 8 (1982). [https://doi.org/10.1016/0304-3991\(82\)90286-8](https://doi.org/10.1016/0304-3991(82)90286-8)
- [199] A.K. Datye, D.J. Smith, The Study of Heterogeneous Catalysts by High-Resolution Transmission Electron Microscopy, *Catalysis Reviews*, 34 (1992). <https://doi.org/10.1080/01614949208021920>
- [200] A.A. Ajibola, J.A. Omoleye, V.E. Efevbokhan, Catalytic cracking of polyethylene plastic waste using synthesised zeolite Y from Nigerian kaolin deposit, *Applied Petrochemical Research*, 8 (2018). <https://doi.org/10.1007/s13203-018-0216-7>
- [201] Z. Ma, F. Zaera, *Characterization of Heterogeneous Catalysts*, 2006, pp. 1-37.
- [202] G. Michel, P. Ludovic, *Catalyse hétérogène : désactivation et régénération des catalyseurs*, Techniques de l'ingénieur Catalyse et procédés catalytiques, base documentaire : TIB325DUO (2014). Access link: <https://www.techniques-ingenieur.fr/base-documentaire/procedes-chimie-bio-agro-th2/catalyse-et-procedes-catalytiques-42325210/catalyse-heterogene-desactivation-et-regeneration-des-catalyseurs-j1265/>
- [203] C. Engtrakul, C. Mukarakate, A.K. Starace, K.A. Magrini, A.K. Rogers, M.M. Yung, Effect of ZSM-5 acidity on aromatic product selectivity during upgrading of pine pyrolysis vapors, *Catalysis Today*, 269 (2016). <https://doi.org/10.1016/j.cattod.2015.10.032>
- [204] J. Goetze, B.M. Weckhuysen, Spatiotemporal coke formation over zeolite ZSM-5 during the methanol-to-olefins process as studied with operando UV-vis spectroscopy: a comparison between H-ZSM-5 and Mg-ZSM-5, *Catalysis Science & Technology*, 8 (2018). <https://doi.org/10.1039/C7CY02459B>

- [205] A. Westermann, PhD thesis, *Élimination sélective d'un mélange d'hydrocarbures imbrûlés Diesel par adsorption sur des matériaux zéolithiques*, in *Université de Lorraine*, 2013.
- [206] B. Wang, PhD thesis, *Zeolite deactivation during hydrocarbon reactions: characterisation of coke precursors and acidity, product distribution*, in *University College London*, 2008.
- [207] J. Weitkamp, Critical Evaluation of Catalytic Testing of Zeolites, in: P.J. Grobet, W.J. Mortier, E.F. Vansant, G. Schulz-Ekloff (Eds.), *Studies in Surface Science and Catalysis*, Elsevier, 1988, pp. 515-534.
- [208] S. van Donk, E. Bus, A. Broersma, J.H. Bitter, K.P. de Jong, Butene skeletal isomerization over H-ferrierite: a TEOM and in situ IR study on the role of carbonaceous deposits and the location of Brønsted acid sites, *Applied Catalysis A: General*, 237 (2002). [https://doi.org/10.1016/S0926-860X\(02\)00326-5](https://doi.org/10.1016/S0926-860X(02)00326-5)
- [209] S. Gomm, R. Gläser, J. Weitkamp, In situ Observation of Coke Deposition on Zeolite Catalysts Using a Tapered Element Oscillating Microbalance, *Chemical Engineering & Technology*, 25 (2002). [https://doi.org/10.1002/1521-4125\(20021008\)25:10<962::AID-CEAT962>3.0.CO;2-J](https://doi.org/10.1002/1521-4125(20021008)25:10<962::AID-CEAT962>3.0.CO;2-J)
- [210] A. Bellare, D.B. Dadyburjor, Evaluation of Modes of Catalyst Deactivation by Coking for Cumene Cracking over Zeolites, *Journal of Catalysis*, 140 (1993). <https://doi.org/10.1006/jcat.1993.1102>
- [211] Y. Zhang, P.T. Williams, Carbon nanotubes and hydrogen production from the pyrolysis catalysis or catalytic-steam reforming of waste tyres, *Journal of Analytical and Applied Pyrolysis*, 122 (2016). <https://doi.org/10.1016/j.jaap.2016.10.015>
- [212] T. Batakliiev, V. Georgiev, M. Anachkov, S. Rakovsky, G.E. Zaikov, Ozone decomposition, *Interdisciplinary toxicology*, 7 (2014). <https://doi.org/10.2478/intox-2014-0008>
- [213] E.P. Barrett, L.G. Joyner, P.P. Halenda, The Determination of Pore Volume and Area Distributions in Porous Substances. I. Computations from Nitrogen Isotherms, *Journal of the American Chemical Society*, 73 (1951). <https://doi.org/10.1021/ja01145a126>
- [214] Horv, Aacute, G. Th, Eacute, Za, K. Kawazoe, METHOD FOR THE CALCULATION OF EFFECTIVE PORE SIZE DISTRIBUTION IN MOLECULAR SIEVE CARBON, *Journal of Chemical Engineering of Japan*, 16 (1983). <https://doi.org/10.1252/jcej.16.470>
- [215] C.A. Emeis, Determination of Integrated Molar Extinction Coefficients for Infrared Absorption Bands of Pyridine Adsorbed on Solid Acid Catalysts, *Journal of Catalysis*, 141 (1993). <https://doi.org/10.1006/jcat.1993.1145>
- [216] P. Duan, K. Schmidt-Rohr, Composite-pulse and partially dipolar dephased multiCP for improved quantitative solid-state <sup>13</sup>C NMR, *Journal of Magnetic Resonance*, 285 (2017). <https://doi.org/10.1016/j.jmr.2017.10.010>
- [217] T. Thonhauser, D. Ceresoli, N. Marzari, NMR shifts for polycyclic aromatic hydrocarbons from first-principles, *International Journal of Quantum Chemistry*, 109 (2009). <https://doi.org/10.1002/qua.21941>
- [218] Y. Ruiz-Morales, A.D. Miranda-Olvera, B.n. Portales-Martínez, J.M. Domínguez, Determination of <sup>13</sup>C NMR Chemical Shift Structural Ranges for Polycyclic Aromatic Hydrocarbons (PAHs) and PAHs in Asphaltenes: An Experimental and Theoretical Density Functional Theory Study, *Energy and Fuels*, 33 (2019). <https://doi.org/10.1021/acs.energyfuels.9b00182>
- [219] J. Pan, G. Liao, R. Su, S. Chen, Z. Wang, L. Chen, L. Chen, X. Wang, Y. Guo, <sup>13</sup>C Solid-State NMR Analysis of the Chemical Structure in Petroleum Coke during

- Idealized In Situ Combustion Conditions, *ACS Omega*, 6 (2021). <https://doi.org/10.1021/acsomega.1c02055>
- [220] D.S. Wragg, G.N. Kalantzopoulos, D.K. Pappas, I. Pinilla-Herrero, D. Rojo-Gama, E. Redekop, M. Di Michiel, P. Beato, L.F. Lundegaard, S. Svelle, Mapping the coke formation within a zeolite catalyst extrudate in space and time by operando computed X-ray diffraction tomography, *Journal of Catalysis*, 401 (2021). <https://doi.org/10.1016/j.jcat.2021.07.001>
- [221] G. Elordi, M. Olazar, M. Artetxe, P. Castaño, J. Bilbao, Effect of the acidity of the HZSM-5 zeolite catalyst on the cracking of high density polyethylene in a conical spouted bed reactor, *Applied Catalysis A: General*, 415-416 (2012). <https://doi.org/10.1016/j.apcata.2011.12.011>
- [222] D.P. Serrano, J. Aguado, J.M. Rodríguez, A. Peral, Catalytic cracking of polyethylene over nanocrystalline HZSM-5: Catalyst deactivation and regeneration study, *Journal of Analytical and Applied Pyrolysis*, 79 (2007). <https://doi.org/10.1016/j.jaap.2006.11.013>
- [223] R.K. Singh, B. Ruj, A.K. Sadhukhan, P. Gupta, V.P. Tigga, Waste plastic to pyrolytic oil and its utilization in CI engine: Performance analysis and combustion characteristics, *Fuel*, 262 (2020). <https://doi.org/10.1016/j.fuel.2019.116539>
- [224] C. Kassargy, S. Awad, G. Burnens, K. Kahine, M. Tazerout, Experimental study of catalytic pyrolysis of polyethylene and polypropylene over USY zeolite and separation to gasoline and diesel-like fuels, *Journal of Analytical and Applied Pyrolysis*, 127 (2017). <https://doi.org/10.1016/j.jaap.2017.09.005>
- [225] C. Kassargy, S. Awad, G. Burnens, K. Kahine, M. Tazerout, Gasoline and diesel-like fuel production by continuous catalytic pyrolysis of waste polyethylene and polypropylene mixtures over USY zeolite, *Fuel*, 224 (2018). <https://doi.org/10.1016/j.fuel.2018.03.113>
- [226] S. Papuga, M. Djurdjevic, A. Ciccioli, S. Vecchio Cipriotti, Catalytic Pyrolysis of Plastic Waste and Molecular Symmetry Effects: A Review, *Symmetry*, 15 (2023). <https://doi.org/10.3390/sym15010038>
- [227] A.C.S. Serra, J.V. Milato, J.G. Faillace, M.R.C.M. Calderari, Reviewing the use of zeolites and clay based catalysts for pyrolysis of plastics and oil fractions, *Brazilian Journal of Chemical Engineering*, 40 (2023). <https://doi.org/10.1007/s43153-022-00254-2>
- [228] D. Zhao, X. Wang, J.B. Miller, G.W. Huber, The Chemistry and Kinetics of Polyethylene Pyrolysis: A Process to Produce Fuels and Chemicals, *ChemSusChem*, 13 (2020). <https://doi.org/10.1002/cssc.201903434>
- [229] B. Liu, D. Slocombe, M. AlKinany, H. AlMegren, J. Wang, J. Arden, A. Vai, S. Gonzalez-Cortes, T. Xiao, V. Kuznetsov, P.P. Edwards, Advances in the study of coke formation over zeolite catalysts in the methanol-to-hydrocarbon process, *Applied Petrochemical Research*, 6 (2016). <https://doi.org/10.1007/s13203-016-0156-z>
- [230] G.L. Woolery, G.H. Kuehl, H.C. Timken, A.W. Chester, J.C. Vartuli, On the nature of framework Brønsted and Lewis acid sites in ZSM-5, *Zeolites*, 19 (1997). [https://doi.org/10.1016/S0144-2449\(97\)00086-9](https://doi.org/10.1016/S0144-2449(97)00086-9)
- [231] A. Corma, J. Planelles, J. Sánchez-Marín, F. Tomás, The role of different types of acid site in the cracking of alkanes on zeolite catalysts, *Journal of Catalysis*, 93 (1985). [https://doi.org/10.1016/0021-9517\(85\)90148-4](https://doi.org/10.1016/0021-9517(85)90148-4)
- [232] M. He, M.-F. Ali, Y.-Q. Song, X.-L. Zhou, J.A. Wang, X.-Y. Nie, Z. Wang, Study on the deactivation mechanism of HZSM-5 in the process of catalytic cracking of n-hexane, *Chemical Engineering Journal*, 451 (2023). <https://doi.org/10.1016/j.cej.2022.138793>

- [233] M. Kuwata, S.R. Zorn, S.T. Martin, Using Elemental Ratios to Predict the Density of Organic Material Composed of Carbon, Hydrogen, and Oxygen, *Environmental Science and Technology*, 46 (2012). <https://doi.org/10.1021/es202525q>
- [234] M. Choi, K. Na, J. Kim, Y. Sakamoto, O. Terasaki, R. Ryoo, Stable single-unit-cell nanosheets of zeolite MFI as active and long-lived catalysts, *Nature*, 461 (2009). <https://doi.org/10.1038/nature08288>
- [235] V. Daligaux, R. Richard, M.H. Manero, Regeneration of coked catalysts via ozonation: Experimental study of diffusion–reaction mechanisms at pellet and reactor scales, *Chemical Engineering Journal*, 476 (2023). <https://doi.org/10.1016/j.cej.2023.146446>
- [236] S.H. Gebre, M.G. Sendeku, M. Bahri, Recent Trends in the Pyrolysis of Non-Degradable Waste Plastics, *ChemistryOpen*, 10 (2021). <https://doi.org/10.1002/open.202100184>
- [237] Lenntech, Ozone reaction mechanisms, 2020. [cited 2021 May]. Access link: <https://www.lenntech.com/library/ozone/reaction/ozone-reaction-mechanisms.htm>,
- [238] J.V. Michael, Thermal Decomposition of Ozone, *The Journal of Chemical Physics*, 54 (1971). <https://doi.org/10.1063/1.1674697>
- [239] J. Jian, H. Hashemi, H. Wu, A.W. Jasper, P. Glarborg, A reaction mechanism for ozone dissociation and reaction with hydrogen at elevated temperature, *Fuel*, 322 (2022). <https://doi.org/10.1016/j.fuel.2022.124138>
- [240] O.R. Wulf, R.C. Tolman, The Thermal Decomposition of Ozone, *Proceedings of the National Academy of Sciences*, 13 (1927). <https://doi.org/10.1073/pnas.13.5.272>
- [241] N. Brodu, M.-H. Manero, C. Andriantsiferana, J.-S. Pic, H. Valdés, Gaseous ozone decomposition over high silica zeolitic frameworks, *The Canadian Journal of Chemical Engineering*, 96 (2018). <https://doi.org/10.1002/cjce.23141>
- [242] M. Stastna, D. Steinmoeller, Chapter 3 - Modeling active tracers, in: M. Stastna, D. Steinmoeller (Eds.), *Physics and Ecology in Fluids*, Elsevier, 2023, pp. 31-50.
- [243] P.B. Weisz, R.D. Goodwin, Combustion of carbonaceous deposits within porous catalyst particles I. Diffusion-controlled kinetics, *Journal of Catalysis*, 2 (1963). [https://doi.org/10.1016/0021-9517\(63\)90104-0](https://doi.org/10.1016/0021-9517(63)90104-0)
- [244] A. Tripodi, M. Compagnoni, R. Martinazzo, G. Ramis, I. Rossetti, Process Simulation for the Design and Scale Up of Heterogeneous Catalytic Process: Kinetic Modelling Issues, *Catalysts*, 7 (2017). <https://doi.org/10.3390/catal7050159>
- [245] O.S. Yazovtseva, I.M. Gubaydullin, E.E. Peskova, L.A. Sukharev, A.N. Zagoruiko, Computer Simulation of Coke Sediments Burning from the Whole Cylindrical Catalyst Grain, *Mathematics*, 11 (2023). <https://doi.org/10.3390/math11030669>
- [246] N. Frikha, E. Schaer, J.-L. Houzelot, Methodology of multiphase reaction kinetics and hydrodynamics identification: Application to catalyzed nitrobenzene hydrogenation, *Chemical Engineering Journal*, 124 (2006). <https://doi.org/https://doi.org/10.1016/j.cej.2006.08.012>
- [247] X. Zhang, Z. Sui, X. Zhou, W. Yuan, Modeling and Simulation of Coke Combustion Regeneration for Coked Cr<sub>2</sub>O<sub>3</sub>/Al<sub>2</sub>O<sub>3</sub> Propane Dehydrogenation Catalyst, *Chinese Journal of Chemical Engineering*, 18 (2010). [https://doi.org/10.1016/S1004-9541\(10\)60265-0](https://doi.org/10.1016/S1004-9541(10)60265-0)
- [248] N. Wakao, T. Funazkri, Effect of fluid dispersion coefficients on particle-to-fluid mass transfer coefficients in packed beds: Correlation of sherwood numbers, *Chemical Engineering Science*, 33 (1978). [https://doi.org/10.1016/0009-2509\(78\)85120-3](https://doi.org/10.1016/0009-2509(78)85120-3)
- [249] R.R. Ratnakar, B. Dindoruk, The Role of Diffusivity in Oil and Gas Industries: Fundamentals, Measurement, and Correlative Techniques, *Processes*, 10 (2022). <https://doi.org/10.3390/pr10061194>

- [250] S. Chapman, T.G. Cowling, *The Mathematical Theory of Non-uniform Gases: An Account of the Kinetic Theory of Viscosity, Thermal Conduction and Diffusion in Gases*. 1990: Cambridge University Press.
- [251] A. Fortin, *Les éléments finis : de la théorie à la pratique* (2006).
- [252] A.A. Zhokh, T.G. Serebrii, P.E. Strizhak, Diffusion of C6 cyclic hydrocarbons in ZSM-5 zeolite: From single nanocrystal to packed pellet, *Microporous and Mesoporous Materials*, 292 (2020). <https://doi.org/10.1016/j.micromeso.2019.109773>
- [253] Y. Sun, S. Han, Diffusion of N2, O2, H2S and SO2 in MFI and 4A zeolites by molecular dynamics simulations, *Molecular Simulation*, 41 (2015). <https://doi.org/10.1080/08927022.2014.945082>
- [254] S. Brosillon, M.-H. Manero, J.-N. Foussard, Mass Transfer in VOC Adsorption on Zeolite : Experimental and Theoretical Breakthrough Curves, *Environmental science & technology*, 35 (2001). <https://doi.org/10.1021/es010017x>
- [255] A.R. Passos, S.H. Pulcinelli, C.V. Santilli, V. Briois, Operando monitoring of metal sites and coke evolution during non-oxidative and oxidative ethanol steam reforming over Ni and NiCu ex-hydrotalcite catalysts, *Catalysis Today*, 336 (2019). <https://doi.org/10.1016/j.cattod.2018.12.054>
- [256] S.H. van Vreeswijk, B.M. Weckhuysen, Emerging analytical methods to characterize zeolite-based materials, *National Science Review*, 9 (2022). <https://doi.org/10.1093/nsr/nwac047>
- [257] G.N. Kalantzopoulos, D. Rojo Gama, D.K. Pappas, I. Dovgaliuk, U. Olsbye, P. Beato, L.F. Lundegaard, D.S. Wragg, S. Svelle, Real-time regeneration of a working zeolite monitored via operando X-ray diffraction and crystallographic imaging: how coke flees the MFI framework, *Dalton Transactions*, 51 (2022). <https://doi.org/10.1039/D2DT02845J>



# List of figures

## Introduction

- Figure 0.1.** Importance de la catalyse hétérogène dans les procédés chimiques .....1  
**Figure 0.1.** Industrial relevance of heterogeneous catalysts in chemical processes .....4

## Chapter 1 – Theory and literature review

- Figure 1.1.** Structures of four particular zeolites and their micropore systems and dimensions (Weitkamp *et al.*, 2000) [10].....8  
**Figure 1.2.** Formation of acid sites in zeolites. M is an electrons acceptor, can be either a compensating cation or extra framework aluminum oxide ( $Al_xO_y^{n+}$ ).....9  
**Figure 1.3.** Illustration of shape-selectivity using zeolites as catalysts in (a) reactant selectivity with the cleavage between linear and branched hydrocarbons and (b) product selectivity during methylation of toluene (Dhakshinamoorthy *et al.*, 2020) [26]. .....9  
**Figure 1.4.** Representation of zeolite material from atomic scale to its pelletized form for industrial use. Adapted from Mitchell *et al.* (2013) [27].....10  
**Figure 1.5.** Spatial representation of ZSM-5 zeolite structure, from tetrahedral primary unit to the framework structure and inherent channel system. Combined scheme adapted from Weitkamp *et al.* (2000) [10], Lounis *et al.* (2018) [32] and Kamaluddin *et al.* (2022) [33].....11  
**Figure 1.6.** Plastic demand by domain and type of polymer in 2019. Illustration taken from report “Plastics – the Facts 2020”. Source: PlasticsEurope. ....12  
**Figure 1.7.** Schematic representation of the different existing methods for plastic waste recycling and their implementation in the circular economy. ....13  
**Figure 1.8.** Product yield comparison between thermal and catalytic pyrolysis of HDPE. Graph adapted from Seo *et al.* (2003) [74].....15  
**Figure 1.9.** Reaction pathways for catalytic pyrolysis of polyolefins (Aguado *et al.*, 2001) [65]. ....16  
**Figure 1.10.** Thermogravimetric analysis (TGA) for determination of degradation temperature for different polymers (Lopez *et al.*, 2011) [67].....17  
**Figure 1.11.** Different possible continuous reactor configurations for catalytic pyrolysis of plastics: (a) fixed bed reactor, (b) fluidized bed reactor, (c) conical spouted bed reactor. Adapted scheme from Ochoa *et al.* (2020) [14]. ....19  
**Figure 1.12.** Schematic representation of catalytic pyrolysis of polyethylene over ZSM-5 with repartition of obtained products .....20  
**Figure 1.13.** Illustration of main catalytic deactivation pathways (Bartholomew *et al.*, 2003) [4].....21  
**Figure 1.14.** Conceptual models representing main mechanisms of metal particles sintering due to thermal degradation (Ochoa *et al.*, 2020) [14]. ....21

<b>Figure 1.15.</b> Deactivation pathways by coke formation from precursors adsorption to structural damages at advanced coke growth stages (Ochoa <i>et al.</i> , 2020) [14].....	22
<b>Figure 1.16.</b> Simplified scheme of coke formation from hydrocarbons and molecular coke over acid zeolite catalysts (Guisnet <i>et al.</i> , 2001) [89]. .....	23
<b>Figure 1.17.</b> Necessary conditions for coke formation over catalysts and major influencing parameters (Guisnet <i>et al.</i> , 2001) [89]. .....	24
<b>Figure 1.18.</b> Rate of coke formation and weight content over steel cylinder during thermal cracking of ethane between 750 and 850°C (Mahamulkar <i>et al.</i> , 2016) [95]. .	25
<b>Figure 1.19.</b> Reaction scheme for coke formation during catalytic cracking of VGO. Adapted from Moustafa <i>et al.</i> (2003) [98] .....	26
<b>Figure 1.20.</b> Scheme of coke formation over pelletized ZSM-5 zeolite, representing coke deposition and pore blocking both at mesopore and micropore level. ....	28
<b>Figure 1.21.</b> Schematic representation of the main coked zeolites regeneration methods with the principal generated products. ....	29
<b>Figure 1.22.</b> (a) Shell progressive regeneration of fouled pellet following shrinking-core mode (Fogler <i>et al.</i> , 2011) [125]; (b) Coke removal during combustion of catalyst pellets in a fixed bed reactor (Müller <i>et al.</i> , 2010) [126]. ....	32
<b>Figure 1.23.</b> Carbocation mechanism for the reaction of oxygen with an adsorbed coke molecule. Dong <i>et al.</i> (1991) [132], adapted by Keskitalo <i>et al.</i> (2006) [118]. ....	34
<b>Figure 1.24.</b> Average coke conversion and temperature profiles in the reactor for different oxygen-inlet concentration strategies (Santamaria <i>et al.</i> , 1991) [115]. ....	34
<b>Figure 1.25.</b> H <sub>2</sub> yield of a metal-impregnated cracking Ni/γ-Al <sub>2</sub> O <sub>3</sub> catalyst after different cycles of regeneration with oxygen for 3h (Lu <i>et al.</i> , 2017) [144]. ....	35
<b>Figure 1.26.</b> Ozone molecule dimensions and resonance structures. Adapted from Chao <i>et al.</i> (2007) [146] and Oyama <i>et al.</i> (2000) [147]. ....	36
<b>Figure 1.27.</b> Criegee mechanism for initial attack of molecular ozone on alkenes (Criegee <i>et al.</i> , 1975) [158]. ....	39
<b>Figure 1.28.</b> Schematic representation of (a) point-to-plate reactor (Pinard <i>et al.</i> , 2019) [129] and (b) fixed-bed dielectric barrier discharge (DBD) reactor for coked catalyst regeneration via NTP (Astafan <i>et al.</i> , 2019) [190]. ....	42
<b>Figure 1.29.</b> Schematic representation of oxidation processes for coke removal from catalysts at pellet and mesoporous scale. ....	44
<b>Figure 1.30.</b> Key takeaways of “Chapter 1”. ....	46

## Chapter 2 – Analytical review and experimental methods

<b>Figure 2.1.</b> SEM images of fresh and aged ZSM-5 zeolite used for catalytic pyrolysis of plastic wastes (López <i>et al.</i> , 2011) [93]. ....	49
<b>Figure 2.2.</b> Determination of free acidity of deactivated USHY zeolite via TPD experiments using NH <sub>3</sub> as probe molecule (Schmidt <i>et al.</i> , 1982) [198]. ....	50
<b>Figure 2.3.</b> TPO curves and deconvoluted peaks of Y-zeolite coked during catalytic pyrolysis of PE at different TOS (Chen <i>et al.</i> , 2021) [79]. ....	52



<b>Figure 2.4.</b> Method for determination of zeolite coke nature and composition developed by Guisnet <i>et al.</i> (graphical abstract from Guisnet <i>et al.</i> , 2009) [89].	52
<b>Figure 2.5.</b> Polyethylene used as plastic feedstock for pyrolysis experiments.	54
<b>Figure 2.6.</b> ZSM-5 catalysts for deactivation (pyrolysis) and regeneration (ozonation) studies.	54
<b>Figure 2.7.</b> Photographs of the pyrolysis experimental pilot with the main different blocks, and bottom part of the reactor where feedstock is loaded.	55
<b>Figure 2.8.</b> PID scheme of pyrolysis experimental setup.	56
<b>Figure 2.9.</b> Scheme of (a) experimental setup for pyrolysis of polyethylene and (b) reactor loading methods. Figure extracted from submitted article (Chapter 3).	58
<b>Figure 2.10.</b> Photographs and scheme of experimental ozonation setup with tubular and syringe reactor configurations.	60
<b>Figure 2.11.</b> Illustration of coked zeolites with corresponding pellet cross-section.	62
<b>Figure 2.12.</b> Different temperature programs for TGA-FTIR analysis of coked samples under air or nitrogen atmosphere.	67
<b>Figure 2.13.</b> Superposed optic and SEM pictures for two partially regenerated samples with corresponding EDX acquisition to illustrate carbon profiles obtained with SEM-EDX method.	68
<b>Figure 2.14.</b> Results obtained with innovative SEM-FEG technique for one cross-section of a partially regenerated sample, with different obtained profiles based on the acquisition method used for analysis (mapping or scanning).	69
<b>Figure 2.15.</b> Key takeaways of “Chapter 2”.	70

### Chapter 3 – Deactivation of catalysts by pyrolysis of LDPE

<b>Figure 3.1.</b> Illustration of pyrolysis yields evolution for thermal and catalytic pyrolysis of plastic wastes experiments (López <i>et al.</i> , 2011) [93].	72
<b>Figure 3.2.</b> Illustration of the PMMA degradation yields evolution using fresh, spent and ozonated ZSM-5 industrial catalysts (Khangkham <i>et al.</i> , 2013) [8].	72
<b>Figure 3.3.</b> Evolution of pyrolysis products repartition after successive reuses of catalysts.	75
<b>Figure 3.4.</b> Evolution of catalysts textural and chemical properties due to coke deposition during several successive runs of pyrolysis of LDPE.	76
<b>Figure 3.5.</b> Correlation between the analyzed carbon content with (a) microporosity, (b) free acid sites and (c) H/C ratio of all catalysts samples (fresh, spent, regenerated and reused).	78
<b>Figure 3.6.</b> Normalized $^{13}\text{C}$ NMR spectra of the different coked samples.	80
<b>Figure 3.7.</b> Schematic representation of coke formation process in industrial ZSM-5 during successive reuses in pyrolysis of LDPE.	82
<b>Figure 3.8.</b> Comparison of pyrolysis products between fresh and regenerated catalysts. Hatched area represents aromatic molecules.	84

<b>Figure 3.9.</b> Evolution of textural and chemical properties of catalysts samples during one cycle of pyrolysis, regeneration with different exposition times and reuse .....	86
<b>Figure 3.10.</b> Evolution of pyrolysis products repartition after successive reuses of catalysts using top mixing method. ....	88
<b>Figure 3.11.</b> Comparative evolution of normalized (a) specific surface, (b) porosity and (c) total acidity between the series of experiments using top and layers mixing. ....	90
<b>Figure 3.12.</b> Normalized $^{13}\text{C}$ NMR spectra for coked samples after top pyrolysis experiments and deconvolution results for the determination of coke nature and composition. ....	91
<b>Figure 3.13.</b> Key takeaways of “Chapter 3”. ....	94

## Chapter 4 – Regeneration of zeolites by ozonation

<b>Figure 4.1.</b> Influence of (a) time-on-stream (TOS) and (b) temperature over carbon removal efficiency during ozonation (Richard <i>et al.</i> , 2017) [9]. ....	96
<b>Figure 4.2.</b> Evolution of the different pathways of $\text{O}_3$ degradation (thermal, catalytic and decoking) for different reactor temperatures (Khangkham <i>et al.</i> , 2013) [8]. ....	96
<b>Figure 4.3.</b> Optical images of catalyst pellet cross-sections (a) and evolution of corresponding carbon removal efficiency (b) for different times of ozonation. ....	98
<b>Figure 4.4.</b> Optical images of catalyst pellet cross-sections (a) and evolution of corresponding carbon removal efficiency (b) for different ozonation temperatures. ...	100
<b>Figure 4.5.</b> (a) Radial carbon profiles for Cok3 and R1 samples (mapping method) and (b) for R2, R3 and R5 samples (scanning method) with corresponding pellets cross-sections. ....	101
<b>Figure 4.6.</b> Catalyst pellet cross-sections (a) and evolution of carbon removal efficiency (b) for different inlet ozone concentrations. ....	103
<b>Figure 4.7.</b> Evolution of coke removal efficiency for (a) different volumetric flowrates of ozone with (b) constant ozone mass flowrate. ....	104
<b>Figure 4.8.</b> Experimental Arrhenius plots of thermal decomposition and catalytic degradation of ozone over HZSM-5 zeolite. ....	107
<b>Figure 4.9.</b> Evolution of ozone decomposition depending on the temperature with repartition of thermal decomposition and catalytic degradation based on apparent reaction rates. ....	108
<b>Figure 4.10.</b> Evolution of ozone degradation efficiency for a catalytic bed (fresh HZSM-5 zeolite) exposed to an ozone-enriched stream. ....	109
<b>Figure 4.11.</b> Optical images of zeolite pellet cross-sections for distinct collected fractions of catalytic bed (high, middle and bottom) to illustrate the influence of time of exposure (a) and temperature (b) of ozonation at reactor scale. Corresponding carbon contents and coke removal are presented with tendencies of coke removal efficiency along the reactor (c,d). ....	110
<b>Figure 4.12.</b> Recording of inlet/outlet $\text{O}_3$ concentrations and temperatures for a typical ozonation experiment. ....	111

<b>Figure 4.13.</b> Visual evolution of catalytic bed during ozonation first run of REG1 and REG2 batches in syringe configuration. ....	113
<b>Figure 4.14.</b> Evolution of (a) temperature difference and (b) outlet ozone concentration during ozonation experiments in syringe reactor. ....	114
<b>Figure 4.15.</b> Key takeaways of "Chapter 4". ....	116

## Chapter 5 – Modelling approach to ozonation reaction

<b>Figure 5.1.</b> Radial profiles of carbon content over a single cylindrical catalyst particle for different regeneration regimes (Kern <i>et al.</i> , 2005) [127]. ....	118
<b>Figure 5.2.</b> Ozone diffusion pathway from catalytic bed level to zeolite crystals active sites located in microporosity (Cejka <i>et al.</i> , 2010) [19]. ....	120
<b>Figure 5.3.</b> Different diffusion mechanisms for molecular transport in a porous volume. Adapted from Ratnakar <i>et al.</i> (2022) [252]. ....	120
<b>Figure 5.4.</b> Different methods for the resolution of 2 <sup>nd</sup> -order derivative equations. ....	125
<b>Figure 5.5.</b> Different steps of photographs treatment by pellet zone detection with developed Matlab® routine, from raw pictures (a, e) to processed image (d, h). ....	128
<b>Figure 5.6.</b> Different steps for the acquisition of radial carbon profiles via grey intensity reading, from processed images (a, e) to smoothed profile (d, h). ....	129
<b>Figure 5.7.</b> Radial profiles of O <sub>3</sub> content (relative to the gas phase) and carbon load (relative to the initial content) alongside a single catalyst pellet at different process times with varying oxidation kinetic constant $k_{oxi}$ (m <sup>3</sup> .kg <sup>-1</sup> .s <sup>-1</sup> ). ....	132
<b>Figure 5.8.</b> Profiles of O <sub>3</sub> concentration and carbon content over catalyst radius at different times with varying diffusion coefficient $D$ (m <sup>2</sup> .s <sup>-1</sup> ). ....	133
<b>Figure 5.9.</b> Profiles of O <sub>3</sub> concentration and carbon content over catalyst radius at different times with varying catalytic degradation kinetic constant $k_{deg}$ (s <sup>-1</sup> ). ....	134
<b>Figure 5.10.</b> Profiles of O <sub>3</sub> concentration and carbon content over catalyst radius at different times with varying initial carbon load $LC_0$ (weight %). ....	136
<b>Figure 5.11.</b> Curve optimization for the determination of diffusion coefficient and oxidation kinetic constant by comparison with experimental profiles at high temperatures (100 to 150°C). ....	137
<b>Figure 5.12.</b> Curve optimization for the determination of diffusion coefficient and oxidation kinetic constant by comparison with experimental profiles at low temperatures (50 to 75°C). ....	138
<b>Figure 5.13.</b> Arrhenius plots of oxidation rate of coke deposited on HZSM-5 obtained by combined numerical and experimental approach. ....	139
<b>Figure 5.14.</b> Determination of the variation range of diffusion coefficient $D_{eff}$ . ....	140
<b>Figure 5.15.</b> Key takeaways of "Chapter 5" ....	142

# List of tables

## Chapter 1 – Theory and literature review

<b>Table 1.1.</b> Overall mechanism for light and heavy coke oxidation with oxygen. ....	30
<b>Table 1.2.</b> Stoichiometry and overall reaction rates for solid carbon and hydrogen oxidation. ....	31
<b>Table 1.3.</b> Standard potential of oxygen, ozone and principal oxygenated radicals under normal conditions (25°C and 1 atm). ....	37
<b>Table 1.4.</b> Kinetic constants for hydrocarbons reactivity towards molecular ozone at ambient temperature (Treacy <i>et al.</i> , 1992) [161]. ....	39
<b>Table 1.5.</b> Experiments of coke removal from catalysts using O <sub>3</sub> found in literature. ....	40
<b>Table 1.6.</b> Coke gasification reactions using H <sub>2</sub> O or CO <sub>2</sub> . ....	41

## Chapter 2 – Analytical review and experimental methods

<b>Table 2.1.</b> Principal analytical techniques found in the literature used for the characterization of fresh and deactivated catalysts. ....	47
<b>Table 2.2.</b> Principal analytical techniques used for the analysis of deactivating species over solid catalysts. ....	51
<b>Table 2.3.</b> Specifications of gases and chemicals used in experimental section. ....	55
<b>Table 2.4.</b> Temperature (T) and pressure (P) sensors of the installation. ....	56
<b>Table 2.5.</b> Catalytic bed and gas stream characteristics for the two different reactor configurations of ozonation experimental setup. ....	59
<b>Table 2.6.</b> Summary of analytical methods used in this work. ....	65

## Chapter 3 – Deactivation of catalysts by pyrolysis of LDPE

<b>Table 3.1.</b> Properties and characteristics of industrial ZSM-5 catalysts given by supplier or experimentally determined (pellet density and binder proportion). ....	73
<b>Table 3.2.</b> Composition of pyrolysis oils analyzed by GC-MS for spent catalysts. ....	74
<b>Table 3.3.</b> Properties of fresh and spent catalysts after successive pyrolysis runs. ....	76
<b>Table 3.4.</b> Nature and composition of coke structures formed during pyrolysis determined by CP-MAS <sup>13</sup> C NMR analysis. ....	80
<b>Table 3.5.</b> Determination of pore blocking contribution in porous volume loss. ....	81
<b>Table 3.6.</b> Composition of pyrolysis oils for regenerated catalysts. ....	83
<b>Table 3.7.</b> Properties of regenerated and reused catalysts. ....	85
<b>Table 3.8.</b> Properties of spent catalysts for repeatability study. ....	87
<b>Table 3.9.</b> Properties of fresh and spent catalysts (top experiments). ....	89

---

## Chapter 4 – Regeneration of zeolites by ozonation

<b>Table 4.1.</b> Coked samples used as initial samples for regeneration via ozonation. ....	97
<b>Table 4.2.</b> Comparison between carbon contents obtained with elemental and microprobe analytical techniques .....	101
<b>Table 4.3.</b> Equations for kinetic constants determination from inlet/outlet O <sub>3</sub> concentrations. ....	107

## Chapter 5 – Modelling approach to ozonation reaction

<b>Table 5.1.</b> Comparison between carbon contents obtained with elemental, microprobe and image processing methods. ....	129
<b>Table 5.2.</b> Extracted values of oxidation kinetic constant and effective diffusion coefficient obtained by curve optimization for samples ozonated at different temperatures. ....	138



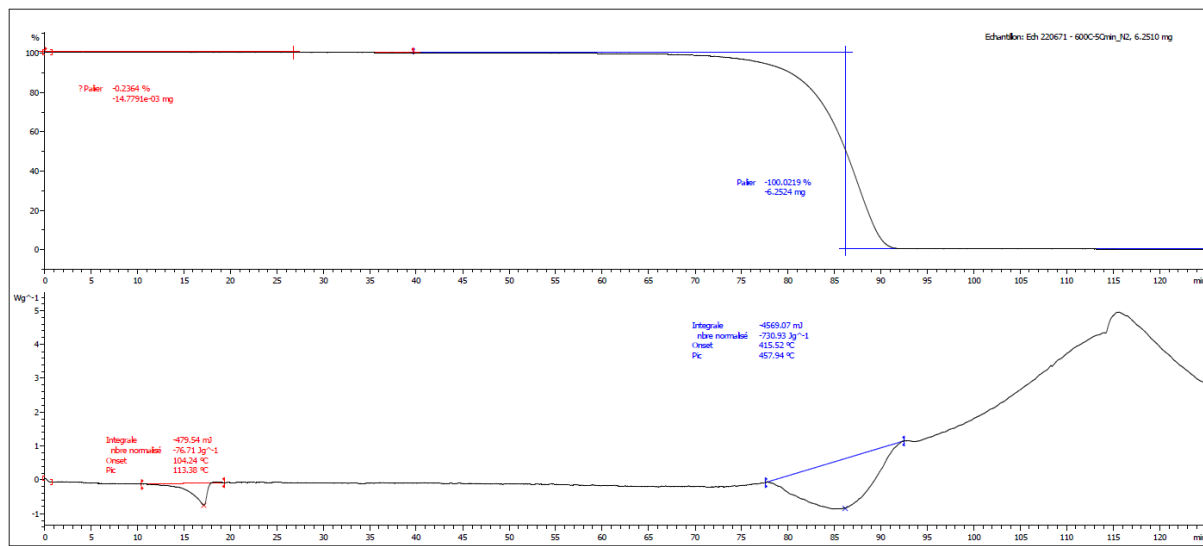
# Appendices

<b>Appendix 1:</b> TGA curves of virgin LDPE under N <sub>2</sub> atmosphere at different temperature heating ramps .....	180
<b>Appendix 2:</b> Calculation of industrial ZSM-5 catalysts pellet density by mass and volume measurements.....	182
<b>Appendix 3:</b> Industrial plans of pyrolysis experimental pilot parts.....	183
<b>Appendix 4:</b> Journal of recorded pyrolysis experiments .....	186
<b>Appendix 5:</b> Calibration of inlet ozone concentration at 20°C as a function of ozone generator electric power .....	187
<b>Appendix 6:</b> Journal of recorded ozonation experiments.....	188
<b>Appendix 7:</b> Supporting information for the experimental calculation of the kinetic constants $k_{th}$ and $k_{deg}$ .....	190
<b>Appendix 8:</b> Complete SEM-FEG results and critical discussion about the method (limitations and perspectives) .....	192
<b>Appendix 9:</b> Correlation between grey intensity and carbon content .....	195
<b>Appendix 10:</b> Image processing code for carbon profiles acquisition .....	196
<b>Appendix 11:</b> Diffusion-reaction PDEs system resolution code.....	197
<b>Appendix 12:</b> Curve-fitting (or optimization) code.....	200

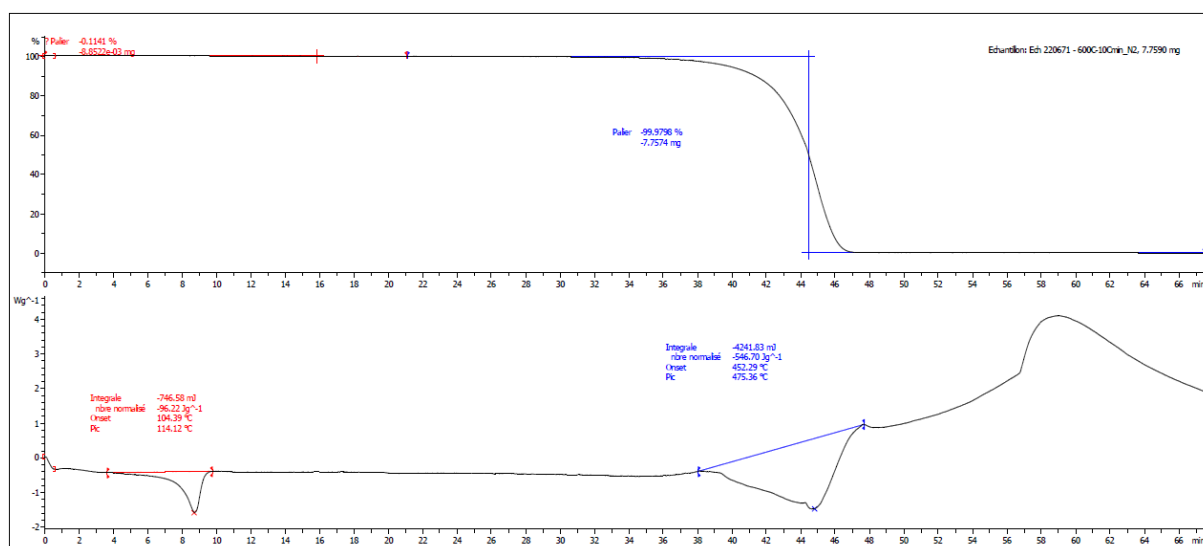


## Appendix 1: TGA curves of virgin LDPE under N<sub>2</sub> atmosphere at different temperature heating ramps

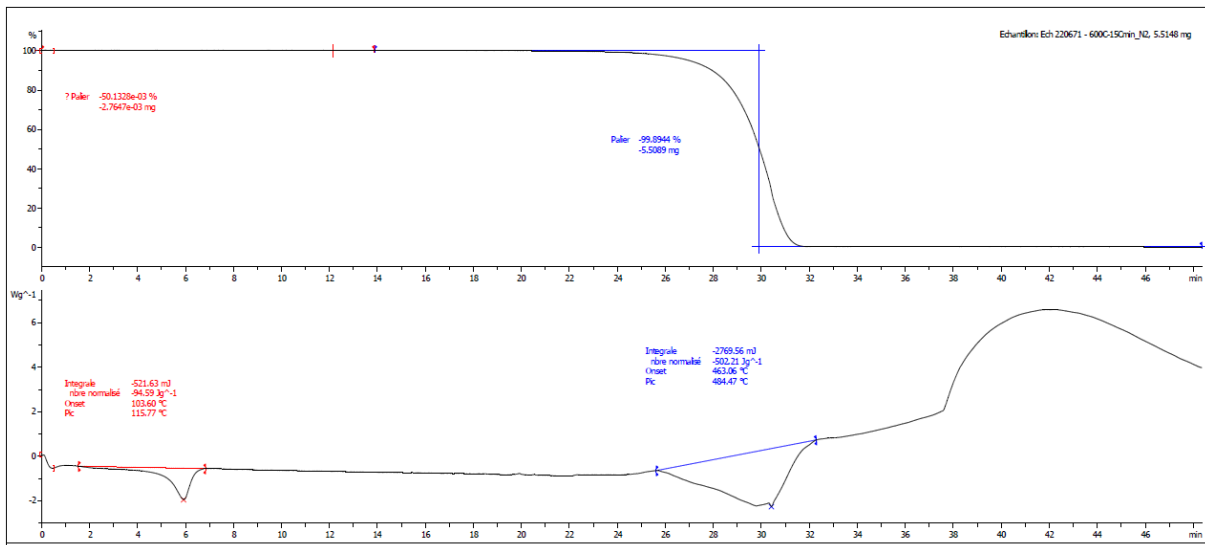
- 5°C.min<sup>-1</sup>:



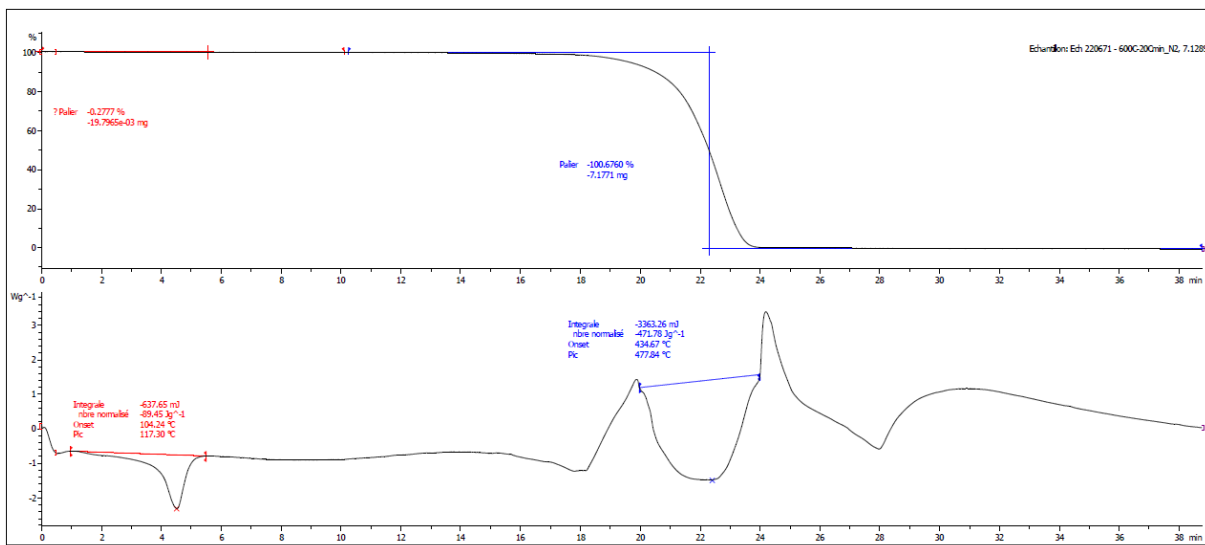
- 10°C.min<sup>-1</sup>:



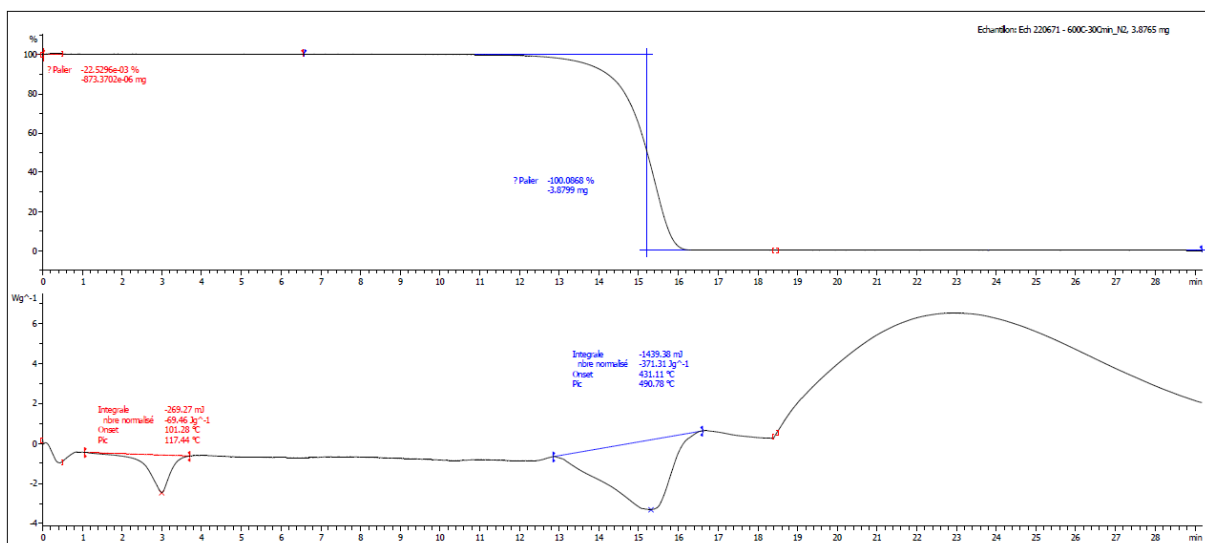
• 15°C.min<sup>-1</sup>:



• 20°C.min<sup>-1</sup>:



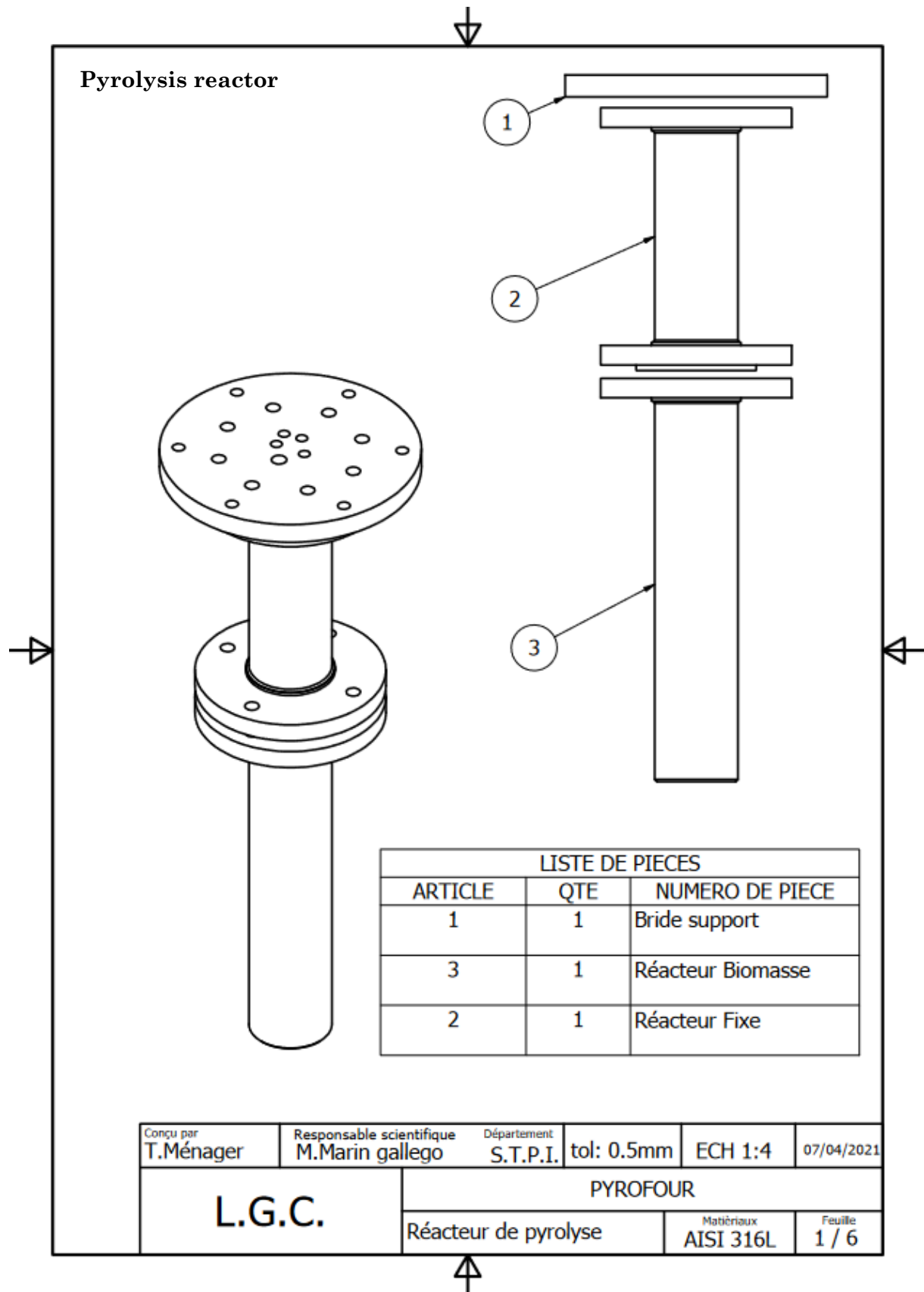
• 30°C.min<sup>-1</sup>:



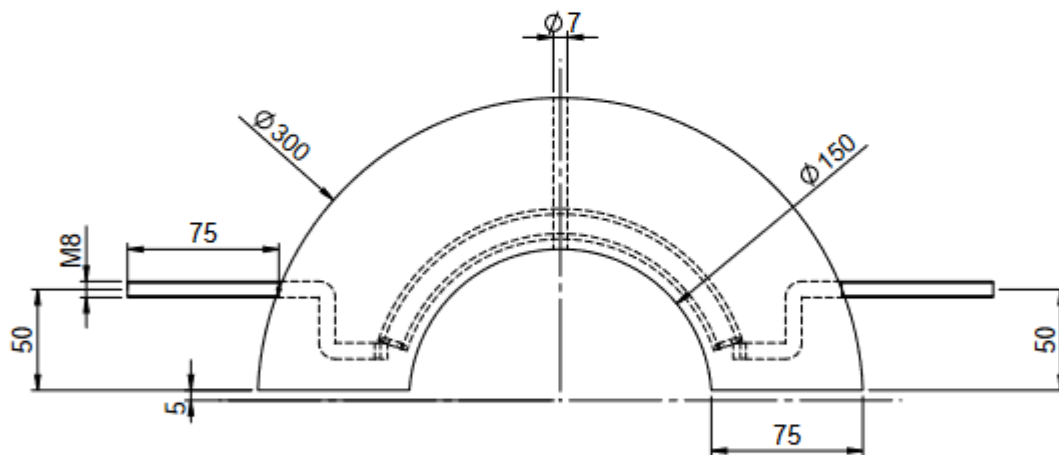
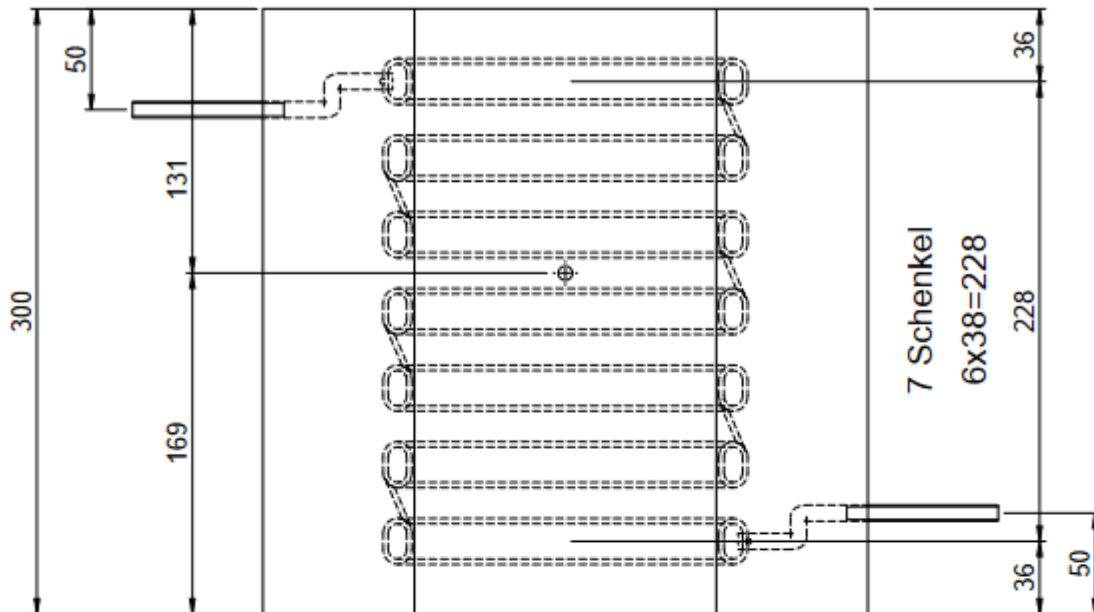
**Appendix 2:** Calculation of industrial ZSM-5 catalysts pellet density by mass and volume measurements

<b>Measure 1</b>					
	L (mm)	D (mm)	V (m <sup>3</sup> )	V <sub>tot</sub> (m <sup>3</sup> )	2.3E-08
Grain 1	6.95	1.47	1.2E-08	m <sub>tot</sub> (kg)	3.01E-05
Grain 2	6.97	1.45	1.2E-08	<b>ρ<sub>cata</sub> (kg/m<sup>3</sup>)</b>	<b>1292</b>
<b>Measure 2</b>					
	L (mm)	D (mm)	V (m <sup>3</sup> )	V <sub>tot</sub> (m <sup>3</sup> )	5.8E-08
Grain 1	4.62	1.5	8.2E-09	m <sub>tot</sub> (kg)	7.45E-05
Grain 2	5.6	1.49	9.8E-09	<b>ρ<sub>cata</sub> (kg/m<sup>3</sup>)</b>	<b>1293</b>
Grain 3	9.26	1.51	1.7E-08		
Grain 4	5.67	1.52	1.0E-08		
Grain 5	7.06	1.52	1.3E-08		

**Appendix 3:** Industrial plans of pyrolysis experimental pilot parts



Oven electric shells

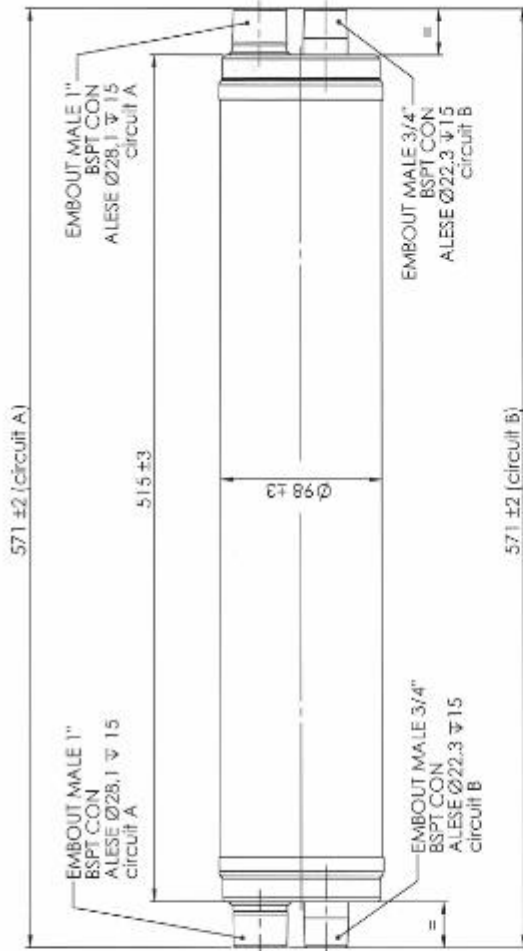


Power: 1150W / 57,5V

Pos.	Qty.	Item Name	Drawing No.	Dimension	Material
1	1	MET.WIR.COI.01.A	-	∅ 2,65	A1
2	2	MET.ROD.TER.01.A	00009388	∅ 8	A1
3	1	FIB.EMB.SHE.01.A	-	∅ 300/150x300	F14
4	1	Isomatte 150x1/2"	-	0,50 m	F14

Date	Name	General tolerances according to document No. 4.05			
Created 2021-05-17	CW	Item No. DFnew	Project No. 000428		
Approved		Title FIB.EMB.SHE.01.A	FIBROTHAL EMBEDDED SHELL 01 A		
Scale 1:3		Drawing No. 00009390	Revision 0.01	Sheet 1/1	A4
Refer to protection notice ISO 16016					

1<sup>st</sup> stage condenser



( ) cotes indicatives

Pression max de service circuit A : 6 bar ; circuit B : 40 bar		<b>spirec</b> Département échangeurs	
Traitement : poids à vide : 9 Kg		ECHANGEUR EC.07.48.RN	
Matière : INOX 316L ; chicane : CHLOROPRENE		SARHAUD CAO N°12324 - 07.48 - K123 N°12324 - 05.36 - 07.48.SI.D.A.S.M	
SPIREC SA - 1207122, rue Léon-Jouhaux 78500 SARROUVILLE - FRANCE		Tél : 01 61 04 65 00 Fax : 01 61 04 65 01	
A3	ECH: 1:2.5	DATE 04/09/2007	1 / 3
		DESS: M.K.	PED:G014 CU
IND.	DATE	MODIFICATIONS	

VA JLD **DAP**

EMBOUT MALE 1" BSPT CON ALESE Ø28.1 ±0.15 circuit A

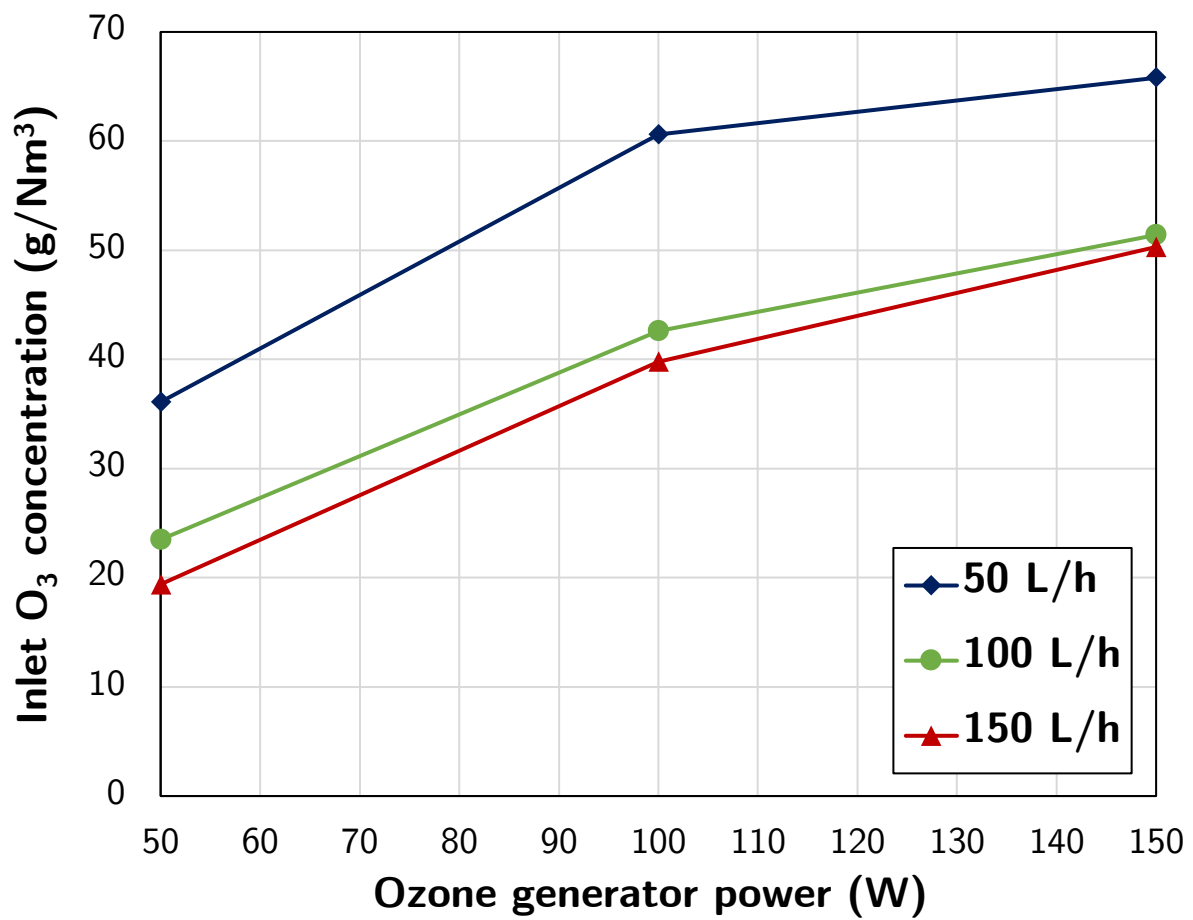
EMBOUT MALE 3/4" BSPT CON ALESE Ø22.3 ±0.15 circuit B

**Appendix 4: Journal of recorded pyrolysis experiments**

Date	LDPE (g)	ZSM-5 (g)	T°C	Used catalysts	Collected samples	Manuscript ID
01/04/2022	200	20	450	PY2_1	PY2_2	T2
12/04/2022	200	20	450	Fresh	PY3_1	-
13/04/2022	200	20	450	PY3_1	PY3_2	-
14/04/2022	200	20	450	PY3_2	PY3_3	T3
19/05/2022	100	10	450	Fresh	PY1_100:10	-
22/05/2022	50	5	450	Fresh	PY1_50:5	-
20/09/2022	200	20	450	Fresh	TOP2	T1'
21/09/2022	200	20	450	Fresh	L1_1	L1
22/09/2022	200	20	450	Fresh	L2_1	L1'
23/09/2022	200	20	450	Fresh	L3_1	L1''
15/11/2022	200	20	450	L1_1	L1_2	L2
16/11/2022	200	20	450	L2_1	L2_2	L2'
17/11/2022	200	20	450	L3_1	L3_2	L2''
22/11/2022	200	20	450	L1_2	L1_3	L3
23/11/2022	200	20	450	L2_2	L2_3	L3'
24/11/2022	200	20	450	L3_2	L3_3	L3''
09/02/2023	200	20	450	Fresh	TOP3	T1''
13/02/2023	200	20	450	L1_3	L1_4	L4
14/02/2023	200	20	450	L1_4	L1_5	L5
11/05/2023	100	10	450	Fresh	PY1_R1	-
12/05/2023	200	20	450	R48 (REG1 + REG2)	PYREG1	R48-P
21/06/2023	200	20	450	R8 (REG3 + REG4)	PYREG2	R8-P
13/07/2023	200	-	450	-	THERM2	Thermal



**Appendix 5:** Calibration of inlet ozone concentration at 20°C as a function of ozone generator electric power



**Appendix 6:** Journal of recorded ozonation experiments

ID	Regeneration conditions					Carbon content and removal results						
	Coked sample	T (°C)	D (L/h)	[O <sub>3</sub> ] <sub>in</sub> (g/Nm <sup>3</sup> )	TOS (h)	%C. init.	Haute (H)	Milieu (M)	Basse (B)	Mean %C	Carbon removal	
R1	PY1	150	50	50	3	3.3	1.2	1.6	1.8	1.5	53%	
R2	PY1	100	50	50	3	3.3	0.6	0.8	0.9	0.8	77%	
R3	PY1	50	50	50	3	3.3	1.7	1.5	1.7	1.6	51%	
R4	PY1	100	50	50	6	3.3	0.5	0.5	0.8	0.6	81%	
R5	PY1	100	50	50	1	3.3	1.1	1.5	1.3	1.3	60%	
R6	PY1	150	50	50	6	3.3	1.1		1.4	1.3	62%	
R7	PY1	125	50	50	3	3.3	0.8	1.0	1.4	1.1	68%	
R8	PY1	75	50	50	3	3.3	1.6	1.3	0.9	1.3	61%	
R9	PY1	100	50	50	4	3.3	0.6	0.7	0.8	0.7	78%	
R10	PY1	100	50	50	2	3.3	0.9	0.8	1.3	1.0	70%	
R11	PY1	100	50	50	0.5	3.3	1.3	1.4	1.6	1.4	57%	
R12	PY1	100	50	50	0.25	3.3	2.6	1.9	2.0	2.2	34%	
R13	PY1	100	50	65-70	3	3.3	0.9		1.3	1.1	67%	
R14	PY1_100:10	100	50	30	3	6	1.9	1.5	1.6	1.7	72%	
R15	PY2	100	50	50	1	5.8	2.5	2.8	2.0	2.4	58%	
R16	PY3	100	50	50	1	7.8	4.9		4.1	4.5	42%	
R17	PY3	150	50	50	1	7.8	4.1		5.2	4.6	41%	
R18	PY2	150	50	50	1	5.8	3.7		3.8	3.7	36%	
R19	PY3	125	50	50	3	7.8	1.9	2.2	3.1	2.5	68%	
R20	PY2	125	50	50	3	5.8	2.2	2.9	2.8	2.7	54%	
R21	PY3	120 100	50	50	7 3	7.8	0.8	1.2	1.8	1.2	84%	
R22	PY1_100:10	100	50	50	3	6.0	1.0	1.1	1.1	1.0	83%	
R23	PY1_100:10	100	100	25	3	6.0	2.1	1.7	1.5	1.7	72%	
R24	PY1_100:10	100	200	12.5	3	6.0	1.5		2.1	1.9	69%	
R25	PY1_100:10	100	50	25-30	3	6.0	1.9		1.8	1.8	69%	
R26	PY1_100:10	100	150	25-30	3	6.0	2.1	2.1	2.0	2.0	66%	
R27	PY3	100 100	50 50	50 50	7 3	7.8	1.1	1.2	1.3	1.2	84%	
R28	PY3	100	150	40	2	7.8	2.8	2.4	2.2	2.5	68%	
R29	PY2	100	125	40	2	5.8	1.9	2.2	1.9	2.0	65%	
R30	PY2	100	100	40	2	5.8	2.2	1.8	1.7	1.9	67%	
R31	PY2	100	75	40	2	5.8	2.2	3.0	2.2	2.7	54%	
R32	PY2	100	50	40	2	5.8	1.9	2.6	2.2	2.4	59%	
R33	PY2	100	150	40	2	5.8	2.1	2.1	2.4	2.2	63%	
R34	PY2	100	50	20	2	5.8	3.1	2.5	2.8	2.8	52%	
R35	Z5_PY2	100	50	60	2	5.8	2.2		2.2	2.2	62%	
R36	PY2	100	50	80	2	5.8	1.6	1.5	1.2	1.4	75%	
R37	PY2	100	50	50	2	5.8	2.4	1.8	1.7	2.0	65%	
R38	PY3	125	50	60	3	7.8	2.5	3.7	4.0	3.4	56%	
R39	PY3	125	75	40	3	7.8	3.3	3.5	3.4	3.4	56%	
R40	PY3	125	100	30	3	7.8	3.7	4.1	4.1	4.0	49%	
R41	PY3	125	125	24	3	7.8	4.1	4.3	4.4	4.3	45%	
R42	PY3	125	150	20	3	7.8	4.0	4.4	4.6	4.4	44%	

ID	Regeneration conditions					Carbon content and removal results						
	Coked sample	T (°C)	D (L/h)	[O <sub>3</sub> ] <sub>in</sub> (g/Nm <sup>3</sup> )	TOS (h)	%C. init.	Haute (H)	Milieu (M)	Basse (B)	Mean %C	Carbon removal	
REG1	PY1_100:10 (V1)	100	50	60	8	5.4		0.5			91%	
				60-80	6							
				70	6							
		80	70	4								
				6								
			100	100	55							6
					6							
REG2	PY1_50:5 + PY1_50:5 (V2)	100	100	60	6	(Non analysé - voir la suite du batch REG2 pour analyse finale)						
		100	100	55	6							
		80	100	55	6							
		80	100	55	6							
R43	L3_3	100	50	50	4	8.3	2.4	2.4	2.7	2.5	70%	
R44	L3_3	125	50	50	4	8.3	1.4	1.8	2.1	1.8	78%	
R45	L3_3	150	50	50	4	8.3	3.6	3.9	4.8	4.3	49%	
R46	L3_3	75	50	50	4	8.3	5.4	5.4	5.1	5.3	36%	
R47	L3_3	50	50	50	4	8.3	6.2	6.3	5.8	6.1	27%	
R48	L3_3	125	50	50	6	8.3	2.7	3.4	4.0	3.4	60%	
REG2	PY1_50:5 + PY1_50:5	100	100	50	6	6.5		0.2			97%	
		100	100	50	6							
		90	100	50	6							
		80	100	50	6							
R49	L3_3	100	50	50	6	8.3	1.5	1.6	1.6	1.6	81%	
R50	L3_3	100	50	50	8	8.3	1.6	1.7	2.0	1.8	78%	
R51	L3_3	100	50	50	1	8.3	5.6	5.0	5.3	5.3	36%	
R52	L3_3	100	50	50	3	8.3	3.6	3.4	3.8	3.6	57%	
R53	L3_3	100	50	50	0.25	8.3	6.3	6.4	6.6	6.4	23%	
R54	L3_3	100	50	50	2	8.3	4.7	4.6	4.4	4.6	44%	
R55	L3_3	100	50	50	0.5	8.3	6.1	5.7	5.9	5.8	30%	
R56	L2_3	125	50	20	4	8.4	3.4	3.6	3.8	3.6	57%	
R57	L2_3	125	50	30	4	8.4	3.2	3.6	4	3.7	57%	
R58	L2_3	125	50	40	4	8.4	2.8	2.9	3.5	3.2	63%	
R59	L2_3	125	50	60	4	8.4	2.2	2.5	2.9	2.6	70%	
R60	L2_3	125	50	70	4	8.4	1.1	1.4	1.5	1.3	84%	
R61	L2_3	125	50	80	4	8.4	1.5	1.8	2.2	1.8	78%	
R62	L2_3	125	75	40	4	8.4	2.2	2.3	2.5	2.3	72%	
R63	L2_3	125	100	40	4	8.4	3.4	3.9	4.2	3.8	54%	
R64	L2_3	125	125	40	4	8.4	2.8	3.2	3.5	3.2	62%	
R65	L2_3	125	150	40	4	8.4	3	3.3	3.6	3.3	60%	
R66	L2_3	125	50	70	1	8.4	1.9	1.9	2.1	2.0	76%	
R67	L2_3	125	50	70	2	8.4	2	2.3	2.2	2.2	74%	
R68	L2_3	125	50	70	8	8.4	1	1.3	1.4	1.3	85%	
REG3	L1_5	75	100	55	8	9.9		4.3			57%	
REG4	L1_5	75	100	55	8	9.9		5			49%	

## Appendix 7: Supporting information for the experimental calculation of the kinetic constants $k_{th}$ and $k_{deg}$

Constants and known data						
L	20	cm	Flowrate	50	L/h	
D	4	mm		1.38889E-05	m <sup>3</sup> /s	
S	1.2566E-05	m <sup>2</sup>	Velocity $u_s$	1.1052	m/s	
M(O <sub>3</sub> )	48	g/mol	$\tau$	0.18	s	
M(O <sub>2</sub> )	32	g/mol	P	1.013	bar	

- Determination of thermal decomposition constant  $k_{th}$

Experimental data (01/06/2022): empty reactor; 50 L/h; 60W.						
Temp. (°C)	Temp. (K)	1/T	[O <sub>3</sub> ] <sub>in</sub> (g/Nm <sup>3</sup> )	[O <sub>3</sub> ] <sub>out</sub> (g/Nm <sup>3</sup> )	[O <sub>3</sub> ] <sub>in</sub> (mol/L)	[O <sub>3</sub> ] <sub>out</sub> (mol/L)
100	373.15	0.002680	39.5	38	1.90	1.82
125	398.15	0.002512	40	34.7	1.92	1.67
150	423.15	0.002363	42.8	24.4	2.05	1.17
175	448.15	0.002231	43.5	9.9	2.09	0.48
200	473.15	0.002113	43	4	2.06	0.19

1 <sup>ST</sup> ORDER				2 <sup>ND</sup> ORDER		
$-\frac{d[O_3]}{dt} = k_{th} [O_3] \rightarrow k_{th} = -\frac{1}{\tau} \cdot \ln\left(\frac{[O_3]_{out}}{[O_3]_{in}}\right)$				$-\frac{d[O_3]}{dt} = k_{th} [O_3]^2 \rightarrow k_{th} = -\frac{1}{\tau} \cdot \left(\frac{1}{[O_3]_{in}} - \frac{1}{[O_3]_{out}}\right)$		
[O <sub>3</sub> ] <sub>out</sub> /[O <sub>3</sub> ] <sub>in</sub>	ln([O <sub>3</sub> ] <sub>out</sub> /[O <sub>3</sub> ] <sub>in</sub> )	$k_{th}$ (s <sup>-1</sup> )	ln( $k_{th}$ )	diff(1/[O <sub>3</sub> ] <sub>in</sub> - 1/[O <sub>3</sub> ] <sub>out</sub> )	$k_{th}$ (s <sup>-1</sup> )	ln( $k_{th}$ )
0.96	-0.04	0.21	-1.54	-0.02	0.12	-2.16
0.87	-0.14	0.79	-0.24	-0.08	0.44	-0.82
0.57	-0.56	3.11	1.13	-0.37	2.03	0.71
0.23	-1.48	8.18	2.10	-1.63	8.98	2.20
0.09	-2.37	13.12	2.57	-4.72	26.10	3.26

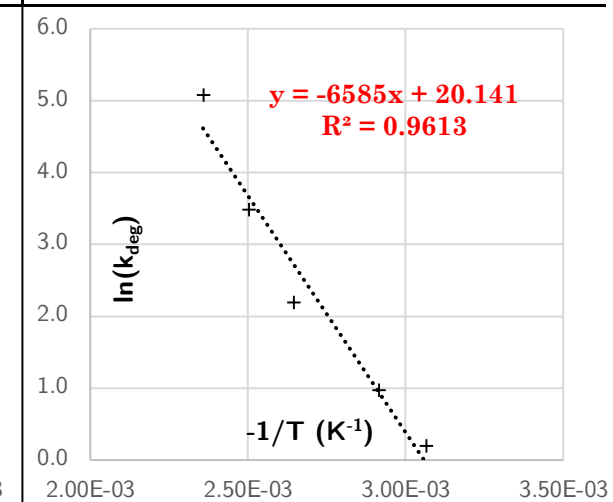
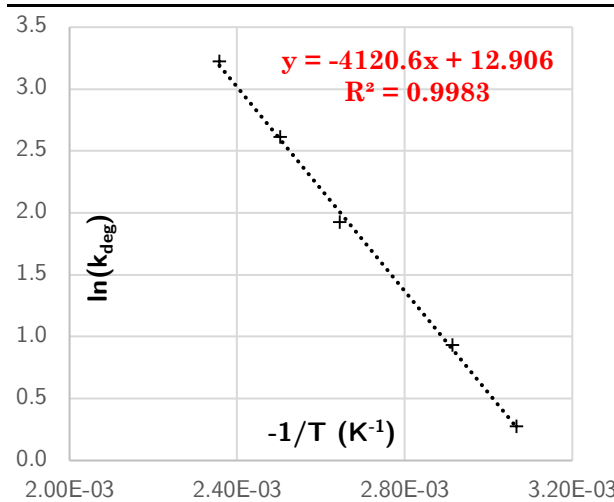
  

<table border="1"> <thead> <tr> <th>-E<sub>a</sub>/R (K<sup>-1</sup>)</th> <th>18.73</th> <th>ln(k<sub>0</sub>)</th> </tr> </thead> <tbody> <tr> <td>E<sub>a</sub> (J.mol<sup>-1</sup>)</td> <td>62625</td> <td>1.36E+08 (m<sup>3</sup>.kg<sup>-1</sup>.s<sup>-1</sup>)</td> </tr> </tbody> </table>	-E <sub>a</sub> /R (K <sup>-1</sup> )	18.73	ln(k <sub>0</sub> )	E <sub>a</sub> (J.mol <sup>-1</sup> )	62625	1.36E+08 (m <sup>3</sup> .kg <sup>-1</sup> .s <sup>-1</sup> )	<table border="1"> <thead> <tr> <th>-E<sub>a</sub>/R (K<sup>-1</sup>)</th> <th>23.93</th> <th>ln(k<sub>0</sub>)</th> </tr> </thead> <tbody> <tr> <td>E<sub>a</sub> (J.mol<sup>-1</sup>)</td> <td>81375</td> <td>2.47E+10 (m<sup>3</sup>.kg<sup>-1</sup>.s<sup>-1</sup>)</td> </tr> </tbody> </table>	-E <sub>a</sub> /R (K <sup>-1</sup> )	23.93	ln(k <sub>0</sub> )	E <sub>a</sub> (J.mol <sup>-1</sup> )	81375	2.47E+10 (m <sup>3</sup> .kg <sup>-1</sup> .s <sup>-1</sup> )
-E <sub>a</sub> /R (K <sup>-1</sup> )	18.73	ln(k <sub>0</sub> )											
E <sub>a</sub> (J.mol <sup>-1</sup> )	62625	1.36E+08 (m <sup>3</sup> .kg <sup>-1</sup> .s <sup>-1</sup> )											
-E <sub>a</sub> /R (K <sup>-1</sup> )	23.93	ln(k <sub>0</sub> )											
E <sub>a</sub> (J.mol <sup>-1</sup> )	81375	2.47E+10 (m <sup>3</sup> .kg <sup>-1</sup> .s <sup>-1</sup> )											

• Determination of catalytic degradation constant  $k_{deg}$

Experimental data (22/04/2022): ZSM-5 bed replaced for each run; 50 L/h; 50W.						
Temp. (°C)	Temp. (K)	1/T	[O <sub>3</sub> ] <sub>in</sub> (g/Nm <sup>3</sup> )	[O <sub>3</sub> ] <sub>out</sub> (g/Nm <sup>3</sup> )	[O <sub>3</sub> ] <sub>in</sub> (mol/L)	[O <sub>3</sub> ] <sub>out</sub> (mol/L)
53	326.15	0.003066	37	31.5	1.78	1.51
70	343.15	0.002914	35.2	25.8	1.69	1.24
105	378.15	0.002644	38	16.1	1.82	0.77
126.5	399.65	0.002502	35.5	6.3	1.70	0.30
151	424.15	0.002358	37.8	1.5	1.81	0.07

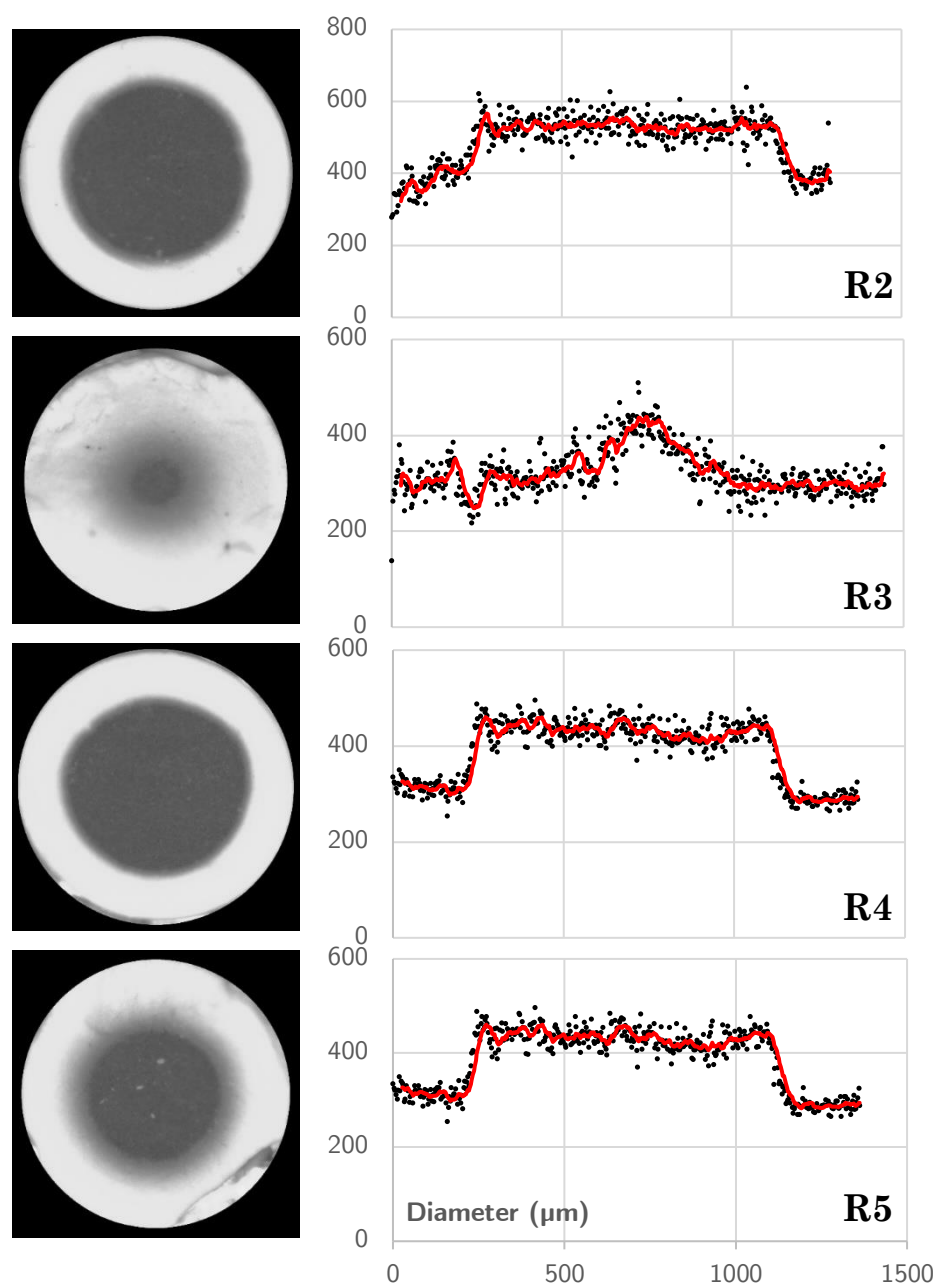
1 <sup>ST</sup> ORDER				2 <sup>ND</sup> ORDER			
$\frac{-d[O_3]}{dt} = \varepsilon k_{th} [O_3]^2 + (1 - \varepsilon) k_{deg} [O_3] \rightarrow$ $\frac{1}{(1-\varepsilon) k_{deg}} * \ln \left( \frac{[O_3]_{out}(\varepsilon k_{th}[O_3]_{in} + (1-\varepsilon) k_{deg})}{[O_3]_{in}(\varepsilon k_{th}[O_3]_{out} + (1-\varepsilon) k_{deg})} \right) = -\tau$ <p style="text-align: center;">(solver <math>k_{deg}</math>)</p>				$\frac{-d[O_3]}{dt} = \varepsilon k_{th} [O_3]^2 + (1 - \varepsilon) k_{deg} [O_3]^2 \rightarrow$ $\frac{1}{\varepsilon k_{th} + (1-\varepsilon) k_{deg}} * \left( \frac{1}{[O_3]_{in}} - \frac{1}{[O_3]_{out}} \right) = -\tau$ <p style="text-align: center;">(solver <math>k_{deg}</math>)</p>			
[O <sub>3</sub> ] <sub>out</sub> /[O <sub>3</sub> ] <sub>in</sub>	$k_{cat}$ (s <sup>-1</sup> )	$k_{cat}/m_{cat}$ (s <sup>-1</sup> .g <sub>cat</sub> <sup>-1</sup> )	ln( $k_{cat}$ )	SOLVER	$k_{cat}$ (s <sup>-1</sup> )	ln( $k_{cat}$ )	
0.85	1.98	1.32	0.28	-0.18	1.21	0.19	
0.73	3.81	2.54	0.93	-0.18	2.64	0.97	
0.42	10.26	6.84	1.92	-0.18	8.93	2.19	
0.18	20.47	13.65	2.61	-0.18	32.49	3.48	
0.04	37.57	25.05	3.22	-0.18	160.29	5.08	



$-E_a/R$ (K <sup>-1</sup> )	-4120.61	12.91	ln( $k_0$ )	$-E_a/R$ (K <sup>-1</sup> )	-6585.01	20.14	ln( $k_0$ )
$E_a$ (J.mol <sup>-1</sup> )	34259	4.03E+05	$k_0$ (m <sup>3</sup> .kg <sup>-1</sup> .s <sup>-1</sup> )	$E_a$ (J.mol <sup>-1</sup> )	54748	5.59E+08	$k_0$ (m <sup>3</sup> .kg <sup>-1</sup> .s <sup>-1</sup> )

## Appendix 8: Complete SEM-FEG results and critical discussion about the method (limitations and perspectives)

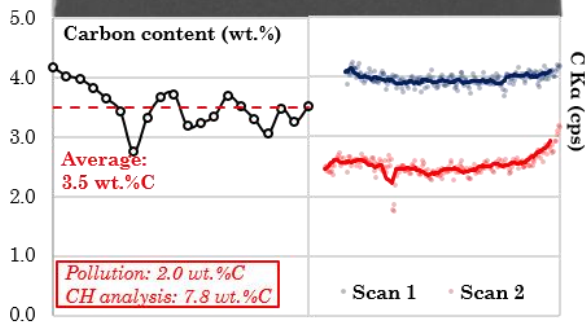
The development and validation of SEM-FEG method for the acquisition of carbon profiles over pellet radius has been conducted using 6 samples: one coked (Cok3 or T3) and five partially regenerated samples (R1 to R5, see Table 4.2). Both mapping and scanning methods were used on all samples. Microprobe analysis results were partially presented in Section 4.2 to meet the article needs. Complete results are presented in the following pages by presenting the acquired profiles with both methods over each sample radius and diameter if applicable as well as carbon pollution measurement. As mentioned previously, the two different methods provide different data: scanning method provides qualitative results while mapping method uses elemental standards for a quantitative analysis.



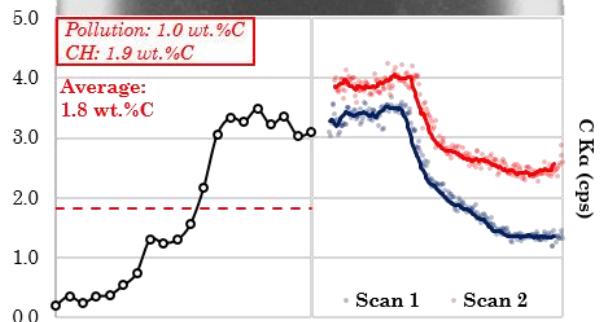
Summary of all SEM-FEG analysis conducted using scanning method (qualitative analysis) over polished catalysts cross-section diameters. Refer to Table 4.2 for regeneration conditions.

**Cok3**

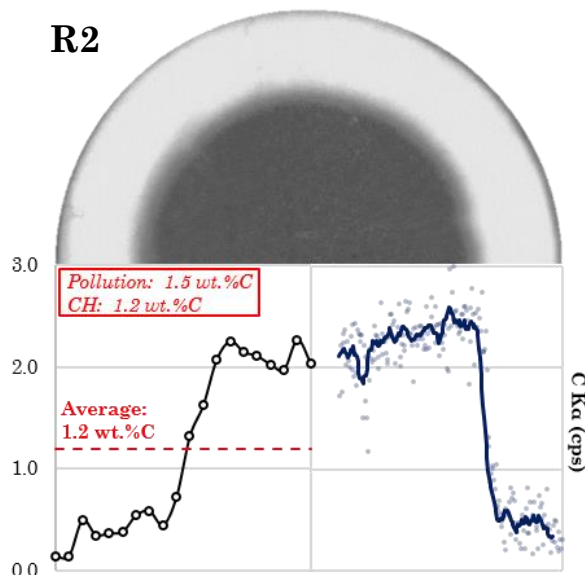
**T3**



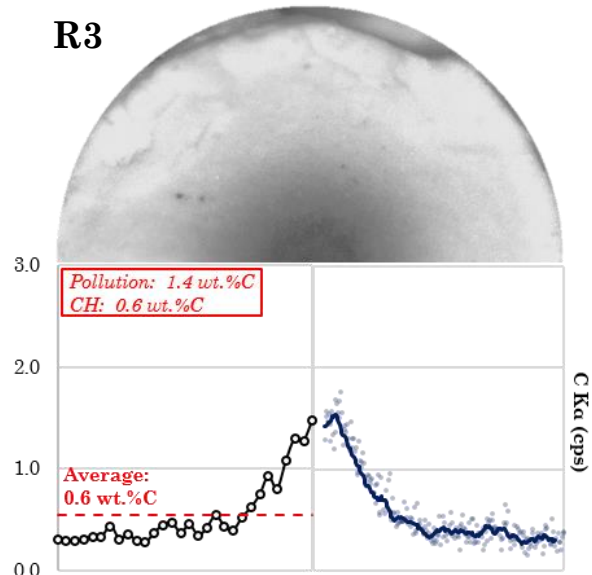
**R1**



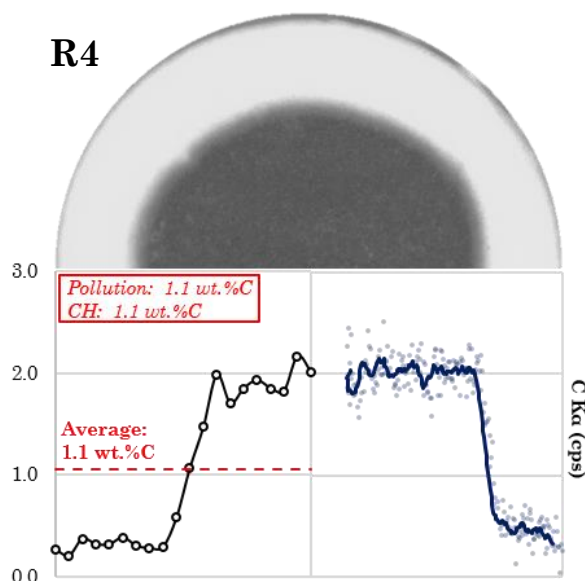
**R2**



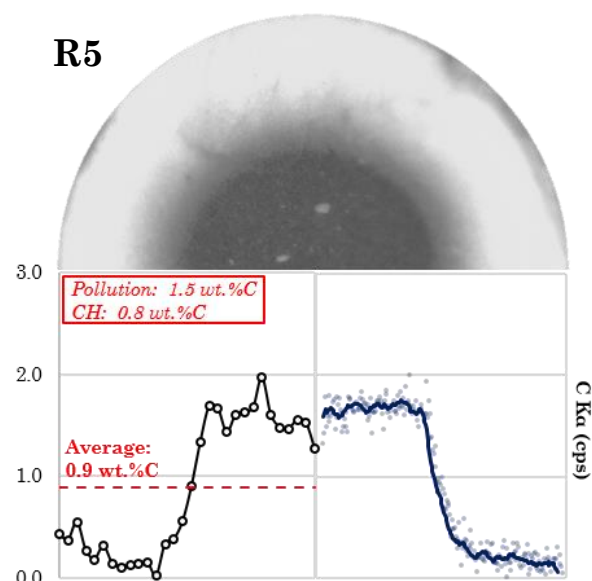
**R3**



**R4**



**R5**



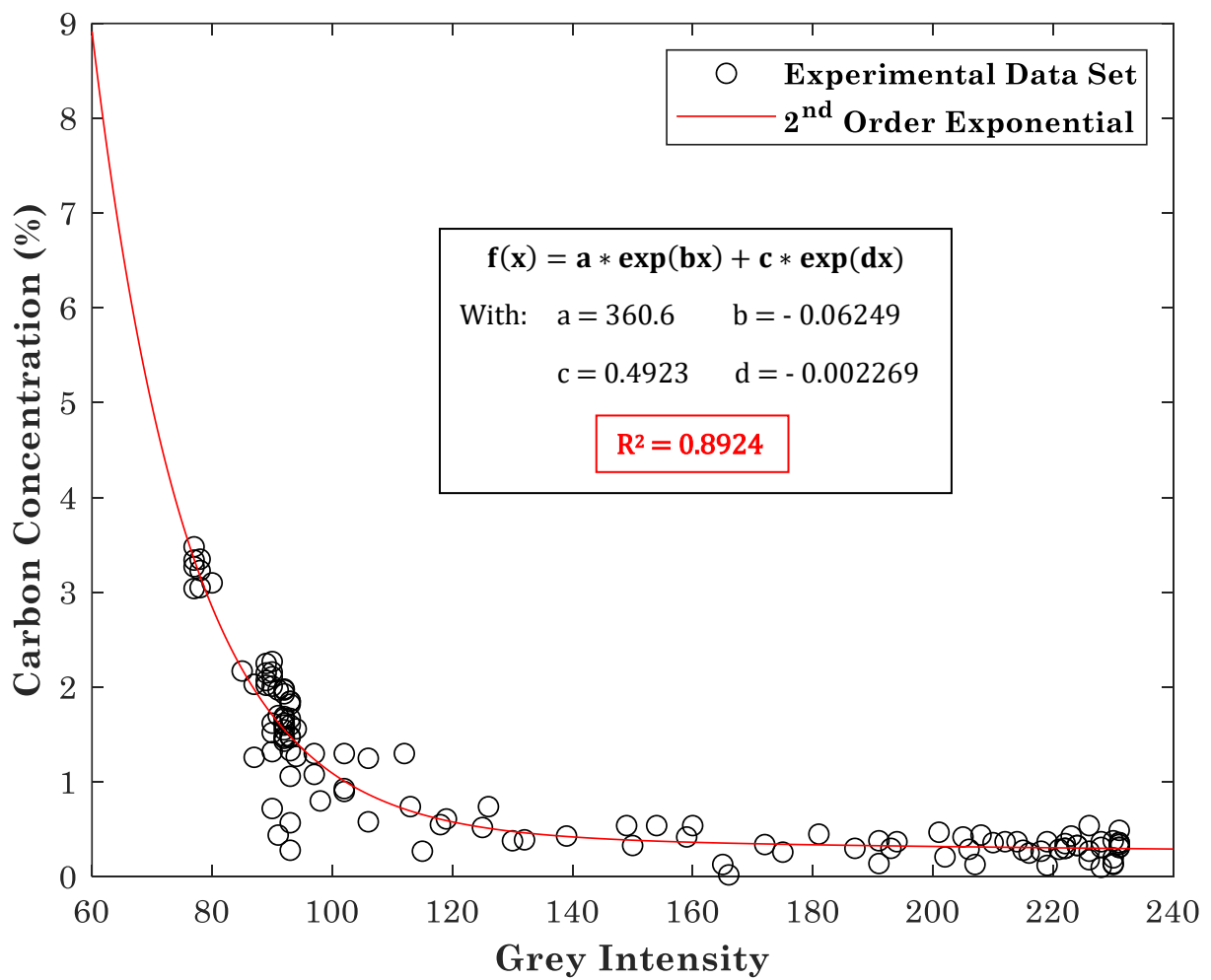
Summary of all analysis conducted with innovative SEM-FEG use for qualitative (scanning method, right graphs) and quantitative (mapping method, left graphs) determination of radial carbon repartition over pellet. Refer to Table 4.2 for regeneration conditions.



Scanning method provides a good image of carbon spatial variation as used mesh over the radius is thin. The different zones of interest consequently appear clearly over pellets presented coke core: completely regenerated outer ring, gradient zone with partial coke removal and unreacted core if relevant. The three zones present visual correspondence with optic images of pellet cross-sections. Initial carbon repartition being homogeneous according to Cok3 analysis, this last zone is visible when the profile presents a plateau near the center of the pellet. Sample R3 is the only one that does not present unreacted core, proving that ozone was able to diffuse through the pellet and oxidize coke until its center during the regeneration. Despite remaining limited noise, use of smoothing function gives exploitable profiles. Smoothed data were here obtained using moving average function (window size: 10). Scanning profile can therefore be used to determine gradient zone width and reaction front, which are important notions in the shrinking-core model [127]. However, this exploitation is not applied here due to limitations of precision measurement. Indeed, the relatively important size of sample at SEM scale does not allow locating precisely the center of the pellet to place the acquisition line. Some profiles are then shorter than 750  $\mu\text{m}$  (expected radial distance). The measure would thus not be precise at micrometer scale as such conclusions on core size or reaction front location would require, but remains a good approximation. Precise measure of such distances could give the possibility to illustrate the influence of time on the progression of shrinking-core. Such observation was intended on samples R2 and R4, exposed to the same conditions during 3 h and 6 h respectively, but bad pellet choice and precision limitations did not permit to differentiate the tiny evolution between them.

As mentioned in Section 4.2, quantitative results obtained with mapping method are consistent with elemental analysis for partially regenerated samples. This conclusion is thrilling, especially considering the usual challenge represented by carbon analysis in such low contents due to its volatility. In this method, raw elemental contents of carbon, but also oxygen, silica and aluminum, are measured after calibration using different standard samples with known proportions (SiC, Al and  $\text{Fe}_3\text{O}_4$  standards). Elemental contents are then normalized so that the total of identified weight is 100%. These carbon content values (given in wt.%) are corrected using the pollution term. This carbon pollution is measured over fresh catalyst pellet and is usually found between 1 and 2 wt.%C. This value is subtracted to the normalized result to obtain the final carbon content consistent with CH analysis. The determination of this pollution term appears as being the main limitation of the method as it changes with time and depending on the carbon content of the analyzed point. The source of this pollution was attributed to electron beam interactions with the pellet: cross-polished surface is a virgin environment with important reactivity and adsorbing capacity. Even though, SEM-FEG analysis is carried out under vacuum, it is suggested that increasing carbon pollution over fresh samples is due to deposition of gas traces present in the initial atmosphere or formed by partial degradation of coke with electron beam. These interactions could also possibly generate a difference of surface pollution between zones initially carbon-free or those containing coke. In this work, carbon pollution was only determined with an average of carbon content analyzed for 4-5 points over fresh sample. After each profile acquisition lasting between 20 and 30 min depending on the number of points, this measure is repeated to take into account the increasing tendency of this pollution. Even though results are valid for the investigated samples, further investigations have to be conducted to understand the source of the polluting species in order to mitigate it or to adapt the correcting term with the type of analyzed surface (fresh, coked or fully regenerated).

**Appendix 9: Correlation between grey intensity and carbon content**



## Appendix 10: Image processing code for carbon profiles acquisition

### Loading the image from the folder

```
sample_name = '...';
folder = '...';
target = strcat(folder,sample_name,'.jpg');
files = dir(target); % can be either a single image or a folder for batch image processing
```

### Defining the number of desired radial profiles

```
N = 360; % Number of acquisition lines
R = 500; % Number of points per line
thetarange = 0:(pi/(N/2)):(2*pi)-(pi/(N/2)); % Polar coordinates
x_standardised = linspace(0,1,R); % Radial coordinates
profile_coordinates = cell(length(thetarange), 1);
intensity_profile = cell(length(thetarange), 1);
coordinates = zeros(length(thetarange), 2);
```

### Experimental grey-to-carbon scale

```
mapping = zeros(256,2); % Initialising the mapping matrix.
mapping(:,1) = (0:1:255); % Grey intensity values between 0 and 255.
a = 360.6; b = -0.06249; c = 0.4923; d = -0.002269; % Coeff. for 2nd order exponential fit
mapping(:,2) = a*exp(b*mapping(:,1)) + c*exp(d*mapping(:,1)); % Attribution of exp. scale
```

### Image processing for carbon profile acquisition from image

```
for i = 1:length(files) % Number of loops determined by the number of images to process

    disp(files(i).name)
    full_name = strcat(folder,files(i).name);
    I = imread(full_name); % Reads the image from the workspace and loads it in.
    imbinarized = imbinarize(I); % Treatment to facilitate circle detection
    [centers, radii] = imfindcircles(imbinarized,[600 700],'Sensitivity', 0.98); % Circle
    detection on the image
    r0 = centers(1,:); % Pellet center based on circle detection
    radius = max(radii) - 1; % Pellet radius based on circle detection
    for j = 1:length(thetarange)
        r = linspace(0,radius,R)';
        theta = thetarange(j); % Angle of single line acquisition
        x = r .* cos(theta) + r0(:,1); % X-Coordinates for a single line
        y = r .* sin(theta) + r0(:,2); % Y-Coordinates for a single line
        coordinates(j, :) = [x(R),y(R)]; % Last point of each profile for plotting
        intensity_profile{j} = mean(impixel(I,x,y),2)'; % Reading grey level for [x,y] pixels
    end
    intensity_profiles_mat = cell2mat(intensity_profile); % Collecting the N acquisitions
    avg_intensity = round(mean(intensity_profiles_mat))'; % Averaging N lines
    carbon_profile = zeros(size(avg_intensity));
    for j=1:length(avg_intensity)
        idx = find(mapping(:,1) == avg_intensity(j)); % Finding intensity corresponding index
        carbon_profile(j) = mapping(idx,2); % Replacing intensity with carbon concentration
    end
    smoothdata = movmean(carbon_profile,10); % Smoothing the experimental profile
    average_content = mean(smoothdata); % Determining average carbon content in the sample

end
```

## Appendix 11: Diffusion-reaction PDEs system resolution code

### Defining Experimental Parameters

```
T_final = 8; % Final time in hours
C_in = 50e-3; % Inlet concentration of ozone in kg/Nm3
LC0 = 3.3; % Initial carbon load in kg/kg of catalyst (wt.%)
```

### Defining Initial Parameters

```
Temp = 150; % Ozonation temperature
D = 3.01e-7; % Diffusion coefficient of ozone in the zeolite
e = 0.55; % Porosity of catalyst
rho_p = 1300; % Density of catalyst in kg/m3
MO3 = 48e-3; % Molar mass of ozone in kg/mol
MC = 12e-3; % Molar mass of carbon in kg/mol
kdeg = 1; % Degradation reaction constant (arbitrary value or Arrhenius expression with Temp)
koxi = 1; % Oxidation reaction constant (arbitrary value or Arrhenius expression with Temp)
C0 = C_in; % Inlet concentration of ozone in mol/Nm3
```

### Establishing Radial Parameters

```
Rx = 0.75e-3; % Radius of catalyst pellet in m
Nr = 200; % Number of intervals in r direction (e.g. radius direction)
nr = Nr+1; % Number of gridpoints in the matrix
dr = Rx/Nr; % Step change in the radial direction
r = 0:dr:Rx; % r values from center (r=0) to external surface (r=Rx)
```

### Establishing Time Parameters

```
tf = T_final*3600; % Final time in seconds
dt = 1; % Time step value in s (up to 10s maximal value)
nsteps = tf/dt; % Number of time steps
```

### Defining Initial Conditions

```
C = zeros(nr,1); % Ozone concentration is null at t = 0
LC = LC0*ones(nr,1); % Homogeneous carbon load along the pellet radius at t = 0
theta = - 0.094.*LC + 0.962; % Experimental correlation between LC and free sites fraction
```

### Newton resolution of C and LC in time and space using Crank-Nicholson scheme

```
alpha = (dt*D)/(2*e*dr^2); % Constant value from discretization scheme
beta = D*dt/(2*e*2*dr); % Constant value from discretization scheme
ksi = dt*koxi/2; % Constant value from discretization scheme

nout = 3600; % Outputting the solution every hour for visualisation (for dt = 0.1)
nitermax = 20; tol = 1e-4; j=1; % Newton resolution iteration and exit parameters

gamma = dt*(kdeg.*theta + rho_p*koxi.*LC)/(2*e); % Reaction term (time dependent)
A = sparse(nr,nr); % Initialization of tridiagonal matrix for C resolution
for k = 2:nr-1
    A(k,k-1) = -alpha + beta/r(k); % South diagonal
    A(k,k) = 1 + 2*alpha + gamma(k); % Principal diagonal
    A(k,k+1) = -alpha - beta/r(k); % North diagonal
end
```

```

A(1,1) = 1 + 2*alpha + gamma(1); % Boundary conditions for the tridiagonal matrix
A(1,2) = -2*alpha;
A(nr,nr) = 1;

% Jacobian matrix for Newton coupled resolution
J = sparse(2*nr,2*nr);
for k = 1:nr
    J(k,k) = 1 + ksi*C(k); % Upper-left quarter (dLC/du)
    J(k,nr+k) = ksi*LC(k); % Upper-right quarter (dC/du)
    J(nr+k,k) = dt*rhop*koxi/(2*e)*C(k); % Bottom-left quarter (dLC/dv)
end
J(nr+1:2*nr,nr+1:2*nr) = A; % Bottom-right quarter (dC/dv). Taken into account in A.
[L,U] = lu(J); % LU factorization of Jacobian matrix

for i = 2:nsteps % Iterate until final time
    % Newton Initialization
    u = LC; v = C; theta = - 0.094.*u + 0.962;
    F = zeros(2*nr,1); % We solve F(u(n+1),v(n+1))=0
    er = 1; niter = 1;
    gamma_o = dt*(kdeg.*theta + rhop*koxi.*LC)/(2*e);
    b = zeros(nr,1); % b doesn't change during the Newton iteration so is out of the loop
    b(1,1) = (1-2*alpha-gamma_o(1))*C(1) + 2*alpha*C(2); % Boundary condition at r=0
    b(2:nr-1,1) = (alpha-beta./r(2:nr-1)').*C(1:nr-2) + (1-2*alpha-gamma_o(2:nr-1)).*C(2:nr-1)
        + (alpha+beta./r(2:nr-1)').*C(3:nr); % Matrix column of CN resolution
    b(nr,1) = C0; % Boundary condition at r=Rx
    while er>tol & niter <= nitermax
        F(1:nr,1) = u - LC + ksi*(u.*v + LC.*C); % nr first equations for LC
        % Diffusion-reaction matrix re-evaluated at (u,v)
        gamma = dt*(kdeg.*theta + rhop*koxi.*u)/(2*e);
        A = sparse(nr,nr);
        for k=2:nr-1
            A(k,k-1) = -alpha + beta/r(k);
            A(k,k) = 1 + 2*alpha + gamma(k);
            A(k,k+1) = -alpha - beta/r(k);
        end
        A(1,1) = 1 + 2*alpha + gamma(1);
        A(1,2) = -2*alpha;
        A(nr,nr) = 1;

        F(nr+1:2*nr,1) = A*v - b; % nr+1:2*nr equations for C
        delta = - U\(L\F); % Solving : J*delta = - F <=> L*U*delta = - F
        u = u + delta(1:nr);
        v = v + delta(nr+1:2*nr); % Updating iterates with correction term
        er = norm(delta);
        niter = niter+1;
    end
    LC = u; C = v; % Solution at t=t(n+1)
    if mod(i,nout)==0 % Saving the solution every process hour for plotting
        cfig(:,j) = C/C0; % Normalizing ozone concentration
        LCfig(:,j) = LC/LC0; % Normalizing carbon concentration
        j = j+1;
    end
end
end

```

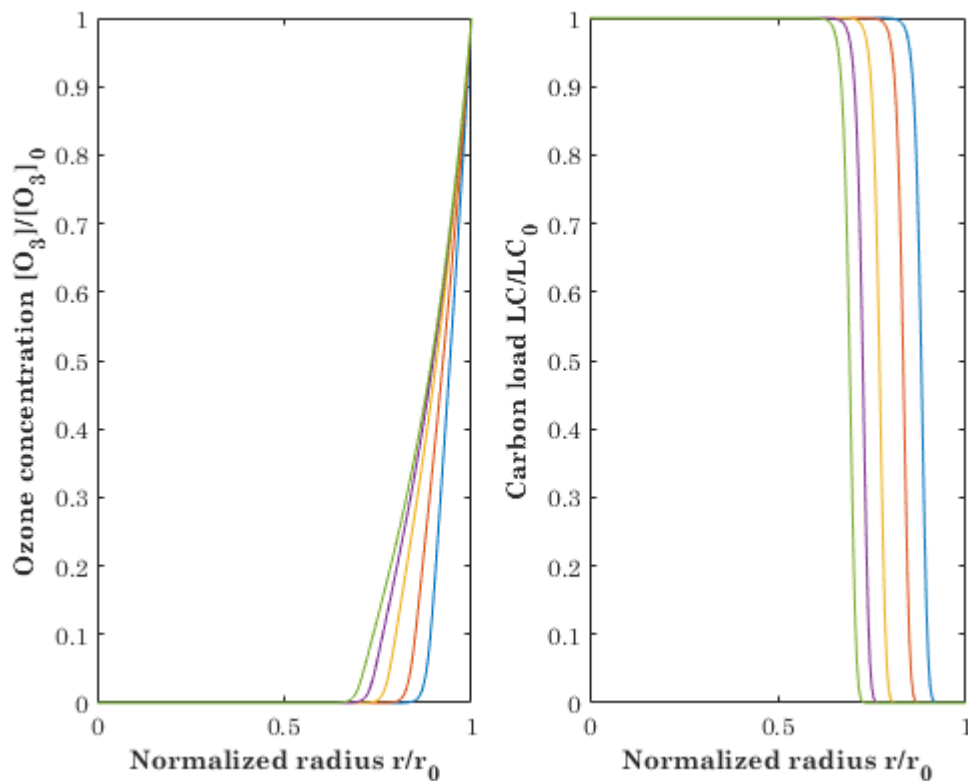
## Plotting Saved Profiles

```

figure(1)
for i = 1:5
    num = [1 2 4 6 8]; % Choosing plotted profiles
    hold on
    subplot(1,2,1)
    plot(r/RX,Cfig(:,num(i)),'Linewidth',1) % Normalizing radial parameter
    hold on
    subplot(1,2,2)
    plot(r/RX,LCfig(:,num(i)),'Linewidth',1) % Normalizing radial parameter
end
% Setting graph appearance
hold on
subplot(1,2,1)
box on
set(gca,'FontName','Century Schoolbook')
xlabel('Normalized radius r/r_0','Fontweight','Bold');
ylabel('Ozone concentration [O_3]/[O_3]_0','Fontweight','Bold');
ylim([0 1])
subplot(1,2,2)
set(gca,'FontName','Century Schoolbook')
xlabel('Normalized radius r/r_0','Fontweight','Bold');
ylabel('Carbon load LC/LC_0','Fontweight','Bold');
ylim([0 1])

```

Elapsed time is 18.138076 seconds.



## Appendix 12: Curve-fitting (or optimization) code

### Loading the Image Processing Results

```
folder = '...';
sample = 'R2';
target = strcat(folder,sample,'_CleanNormalized.mat'); % Specifying exp. profile file name
file = load(target); temp = fieldnames(file); data = file.(temp{1});
exp_profile = data'; % Experimental profile for comparison with numerical resolution
```

### Establishing Radial and Time Parameters

```
Rx = 0.75e-3; % Radius of catalyst pellet in m
Nr = 99; % Number of intervals in r direction (reduced to minimize optimization constraints)
nr = Nr+1; % Number of gridpoints in the matrix
dr = 1/Nr; % Radial step
r = 0:dr:1; % Normalized radius range
tadim = 1e-1; % Time parameter to remove parameters dimensions
```

### Parametric Study with Gauss-Newton Method

```
D = 3e-7; % Diffusion coefficient of ozone in catalyst (arbitrary value)
kdeg = 20; % Catalytic degradation kinetic constant (arbitrary value)
koxi = 1; % Coke oxidation kinetic constant (arbitrary value)
param = [D, kdeg, koxi]; % Initialization of parameters triplet [D, kdeg, koxi]
deltaparam = [1e-3 1e-3 1e-6]; % [deltaD, deltakdeg, deltakoxi]

max_iterations = 10; % Maximum number of loops. Modify if necessary.
tol = 1e-10; er = 1; iteration = 1; % Gauss-Newton iteration and exit parameters
param = param.*[(tadim/(Rx^2)), tadim, tadim]; % Remove parameters dimension to have a triplet
with similar magnitude and balance the optimization resolution

plot(r, exp_profile,'Linewidth',2,'Color','Black') % Plotting reference experimental profile

while er > tol & iteration <= max_iterations
    disp(iteration)
    num_profile = ynum(param); % Resolution of PDEs system with initial parameters. Function
    ynum is the code presented in Appendix 11 adapted for dimensionless parameters input.
    save_cost(iteration) = cost(exp_profile,num_profile); % Cost function between profiles
    hold on
    plot(r,num_profile,'Linewidth',1,'Color','Red') % Plotting resolution at each iteration
    F = gradient_J(exp_profile,num_profile,param,deltaparam); % Gradient function
    H = hessienne(exp_profile,num_profile,param,deltaparam); % Hessian matrix function
    delta = - H\F; % Correction term according to optimization algorithm.
    % Size of delta varies from 1 to 3 according to the number of varying parameters.
    param = param + 0.1*delta'; % New set of parameters (0.1 factor is optional)
    er = norm(F);
    disp(param)
    save_er(iteration) = er; % Saving evolution of error
    save_param(iteration,:) = param; % Saving parameter sets at each iteration
    iteration = iteration + 1;
end

save_param = save_param./[(tadim/(Rx^2)), tadim, tadim]; % Restoring parameters dimensions
num_profile = ynum(param); % Solving PDEs system with final parameters triplet
plot(r,num_profile,'Linewidth',1,'Color','Green') % Plotting final optimized profile
```



## Cost function

```
function [J] = cost(yexp, ynum)
J = sum((yexp - ynum).^2); % Evaluation of residual sum of squares between profiles
end
```

## Gradient function

```
function [gradJ] = gradient_J(yexp, ynum0, P, delta)
% Gradient function can be adapted according to the number of varying parameters by commenting
the different coefficients. Output matrix will vary from 1 to 3 coefficients.
dB = sum(2.*(yexp - ynum0).*(ynum(P + delta.*[-1 0 0])
        - ynum(P + delta.*[1 0 0]))/(2*delta(1)));
dkdeg = sum(2.*(yexp - ynum0).*(ynum(P + delta.*[0 -1 0])
        - ynum(P + delta.*[0 1 0]))/(2*delta(2)));
dkoxi = sum(2.*(yexp - ynum0).*(ynum(P + delta.*[0 0 -1])
        - ynum(P + delta.*[0 0 1]))/(2*delta(3)));
gradJ = [dB; dkdeg; dkoxi];
end
```

## Hessian matrix function

```
function [H] = hessienne(yexp, ynum0, P, delta)
% Hessian matrix function can be adapted according to the number of varying parameters by
commenting the adequate coefficients. Output matrix size will vary from 1x1 to 3x3.

coeff1 = (cost(yexp, ynum(P+delta.*[2 0 0]))- 2*cost(yexp, ynum0)
        + cost(yexp, ynum(P+delta.*[-2 0 0])))/(4*delta(1)^2);
coeff2 = (cost(yexp, ynum(P+delta.*[1 1 0]))-(cost(yexp, ynum(P+delta.*[-1 1 0]))
        + cost(yexp, ynum(P+delta.*[1 -1 0]))
        + cost(yexp, ynum(P+delta.*[-1 -1 0])))/(4*delta(1)*delta(2));
coeff3 = (cost(yexp, ynum(P+delta.*[1 0 1]))-(cost(yexp, ynum(P+delta.*[-1 0 1]))
        + cost(yexp, ynum(P+delta.*[1 0 -1]))
        + cost(yexp, ynum(P+delta.*[-1 0 -1])))/(4*delta(1)*delta(3));
% coeff4 = (cost(yexp, ynum(P+delta.*[1 1 0]))-(cost(yexp, ynum(P+delta.*[1 -1 0]))
        + cost(yexp, ynum(P+delta.*[-1 1 0]))
        + cost(yexp, ynum(P+delta.*[-1 -1 0])))/(4*delta(1)*delta(2));
coeff5 = (cost(yexp, ynum(P+delta.*[0 2 0]))-2*cost(yexp, ynum0)
        + cost(yexp, ynum(P+delta.*[0 -2 0])))/(4*delta(2)^2);
coeff6 = (cost(yexp, ynum(P+delta.*[0 1 1]))-(cost(yexp, ynum(P+delta.*[0 -1 1]))
        + cost(yexp, ynum(P+delta.*[0 1 -1]))
        + cost(yexp, ynum(P+delta.*[0 -1 -1])))/(4*delta(2)*delta(3));
% coeff7 = (cost(yexp, ynum(P+delta.*[1 0 1]))-(cost(yexp, ynum(P+delta.*[1 0 -1]))
        + cost(yexp, ynum(P+delta.*[-1 0 1]))
        + cost(yexp, ynum(P+delta.*[-1 0 -1])))/(4*delta(1)*delta(3));
% coeff8 = (cost(yexp, ynum(P+delta.*[0 1 1]))-(cost(yexp, ynum(P+delta.*[0 1 -1]))
        + cost(yexp, ynum(P+delta.*[0 -1 1]))
        + cost(yexp, ynum(P+delta.*[0 -1 -1])))/(4*delta(2)*delta(3));
coeff9 = (cost(yexp, ynum(P+delta.*[0 0 2]))-2*cost(yexp, ynum0)
        + cost(yexp, ynum(P+delta.*[0 0 -2])))/(4*delta(3)^2);
coeff4 = coeff2;
coeff7 = coeff3;
coeff8 = coeff6; % Symetric coefficients are not calculated twice to reduce calculation time

H = [coeff1 coeff2 coeff3; coeff4 coeff5 coeff6; coeff7 coeff8 coeff9];
end
```





## RÉSUMÉ

---

Cette thèse s'inscrit dans une stratégie de développement de procédés pour répondre aux enjeux environnementaux actuels, dont la transition énergétique de l'industrie chimique. Deux procédés sont ici étudiés : la pyrolyse catalytique du polyéthylène et la régénération des catalyseurs par ozonation. La pyrolyse est un procédé permettant la revalorisation des déchets plastiques en carburants. Son développement est freiné par la désactivation rapide des catalyseurs par formation de dépôts carbonés appelés « coke ». La méthode classique de combustion pour leur régénération nécessite des températures élevées (500°C). L'ozonation est un procédé alternatif moins énergivore permettant d'oxyder le coke aux alentours de 100°C. L'approche expérimentale et numérique menée dans cette thèse ont permis l'étude approfondie de la désactivation et la régénération par ozonation des catalyseurs, apportant d'importants résultats pour la compréhension et l'application industrielle de ces procédés.

### Mots-clés :

Régénération de catalyseurs ; Ozone ; Procédé d'oxydation avancée (POA) ; Zéolithe ; Pyrolyse de plastiques ; Coke

## ABSTRACT

---

This PhD thesis is embedded in a strategy for the development of processes to answer contemporary challenges such as the energetic transition of chemical industry. Two processes are investigated in this research project: catalytic pyrolysis of polyethylene and regeneration of catalysts by ozonation. Pyrolysis of plastics is a promising process allowing wastes revalorization into fuels. However, its industrial application is restrained by an important decrease of performances due to the formation of carbon deposits, called "coke", over the used catalysts. While the usual process for their regeneration operates at 500°C, ozonation is a less energy intensive method to remove coke under milder conditions (around 100°C). The combined experimental and numerical approach conducted in this work allowed intensive study of coke formation during pyrolysis and regeneration via ozonation, providing important data for the comprehension and future industrial application of these processes.

### Keywords:

Catalysts regeneration ; Ozone ; Advanced oxidation process (AOP) ; Zeolite ; Plastics pyrolysis ; Coke